The synthesis of estuarine bathymetry from sparse sounding data

by

Janet Eirlys Burroughes

A thesis submitted to the University of Plymouth

In partial fulfilment for the degree of

DOCTOR OF PHILOSOPHY

Institute of Marine Studies

Faculty of Science

September 2001

Abstract

The two aims of the project involved:

1. Devising a system for prediction of areas of bathymetric change within the Fal estuary
2. Formulating and evaluating a method for interpolating single beam acoustic bathymetry to avoid artefacts of interpolation.

In order to address these aims, sources of bathymetric data for the Fal estuary were identified as Truro Harbour Office, Cornwall County Council and the Environment Agency. The data collected from these sources included red wavelength Lidar, aerial photography and single beam acoustic bathymetry from a number of different years. These data were input into a Geographic Information System (GIS) and assessed for suitability for the purposes of data comparison and hence assessment of temporal trends in bathymetry within the estuary

Problems encountered during interpolation of the acoustic bathymetry resulted in the later aim of the project, to formulate an interpolation system suitable for interpolation of the single beam, bathymetric data in a realistic way, avoiding serious artefacts of interpolation. This aim was met, successfully, through the following processes:

1. An interpolation system was developed, using polygonal zones, bounded by channels and coastlines, to prevent interpolation across these boundaries. This system, based on Inverse Distance Weighting (IDW) interpolation, was referred to as Zoned Inverse Distance Weighting (ZIDW).
2. ZIDW was found, by visual inspection, to eliminate the interpolation artefacts described above.
3. The processes of identification of sounding lines and channels, and the allocation of soundings and output grid cells to polygons, were successfully automated to allow ZIDW to be applied to large and multiple data sets. Manual intervention was maintained for processes performed most successfully by the human brain to optimise the results of ZIDW.
4. To formalise the theory of ZIDW it was applied to a range of idealised, mathematically defined channels. For simple straight and regular curved, mathematical channels interpolation by the standard TIN method was found to perform as well as ZIDW.
5. Investigation of sinusoidal channels within a rectangular estuary, however, revealed that the TIN method begins to produce serious interpolation artefacts where sounding lines are not parallel to the centre lines of channels and ridges. Hence, overall ZIDW was determined mathematically to represent the optimum method of interpolation for single beam, bathymetric data.
6. Finally, ZIDW was refined, using data from the Humber and Gironde estuaries, to achieve universal applicability for interpolation of single beam, echo sounding data from any estuary.
7. The refinements involved allowance for non-continuous, flood and ebb type channels; consideration of the effects of the scale of the estuary; smoothing of the channels using cubic splines; interpolation using a 'smart' ellipse and the option to reconstruct sounding lines from data that had previously been re-ordered.

Contents

Appendices

Appendix 1 - Example of Satellite Elevation Plots used for GPS Survey Planning

Appendix 2 - Example of Station Description Form used during GPS Ground Control Survey and Co-ordinates of Ground Control Points

Appendix 3 - Results of the Triangulation of Aerial Photography, with GPS Ground Control, for 1988 and 1996

Appendix 4 - Conversion of Heights from OD Liverpool to OD Newlyn

Appendix 5 - Publications Resulting from this Project

Appendix 6 - Users Guide to the ZIDW Program Suite for Interpolation of Bathymetric Data

Appendix 7 - File Formats for the ZIDW Program Suite

Appendix 8 - Glossary of Technical Terms

Appendix 9 - Transformation of Gironde Data from Latitude and Longitude on Clarke 1880 Spheroid to Lambert 1993 Grid Co-ordinates

List of Figures

List of Tables

Glossary of Common Acronyms

DEM – *Digital Elevation Model*, the numerical representation of the height or depth at all points on a surface.

DGPS – *Differential Global Positioning System*, increased accuracy Global Positioning System using corrections generated by a fixed reference station.

GIS – *Geographic Information System*, a computer based system designed to store, manipulate, analyse and display all forms of geographically referenced data.

GPS – *Global Positioning System*, a navigation tool using artificial satellites.

IDW – *Inverse Distance Weighting*, an interpolation method weighting the effect of each input data point inversely according to its distance from a given output point.

OD – *Ordnance Datum*, height reference (zero) used by the Ordnance Survey to map Great Britain.

TIN – *Triangular Irregular Network*, an interpolation technique based on a network of triangles joining input data points.

ZIDW – *Zoned Inverse Distance Weighting*, the interpolation method formulated and developed in this thesis, based on Inverse Distance Weighting.

Acknowledgements

I would like to thank Vic Abbott and Keith Miller for setting up and supervising the early stages of this project, and Vic for his continuing help and support throughout the duration of the work. Also, particular thanks to Ken George for his invaluable assistance after taking over as Director of Studies, and to Andrew Williams for his additional help and supervision.

In addition, I wish to thank the many other academic, technical and administrative, staff at the University of Plymouth and Plymouth Marine Laboratories, who have provided assistance though the course of this work. Also a huge 'thank you' to the many friends and members of my family who have provided help, support and encouragement, especially during difficult phases of the project.

List of Publications

1. Burroughes, J. E., Abbott V. J. & Morris, K. P. (2000) Management of Hydrographic Survey Requirements. **Proceeding of Conference: Oceanology International 2000**, Brighton, UK.

2. Burroughes, J. E., George K. J. & Abbott V. J. (2001a) Interpolation of Hydrographic Survey Data. **The Hydrographic Journal** 99.

3. Burroughes J. E. & George K. J. (2001b) Automation of Interpolation by Zoned Inverse Distance Weighting for Linearly Distribution of Soundings. **GeoCoast**. In Press.

Authors Declaration

At no time during the registration for the degree of Doctor of Philosophy has the author been registered for any other University award.

This study was financed with by the Hydrography Section of the Institute of Marine Studies (IMS) at the University of Plymouth.

During the period of study relevant scientific seminars and conferences were attended. Conference papers and publications prepared during the period of study are listed on page xiii, full copies of these papers are given in appendix 5.

Signature: Janet Brooks

Date: 27-11-01

Chapter 1 – Introduction

1.1 Introduction to the Project

As a result of frequent hydrographic surveys within large busy estuaries, such as the Thames or Humber, data are available to allow the recognition of sedimentary patterns, even if they are not always fully understood. In the case of smaller estuaries with fragmented commercial interests, such as the Fal estuary in Cornwall, sufficient resources are rarely available to carry out frequent and comprehensive hydrographic surveys.

Despite this limitation a variety of data providing mud-bank heights and/or channel depths is available, though widely scattered amongst various authorities. These data include occasional hydrographic surveys, aerial photography at low water and Lidar flights. This research, based at the University of Plymouth, uses the Fal estuary as a typical example of a small port and aims to rationalise the available information into a standard format and refer it to a single datum, within a Geographic Information System (GIS). The result of this process was intended to provide a basis for statistical prediction of areas of change within the estuary. The development of this prediction system, in conjunction with airborne data to be acquired in the future, would aid the port authorities in evaluating sediment movement within their area of jurisdiction and in managing further hydrographic survey requirements economically.

During the development of this small port system, based on the Fal estuary, it became necessary to interpolate single beam bathymetric data on to a regular grid for the purpose of comparison with the other data sets. A regular grid with 10 metre cell size was considered applicable for the initial interpolation of the single beam data sets, a 1 metre grid was subsequently introduced during the development of Zoned Inverse Distance Weighting (ZIDW), in Chapter 5. The use of standard interpolation methods available within GIS software, such as Inverse Distance Weighting (IDW), Kriging and Triangular Irregular Network (TIN), on the linearly inhomogeneous single beam data produced clearly identifiable interpolation artefacts. Although it was possible to reduce these artefacts, by manual input to the interpolation process, this method was subjective and inefficient. Hence, it was decided to concentrate on the development

of an interpolation method suitable for dealing with inhomogeneously distributed data crossing narrow, deep channels.

An interpolation method, entitled Zoned Inverse Distance Weighting (ZIDW), was devised, and successfully tested on small data sets from the Fal estuary. Subsequently ZIDW was automated to facilitate the interpolation of larger data sets and further improved for universal application to estuaries of any size. In addition to the Fal, data from the larger Humber estuary, in north-east England, and very large Gironde estuary, in western France, was used to ensure applicability at a variety of different scales.

1.2 The Fal Estuary

The Fal estuary in SW Cornwall forms the largest estuarine system in the Duchy, covering an area of approximately 2,500 hectares. Significantly, some 26 % of this area consists of intertidal mud flats (Hughes, 1999). The estuary has a spring tidal range of 4.6m (Admiralty Tide Tables, 1999) and a tidal limit at Tresillian, 18.1 km inland (Stapleton & Pethick, 1995).

The estuary system comprises a drowned river valley or ria, formed by the sea level rise associated with the end of the last ice age. The deep tidal basin, known as Carrick Roads, which forms the lower section of the estuary is fed by six major tidal tributaries (see figure 1.1). The River Fal, Tresillian River, Truro River and Restronguet Creek, which flow into the head of the estuary, have experienced rapid siltation historically as a result of mine waste deposits (Pirrie et al, 1996, 1997). According to these authors, the greatest degree of siltation occurred in the Fal River, which drains the china clay mining district, and Restronguet Creek, draining the metal mining district to the north and west. The Percuil River, Penryn River and Mylor Creek are considered to have experienced far less siltation over the past 500 years.

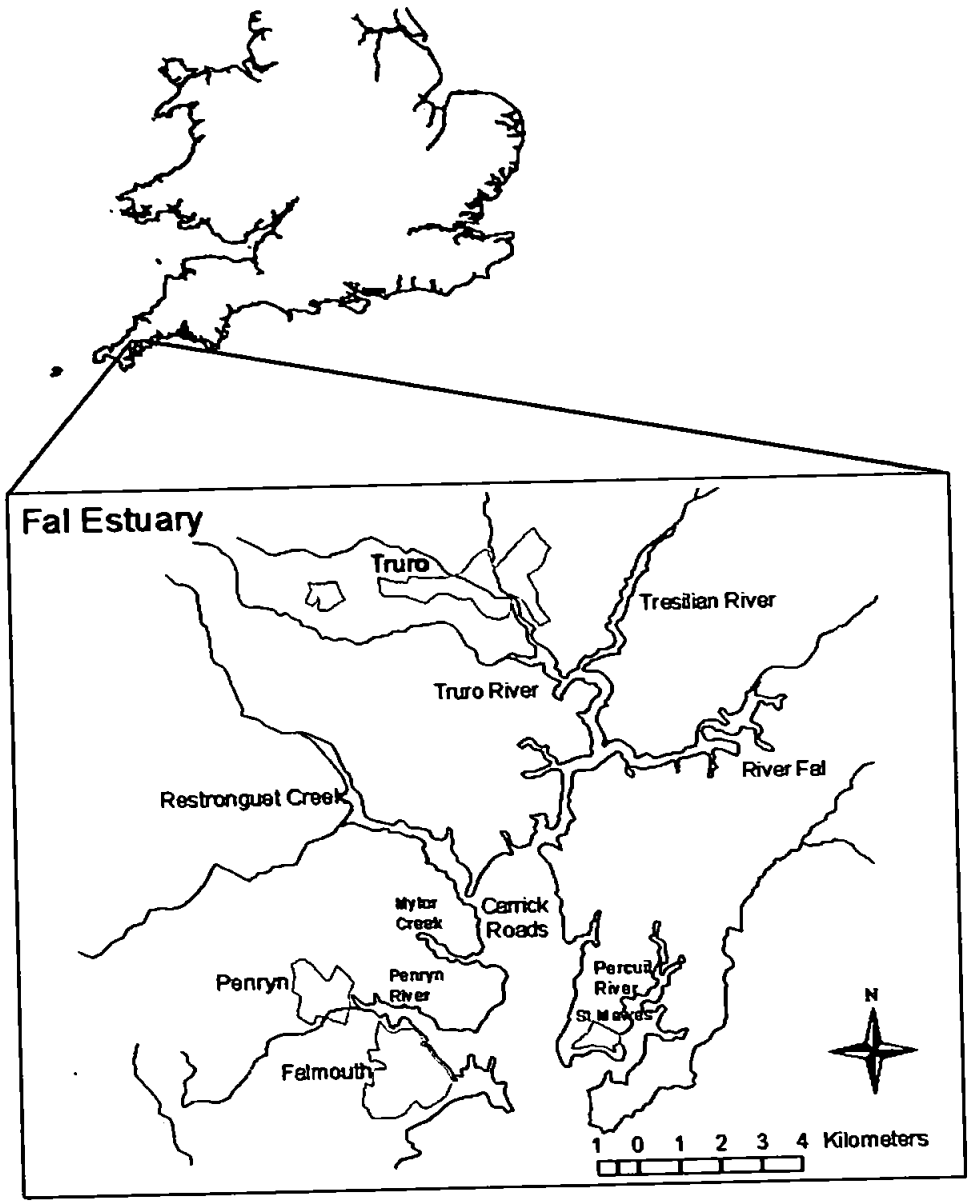

Figure 1.1 – Location and geography of the Fal

The geology of the area comprises metamorphosed sandstones and mudstones along the north and eastern edges of the estuary, drained by the Truro, Tresillian, Fal and Percuil Rivers. Further east the Fal River catchment consists of St Austell Granite associated with the china clay workings. To the west, the estuary is bordered by the Devonian Mylor Slate Formation with Carnmenellis Granite underlying the higher ground further west (Pirrie et al, 1996).

The main commercial ports within the Fal estuary are those of Truro, Penryn and Falmouth, with major waterfront activities consisting of:

- Cargo handling and the landing of calcified seaweed at Newham and Lighterage Quays in the Truro River
- Fishing activities at Penryn Quay, Bowyers Cellars and Little Falmouth
- Boatyards, lay ups and maintenance on the south bank of the Penryn River.

The main commercial area is at Falmouth Docks, supporting cargo handling, ship repair and maintenance, dry docking facilities and the building and fitting of large yachts. Bunkering services for ships using the English Channel and sheltered anchoring for large vessels in Carrick Roads and Falmouth Bay are also commercially important to the Falmouth area (Ratcliffe, 1997).

1.3 The Humber Estuary

The Humber estuary, in eastern England (location shown in figure 1.2), extends from the confluence of the Rivers Trent and Ouse, at Trent Falls, to the North Sea. The estuary covers an area of approximately 250 km^2, making it the largest estuary on the East Coast of England. The distance from Trent Falls to the mouth of the Humber, at Spurn Head, is more than 62 km. The width of the estuary increases from 1 km to more than 8 km along the length of the estuary (Barr et al, 1990). The River Ouse is tidal for some 40 km and the Trent for about 80 km above their confluence.

The Humber exhibits a spring tidal range of over 7 m, with extensive intertidal, mud flats being exposed around low water. Current velocities within the estuary reach between 2 and 3 m/s during spring tides (Barr et al, 1990).

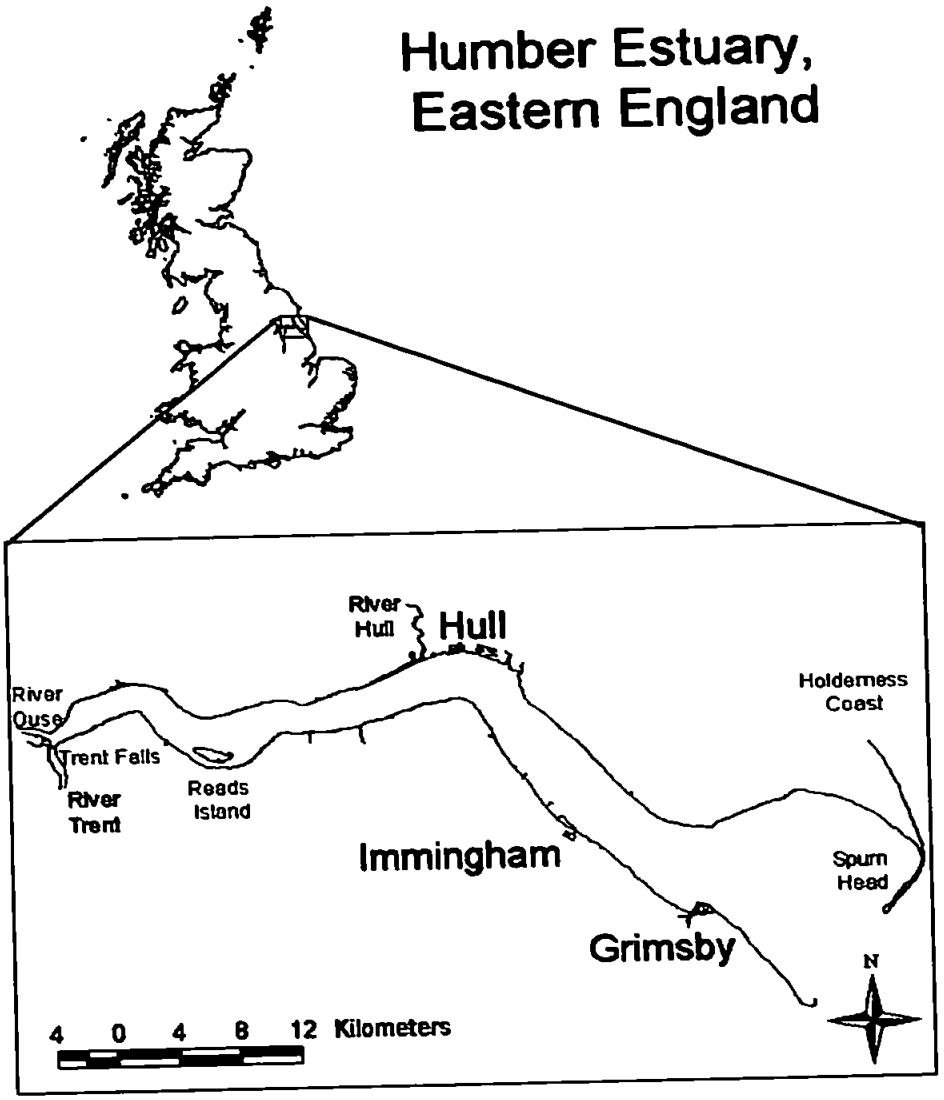

Figure 1.2 – Location and geography of the Humber

The main commercial ports within the Humber estuary are those of Grimsby, Immingham and Kingston upon Hull. The port of Grimsby, via a long standing importance in the fishing industry, has become a centre for the frozen food industry. It also operates roll-on-roll-off (ro-ro) and container terminals and, combined with Immingham, handles over 300,000 cars per year (ABP Ports Handbook, 1998). In addition to cars, Immingham specialises in dry and liquid bulk commodities, particularly grain, iron ore and petrochemical products and operates ro-ro and container terminals. The Port of Hull provides berthing for passenger and ro-ro ferries and has recently expanded its container handling facilities, in addition to a range of general cargoes.

The ports of Goole, on the River Ouse, and Gainsborough, on the River Trent, also gain access to the North Sea via the Humber estuary. In addition to the ports, numerous river-side wharves operate on the banks of the Humber estuary, and rivers Hull and Trent.

1.4 The Gironde Estuary

The Gironde estuary (figure 1.3) in South-West France is the largest estuary in Europe, covering an area of 625 km^2 at high tide (Jouanneau & Latouche, 1981). It extends almost 80 km from the confluence of the rivers Garonne and Dordogne to the Atlantic coast of France, with widths varying from 3 km to 12 km along its length.

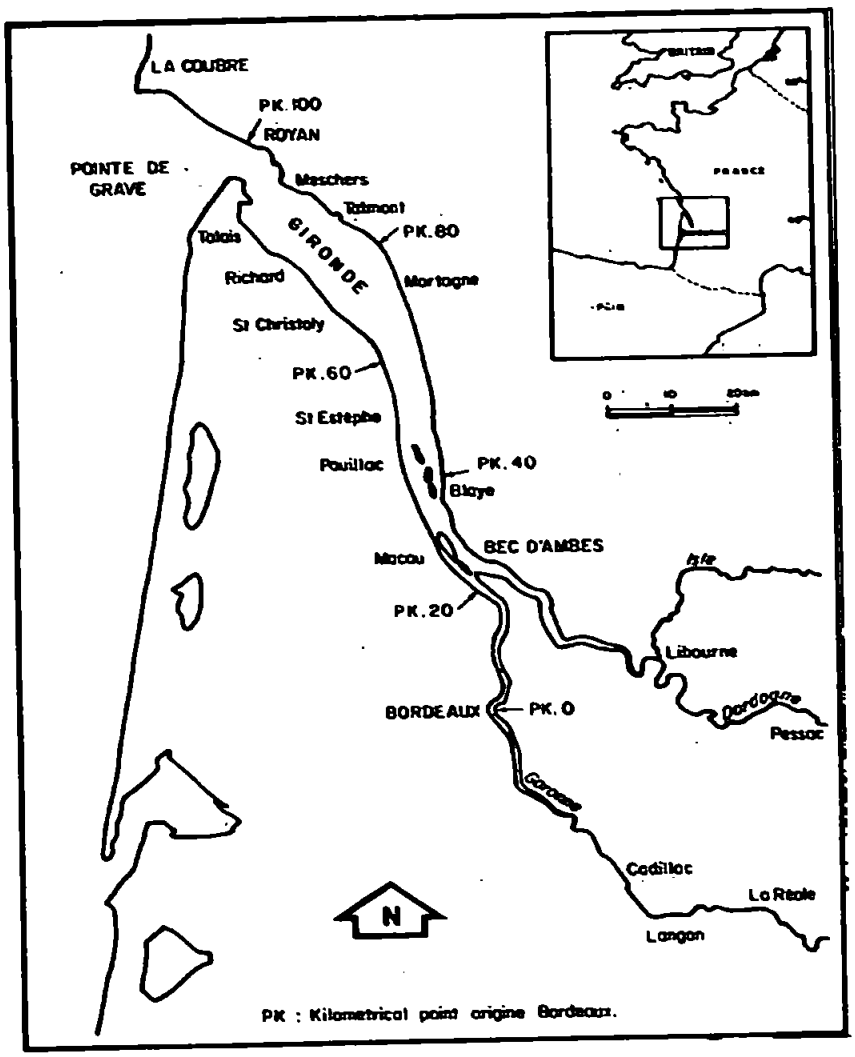

Figure 1.3 – Location and geography of the Gironde (from Jouanneau & Latouche, 1981)

The estuary experiences semi-diurnal tides, with tidal ranges at the mouth varying from 1.5 m during neap tides to 5 m at spring tide. The spring tidal range further upstream reaches as much as 5.5 m (Jouanneau & Latouche, 1981). The tides in the middle reaches, around Bordeaux, exhibit extreme shallow-water distortion (George & Simon, 1984).

Human activities in and around the Gironde estuary were traditionally dominated by viticulture, with famous vineyards situated on alluvial terraces along the banks of the estuary, and by fishing. In recent times the port of Verdon, at the mouth of the estuary, has become particularly successful providing container facilities and a petroleum outport accessible to fully laden ships of 150,00 to 250,00 tons (Jouanneau & Latouche, 1981). Access to shipping of 9.5 – 10.5 m draught, allows the port of Bordeaux, some 100 kilometres from the mouth of the estuaries to remain an important port particularly in the hydrocarbon industry.

Other ports along the Gironde include:

- Pauillac, 50 km from the mouth and the site of a petrol refinery
- Blaye, trading mostly in cereals and liquid chemical products
- Bec d'Ambès situated at the confluence of the Garonne and Dordogne rivers, comprising two petrol refineries and a thermo-electric power station

(Jouanneau & Latouche, 1981).

1.5 Aims & Objectives

1.5.1 Aims of the Project

When considering a small port, the term 'small' may refer to one of a number of different aspects of the port. In the context of Truro and many other ports in the UK 'small' refers to the commercial turnover, yet the waters for which the port is responsible extend to about 80 hectares. Management of the area, which consists of the main river and several tributaries, has to be undertaken on the small revenue that

is generated. One element of the management is hydrographic surveying (which is put out to contract) and only a small section of the area is surveyed at intervals of several years. The original aim of this project was to investigate how modern data management techniques in conjunction with data which is readily available can assist the harbour master in assessing survey requirements.

As a result of research work to fulfil this aim, the need for an interpolation system suitable for application to estuarine bathymetry, consisting of relatively narrow, deep channels crossing wide inter-tidal zones, was identified. This resulted in the further aim of this study to develop such a system. The proposed technique was investigated practically in the Fal estuary, formalised by statistical testing using mathematically defined channels and finally extended to provide universal applicability to bathymetric data collected in any estuary.

1.5.2 Objectives

In order to meet the two aims, described above, five objectives were identified. These objectives are summarised as follows:

1. To collect and integrate various data sets for the Fal estuary within a GIS.
2. To assess the suitability of each data set for comparison and hence for monitoring changes and predicting trends.
3. To formulate an interpolation system suitable for single beam acoustic bathymetry collected in the Fal estuary.
4. To assess this interpolation method, named Zoned Inverse Distance Weighting (ZIDW), using idealised, mathematical channels.
5. To refine ZIDW to achieve universal applicability, using the Humber and Gironde estuaries as examples.

1.5.3 Layout of the Project

Currently the harbour master decides on a particular area appropriate for survey and the work is put out to contract. The contractor uses traditional survey techniques to undertake the work and results are provided in the form of paper charts including fair sheet and contour sheet (**Chapter 4 – Acoustic Bathymetry**). This procedure has

been carried out for the last ten years; previously the Admiralty were responsible for survey work in the Fal. At the current rate it will take many decades to survey the whole area which may be subject to change due to environmental and industrial factors. Additional data exist in the hands of local government and agencies that may be able to contribute to the survey issues within the port, yet these data are not currently considered. Remotely sensed airborne data are acquired and held by the Environmental Agency (**Chapter 2 - Lidar**) and aerial photographs (**Chapter 3 – Aerial Photgraphy**) are available through the County Council and the Ministry of Defence. The first aim of this investigation is to consider all data that have been acquired over the last 40 years, and through the use of GIS, to develop a tool for the assessment of variation of the waterways for which the harbour master has responsibility. The remotely sensed data do not indicate water depth, but provided they are acquired at low tide, drying heights will be shown. It is not intended that the tool will provide quantitative hydrographic survey information, rather it will indicate areas of change and assist in the decision making process as to where detailed work is required. Furthermore, the introduction of a GIS based system into small port management will provide a focus for information enabling trends and influences to be identified and managed.

During research to fulfil this initial aim, a particular problem was identified in interpolation of acoustic bathymetry to a format suitable for comparison between data sets of this type, collected at different times, and with data from other sources (**Chapter 4 – Acoustic Bathymetry**). In response to this requirement a suite of software was developed, to interpolate such data for the Fal estuary (**Chapter 5 – Development of Zoned Inverse Distance Weighting, ZIDW**). The theory behind these initially practical based programs was investigated statistically (**Chapter 6 - Formulating the Theory of ZIDW**), and in response to demand for other purposes, such as tidal modelling, the program suite was extended to cover bathymetric data collected in any estuary. To ensure this universal applicability the programs were tested, not only for the small Fal estuary, but also for two larger estuaries. The Humber, in north-east England provided an example of a large estuary and a very large example was provided by the Gironde, in western France (**Chapter 7 – Application of ZIDW to the Humber and Gironde**). **Discussion and Conclusions** of the thesis are documented in **Chapters 8** and **9**.

Chapter 2 – GIS and Lidar

A Geographic Information System (GIS) forms an integral part of this project, by providing a medium through which the various data sets, including Lidar, are visualised, manipulated and analysed. Thus, a review of GIS literature will precede the review and discussion of each individual data set contained in chapters 2, 3 and 4.

2.1 Review of GIS Literature

A number of applications of GIS for the combination of data sets, including data obtained by different sensors, are identified within this section of the project. Necessarily these studies cover many aspects of rationalisation of data format. Despite this overlap, the aim of the section is to concentrate on specific functions within the GIS which make it fundamental to the successful outcome of this study.

2.1.1 Rationalisation of Data Format using GIS

Neilson & Costello (1999) provide an example where rationalisation of data sets provides the justification for use of a GIS. These authors make successful use of the GIS to allow comparison of many marine charts with different original scales and projections. The GIS allows Neilson & Costello to identify length and type of coastline for the various counties of Ireland, thus enhancing information input to coastal zone management. The unique information obtained by use of the GIS allowed a detailed assessment of the habitats requiring protection under the European Union Habitats Directive.

Livingston et al (1999) aimed to compare airborne video and digital camera imagery with terrain data from ground survey, using a GIS on a standard desktop computer, in order to minimise costs. This comparison requires the investigation of differently geo-referenced data. In addition the authors stressed the trade-off made involving spatial resolution and temporal control compared to absolute accuracy.

Work carried out by Stevens and Olsen (1999) demonstrated the value of a GIS in the treatment of data sets of various formats. The incorporated aquatic data includes finite discrete populations within lakes; continuous linear populations within bounded areas, such as streams; and continuous, two-dimensional populations associated with coastal waters. A unified approach consisting of survey theory for continuous populations; explicit control of spatial dispersion of samples; variable spatial density; nested sub-sampling and incorporating panel structures for sampling over time is used to combine the data within the GIS.

Further examples of work involving some component of rationalisation of data formats are discussed in sections 3.1.3 and 3.1.4.

2.1.2 Interpolation of Data via GIS

Creation of Digital Elevation Models (DEMs) and rasterised data from data sets consisting of discrete point samples is a vital GIS function to many users. A number of such interpolation methods are investigated within this study:

1. The triangular irregular network (TIN) method joins points within the data set to form triangles. The condition that all triangles are as close to equilateral as possible controls this process. Interpolation is then carried out along each side of each triangle, hence all original data point values are maintained.
2. The method of inverse distance weighting (IDW) uses all data points within a specified radius of each grid value required. The effect of these selected points is applied with weighting of decreasing importance according to increasing distance from the required position.
3. Based on the regionalised variable theory, Kriging has been extensively used as a method of data interpolation. Kriging assumes statistical homogeneity throughout a surface i.e. the same pattern of variation at all locations on that surface.

(Petrie & Kennie, 1990).

Blomgran (1999) used Kriging within an Arc/Info based GIS to produce a digital elevation model from discrete elevation points. The investigation of variogram

models produced by the GIS allowed Blomgran to improve the fit between theoretical and actual variograms, thus the probability of accurately interpolated DEMs could be increased by the removal of clustered input points. The resultant DEM of 5 × 5 metre grid size and vertical resolution of 0.1 metres provided a valuable tool for visualisation of flooding scenarios. Orum et al (1999) used variograms to identify spatial structure within soil fungus populations on two different scales (2 to 6 km and 20 to 30 km), from point sampled data. From this information these authors were able to produce surface maps showing spatial patterns by means of Kriging.

The use of Kriging interpolation, within a GIS-based model, is taken a stage further by vanHorssen et al (1999). Having interpolated point sample data of wetland plant species using Kriging, these authors validated their model by an uncertainty investigation. This investigation was carried out by examining the effect of errors input to the model as they propagated through it. It was found that the number of valid predictions, output by the model, declined approximately 10-20% when 95% confidence intervals were used in the validation.

Oberthur et al (1999) compared interpolation of soil sample points by Thiessen polygons (constructed in deriving TINs) and indicator Kriging. Their results showed that Thiessen polygons performed well in areas of undulating, rain-fed land but that Kriging provided the more reliable interpolation method for gradually changing, irrigated lands. Interpolation was found to be of lower accuracy in areas of sparse data and highly variable, young, alluvial soils.

2.1.3 GIS, Modelling and Statistical Testing

Examples of linking site specific models with a GIS in order to examine spatial as well as temporal phenomena are reviewed by Hartkamp et al (1999). The review places particular importance on data issues and scale as well as computer programming and interfacing considerations. The problems associated with the greatly increased data volumes produced by the use of spatial data rather than individual point sampling are also discussed.

Townsend and Walsh (1998) integrated satellite images, time series data and GIS coverages to model the potential for flood inundation within the lower Roanoke River floodplain, North Carolina. Initially a DEM was developed and from this models of potential wetness and potential for flood inundation, using both raster and vector analysis, were generated. Comparison with statistical results indicated the success of these GIS-derived models for identification of flooded areas.

A clear parallel can be seen between this type of GIS based, flood potential modelling, involving very gently sloping surfaces, and the prediction of areas of estuary channel change documented in this study. Both areas of investigation use historical data of various sources and types, rationalised within a GIS, to provide a basis for future prediction. Townsend and Walsh identified areas at high risk of inundation by floodwaters, whilst this study aims to distinguish regions of rapid channel change in order to target resources for hydrographic surveys effectively.

2.2 Review of Literature on Lidar

2.2.1 Lidar Bathymetry

Lidar provides an important source of inter-tidal zone bathymetry for this study. This section reviews marine and land based application of Lidar potentially relevant to this type of area, which forms the interface between land and sea.

A review of airborne Lidar hydrographic (ALH) systems, produced by Estep (1993a), identifies a number of systems being developed by various countries, including Australia, America, Canada, Russia, China and Sweden. This wide ranging review allows modern, commercially successful Lidar systems to be viewed in their wider historical context. Since that time, three systems have emerged for commercial development, namely the Australian 'LADS', Swedish 'Hawk Eye' and American 'SHOALS' systems. The stages involved in the development of all three systems have been extensively reviewed with many example surveys documented.

The WERLADS II system, a trial system for LADS, was reviewed, by Penny et al back in 1986. The author concludes by identifying improvements expected for the operational LADS system, including DGPS positioning, a digital acquisition subsystem, improved software, a sounding rate of 168 Hertz (Hz) and a spot sounding density of 10m × 10m. These positioning and data acquisition features combined with ever increasing sounding rates and densities characterise present day Lidar systems. Mortensen (1996b) documented the performance of the first operational LADS system. The system is quoted to be capable of surveying a 240m wide swath, with a maximum depth capability of 50m and resolution of 0.22m. The importance of an airborne surveying system surveying the vast expanses of Australia's coastal waters, particularly environmentally sensitive areas such as the Great Barrier Reef is stressed by Mortensen (1996b). Remote monitoring of difficult to access, often environmentally sensitive, inter-tidal mudflat areas is a useful aspect of both the Lidar and aerial photographic data used in this study. Specifications for the recently developed LADS MK II are detailed in Sinclair (1999). The author emphasises the sounding rate of 900 Hz, selectable sounding densities of between 2m × 2m and 5m × 5m and a depth range of 70m, representing significant improvements over the first LADS system. A high sounding density of 2m × 2m allows the fine detail of channels crossing inter-tidal areas within the Fal estuary to be identified from the Lidar data used in this study. A survey for nautical chart production off the Norwegian coast and a site survey for oil and gas exploration off Western Australia are cited as examples of the first contract surveys carried out by LADS MK II.

Following system trials from 1989 to 1992, Sunberg (1992) debated the concept of developing the Hawk System for helicopter mounting in addition to operation from a fixed wing aircraft, similar to that used with the LADS systems. Helicopter mounting provided the advantages of increased manoeuvrability, higher sounding density and the ability to select sounding patterns and carry out repeats. These advantages, particularly for surveying complex areas such as Swedish coastal waters, were considered to justify additional system development costs incurred in combating problems caused by helicopter vibration. Koppari et al (1994) reviewed the improvements made to the operational Hawk Eye system compared to the trial system FLASH. These improvements included DGPS positioning, an inertial reference

system, increased storage and improved system software. The Hawk Eye system was also more compact and easier to install than FLASH. Factors affecting the depth range and depth measurement accuracies achievable by Hawk Eye are discussed in detail by Steinvall & Koppari (1996). They also identified limitations of Lidar systems at that time and improvements which may be made possible by technical advances in the future. Recently, Axelsson & Alfredsson (1999) gave details of the Hawk Eye II system and compared its capabilities with those of a state-of-the-art, multi-beam echo sounder. Financial constraints currently preclude the majority of small ports such as Truro from the use of a multi-beam echo sounder, however, this may be an issue for the future.

A case study of SHOALS operation in Florida Bay, USA is presented by Parson et al (1997). Irish & Lillycrop (1999) review five years of SHOALS operation. A survey of the Saco River, Maine, New England, is presented as an example of remotely measured bathymetry and topography. In addition to bathymetric applications, SHOALS' capability to survey topographic heights enables its use in assessing breakwaters and in beach and reef damage monitoring. The benefits of such a system compared to LADS, a purely bathymetric measurement system, are discussed by Lillycrop et al (1997).

The majority of systems reviewed by Estep (1993a) use a Nd: YAG laser producing infra-red (IR) radiation, wavelength 1064nm, to measure the aircraft height above the sea surface, and the same laser output, frequency doubled to 532nm wavelength, to measure aircraft-seabed separation. The feature distinguishing the LADS, SHOALS and Hawk Eye systems from those developed in other countries were far higher sounding rates of 168 – 200 Hz in 1993. Laser pulse rate continues to be the major development area for bathymetric Lidar systems. LADS MK II operates with a sounding rate of 900 Hz, allowing it to cover 64 square kilometres per hour, with a sounding density of 5m * 5m (Sinclair, 1999). Hawk Eye II, normally helicopter mounted to give a very high-resolution capability, claims to be close to providing a sounding rate of 1000 Hz (Axelsson & Alfredsson, 1999). The third commercial Lidar system, SHOALS, lags behind its major competitors in terms of performance figures. Instead the system developers have chosen to integrate the Lidar with a Compact Airborne Spectrographic Imager (CASI) to monitor water quality and sea

bed characteristics, which affect the energy and wavelength of Lidar returns (Estep et al, 1994).

Originally it was hoped that data from a hydrographic Lidar system, such as those detailed above, would be available for this project. Unfortunately an operational blue-green laser system, providing water penetrating capabilities, is not available within the United Kingdom (UK) at present. The Lidar data collected using the red laser operated by the Environment Agency UK, provides topographic elevations, but red wavelengths provide little or no penetration into the water column. Despite this limitation, red Lidar collected over inter-tidal areas at low water provides a valuable, high resolution (2m * 2m pixel size) source of data for this study. Related applications of Lidar in oceanographic and land use fields are discussed in the following section.

2.2.2 Lidar used in Oceanography and Vegetation Monitoring

The UK Environment Agency use a purely topographic, Lidar system for detailed mapping of flood plains. The rapid production of high resolution flood plain maps provides a vital input into flood early warning systems and a basis for flood defence projects. Data collected by this system, at low water, provides mud-bank topography and channel position data for this project. Other land-based uses of Lidar include extensive vegetation monitoring programs. The volume of timber in forested areas was estimated using Lidar, by Naisset (1997), whilst Saito et al (1998) used a pulsed laser to identify stresses on vegetation, and in some cases vegetation type. Identification of minerals including quartz, feldspar, garnet, talc, dolomite and amphibole and mixtures of these minerals by airborne, infra-red laser is the subject of work carried out by Mortensen (1996a).

2.2.3 Passive Airborne Sensors

The use of a passive, optical sensor to determine shallow water bathymetry is documented by Estep (1993). The method, which compares the ratios of different up-welling wavelengths, is quoted to provide depth information with variation from

reality of between 0.1m and 1.5m, depending on the reflectance properties of the seabed. George (1997a) refines this technique using a CASI. During tests carried out in Lake Windermere, returns in 15 discrete wavebands between 430 to 870nm were input to multi-band algorithms to produce an estimation of water depth. A good correlation between actual depth and that produced by the algorithms was found for uniform bottom sediments, but variation in sediment type and live or decaying vegetation remain a serious limitation to the measurement of bathymetry by passive, optical sensors. Other applications of CASI include classification of sediment and vegetation types in inter-tidal areas (Thomson et al, 1996) and vegetation mapping on land, for example estimation of crop yield and crop stress in coniferous forests (Gong et al, 1995).

Although the main focus of this study is active laser sensors, the Environment Agency has supplied Compact Airborne Spectrographic Imager (CASI) data of the Truro River, flown at high water in 1995 and low water in 1996. Hence, it was felt that, a brief mention of the increasingly important area of passive airborne remote sensing should be made. Selective examples have been cited specifically for their relevance to remote sensing of estuaries and coastal waters.

The very positive assessment of the benefits of Airborne Thematic Mapper (ATM) for monitoring coastal waters, provided by Malthus et al (1996), is supported by the wide range of documented applications of its use. River channel bathymetry and flood plain sediment distribution in the Tay (River) valley, Scotland, was estimated using ATM (Watson & Gilvear, 1993). Ferrier & Anderson (1997) used the system to study thermal and colour changes across fronts also in the Tay estuary. The results of the ATM work were correlated with mathematical and physical models in an attempt to assess the nature of, and temporal and spatial extent of the fronts. ATM data were correlated with helicopter-borne scatterometer to compare thermal and visible changes with surface roughness patterns across the Rhine frontal plume (Matthews et al, 1997). George (1997b) measured phytoplankton concentrations in lakes and tarns using ATM whilst Garciasoto et al (1996) applied the system to mapping the detail of coccolithophorid blooms. Pollution monitoring is another area in which ATM has produced significant advancements. George and Happey-Wood (1996) used the system to monitor a power station effluent plume into Llyn Peris, Snowdonia, whilst

Rainey et al (1996) and Atkin et al (1996) used ATM combined with CASI to map radionuclide dispersion in estuaries via recording of sediment sizes and loading.

Clearly the use of ATM for determination of river channel bathymetry and flood plain sedimentation would provide a useful input to this study. ATM data covering the Truro River has not been made available to this project, at present. The GIS being developed would, however, allow such data to be included should it became available in the future.

2.3 The Lidar Data

Lidar data collected in 1998, covering the entire Fal estuary, have been obtained from the Environment Agency (EA). The red wavelength Lidar used by the EA provides very little penetration into the water column, thus mud bank heights, but not water depths are obtainable from the data set. Since the Lidar data was flown at low water, coverage of the inter-tidal zone in the Truro River was achieved at very high resolution, using a square pixel size of 2 × 2 metres. From information supplied by the EA, the accuracy of Lidar height information is estimated to be ±0.35 metres with positional accuracy of ±1.7 metres. An example of Lidar data for a section of the Truro River is given in figure 2.1.

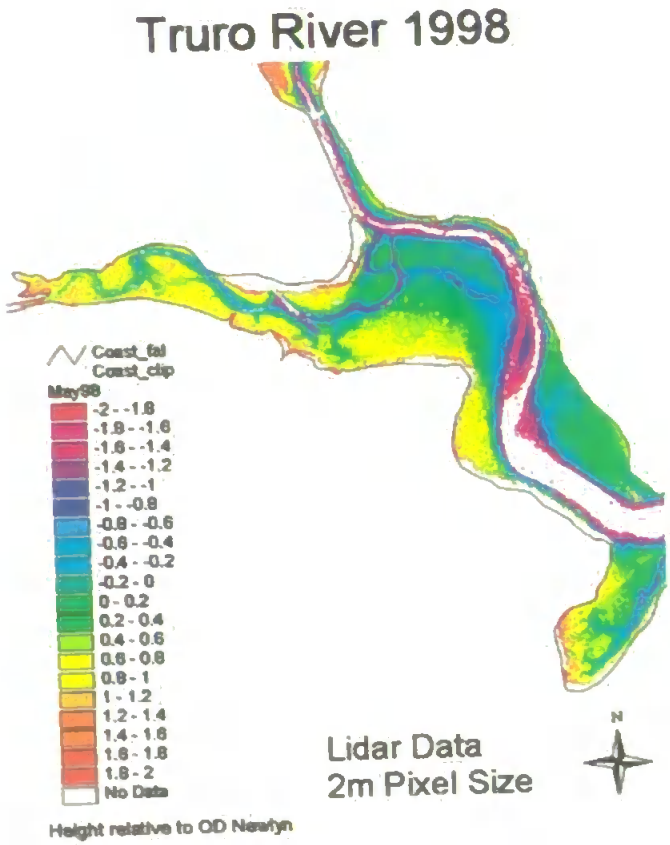

Figure 2.1 – Lidar Data for a Section of the Truro River, 1998

2.4 Data Units and Format

The Lidar data were supplied to the project in digital, Arc/View input format, allowing for straightforward input into the GIS. These data were datum converted from the GPS global reference ellipsoid WGS84 to OSGB36 grid by the Ordnance Survey, before being supplied to this study by the Environment Agency. The Ordnance Survey estimate that the horizontal accuracy of this conversion is within 1-2 metres. The vertical datum used in the collection of the Lidar data was OD Newlyn, so no vertical conversion was required.

2.5 Interpolation

The Lidar data were supplied on a grid of 2 metre, square cells. This high resolution allows the fine structure of channels flowing across mud banks to be identified. However, it has been determined by trial interpolation that the other types of data used in this study (single beam acoustic bathymetry and aerial photography) do not support interpolation to this high resolution. In addition, calculation times for such interpolation are extremely long, taking several tens of minutes on a modern PC. Fortunately the GIS allows the fine resolution of the Lidar data to be maintained, and will perform data comparison with data sets of lower resolution. This is achieved, within the GIS, by automatic selection of the fine grid cells covered by each large cell and calculation of their mean value. These mean values can then be compared with the corresponding value within the coarse grid. If required the GIS supports other 'averaging' processes, such as median values. These could be used to convert the Lidar from a 2 metre to 10 metre grid before comparison with the other data sets.

During the production of navigational charts it is normal to display sounding values demonstrating the worst case scenario, that is the largest drying height or shallowest depth in each selection area. In view of the aim of this study, namely to predict areas of change rather than actual height or depth values, the decision between using average values or worst case values for navigational safety can be seen to be an arbitrary one. Clearly it is essential, however, to maintain a consistent selection method between data sets for comparison purposes. For convenience average values will be used in data selection throughout this study.

Considering the 'smooth' nature of mud banks it would be expected that a grid of 10 metre cell size generated from the 2 metre grid using the mean or median cell value would produce very similar results. Comparison of grids generated by each method shows them to be almost identical. Hence, it is considered appropriate to use the automatic meaning of values, performed within the GIS, during comparison of the Lidar data with other data sets within this study.

Lidar height information is displayed at decimetre resolution using Arc/View legend files constructed to highlight depth bands of particular interest, whilst masking out land heights which are not relevant to this investigation.

Chapter 3 – Aerial Photography

3.1 Review of Literature on Aerial Photography

3.1.1 Aerial Photogrammetry

Aerial photogrammetry is used to produce planimetric and topographic maps from aerial photographs. In order to provide quantitative map information the photographs should ideally be taken vertically or near vertically as stereopairs, that is with an end overlap of between 55 and 65% (Wolf, 1974). Two sets of aerial photographs, for 1988 and 1996, forming stereo-pairs and covering the Truro River at low water have been obtained for use in this project.

In addition to the precision of the photogrammetric instrumentation used, the production of accurate mapping depends upon good quality photo ground control, ground checkpoints and reliable camera calibration information (Chandler, 1999). Ground control points for the Truro River aerial photography were surveyed in using Rapid Static GPS. This system will provide centimetric accuracy in both horizontal directions (x, y) and height (z). Camera calibration certificates for 1988 and 1996 have been supplied by the Natural Environmental Research Council (NRSC) and BKS Surveys, respectively.

Despite the apparently long list of requirements, aerial photography provides a method of mapping often difficult-to-access areas along the land-sea interface. Jimenez et al (1997) made effective use of vertical aerial photography taken at intervals over a four-month period to monitor coastal change along the Ebro delta in Spain.

3.1.2 Digital Photography

Recent developments in digital photogrammetry combined with ever-increasing computational capacities have provided an automated tool capable of generating high density Digital Elevation Models (DEMs). Digital photogrammetry will be used to

obtain topography, from scanned aerial photographs, for direct input into the GIS being developed within this study.

The necessary hardware and software is available at lower cost than previous generations of photogrammetric instrumentation (Chandler, 1999). Light (1999) calculates a dimensionless measure of precision, known as the C-factor, for digital photogrammetric workstations. These digital systems are found to achieve a similar range of precision levels to those exhibited by conventional plotters. C-factors for conventional systems are accepted (referenced in Light, 1999) to range from 900 to 2200, whilst those of digital photogrammetric workstations are found, by Light (1999), to be between 800 and 2200, with state-of-the-art digital and conventional photogrammetric systems giving C-factors of 2200.

In addition to being relatively low cost and of equal precision, a digital approach to aerial photograph interpretation provides:

- Facilities for change detection in time-series images
- Digital, morphological characterisation
- Geo-referencing with other digital data sets

(Matioli et al, 1996).

The advantages of digital systems are taken a stage further by the development of an expert system to aid coastal management (Moore et al, 1998). The system prototype, for the Holderness Coast, eastern England, allows the user to draw on a series of Digital Elevation Models, derived from aerial photography, to address coastal management issues. The system development is ongoing at Plymouth Marine Laboratory, at the time of writing.

Despite the shift to digital aerial photogrammetry, Light (1996) concludes that the use of a film camera and scanner, as in this project, is currently more cost effective than a digital camera for aerial use. However, with larger arrays, refinement of attitude sensors, increasingly widespread GPS co-ordinate readouts and more affordable

storage capacity, Light predicts that digital cameras may represent the future for aerial photography. Mason et al (1997) suggest that digital cameras may be a viable alternative to film for small-format, local area mapping. However, the quoted accuracy of mapping from stereopairs, in the horizontal and vertical, is low. The authors admit that limited format size and slow image download speed currently restrict the use of digital cameras to the mapping of small areas.

3.1.3 Historic Surveys

The increasing demand for historical aerial photography for land use, geological and litigation investigations is highlighted by Shuey (1996). The availability of this type of historic information from local authorities, research institutes and military sources has provided the basis for extensive research into coastal change. Stereo aerial photography is vital to this study in that it provides a unique source of historic, bathymetric data.

Sanderson et al (1998) used aerial photography dating back as far as 1944 to study coastal accretion at Desperate Bay in Western Australia. Analysis of sequential aerial photography and coastal maps within a GIS allowed the authors to identify a period of particularly rapid deposition between 1965 and 1990, the causes of which are the subject of continuing investigation. Long-term deterioration of Louisiana's barrier coastline is documented by McBride & Byrnes (1997). In this case a computer mapping system was used to compile a large number of shoreline transects from aerial photography taken between 1855 and 1959. Digital comparison of data over this long time frame allowed periods of rapid coastal deterioration to be clearly identified.

Historic aerial photography, between 1951 and 1990, is used by Shoshany et al (1996) to support their model of littoral drift along the Israeli coast, demonstrating the potential value of sequential photography in the modelling of long term trends. Miller (1999) provides an example of the study of historic aerial photography to predict future trends. The study of photographs taken between 1935 and 1991 are analysed within a GIS. Trends identified by this analysis are then used to predict changes in vegetation around the Negrito Creek in New Mexico up to the year 2047.

The importance of historic aerial photography is further emphasised by Luman et al (1997). They propose a method for preserving early photographic prints by high quality precision scanning, rather than traditional methods of photograph reproduction.

3.1.4 Combining Aerial Photography with other Data Sets

As mentioned previously, traditional hydrographic surveys, Lidar and aerial photogrammetry will provide the bathymetric data forming the basis of this study.

The combination of data sets raises several issues, including rationalisation of data formats and normalisation to the same co-ordinate system and vertical datum, issues which will be discussed in detail later in this study. Gorman et al (1998) provide an American example of reference frames to be rationalised when combining aerial photography, satellite imagery, profile surveys and hydrographic records.

The potential of combining airborne multi-spectral imagery and aerial photography for mapping channel morphology in shallow gravel-bed rivers is examined by Winterbottom & Gilvear (1997). Aerial photography is combined with high resolution seismic profiling and sediment coring to investigate sediment trapping in the Florida Keys (Shinn et al, 1996). Multiple data sources, including aerial photography, a small scale topographic map, georeferenced satellite imagery and surveyed control points, are used to produce accurate, large scale mapping of areas of Antarctica (Fox, 1995). Jallow et al (1996) used aerial video recording in conjunction with aerial photography, topographic maps and bathymetric charts to investigate the vulnerability of Gambia's coast to sea-level rise.

The volume of recent work using historic aerial photography combined with other types of data within a GIS demonstrates the value of the type of data analysis to be used in this project. Examples such as the work of Miller (1999), discussed in section 4.3, highlight the interest in extending investigation of historic data to provide a means of prediction of future trends.

3.2 The Aerial Photographic Data for the Truro River

Sets of aerial photographs, forming vertical, stereo pairs, at a scale of 1:10,000, were obtained from the National Remote Sensing Centre Ltd (NRSC) and BKS Surveys Ltd, Londonderry, Northern Ireland with the permission of Cornwall County Council (CCC). An example photograph is shown in figure 3.1. Unfortunately colour photocopies of the photographs supplied to the project free of charge, by CCC could not be used to obtain quantitative information because stereo interpretation must assume each photograph to be free from distortion. Photocopying has been shown to produce 10-15% distortion of images.

Figure 3.1 – Reduced aerial photograph of a section of the Truro River, taken in 1996 at an original scale of 1:10000

The two sets of nine photographs obtained were flown at low water and therefore provide inter-tidal zone height information for 1988 and 1996. As with the Lidar data aerial photography does not provide depth information for areas covered by water.

The camera calibration certificates, necessary to resolve the inner orientation of the photographic system for the purposes of stereo interpretation, have also been obtained from NRSC and BKS Surveys Ltd. Ground control for the aerial photography will be surveyed using carrier phase global positioning system (GPS). The carrier phase receivers, manufactured by Trimble and loaned to the project by the University of Plymouth, provided centimetric accuracy in both horizontal position and height on the

WGS84 spheroid. Conversion to the OSGB36 co-ordinate system was performed using the Ordnance Survey Grid-Inquest software (see section 4.2.3). The quoted accuracy of this conversion is to within 10 centimetres in the horizontal and 20 centimetres in the vertical.

3.3 GPS Ground Control

In order to perform co-ordination of sets of aerial photography, by means of triangulation, the digital photogrammetry software requires a minimum of four ground control points within the overlap of each pair of photographs. Clearly the quality of the triangulation solution is increased by the provision of additional, redundant measurements. To provide this redundancy, the project aimed to survey seven ground control points within the overlap of each stereo pair of photographs. This was achieved by careful selection of 36 points over the entire area covered by the two sets of nine photographs (1988 and 1996). Due to the geometry of the system some overlaps actually contained more than the seven points, up to eleven for a central pair of photographs within a set.

3.3.1 Selection of Ground Control Points

Selection of suitable locations for the ground control points required that each point was clearly visible and uniquely identifiable on both photographs of the stereo pair. Ideally the points should be spread evenly over the entire overlap of each pair of photographs to provide the best possible positioning solution. This was not, however, always achievable as point visibility was a problem in wooded areas and built-up areas presented the potential for GPS error resulting from multi-path.

The GPS equipment was provided with back-packs, so vehicular access was not necessarily required to all control point sites, though it was preferable for the majority of points to prevent the survey work becoming disproportionately time consuming. In general, points with public access were selected for convenience. It was, however, necessary to obtain permission to survey points on the Tregothnan Estate, east of the Tresillian River. This estate is very extensive (several square kilometres), thus

rendering it impossible to obtain ground control points spread over all overlaps, without access to estate land.

3.3.2 Choice of Survey Method

The rapid static method of carrier phase GPS survey was selected as most suitable for obtaining the ground control measurements. This survey method requires data to be recorded at each point for between 8 and 20 minutes, depending on the number of satellites visible. The slight loss of accuracy compared to that of static survey (accuracy within a few millimetres for static survey compared to centimetres for rapid static) was more than justified in the time saving as each static point takes over an hour to survey. A kinematic survey method was not appropriate as satellite lock could not be maintained whilst travelling between points in wooded and built up areas. Using rapid static survey all co-ordinates are post-processed from combined base and rover data. A hand held GPS unit was used in the field to provide an approximate location of each point in real time.

3.3.3 Performing the Survey

Rapid static GPS surveying requires a base station to be set up, at an approximately known location, whilst a second, roving GPS unit records at each unknown point in turn.

An Ordnance Survey triangulation pillar was used as the base station for this survey. Permission for access to the site was obtained from the landowner and pillar co-ordinates were, kindly, supplied by Truro Harbour Authority. These co-ordinates were converted from OSGB36 to WGS84, for input into the GPS, using the Grid Inquest software. This conversion software is based on the Ordnance Survey geoid model, thus providing an accuracy of better than 10 centimetres in the horizontal and 20 centimetres in the vertical. The software is now available in the public domain via the Internet (http:\\www.gps.gov.uk/convert.asp).

The triangulation pillar did not represent a secure site; hence someone was required to remain at this location throughout survey operations. It proved desirable to leave a

vehicle at the site to provide shelter for this person, in addition to the estate car needed to transport the roving station to each ground control site. It was also necessary to clear thick vegetation from around the triangulation pillar the first time it was used.

The Trimble base station antenna was set up on the triangulation pillar, by means of an improvised tribrac with the recording unit and power supply, consisting of four 12 volt camcorder batteries, housed in a weather proof box at the base of the pillar. The station parameters, including antenna height measured from the Ordnance Survey Bench Mark (OSBM) on the pillar, was set-up using the Trimble Survey Controller (TSC1). It was necessary to return to the base station every four hours in order to reinitialise the base unit using the TSC1 after changing the batteries. Providing a longer running period by powering the base from a car battery (with specially constructed cable) was considered, but practically it was found necessary to swap the person guarding the base station every four hours due to boredom.

The ground control stations were surveyed in a planned order, to minimise travelling time, as the survey area of nearly 20 square kilometres was largely accessed by narrow country roads. Satellite visibility and elevation plots (see examples in appendix 1) were generated for each survey period using Trimble survey planning software, available via the Internet (http:\\www.trimble.com/cgi/satview.cgi). These plots showed a minimum of four satellites to be in view at all times. The satellite availability information provided by the plots was then used to predict the likely time required for data logging at each point and checking the site.

Having located a ground control point using Ordnance Survey 1:2500 map sheets, the exact survey point was checked against the aerial photographs to ensure visibility. The rover antenna was set-up on a tripod and point details stored along with the logged data in the TSC1. Data were logged for the time specified by the GPS system, dependent on number of satellites visible, during the which time station description sheets, including sketch maps (see appendix 2), were produced to aid identification of each point on the aerial photographs during the photogrammetry process. A photograph of each station was taken and its approximate position obtained using a

handheld, stand alone GPS unit. The photograph number and GPS position obtained by the stand-alone GPS were noted with the station description for checking purposes.

Having initially located and cleared the base station site the ground control survey over this rural area could be carried out at a rate of nine survey points per day. Due to time taken for initial base mobilisation, obtaining access to the Tregothnan Estate and surveying of final check points, the 36-point survey campaign took five full days in the field.

The rapid static GPS data was downloaded from the base receiver and TSC1 into Trimble Survey Office software for processing. All data was maintained in the WGS84 reference framework throughout processing to avoid loss of data accuracy. Datum conversion from the WGS84 ellipsoid to OSGB36 on Airy's spheroid was performed only on the final point positions, using the high accuracy GridInquest software (see above).

A gross error check was carried out on all ground control co-ordinates by comparison with Ordnance Survey 1:2,500 sheets and no problems were found. Unfortunately the known point to be used for a final check on the system turned out to be a flagpole mounted several storeys up on the side of Falmouth Harbour Office building. Alternative points had been derived from this using Differential GPS (DGPS) and thus represented a lower accuracy than the carrier phase survey. These points were found to correlate with the rapid static measurements to within 3 metres, a result consistent with the accepted accuracy of DGPS of between 2 and 5 metres.

3.4 Digital Photogrammetry

3.4.1 Method

The optimum scanning resolution for aerial photography is 800 dpi, since higher resolutions merely perform interpolation between the inherent pixel size of the photographs. Hence the image is apparently enhanced, but no additional information is obtained. The vertical, stereo-paired aerial photographic prints were scanned into a

PC using a high-resolution scanner capable of scanning to a resolution of 1200 dpi. The resolution used was, however, limited to 300dpi by the available data storage capacity and processing power of available PCs and workstations. Aerial photographs scanned at a resolution of 300 dpi produce a file size of 25 MB compared to 95 MB for 400 dpi and 250 MB for 800 dpi. DEM production took 30 minutes using a stereo pair of photographs scanned at 300 dpi, compared to more than 3 days for photographs scanned at 400 dpi (Simpson, 2000). At the photograph scale of 1:10,000 the 300 dpi resolution corresponds to slightly more than one scanned dot per metre, representing an order of magnitude better resolution than the 10 metre cell size required for comparison with other data sets.

Photogrammetry was performed using the Orthomax module of Erdas Imagine. Initially a block was created, using the Orthomax 'Block Tool', for each data set (1988 and 1996). All data relating to this block is then assigned to it, as follows:

1. The camera calibration information, including focal length, fiducial co-ordinates and radial distortions, was added for each camera used.
2. The scanned aerial photographs were input as *.tif files, with the correct balance of coloured layers (red, green and blue); these are referred to within the software as frames. The camera corresponding to each frame was selected where more than one camera was used within a set of photographs.
3. The co-ordinates of ground points were input, from file, in the comma-separated form: 'id number, easting, northing, height'.
4. Using the 'Activities' menu the fiducial marks were pinpointed in each frame. Fiducial marks are then automatically related to the fiducial co-ordinates specified previously.
5. Each ground control point was then identified on each frame in which it appears. Up to three frames may be displayed at a time to aid consistent location of points. Measurements are taken, within the software, to relate all occurrences of a given point to each other and to the relevant co-ordinate system, in this case OSGB36.

A triangulation solution was then performed for the whole block, a set of nine frames, using a convergence value of 0.1 metre and a specified maximum of 10 iterations. A

summary of the triangulation results for 1988 and 1996 is given in section 3.4.2 and the detailed, statistical results form appendix 3.

A Digital Elevation Model (DEM) for the overlap of each pair of photographs could then be created from the triangulated solution of the block. A 10 metre cell size was selected for the DEMs to correspond to the 10 metre cell size used to display the other types of data within the GIS. Only areas of the overlap containing the inter-tidal zone were chosen to minimise DEM compilation time. The DEMs were exported from Imagine in Arc/Info Grid format for input into the project GIS.

Orthorectified photographs were also produced in Imagine. These were input into the GIS as Imagine images, i.e. *.img format, in order to maintain the true colour of the original photographs.

3.4.2 Results of Photogrammetry

The triangulation of the 1996 data took only 4 out of the 10 allowable iterations and produced a Standard Deviation of Unit Weight of 2.60. The 1988 data took 5 iterations producing a Standard Deviation of Unit Weight of 0.67 (see appendix 3 for the full results of the triangulation process). The Standard Deviation of Unit Weight provides a measure of the conformance of the adjustment to its estimated parameters and parameter precessions. Ideally it should have a value close to unity; values in the range 0.5 to 2 are acceptable (IMAGINE Orthomax User's Guide, 1995). Hence, the 1988 value is considered to be acceptable, whilst the 1996 value is slightly higher than is ideally required.

Orthorectification of each aerial photograph produces a co-ordinated image tying closely other images from the set and data from other sources. The positioning of photographs within a set was found to tie together with discrepancies of not more than one pixel size, i.e. less than 1 metre in all areas except those hidden by shadows. Comparison with other data sets, within the GIS, also produced good correlation. For example, coastlines identified from the orthorectified photographs correspond to a coastline digitised from the large scale Admiralty Chart, to within the levels of accuracy expected from photogrammetric positioning, exhibiting positioning

discrepancies of between 1 and 6 metres. The larger differences (4 to 6 metres) occur in areas of wooded coastline where tree shadowing makes the coast difficult to identify from the photographs.

Comparison of elevation data, in the form of DEMs, even within a set of photographic data (i.e. from photographs taken at 20 second intervals), revealed height differences of between 3 and 6 metres. These differences occurred over the entire DEM, precluding the theory that reflection of light by surface water on inter-tidal mudflats might be the cause of such large discrepancies. Calculation of grids showing the difference between DEMs, within the GIS, showed the identified differences to be distributed randomly throughout the photograph overlap area, even having trimmed the edges to remove obvious large anomalies resulting from edge effects.

In an attempt to reduce the large and apparently random errors ten additional tie points, identified on each of a pair of photographs but without co-ordinates, were added to each overlap, and the data retriangulated. The addition of tie points to the 1996 data improved the Standard Deviation of Unit Weight of the triangulation process to 1.89, i.e. significantly closer to unity. Unfortunately, however, no corresponding reduction in the discrepancies between overlapping DEMs was observed. Thus it must be concluded that **standard, vertical aerial photography provides insufficient vertical accuracy to allow the study of inter-tidal zones,** whose total vertical extent will often be less than the maximum error exhibited by the DEMs.

This conclusion is supported by information obtained from the photogrammetry software providers, Erdas, and major providers and users of this type of aerial photography the National Remote Sensing Centre Limited (NRSC). Other studies undertaken at the University of Plymouth have also been restricted by inaccuracies identified in DEMs, derived digitally from vertical, stereo aerial photography, using the Orthomax module of Erdas Imagine. DEMs produced by Richards (1997) exhibited peaks of several metres on the beach and cliffs, as well as positioning problems of 80 to 90 metres. Richards attributes these anomalous peaks in elevation to reflectance produced by surface water on the beach. Duclos (1998) also fails to achieve reliable quantitative results from digital photogrammetry, blaming

inaccuracies in ground control by DGPS (quoted error ± 2.5 metre) and problems with scanning accuracy. Clearly the use of carrier phase GPS in this study, producing ground control point to decimetre accuracy, renders the former reason irrelevant. Whilst scanning problems may be a contributing factor, the high quality, flat-bed scanner used in this study is not considered to be the dominant factor in producing elevation accuracies at best 3-6 metres.

At this point it became necessary to undergo further research into sources of error and inaccuracy in heighting from stereo aerial photography. Using an idealised equation for height accuracy (Kilford, 1979) the expected accuracy from the photography of the Fal estuary was calculated to be 0.18 metre. However, this idealised equation does not account for the very significant effects of aircraft tilt and variations in plane height on the accuracy of photogrammetry. An example, given by Wolf (1974), showed a height accuracy, from manual photogrammetry, of ± 9.7 feet, equivalent to ± 2.96 metres, associated with an aircraft height above ground of approximately 650 metres. As documented in section 3.1, Light (1999) determined that digital photogrammetric systems exhibit similar levels of accuracy to conventional plotters. Thus, for the greater aircraft-ground spacing, of around 1600 metres, within the Fal estuary scheme an accuracy of heighting worse than ± 2.96 metres would be expected. Hence, the height variations of between 3 and 6 metres exhibited in Digital Elevation Models derived from the aerial photography used in this study appear to be consistent with other findings.

As a final check a pair of aerial photographs from the Fal estuary were sent away for processing by a company specialising in photogrametry, Harvey Map Services, Doune, Scotland. Comparison of their results with those obtained in this study revealed discrepancies in elevation of 3-5 metres or more. A result that further strengthens the conclusion that **the accuracy of heighting obtained from 1:10,000 stereo, aerial photography,** such as that commissioned by Cornwall County Council covering the Fal estuary, **is insufficient for the study of heights within the intertidal zone.**

Chapter 4 – Acoustic Bathymetry

Acoustic bathymetry collected by the Harbour Master's Department has, to-date, provided the only basis for monitoring siltation and assessing survey requirements within the Truro River. Such data are limited, by financial constraints and equipment availability, to relatively infrequent surveys, with often more than 10 years between them, gathered using a single beam echo sounder. This project aims to accumulate such data, in conjunction with data from other types of survey and supporting historic information to provide a fuller picture of changes within this part of the Fal estuary. Data have been accumulated for the Truro River from 1960 to the present.

4.1 The Data

Depths and drying heights are provided by a number of boat-based acoustic surveys. The United Kingdom Hydrographic Office (UKHO) provided the source of earlier data of this type. The 1961 survey supplied by the UKHO provides coverage of the upper part of the Truro River at a scale of 1:2,500. Complete coverage is provided by a survey undertaken in 1974 to a smaller scale of 1:7,500. It was decided that survey data collected, by the Admiralty, prior to 1961 could not provide a valuable input to this study largely due to positioning problems. Investigation of positioning of permanent features, such as walled stretches of river bank and jetties, revealed positioning errors of several tens of metres, well outside the allowable tolerances in a study using a ten metre cell size to facilitate data comparison.

Truro Harbour Authority has supplied more recent acoustic bathymetry, also collected using a single beam echo sounder. Coverage, at a scale of 1:2,500, of the entire Truro River is provided during the 1990s, comprising three surveys carried out in 1991, 1995 and 1996.

Data obtained using the single beam sounder is collected along survey lines at time intervals of 0.1 second, corresponding to a data spacing of 0.3 m, for a vessel speed of 3 m/s. Clearly this high density of depth information can not practically be displayed

on a chart. Density of soundings on the chart is scale-dependent, with a typical sounding spacing of 12 metres at the scale of 1:2,500. Survey line spacing is variable due to the curved course followed by the Truro River; the average spacing is approximately 40 metres at the same scale. An example of the positions of soundings within single beam bathymetric data is given in figure 4.1.

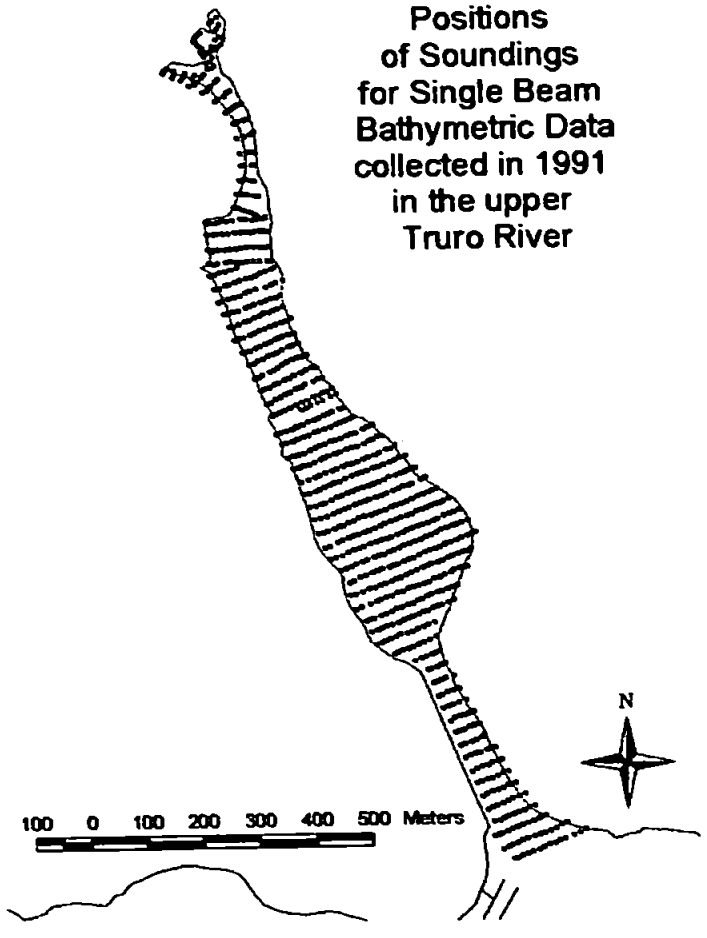

Figure 4.1 – Positions of soundings within single beam bathymetric data collected in 1991, in the upper Truro River.

The positional accuracy of depth information is estimated to be ±3 metres for 1961 and 1974 data and ±2.5 metres for surveys undertaken in the 1990s. Depth accuracy, excluding the effects of position, but including tidal correction is expected to be ±0.3 metres (Reference Admiralty publications).

4.2 Data Units and Format

As the bathymetric data were available only in paper chart form the first stage of preparing these data, for analysis within the GIS, was data digitisation. All charts were hand drawn by different cartographers and therefore not suitable for input to the computer system by means of scanning and character recognition techniques. Hence, the time intensive process of hand digitising the charts had to be undertaken. An A0 digitising table linked to a PC running Arc/Info, provided at the Natural Environment Research Council (NERC) laboratory, situated within the University of Plymouth was used in this process.

The next stage of the data preparation process was to convert the bathymetric data to a common unit system and reference framework. This process was carried out within the Arc/Info based GIS. Initially depth and height data from the early surveys were converted from feet into metres.

It was decided to resolve all positions to the Ordnance Survey (OS) grid, OSGB36, because this system is widely used and well understood within the British scientific community. In addition, the choice of grid co-ordinates rather than latitude and longitude, simplify geometric issues associated with interpolation of spatial data, during later stages of the project. The limitations imposed on OSGB36 by internal inconsistencies within the system (Ashkenazi et al, 1972 & 1980) were not considered to represent a major problem over the size of the survey area covered by the Truro River, an area of approximately 4 by 5 kilometres.

All the acoustic bathymetry to be used in the project was already referenced to OSGB36, so datum conversion was not required here. However, the other data sets to be included within the project made issues of datum conversion inevitable. The choice of OSGB36 resulted in a requirement for conversion from the GPS reference ellipsoid, WGS84, to OSGB36 for Lidar data and aerial photographic ground control.

It was decided to relate all depth and height information to Ordnance Datum (OD) Newlyn. This datum provides a single, continuous vertical reference level coincident

with an equipotential gravity surface and approximating a horizontal plane, throughout the area of interest, unlike the more obvious choice of local chart datum. Chart datum forms a series of six steps along the Truro River, between the north end of Carrick Roads and Truro. These steps form an approximation to the rise of river bed level in this area. Hence, a stepped conversion was required for conversion of some data supplied by the Admiralty. Older bathymetric information, from the Admiralty Hydrographic Office, required conversion from OD Liverpool to OD Newlyn, a constant correction calculated to be 0.15 metres (see appendix 4). Charts produced by Truro Harbour Authority, during the 1990s, were converted from Chart Datum at Falmouth to OD Newlyn, a 2.91 metre constant correction.

Depth data is to be displayed within the GIS at decimetre resolution, using Arc/View legend files constructed to ensure that depth bands of particular interest are clearly differentiable.

4.3 Review of Digital Elevation Modelling

The term digital elevation model (DEM) refers to *any digital representation of the continuous variation of relief over space* (Burrough, 1986). This review section considers, in particular, various methods of interpolation of spatial data to produce DEMs. These methods are of particular significance to the project as the interpolation of the single beam echo sounding data, described in section 4.1 and 4.2, is required to produce continuous representations of the estuary bed, for comparison with other data sets.

4.3.1 Interpolation of Data to Produce DEMs

The various interpolation methods used to model data over a continuous surface follow one of two main approaches, based either

1. on a regular grid of height data, or
2. on a triangular network of irregular size, shape and orientation.

(Petrie & Kennie, 1990).

Regular grid methods support efficient data storage; ease of comparison with other data sets and straightforward calculation of surface parameters, such as gradient and attitude of slopes. Irregular triangular networks (TINs), however, provide flexibility in dealing with data containing terrain features of various scales. Kidner et al (2000) detail the production of a Multiscale Implicit TIN to provide storage and access to terrain data which is retrieved and triangulated, by Delaunay triangulation, according to the feature content and level of detail specified by the user.

Regular grid systems support a number of interpolation methods. The methods most commonly available via conventional DEM and GIS software appear to be Inverse Distance Weighting and Kriging. Inverse Distance Weighting (IDW) determines the height/depth at a given point as the distance weighted average of all data values within a specified search area around the point. Kriging uses a predefined autocorrelation function related to the local data, the point to be interpolated and regional trends in the surface by means of a matrix equation system. This system of equations is solved to calculated coefficients used in the interpolation and producing an estimate of error (Petrie & Kennie, 1990).

Triangulation-based terrain modelling produces a unique set of triangles that are as equilateral as possible and of minimum side length (McCullagh, 1983). The two main algorithms used to implement these requirements are the Delaunay triangulation and radial sweep methods (Petrie & Kennie, 1990).

Delaunay triangulation (see figure 4.2) is performed by initially defining a set of boundary points defining the perimeter of the data set area. Triangulation begins at a pair of these boundary points, known as the initial known neighbours. An expanding circular search, beginning with a circle of diameter joining the initial known neighbours, is then used to identify data points close to these two points. All data points found within the circle are tested against a set of criteria to find the nearest

Theissen neighbour. This new neighbour is used to continue the search, until the entire domain has been covered by triangles.

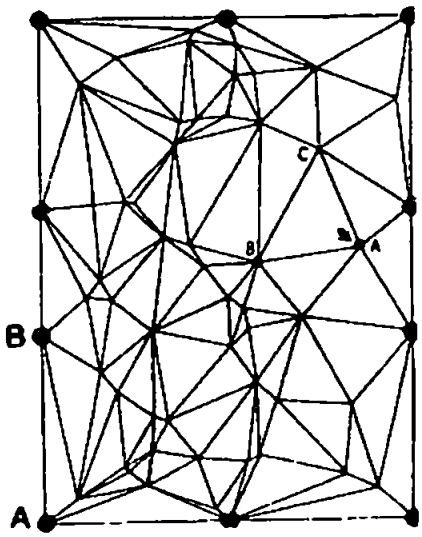

Figure 4.2 – Delaunay triangulation. Triangulated surface and boundary points, from Petrie and Kennie, 1990.

The radial sweep method initially identifies the point closest to the centroid of the data. The distance and bearing of all other data points from the central point are calculated, and the points are arranged in order of bearing. Radiating lines joining all points to the central one produce a set of long thin triangles. After this initial sweep each point is compared with the next two points in the list to determine whether an inside triangle can be formed. The triangulation produced is then optimised by forming quadrilaterals from each pair of triangles. The distances between opposite corners of this quadrilateral are compared, if the distance between the two common points is greater than that between the two unique nodes then the triangle indices are switched. This process is repeated until successive checks of the data-base produce no further changes.

4.3.2 Applications of DEMs

As previously mentioned, the DEMs produced by interpolation of the bathymetric data were required to allow comparison between data sets. Diverse data sets collected over several decades could then provide the basis for analysis of long term trends. DEMs,

produced by various interpolation methods, are also important for many other applications. For example, Dobosiewicz (2001) uses DEMs in conjunction with a GIS for prediction of flooding in the coastal zone along the Shoreline of Raritan Bay, New Jersey. Dobosiewicz successfully uses DEMs in conjunction with tidal data and road details to determine zones 1% probability of flooding, so called 100-year flood, zones.

A method for automatic extract of channel networks from DEMs, obtained from remotely sensed data, is described by Sagar et al (2000). Kenward et al (2000) also consider the use of DEMs as a basis for hydrological modelling and prediction of runoff volumes. Tests using three different DEMs of varying accuracy show variations in predicted mean annual runoff of 0.3% and 7% for the different DEMs, with larger differences predicted peaks and base flow levels.

4.4 Methods of Interpolation

To allow inter-comparison of the data, spatial and depth resolution required rationalisation between the various data sets. A 10 metre cell size was chosen as the most suitable resolution in both horizontal directions. This choice of optimum resolution represents a compromise between requirements for a sufficiently high resolution to allow comparison of fine detail within the channel bed structure and the limitations imposed by the single beam sounding data with average resolutions of 11 metres along line and 40 metres between lines. Averaging of the high resolution, Lidar data to this cell size unfortunately resulted in the loss of interesting detail during data comparison, but presented no technical difficulties within the GIS. Interpolation of the lower resolution single beam echo sounder data to the 10 metre cell size was, however, far less straightforward.

Initially a triangular irregular network (TIN) model was used to interpolate point depths on to the 10 metre grid. This method creates a network of triangles joining each point to all its near neighbours; point values are maintained and intermediate values are interpolated along each side of each triangle. The method applies the condition that all triangles are as close to equilateral as possible. Within this study, the

interpolation was constrained by the use of coastline information. This information was digitised as a polygon coverage, from an Admiralty chart of the largest scale available. The resulting boundary coverage prevented artificial water depths from being interpolated for areas of land effectively contained on three sides by curves in the river. Initial data comparisons showed greatly increased variation in cell values for cells immediately adjacent to the coastline compared to more central cells. Variations of up to 0.3 metre for edge cells compared to <0.05 metre for central cells are observed. These results are unsurprising in that fewer data are available for interpolation of edge cells than central ones, but must be taken into consideration when assessing the results of the model later in this study.

In addition, interpolation of the linearly inhomogeneous, single beam echo sounder data by the TIN technique produced features identified as 'artificial interpolation artefacts'. These features appeared as shoal 'ridges' across the centre line of the deep water channel, between lines of depth data (figure 4.3). Interpolation between shoal depths on either side of the channel was identified as the cause of such artefacts, see figure 4.4.

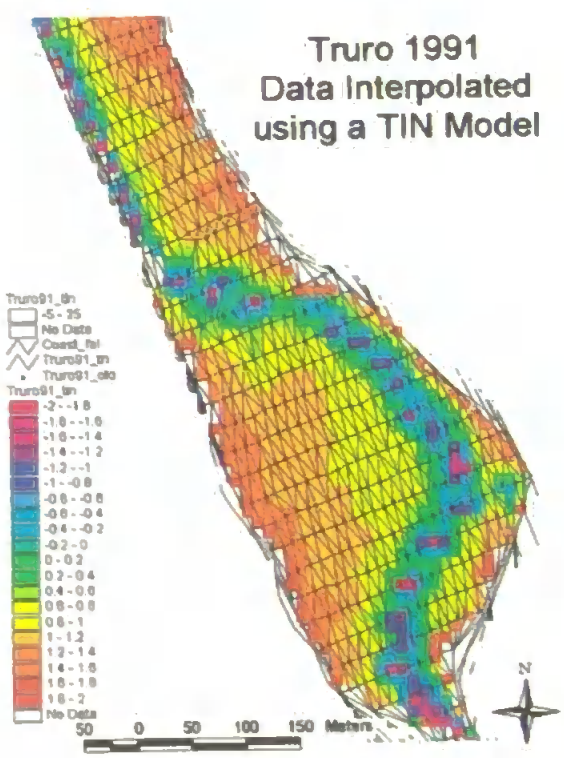

Figure 4.3 – Truro 1991 data interpolated onto a 10 metre grid using TIN.

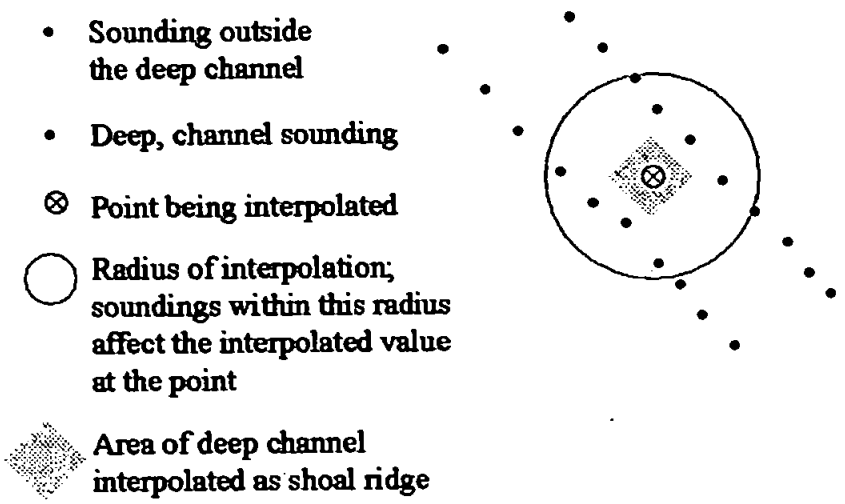

Figure 4.4 – Shoal 'ridges' across the deep channel caused by the interpolation process.

Further investigation, using a 1 metre cell size, revealed the interpolation artefacts to be most pronounced where the direction of the sounding lines is not perpendicular the channel. Due to the differing density of soundings along, compared to across, the sounding line direction, the TIN model produces interpolation triangles elongated in the cross line direction. Consequently interpolation becomes increasingly poor as the angle between sounding lines and the channel decreases from 90°.

A number of techniques were identified as possible methods of eliminating this interpolation problem. Manual interpolation and the addition of data points along the centre line of the channel was attempted before re-running the TIN. This method proved successful in greatly reducing, but not eliminating, the interpolation artefacts. Some artefacts of smaller horizontal extent and lesser depth differential were still generated by the TIN model after this process had been undertaken (figure 4.5). These

artefacts were particularly apparent for non-perpendicular sounding lines to channel, for the reasons described above.

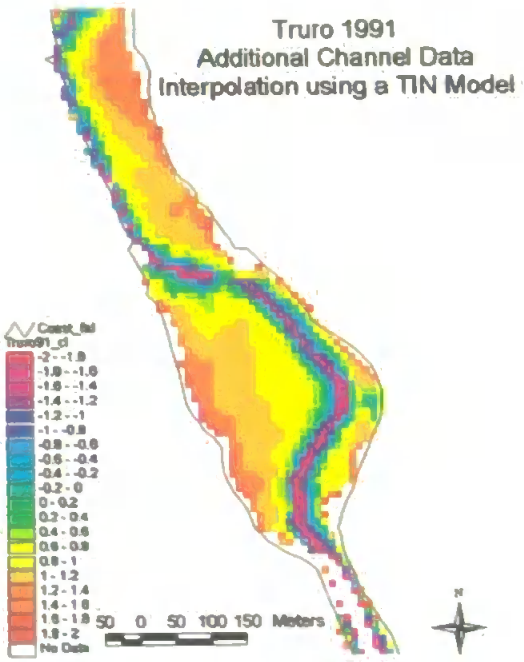

Figure 4.5 – Truro 1991 data, with additional channel data, interpolated onto a 10 metre grid using TIN.

The use of Inverse Distance Weighting (IDW) as an interpolation technique was also investigated. This method weights surrounding depth values according to their distance from each point where an interpolated depth value is required. A number of interpolation radii were tested during the investigation of the IDW technique. For the echo sounder data of 40 metre line spacing a 50 metre radius appeared to produce the most realistic interpolation. Interpolation radii of less than 50 metres produced very prominent linear 'artefacts' across the channel, whilst larger radii tended to generate an unrealistic 'speckled' effect. Clearly channel bed contours consisting of small spikes and hollows are not realistic for sediment consisting of fine mud particles. An example of sounding data interpolated using the IDW method is given in figure 4.6.

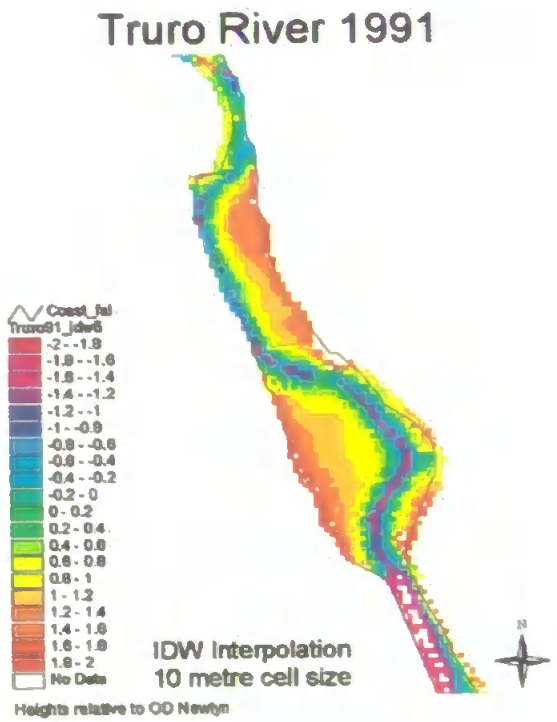

Figure 4.6 – Truro 1991 data interpolated on to a 10 metre grid using IDW.

Finally the statistical interpolation technique of Kriging was applied to the bathymetric data. Investigation of the most suitable type of interpolation model and interpolation radius required was carried out through the study of semi-variograms and contoured variance models produced within the GIS. A Gaussian interpolation model with a radius slightly larger than the maximum line spacing of the point data (a 50 metre radius for 40 metre line spacing) was applied to the sounding data containing additional soundings interpolated along the centre line of the channel. The results of this interpolation exhibited an apparent minimum of interpolation artefacts. Results produced by this method also generate the smooth channel bed profile, without any sudden 'jumps', one would expect for the fine sediment type. Examples of sounding data interpolated using the Kriging by the Gaussian model is given in figure 4.7. It is worth noting that interpolation by Kriging is relatively slow and computer intensive compared to the other interpolation methods mentioned above. When tested on the Truro 1991 data set, interpolation by Kriging was found to be more than twenty times slower than interpolation by standard IDW or using a TIN model and over five times slower than using full ZIDW interpolation.

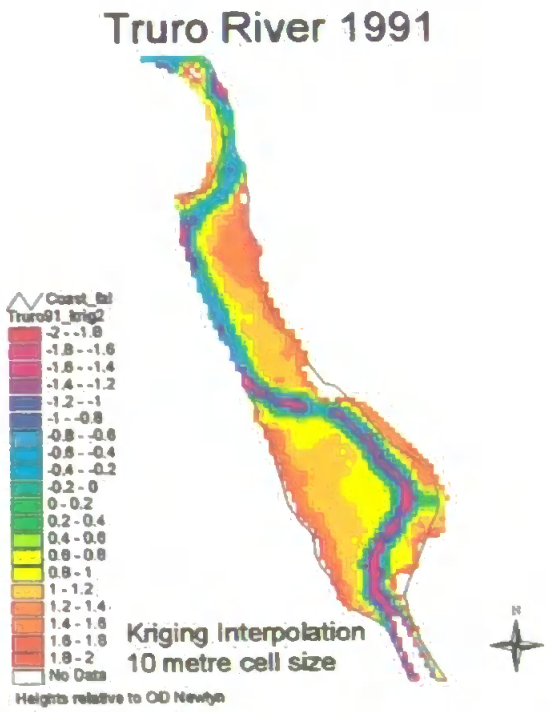

Figure 4.7 – Truro 1991 data interpolated onto a 10 metre grid using Gaussian Model Kriging.

Although it was possible to reduce the scale of interpolation artefacts (generated by interpolation between soundings across the centre line of the deep channel) by means of manual addition of soundings along this line, these artefacts remained for all three interpolation methods (TIN, IDW and Kriging). Hence, it was decided to devise an interpolation method which splits the estuary into a number of polygons, with the centre line of the channel forming an important polygon boundary. This method, entitled Zoned Inverse Distance Weighting (ZIDW), is described in Chapter 5.

Chapter 5 - Zoned Inverse Distance Weighting (ZIDW)

As part of this study, a method has been developed to overcome the limitations of standard interpolation procedures for estuaries consisting of a narrow, deep channel crossing extensive mud flats. This method, referred to as Zoned Inverse Distance Weighting (ZIDW), recognises and accounts for the deep channel during interpolation and was described in chapter 4 and Burroughes et al (2001a). The development of a suite of programs to automate the ZIDW process is documented in this chapter and Burroughes et. al. (2001b). Published works resulting from this project, to date, are included in appendix 5.

Within the program each sounding in the data set was assigned to one of a number of zones or polygons, bounded by the coastline, main channel and any subsidiary channels. Initially the ZIDW process is described for the 1991 data set, a relatively straight-forward case exhibiting a single main channel only. Anomalies arising when the program suite was applied to more complex data sets, such as those collected in the Fal estuary in 1974 and 1995, are described in section 5.3.

5.1 Developing Manual ZIDW

The general trend of the river channel in the Fal estuary is north south. Hence, polygonal zones were assigned to the area, as follows:

1. W = west of the channel bed
2. C = in the channel bed
3. E = east of the channel bed

Each point in the local, rectangular grid on to which points are to be interpolated were similarly assigned to one of the three zones W, C or E. The allocation of zones to the sounding data is illustrated in Figure 5.1.

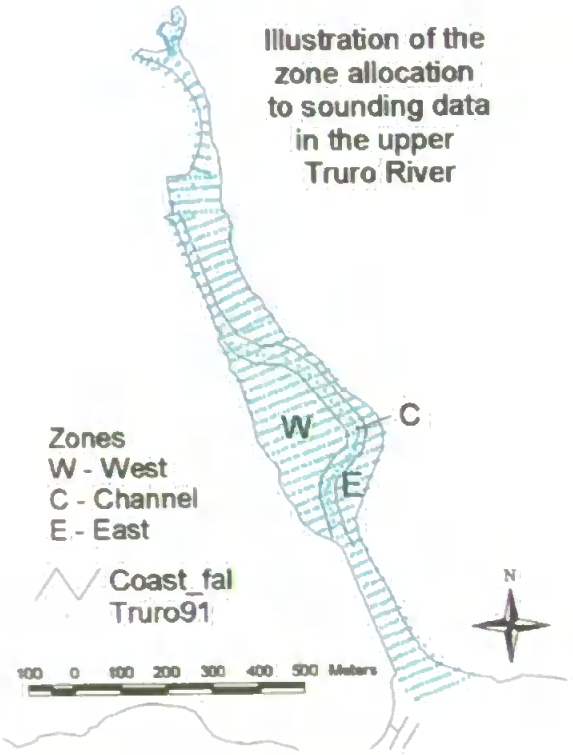

Figure 5.1 – Allocation of the three zones to bathymetric data in part of the Upper Truro River.

Initially, these zones have been assigned by manually editing soundings and grid cells within the data files. Clearly for large and/or multiple data sets it was desirable to devise a method of automating this process (see section 5.2).

Interpolation was performed by the method of inverse distance weighting (IDW), with an interpolation radius of 50 m, but taking the zones into account, thus:

Zone of Specified Point	**Zone of Sounding**
West	West or Channel
Channel	Channel
East	Channel or East

The success of zoning the channel and mud bank areas in the interpolation process is clearly shown in Figure 5.2. It can be seen from the figure, that allowing for the channel, by zone allocation, removes artificially interpolated ridges across the channel produced by interpolation without zoning (as illustrated in Figure 5.2).

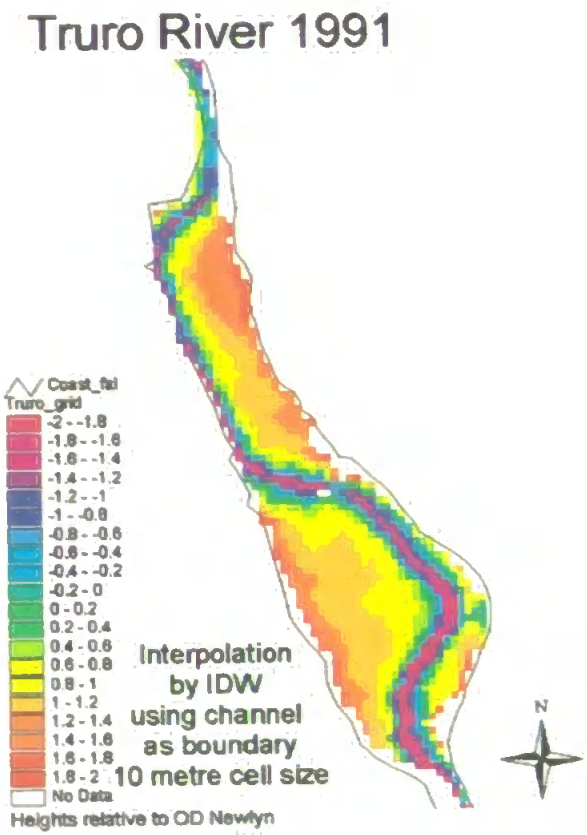

Figure 5.2 – Interpolation of bathymetric data using Zoned Inverse Distance Weighting to allow for the channel.

5.2 Automating the ZIDW Process

To facilitate allocation of soundings and interpolated data points a rectangular domain covering the entire survey area was defined. This rectangle had dimensions 4 km by 5 km for the Truro River study, thus enclosing the areas covered by various surveys carried out over the 40 year study period. The domain contained within this rectangle was then covered by a fine mesh of 1 metre cells. This cell size was chosen on the basis of a compromise between a sufficiently high resolution to maintain data accuracy for any sounding and output resolutions to be dealt with in the Truro River study, whilst maintaining manageable file sizes.

The stages required to produce ZIDW with automated zone allocation are shown in Figure 5.3.

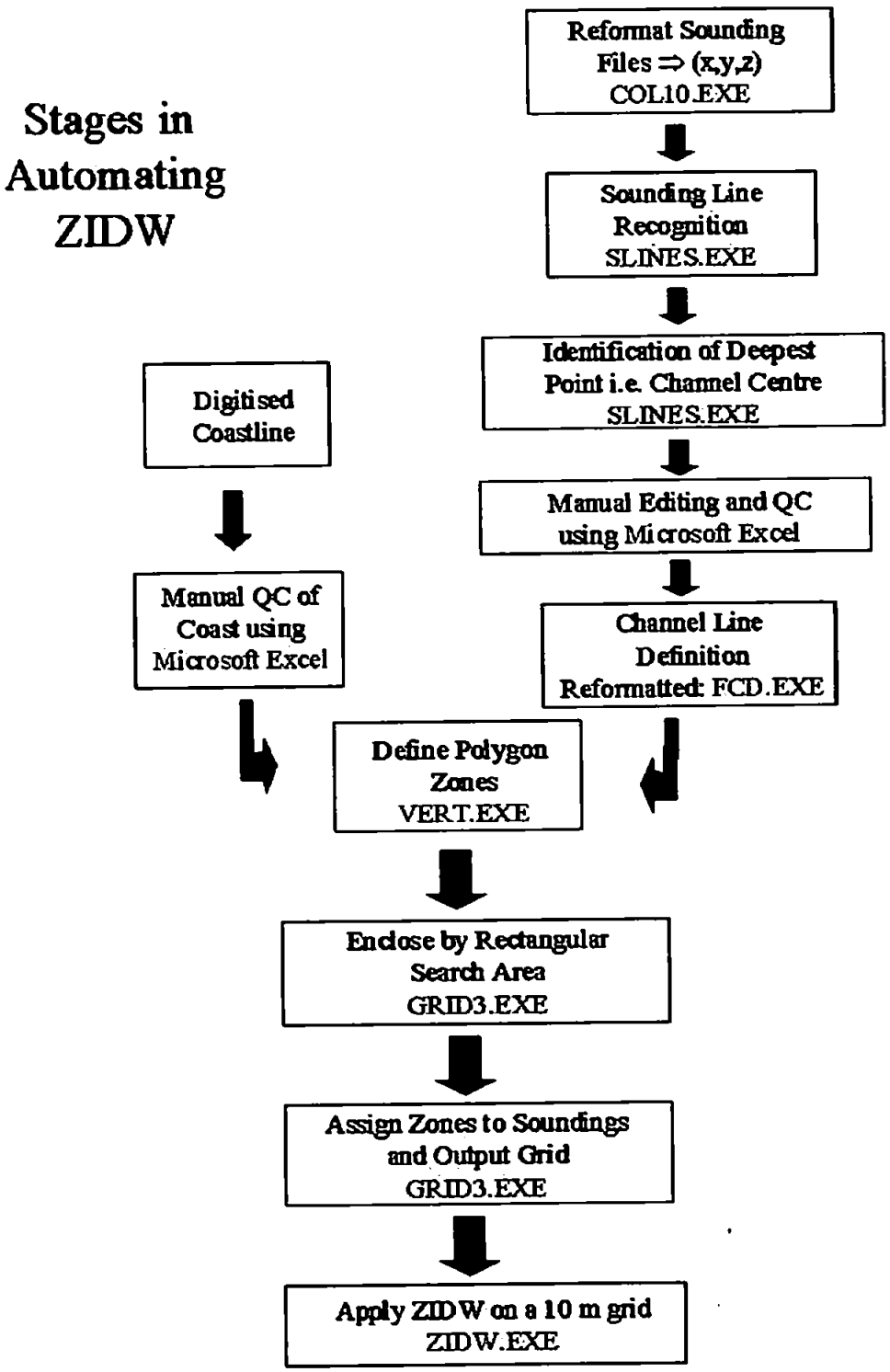

Figure 5.3 – Flow Diagram illustrating the processes involved in producing automated ZIDW software. The program used to apply each process appears in blue. QC = Quality Control.

The first stage of the automation process was to define the centre line of the deep channel (right branch of the flow diagram, Figure 5.3). Initially the separate position (x, y) and depth (z) files produced by digitising depth data within Arc/Info were combined into a single file of co-ordinates and depth (x, y, z), using the COL10.EXE program. The output (x, y, z) file could then be input into the ZIDW software suite.

To maintain consistency all file names consist of a three-character code for the data set, of the form 'Txx', where 'T' denotes data from the Truro river and 'xx' is the two figure year in which the data was collected. This three-character code is followed by the abbreviation for the file type, separated by a dash. For example, the (x, y, z) file for the Truro 1991 data set is named 'T91-xyz'. The format of each file used within the final ZIDW program suite is given in appendix 7.

As the depth within the deep channel is unlikely to remain constant (in the case of the Truro River the channel shoals moving landward) an overall depth threshold can't be used to identify the line of deep soundings delineating this channel. Instead advantage was taken of the requirement for survey lines of single beam echo sounding data to be run at a high angle (near perpendicular) to depth contours, and hence to the channel. Consequently the deepest sounding on each line will represent the point of intersection of the deep channel with that line. Identification of this intersection point on all sounding lines will thus produce a series of points through which the channel line may be drawn.

To apply this process it was first necessary for the next program in the ZIDW suite (SLINES.EXE) to recognise sounding lines within the (x, y, z) data file. Here it was possible to have recourse to the order by which linearly distributed data are most straightforwardly digitised, i.e. across the river along the first line then returning in the opposite direction via the next (see figure 5.4). The SLINES.EXE program considered the direction between consecutive pairs of soundings to determine whether they lie on the same line. An inter-sounding direction of less then 60° implies that the pair of soundings lie on the same line, whilst a directional change of greater than 60° identifies a line change. Hence, a column containing line numbers can be added to the (x, y, z) data file.

This method would also operate successfully for sounding data digitised line by line in the same direction. Digitally logged data will normally contain line numbers, and thus allow this stage of the automated ZIDW process to be by-passed. However, the line identification method within ZIDW would deal with data logged consecutively along vessel survey lines if required.

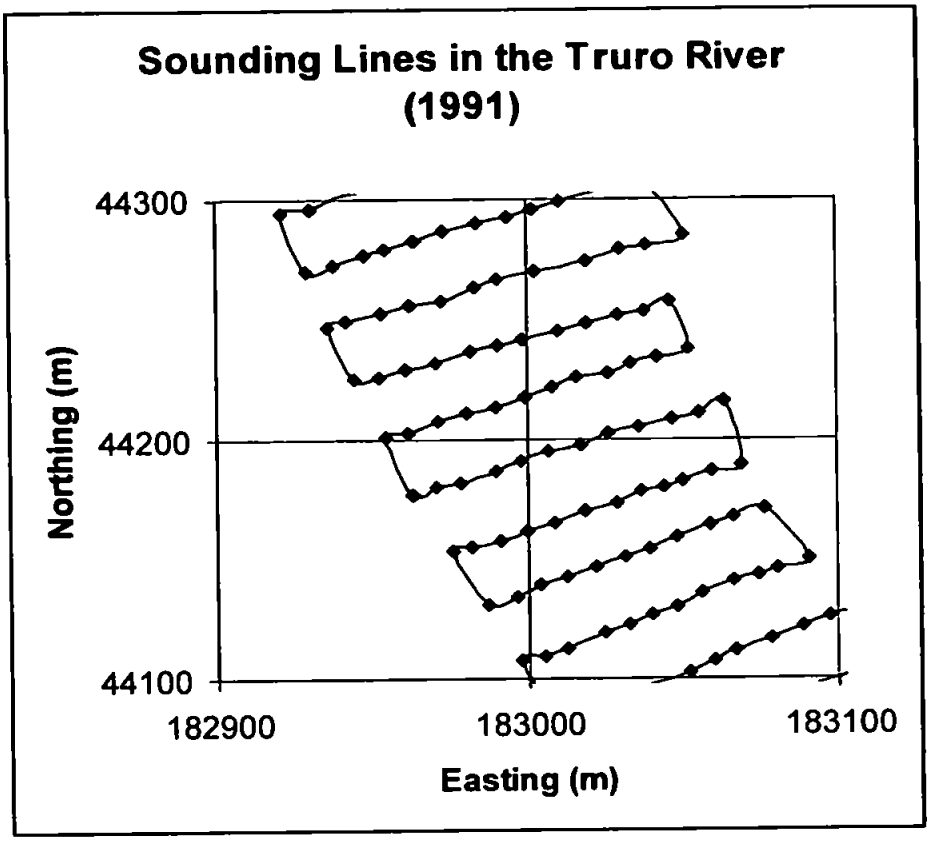

Figure 5.4 – Sounding data for the Truro River (1991) digitised along the sounding lines. A diamond shaped symbols represents each sounding, lines show the order of digitising.

Having identified the survey lines the program then determined, and allocated a code number, to the deepest sounding within each line. The record (co-ordinates, depth, line number, and code) for each of these deepest points was automatically copied to the end of the data file, to allow straight-forward investigation and display of the results. Local minima were also ascertained, with a different code number, to facilitate interpolation in the area of any subsidiary channels.

Examination of the program outputs from this stage of the ZIDW software revealed a number of anomalies. These anomalies resulted from peculiarities in the survey method and complex channel features, supporting the decision to incorporate a manual quality control (QC) stage within the program at this point, see Figure 5.3.

5.2.1 Details of Anomalies

Anomalous channel points selected by the program were identified as resulting either from unusual survey practice or from genuine anomalies in the estuarine channel system. Within these two broad categories a number of specific problem factors were detected:

1) Factors of unusual survey practice

   a) Partial survey lines - where occasional large gaps between survey lines have been in-filled by a line stretching only part way across the estuary. Anomalies occur where these part lines do not cross the deep channel, as the deepest sounding covered is selected rather than the deep channel (Figure 5.5a).

   b) Lines run parallel to the deep channel – an unusual practice undertaken in a small part of the Truro River where channel straightening has produced a very narrow channel. The program is not designed to select the channel in these areas (Figure 5.5b).

   c) Very irregular lines – where direction changes of greater than 60° occur within a survey line. These direction changes will be wrongly identified as a line change (Figure 5.5c). In this case, extra channel maxima are deduced, one for each incorrectly identified line.

   d) Gaps in the line corresponding to the deep channel – induced by the deliberate practice of selection of shoal soundings for navigational safety. This may result in secondary maxima being labelled as the main channel (Figure 5.5d).

2) Complex features of the channel system

   a) Discontinuities in the channel – In tidal estuaries separate flood and ebb channels may occur. These channels do not join producing a discontinuity in the channel line identified (Figure 5.6a).

   b) Branching channels and middle grounds – areas where the channel branches or divides around an island or central mud-bank (Figure 5.6b).

Figure 5.5 – Anomalous Channel Selection due to Unusual Survey Practice

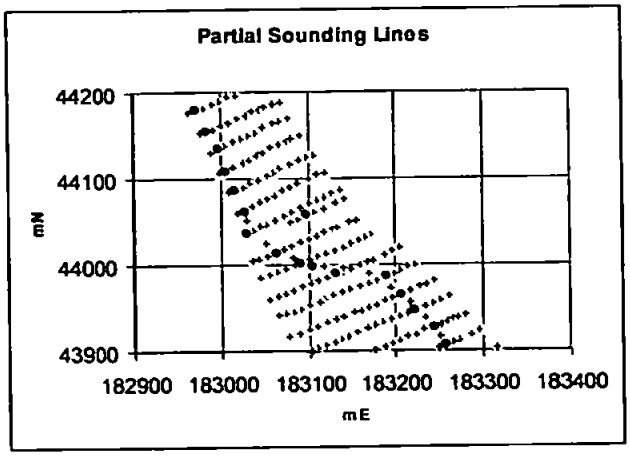

Figure 5.5a – Partial Survey Lines

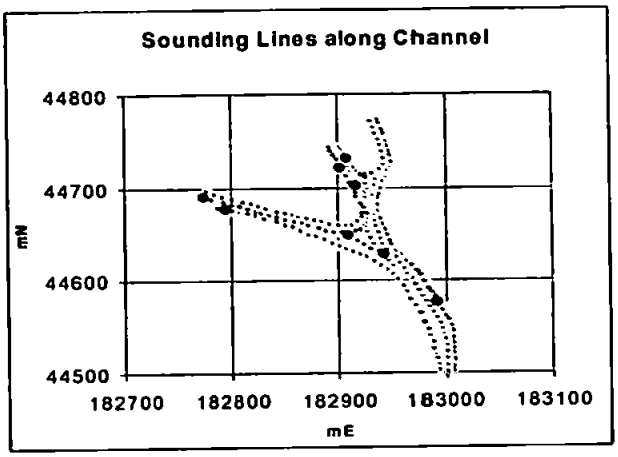

Figure 5.5b – Survey Lines Parallel to Channel

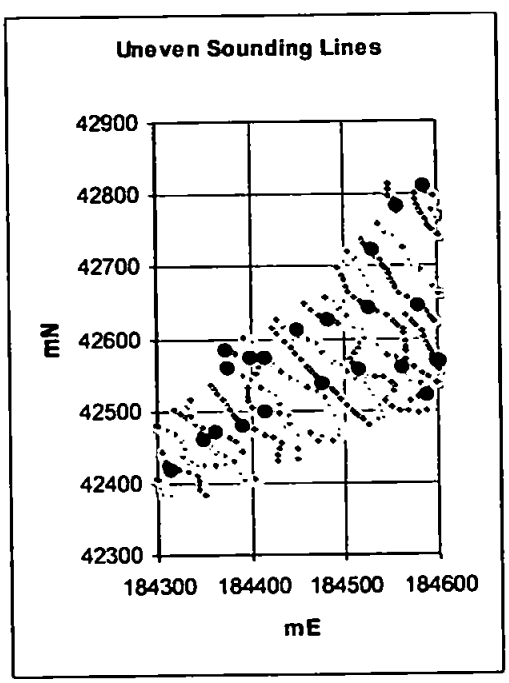

Figure 5.5c – Irregular Survey Lines

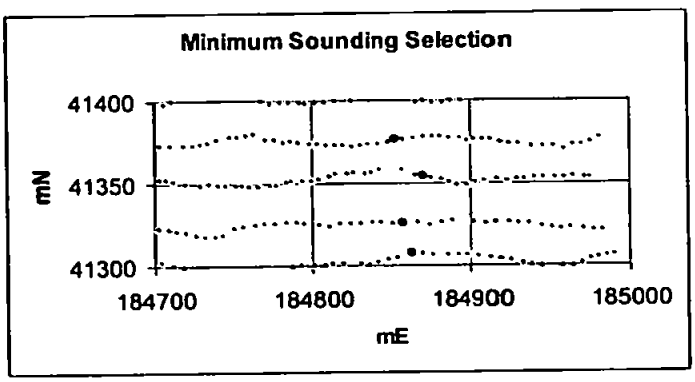

Figure 5.5d – Gaps in Lines due to Sounding Selection

Figure 5.6 – Anomalies in Channel Selection due to Complex Natural Systems

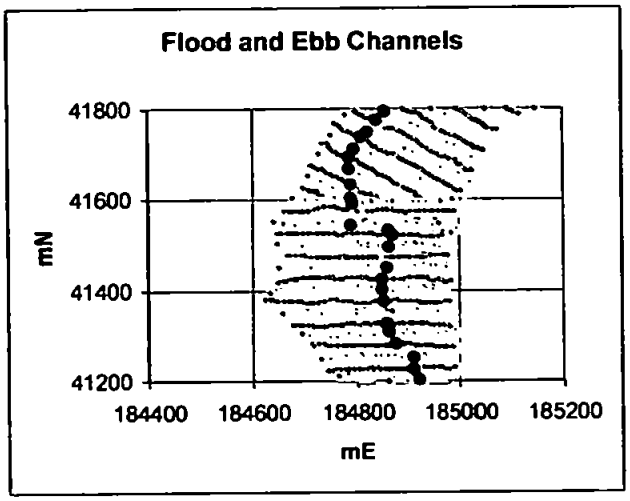

Figure 5.6a – Flood and Ebb Channels

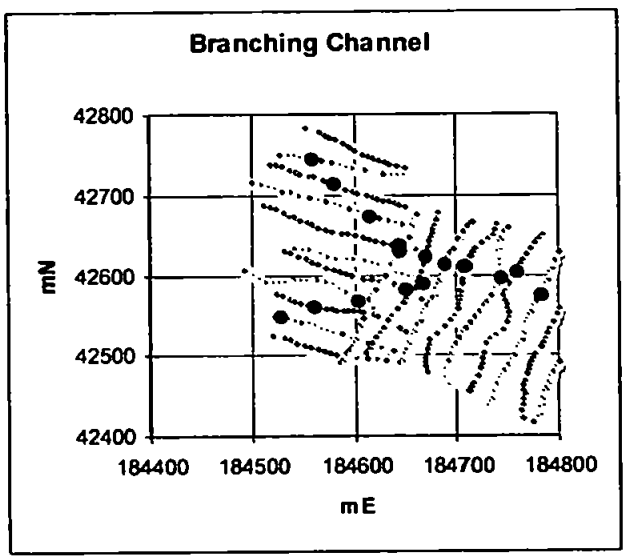

Figure 5.6b – Channel Branching

Despite the presence of these unusual features, the automated channel selection process was found to select the deep channel correctly on more than 91% of survey lines when tested on four historic data sets surveyed in the Truro River between 1961 and 1996. Inclusion of the fifth available data set surveyed in the same area, in 1995, produced a lower rate of correct channel selection, just over 82%, due to a large number of survey lines containing bends of greater than 60° (an unusual survey practice).

5.2.2 Manual Quality Control

Manual quality control was used to identify erroneous channel points resulting from the anomalies identified above. The number and complexity of their causal factors made automation of the quality control process unrealistic (and arguably undesirable) to ensure adequate treatment of unusual channel features.

During quality control, rogue channel points were given an error code in place of the channel code assigned by the program, to avoid incorrect channel definition in the next stage of the ZIDW automation process. Out of sequence points resulting from bends and branches in the main channel and the presence of secondary channels were reordered in preparation for the fitting of channel lines to the data. A separate number code was allocated to each subsidiary channel to facilitate correct joining of channel systems.

Having completed the manual quality control of channel points it was necessary to reformat the channel data using a program entitled FCD.EXE. This program merely converted the data from a space delineated text format output by Microsoft Excel to a format suitable for input into the next program in the suite (VERT.EXE).

5.2.3 Defining the Channel and Coastline

The channel line was defined by linking all the deepest points determined above with straight lines. From investigation of small samples of data, the use of actual data points joined by straight lines was determined to be the most sensible method of producing an interpolation boundary. This approach eliminates the assumptions involved in curve fitting.

It was originally intended to define the channel and coastline by points at 1 metre intervals at this stage of the process. This would, however, produce very large file sizes, particularly for the coastline. Hence, the generalisation strategy was amended so that each polygon enclosed by the coastline and channel would be defined using the lines joining existing points along the channel and coast. The sides of the polygons

were defined on a 1 metre grid during the zone assignment process, immediately before the final stage of performing the ZIDW interpolation.

The line definition program, originally designed for coastlines, was amended to recognise a change in point code and thus avoid adding additional join lines when moving from the main channel to a subsidiary channel and between successive subsidiary channels. It was also necessary to edit the input channel data files, generated above, to include a duplicate, joining point associated with the data for the incoming channel. This prevented gaps occurring at junctions of channels and thus 'leakage' in the polygons outlined by the channels and coastline. The channel was specified in an upriver direction.

For consistency the coastline was to be specified in an anticlockwise direction around the UK. The start of this file was taken as the southern-most data point; necessarily the point on the opposite bank must become the last data point. To achieve the desired file format a number of stages of editing were identified. These are as follows:

1. Reordering of digitised segments of coastline, to ensure that they are consecutive in an anticlockwise direction. This was required as the chart, from which the coastline was digitised, contained inserts of the upper sections of each river, necessitating an apparently illogical digitising order.

2. 'End' statements and code numbers assigned to the data by Arc/Info during digitising were removed. This was straightforward during editing. Minor changes to the program could, however, be made to recognise and ignore these statements if necessary.

3. A program to reverse the order of data points in one of the digitised segments. The reason for digitising this section in a clockwise direction is unclear. However, it is likely that point order was non-critical in the original use for the digitised coastline. This point reordering algorithm will also be required during compilation of polygons as the channel is required in the opposite sense for polygons on the west side of the estuary compared to those to the east.

4. Reversal of the point order of the complete file to achieve the preferred anticlockwise data direction.

5. Addition of 'close off' lines where the edges of the survey area cut across rivers and creeks, leaving open ends.

All these stages may be carried out using the functionality of the Microsoft Excel software package.

5.2.4 Construction of Interpolation Polygons

Two vector topology files were constructed for the purpose of defining the required polygons. The first file contained node names and their co-ordinates (nodes being points at the junctions of every line (arc) forming the edge of one or more polygons). This file was given a name Txx-node.txt, where 'T' implies data from the Truro River 'xx' contains the relevant two-figure year of the survey. The second file defined each polygon according to the nodes surrounding it in clockwise order; the type of line joining consecutive pairs of nodes, e.g. main channel (MC), coast (AC) or free boundary (F), and the direction to be followed along each line (positive '+' or negative '-'). This file has the name Txx-poly.txt, as before, 'T' is for the Truro River and 'xx' represents the relevant two-figure year of the survey.

Samples of the node and polygon topology files are given in Figure 5.7.

An algorithm was then developed (within a program entitled VERT.EXE) to produce interpolation polygons from a file containing coded coastline and channel vertices according to the relevant vector topology files. This algorithm deals with each polygon, in turn, as follows:

- for each bound segment (i.e. along a coast or channel), working from one node to the next:
  - identify the vertex closest to the start node
  - identify the vertex closest to the end node
  - trace along the line (coast or channel) from the start node to the end node

- ➢ extract the co-ordinates of the intervening vertices

- for each free segment (direct from one node to another):

  - ➢ extract just the co-ordinates of the vertices closest to the start and end nodes.

Node Identifier	Easting (m)	Northing (m)
96 A1	184812	40563
96 A2	184519	42445
96 M1	184910	40422

Start Node	Type and Direction of Joining Arc
A1	AC+
A2	F
M3	MC-

Figure 5.7 – Top Box: An example node definition file, '96' gives the year of survey, 'A' represents a node on the coastline and 'M' a node on the main channel and nodes are numbered consecutively along the relevant arc. **Lower Box:** Node numbers identify arcs enclosing each polygon, with associated arc type and direction. **Note:** Free boundaries join nodes with a straight line having no direction.

For the successful operation of this program it was necessary to avoid anomalous topologies of two types:

1. Polygons must not be specified starting with a free section (Code F). This is easily avoided by careful choice of start node.

2. Two free sections must not occur consecutively within the polygon topology. Two very closely spaced nodes on the same arc, joined by a short section of this arc, must be input between free sections to allow the program to correctly define the polygons.

The codes of defined nodes were maintained in the output file to allow them to be distinguished from vertices for checking purposes. The vertices were allocated a code 'v' within the polygon definition program.

5.2.5 Allocation of Soundings and Output Grid Cells to Polygons

The rectangular domain, described in section 6.2, was employed to facilitate the process of allocating soundings and output cells on to a fine mesh grid of 1 metre cell size.

The program was then able to represent all coastline and channel data on the 1 metre grid by allocating their data codes to the appropriate grid cells. At this stage any grid cells containing neither coastline nor channels, i.e. cells covered by land or non-channel parts of the estuary were allocated a blank code (..). These processes were performed using the program entitled GRID3.EXE, within the ZIDW suite of programs.

To avoid difficulties resulting from boundaries shared by more than one polygon the program would fill each polygon individually, using a different code letter for each. For example, all cells on the 1 metre grid within the western polygon, i.e. between the western coast of the estuary and the channel would be assigned a code 'W'. A single character code was chosen to maintain manageable file sizes, whilst using a grid of 1 metre cell size over an area of several square kilometres.

Polygon filling, to assign the correct polygon code to all cells within the polygon, was undertaken using the method of scan-line filling (as explained in Mielke, 1991). Within the polygon-filling program, it was necessary to design an algorithm to resolve the anomalous situation of polygon boundaries and turning points of these boundaries appearing identical when detected by the line-by-line scanning approach. For example, scanning from left to right across the grid in figure 5.8:

1. The first scan line encounters no polygon boundaries

2. The second scan detects only one turning point and thus would require no filling

3. The third line finds two turning points, also requiring no filling

4. The fourth line contains four polygon boundary crossings, conforming to the odd-even rule (Mielke, 1991) and would therefore be filled correctly

5. The fifth scan line would detect two polygon boundaries, require fill between, but also a minimum turning point which does not represent a boundary where filling is stopped.

.	.	.	.	.	.	.	.	.	.	.
.	.	.	.	B	.	.	.	.	.	.
.	.	.	B	B	B	.	.	B	.	.
.	.	B	B	.	B	.	B	.	B	.
.	B	B	.	.	.	B	.	.	B	.
.	B	.	.	.	.	.	.	.	B	.
.	B	.	.	.	.	.	.	.	B	.

Figure 5.8 – Part of a polygon, defined on the grid, illustrating typical problems associated with the polygon filling process. 'B' represents a cell identified as a boundary.

5.2.6 Performing ZIDW

Having successfully assigned all cells, within the 1 metre grid, to a polygon, the ZIDW interpolation process could be performed. It was necessary to decide whether to average the data on to the 10 metre grid, initially identified for comparison with other data sets, during the process interpolation. The polygonal zones would need to be taken into account during any averaging processes. Otherwise, the benefits of zoned interpolation would be partially negated by the effects of averaging across channels. After consideration, it was decided to maintain the high resolution, 1 metre grid during interpolation. This would provide data at 1 metre grid scale, for comparison and calculations. Then averaging to a 10 metre resolution could be applied later if required.

According to the zoning theory the choice of soundings to be included in the determination of each point on the grid must obey the following rules:

1. For each trial point in the channel, i.e. coded C or c, only soundings within the channel are allowed in the ZIDW process.

2. For non-channel trial points, i.e. points in any polygon, only soundings in the same polygon or in the channel are permitted in ZIDW.

Initially all soundings were detected within a square of 100 metres side length; centred on each non-channel test point and divided into four quadrants. The sounding closest to the test point, from each quadrant, was selected and inverse distance weighting applied for the resultant four values. Test points in the channel were treated separately, applying inverse distance weighting for all channel soundings within the 100 metre square. Although generally satisfactory the results of this interpolation strategy suffered from insufficient soundings in quadrants close to polygon boundaries. As a result areas of no data were generated along the coastline and channel edges (see Figure 5.9).

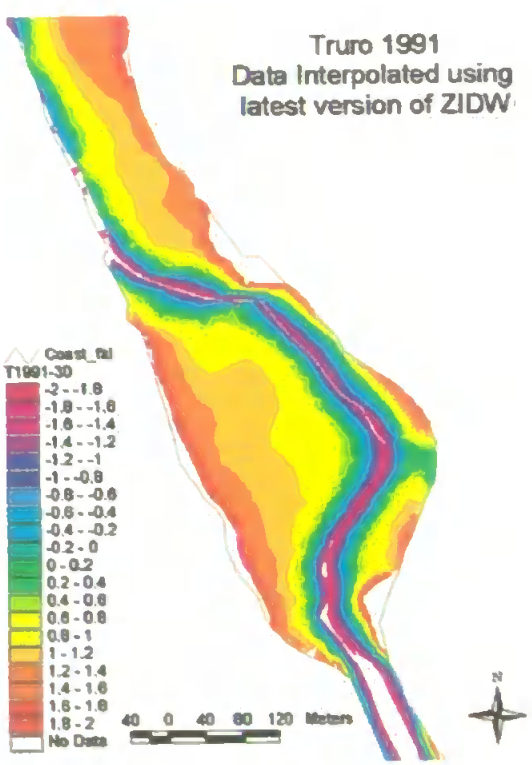

Figure 5.9 – Truro 1991 data interpolated using automated ZIDW, exhibiting loss of data near channel and coastlines.

A revised interpolation strategy was then produced. This method identified the closest three soundings to the test point. These soundings are required to be in the same polygon as the test point or in the channel. A plane equation of the form $z = a + bx + cy$ was fitted to these three points, using an origin which is coincident with the test point, and such that the equations of condition are:

$$a + bx_1 + cy_1 = z_1$$

$$a + bx_2 + cy_2 = z_2$$

$$a + bx_3 + cy_3 = z_3$$

Hence the solution, for 'a' gives the value of depth (z) at the test point, where:

$$a = \begin{vmatrix} z_1 & x_1 & y_1 \\ z_2 & x_2 & y_2 \\ z_3 & x_3 & y_3 \end{vmatrix} \div \begin{vmatrix} 1 & x_1 & y_1 \\ 1 & x_2 & y_2 \\ 1 & x_3 & y_3 \end{vmatrix}$$

This revised interpolation method produced more spatially complete results, but exhibited anomalous data in blocks running parallel to the sounding lines. The likely cause of this is difficulty in fitting a plane to three points lying on or close to a straight line. Programming error has not been ruled out as an additional factor contributing to this problem.

The program was rewritten to include plane fitting and inverse distance weighting. All soundings lying within a circle, of radius 50 metres, centred on the test point (except those outside the polygon containing the test point) were used in this interpolation procedure. This resulted in up to 40 soundings being used to interpolate the depth at certain test points. Hence a least squares solution was used to fit a plane through the soundings, with normal equations:

$$(\Sigma W_i)a + (\Sigma W_i\, x_i)b + (\Sigma W_i\, y_i)c = (\Sigma W_i\, z_i)$$

$$(\Sigma W_i\, x_i)a + (\Sigma W_i\, x_i^2)b + (\Sigma W_i\, x_i\, y_i)c = (\Sigma W_i\, x_i\, z_i)$$

$$(\Sigma W_i\, y_i)a + (\Sigma W_i\, x_i\, y_i)b + (\Sigma W_i\, y_i^2)c = (\Sigma W_i\, y_i\, z_i)$$

The results of this third method produce a smoothly contoured surface, apparently consistent with the smooth shape expected for mud bank features (figure 5.10).

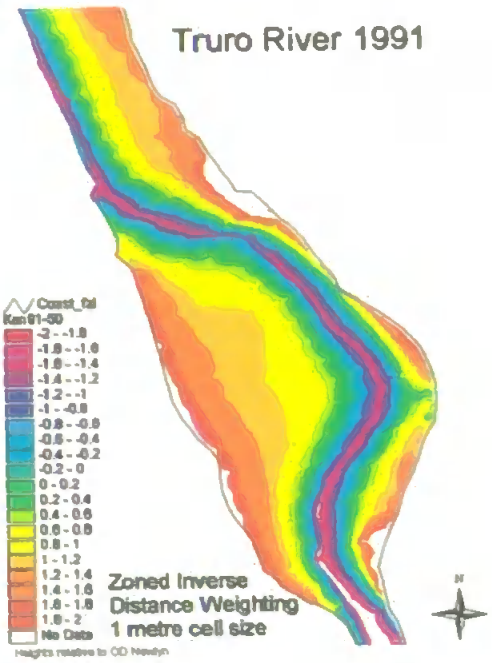

Figure 5.10 – Results of Automated ZIDW, using a 30 metre radius, for 1991 data from the Truro River.

For certain data sets the isobaths exhibit slight arcuate cusps in some areas. These features appear to coincide with the intersection of the isobaths with sounding lines. To minimise this effect, the program was improved to remove rounding errors imposed on the locations of sounding points. Also, various interpolation radii were tested to determine which was best suited to the average line spacing exhibited by each individual data set.

For the 1991 and 1996 data the arcuate cusps were removed from the interpolated isobaths by reduction of the 50 metre interpolation radius to 30 metres (Figure 5.10). The 1961 data, however, exhibit a greater spacing between certain pairs of sounding lines than the more recent data sets, probably as a result of running lines along transects. This early data set contains line spacings of up to 50 metres compared to 40 metres for subsequent surveys. Consequently, the use of a 30 metre interpolation radius for 1961 produced narrow bands of 'no data' between some survey lines. After experimenting with various interpolation radii, a 50 metre radius was determined, by visual inspection, to produce the most realistic isobath model from this data set.

The ZIDW.EXE program was subsequently amended to prompt the user to input an interpolation radius of their choice each time the program is run. This radius is chosen according to the spacing of sounding lines within the data set, to ensure that it encompasses a sounding line to either side of that containing the test point.

5.3 Application of the ZIDW Suite to Data Sets of Increased Complexity

Some additional problems were identified when applying the ZIDW program suite to the 1974 and 1995 data. The 1974 data set covers a larger part of the estuary than any other, and data collected in 1995 contain very irregular sounding lines.

5.3.1 More than five boundary intersections

The first such anomaly occurred whilst running the GRID3.EXE program (to define a very fine-mesh grid, of 1 metre cell size, for the 4 × 5 km area including all surveys) on the 1974 data set. Further anomalies were subsequently discovered in the 1995 data.

The GRID3.EXE program is limited to a maximum of 5 intersections of each scan line with the coastline and channel, all possible polygon shapes resulting from any given set of intersections can then be defined uniquely within the program. If more than 5 intersections are encountered the program is terminated and a 'Fatal Error' message displayed. After examination of the data sets it was determined that the number of intersections could be reduced to a maximum of 5 for all scan lines by blocking out small tributaries and creeks, such as Calenick Creek. These small creeks contain no soundings and thus the display 'no-data' would be present in them after interpolation. Hence, no information is lost if the small tributaries and creeks are removed from the interpolation polygons.

Initially the creeks were blocked out by means of a free boundary across the mouth of each, input via the polygon topology files (Txx-poly.txt). This allowed the program to progress further than previously, but fatal errors (due to more than 5 intersections with the coastline and channel) were still returned by the program, for both the 1974

and 1995 data sets. These errors were found to result from repeated intersections along short sections of very irregular channel boundaries.

The uneven nature of the channel was investigated by means of plotting profiles across the channel, along each sounding line within the problem area. A number of consecutive profiles were plotted coincidentally on the same axes for comparison purposes. The results of this investigation ascertained that the data set contains insufficient information to determine whether the uneven channel is a genuine phenomenon, resulting from complex hydrography at the confluence of the Truro and Tresillian Rivers, or due to factors of the survey. These survey induced factors could result from the selection method used to determine which sounding values are displayed on the chart combined with the closeness and irregularity of sounding lines in this area.

In the light of this investigation it was considered inappropriate to apply any form of smoothing to the uneven channel, for the purpose of polygon delineation. If it had been possible to ascribe channel irregularities to facets of the survey process it would have been relatively straightforward to assign a best fit curve through the channel points. This could be achieved during the manual checking of the channel output from the SLINES.EXE program or via a smoothing algorithm added to the FCD.EXE program, currently used only to reformat the manually edited channel data. To avoid the danger of losing genuine channel information via a smoothing process, however, it was determined necessary to edit the GRID3.EXE program to cope with more than 5 intersections of the coastline and channel.

The counting of intersections is a fundamental part of polygon definition within GRID3.EXE; hence this alteration is apparently not straightforward. Initially part of the program was modified to count the maximum number of intersections that could be encountered within a data set representing the worst case scenario. Hence, it was shown that a maximum of nine intersections are present in the data sets from the Fal estuary. Clearly more might be present in data for other areas.

In order, to maintain the universal applicability of the ZIDW program suite, it was decided to replace the GRID3.EXE program by a GRID4.EXE program, employing a different approach for assigning grid cells to the appropriate polygonal zone. The

GRID4.EXE program initially ensures that no vertices of polygons fall exactly on a scan line. This is achieved, within the program, by displacing all vertices with co-ordinates of a whole number of metres by a negligibly small amount. Consequently a scan line will never exactly intersect with a maximum or minimum turning point of a polygon boundary. This ensures that every scan line will encounter an even number of intersections with polygon boundaries. Each consecutive pair of intersections will, therefore, represent entering and then leaving the polygon. By this method the GRID4.EXE program is able to deal with a greater number of boundary intersections, as it is no longer necessary to specify each unique combination of intersections individually.

Basing the GRID4.EXE program on initially searching for intersections around the polygon, rather than along the scan line as in GRID3.EXE, resulted in listings of intersections being generated in a non-sequential order. This difficulty was overcome by the addition of a simple sorting sub-routine to place the previously identified intersection points into numerically ascending order according to their east-west co-ordinates, that is parallel to the direction of scanning.

5.3.2 Coastal Artefacts

As a result of replacing GRID3.EXE by GRID4.EXE (for reasons described above) artificial artefacts were interpolated outside the coastline, i.e. on land. These occurred as a result of the revised method of assigning grid cells to polygons, used in the GRID4.EXE program, and were eliminated by ensuring that no pixels outside the polygons are filled.

5.3.3 Loss of data along the Centre Line of the Channel

A further side effect of the development of GRID4.EXE, to deal with data sets with more than five polygon boundary intersections, was a narrow band of 'no-data' generated along the centre line of the channel during ZIDW interpolation. Initially this was thought to result from vertices labelled 'C' (Channel) and 'A' (Anti-clockwise coastline) being overwritten by points assigned at 1 metre intervals, labelled 'c' and 'a'. A sub-routine to re-write vertex labels at the end of GRID4.EXE, however, failed to rectify this problem.

Further investigation revealed that not all soundings within the channel were being correctly identified as channel soundings. This occurred as soundings not lying exactly on the centre line of the channel were being assigned to an adjoining polygon rather than to the channel. This difficulty was overcome by using the original list of channel points, which had been preserved, to overwrite the channel data after polygon delineation.

5.3.4 Other Anomalies

A number of further anomalies were identified whilst testing the ZIDW program suite on the data from 1995. These included:

1. A circle of 50 m radius containing values offset from interpolated values outside the circle
2. Straight lines of erroneous data cutting across the domain
3. Interpolation artefacts corresponding directly with sounding line spacing.

The causes of these problems were traced back to peculiarities in the data set rather than the suite of programs. Checking data for the following should eliminate such difficulties:

1. Gross errors in sounding values, for example 1 m input as 41 m
2. Repeated points
3. The order of all points in coast or channel files in reverse order. The coastline should be specified in an anti-clockwise direction around the coast of the country. Channel data must be in the order implied by the polygon topology file.
4. Erroneous allocation of points to the channel
5. Channels gradually disappearing, for example the ends of flood and ebb channels.

The genuine hydrographic phenomenon of non-continuous channels, caused by flood and ebb currents, represents a particularly important situation which the initial version of the ZIDW program suite, developed in this chapter, was unable to deal with adequately. Clearly, non-continuous channels will not produce the closed polygonal

boundaries necessary for application of ZIDW in this initial form. Only one case of a flood and ebb channel situation was identified within the Fal estuary, hence it could be treated individually as a minor anomaly. However, non-continuous channels would become a significant factor, necessitating the re-appraisal of the whole ZIDW procedure, for application to large estuaries, with multiple channels, such as the Humber and Gironde.

5.4 Universal Application of Automated ZIDW

This chapter has described, in detail, the development of a suite of programs to perform Zoned Inverse Distance Weighting (ZIDW). The program suite was initially developed using data sets from the Fal estuary. However, the requirement for a universally applicable suite of programs was identified at this stage in the research work. To this end, it was necessary to formalise the theory behind ZIDW, by means of statistical testing of the method using idealised mathematical channels. Discussion of this process forms the next chapter of this thesis (Chapter 6).

To produce a suite of programs, which is universally applicable to even large estuaries, such as the Humber or Gironde, it was necessary to investigate in more detail the effects of hydrographic features, poorly dealt with by the methods described in this chapter. Flood and ebb channels are thus covered in detail, during the development of ZIDW for application to the large estuaries, as described in Chapter 7.

Chapter 6 – Application of ZIDW to Theoretical Cases

Having successfully developed the ZIDW interpolation method as a practical solution to data interpolation problems discovered whilst working with data from the Fal estuary, it was decided to test the method rigorously using a number of idealised estuaries. This statistical testing will formulate the theory behind ZIDW, thus providing a sound basis for application of the method to other estuaries (Chapter 7).

6.1 The Idealised Channels

Four idealised estuaries were utilised in formulating the theory of ZIDW. In each case the channel was defined by a known mathematical expression, allowing the level of the bed to be precisely defined everywhere. This 'real' case could then be compared, both visually and statistically, with models generated by any given interpolation method.

Each idealised channel has a length (specified as the x direction) of 400 metres and a width (y direction) of 100 metres. The three Gaussian channels are of the general form:

$$z(x,y) = b(x) - d(x)\exp\left[-\left(\frac{y}{20}\right)^2\right]$$

where b(x) and d(x) are defined below, for each Gaussian channel.

The four idealised channels were then defined as follows:

1. Gaussian Prism – This channel has a uniform cross section formed by an inverted Gaussian curve (figure 6.1). The maximum depth in the channel is specified as 4 metres and the banks of Gaussian channels tend towards datum. Hence, the parameters b(x) and d(x) in the equation for Gaussian channels are:

$$b(x) = 4$$
$$d(x) = 4$$

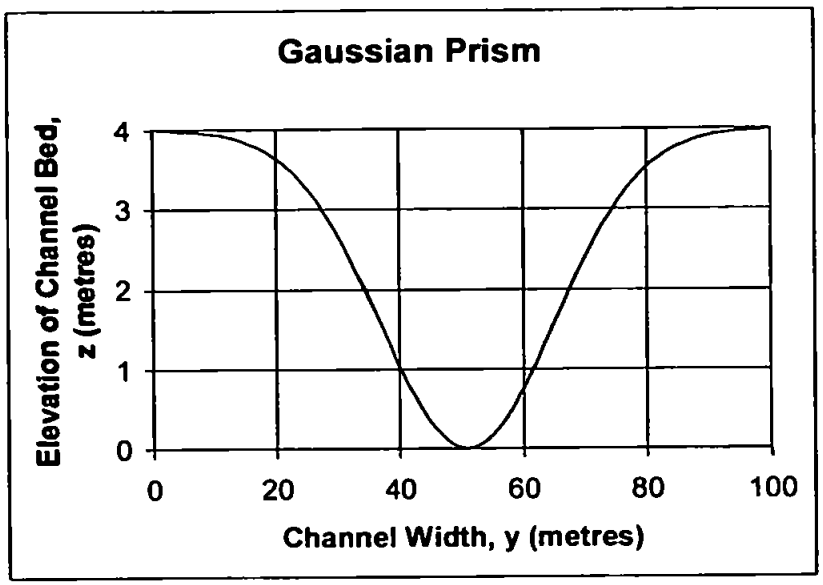

Figure 6.1 – Channel 1 = Gaussian Prism of uniform cross-section.

2. Triangular Prism – The triangular prism is a mathematically simple channel, having a uniform triangular cross section. The channel has a width of 100 metres, length of 400 metres and maximum depth of 4 metres (see figure 6.2). The depth (z) at any point in the channel is thus given by the equations:

$$z = 4\left[1 - \frac{y}{50}\right] \quad \text{for } 0 \leq y \leq 50$$

$$z = -4\left[1 - \frac{y}{50}\right] \quad \text{for } 50 \leq y \leq 100$$

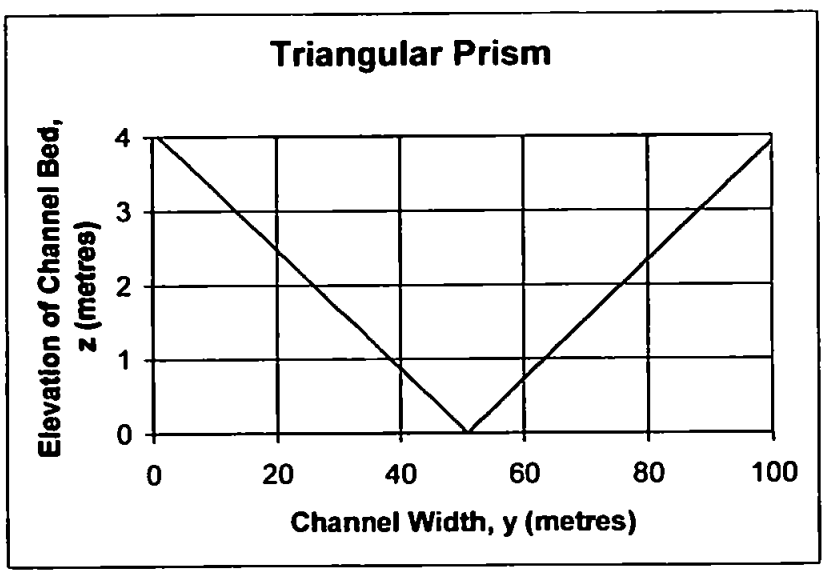

Figure 6.2 – Channel 2 = Triangular Prism of uniform cross-section.

3. Gaussian Sloping – The Gaussian sloping channel forms an inverted Gaussian curve in cross section, at any point along its 400 metre length. The channel depth, however, varies linearly with distance along the channel (x direction), figure 6.3.

   The depth at the mid-point along the channel, i.e. x = 200 metres, is 4 metres and the depths at x = 0 and x = 400 metres are 3 and 5 metres, respectively. Hence, the parameters b(x) and d(x) in the general equation for Gaussian channels become:

$$b(x) = 4$$

$$d(x) = 3 + \frac{2x}{400}$$

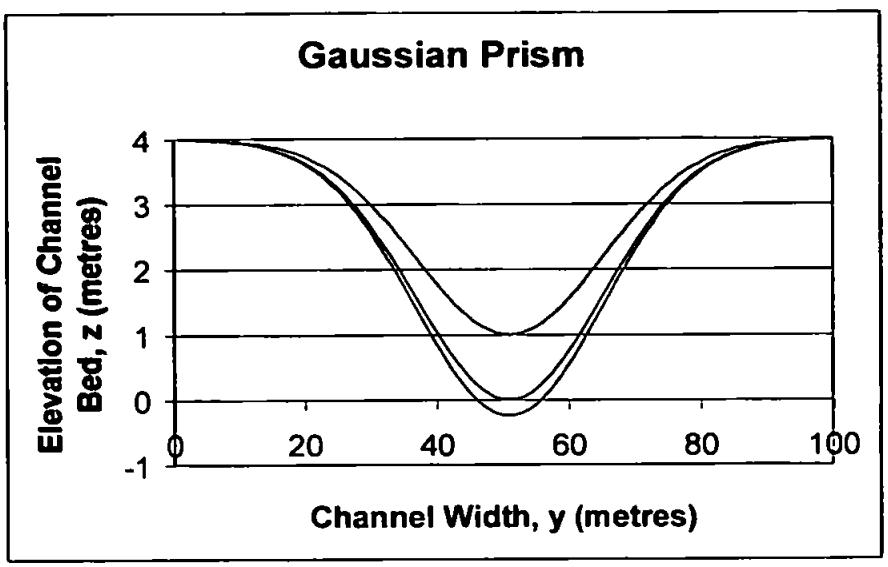

Figure 6.3 – Channel 3 = Gaussian Sloping, cross-sections at x = 0 metres (green curve), x = 200 metres (blue curve) and x = 240 metres (pink curve).

4. Gaussian Variable – In this case a Gaussian channel is defined as one end of the 400 metre long domain and an equal and opposite Gaussian ridge at the other. A saddle point forms in the centre of the domain (figure 6.4 & 6.5). This more complex case was designed to simulate the occurrence of flood and ebb channels in real estuaries. The parameters b(x) and d(x) are given by:

$$b(x) = 2 + 2\cos\left[\frac{\pi x}{400}\right]$$

$$d(x) = 4\cos\left[\frac{\pi x}{400}\right]$$

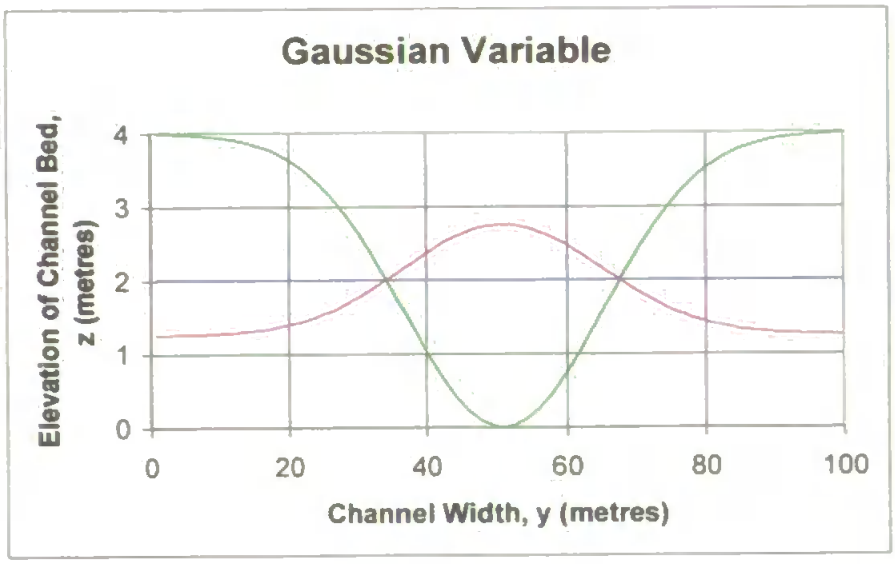

Figure 6.4 – Channel 4 = Gaussian Variable, cross-sections at x = 0 metres (green curve), x = 200 metres (blue curve) and x = 240 metres (pink curve).

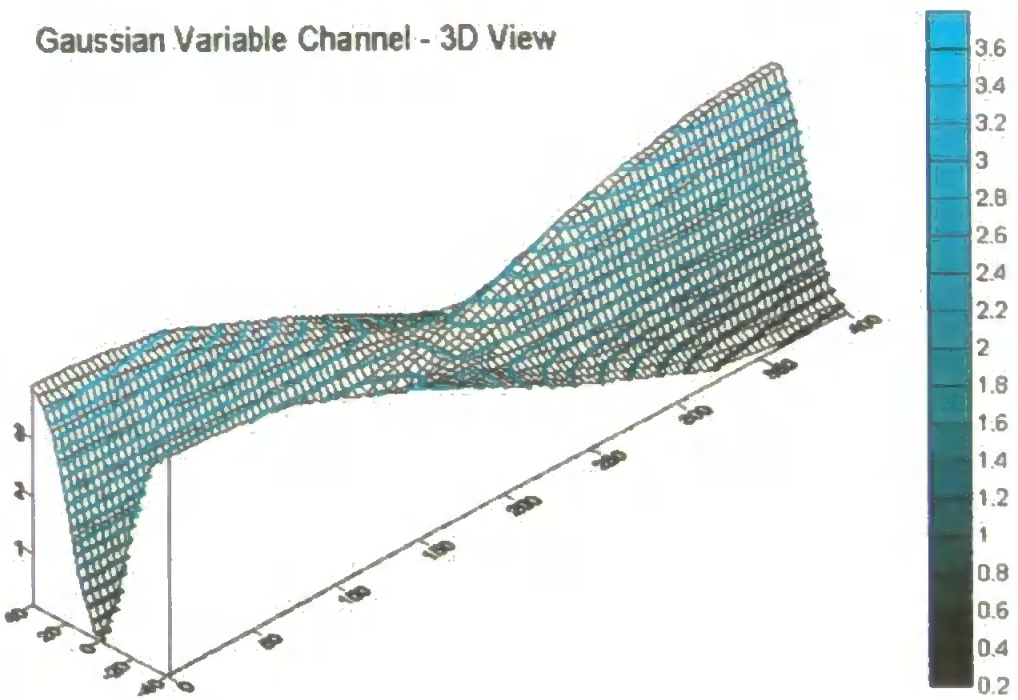

Figure 6.5 – Channel 4 = Gaussian Variable, 3D view of channel bed elevation. All elevations are in metres above datum.

6.2 Methods of Interpolation

Each of the four idealised channels, described in section 6.1, were subjected to standard interpolation by inverse distance weighting (IDW); inverse distance weighting with various combinations of improvements (see below) and interpolation utilising triangular irregular networks (TINs) and Kriging. A 50 metre radius of interpolation was used for all IDW interpolation, unless otherwise stated.

The three improvements to the inverse distance weighting method were as follows:

1. Introduction of a co-ordinate system based on sounding lines. This method involved transforming all data from the standard (x,y) Cartesian co-ordinate system to a distorted system using spacing between sounding lines (l) compared to sounding spacing along a line (s). For single beam echo sounding data $l >> s$, for example in the Fal estuary $l \approx 40$ metres, $s \approx 11$ metres; transformation to the sounding line co-ordinate system results in $l = s$. The data are then interpolated as regularly spaced points in the sounding line system. An interpolation radius of 1.2 units in the sounding line co-ordinate system was chosen, representing the region within the 'smart' interpolation ellipse, with semi-major axis of 48 metres and semi-minor axis of 12 metres, in the real world. The 'smart' ellipse is defined in the Glossary of Technical Terms (appendix 8). Finally the interpolated data are re-transformed for output in Cartesian co-ordinates.

2. Use of zoning, with zone boundaries along the centre-lines of channels and ridges, i.e. ZIDW as described in Chapters 4 and 5.

3. Application of plane fitting as opposed to simple weighted averaging. This technique also applied via the ZIDW program suite, see section 5.2.6 for details of the calculation process involved.

The standard errors resulting from interpolation of the four idealised channels using all possible combinations of improvements to the inverse distance weighing

interpolation method are detailed in table 6.1. Standard Error (SE) was calculated using the equation:

$$SE = \sqrt{\frac{\sum (Z_r - Z_i)^2}{n}}$$

Where: Z_r = Real depth at a point

Z_i = Interpolated depth at that point

n = Number of points

Elevation models produced by interpolating the data, for all four idealised channels, are displayed in figures 6.6 - 6.17. From the figures, each improvement can be seen to reduce the undesirable effects of sounding lines, as compared to the standard IDW method of interpolation (figure 6.6 - 6.17). The standard errors displayed in table 6.1 confirm statistically improvements identified by visual inspection. The greatest improvements can be seen, from both visual inspection and the Standard Error values, to result from the use of the sounding line co-ordinate system (lower half of table 6.1).

Co-ordinate System	Zoning	Algorithm	Gaussian Prism (1)	Triangular Prism (2)	Gaussian Sloping (3)	Gaussian Variable (4)
Cartesian Co-ordinates (1) (x,y)	No Zoning (1)	IDW Only (1)	1.037	0.873	1.049	0.738
		Plane Fitting (2)	0.800	0.449	0.807	0.563
	Zoning (2)	IDW Only (1)	0.937	0.825	0.947	0.667
		Plane Fitting (2)	0.391	0.000	0.395	0.275
Sounding Line Co-ordinates (2) (ξ,η)	No Zoning (1)	IDW Only (1)	0.148	0.267	0.138	0.114
		Plane Fitting (2)	0.104	0.193	0.104	0.097
	Zoning (2)	IDW Only (1)	0.143	0.265	0.134	0.111
		Plane Fitting (2)	0.094	0.190	0.094	0.091

Table 6.1 – Standard Errors in the output from all combinations of improvements applied to IDW interpolation of the four idealised channels. (1) = code for no improvement, (2) = code for improvement used, **(1)**, **(2)**, **(3)** or **(4)** = channel type used.

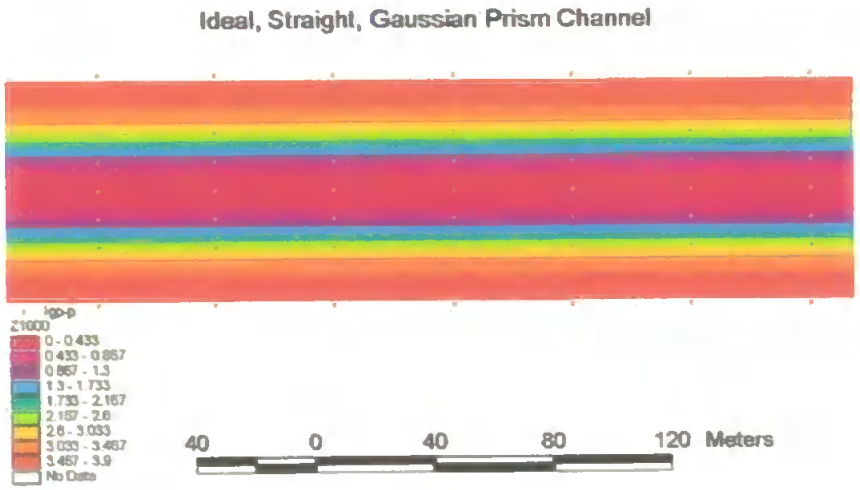

Figure 6.6 – Mathematically defined Channel – Gaussian Prism.

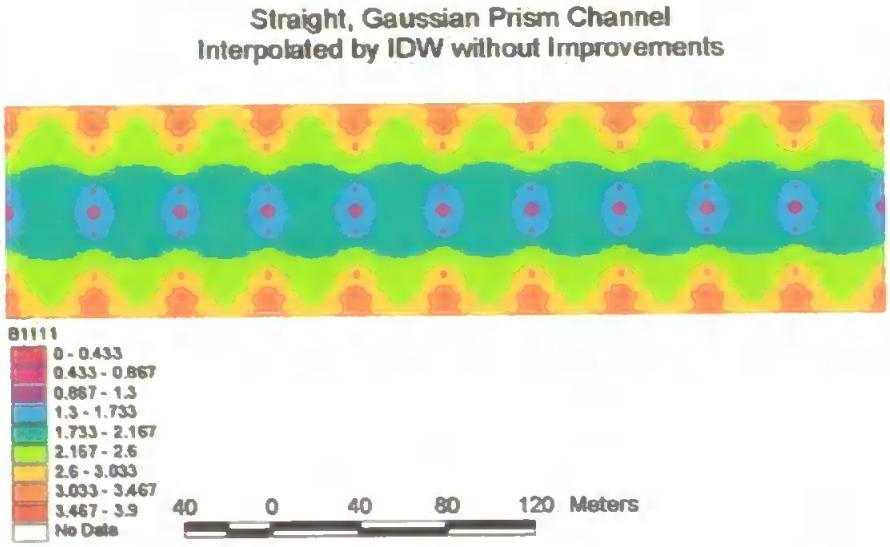

Figure 6.7 – Channel Interpolated by Standard IDW – Gaussian Prism.

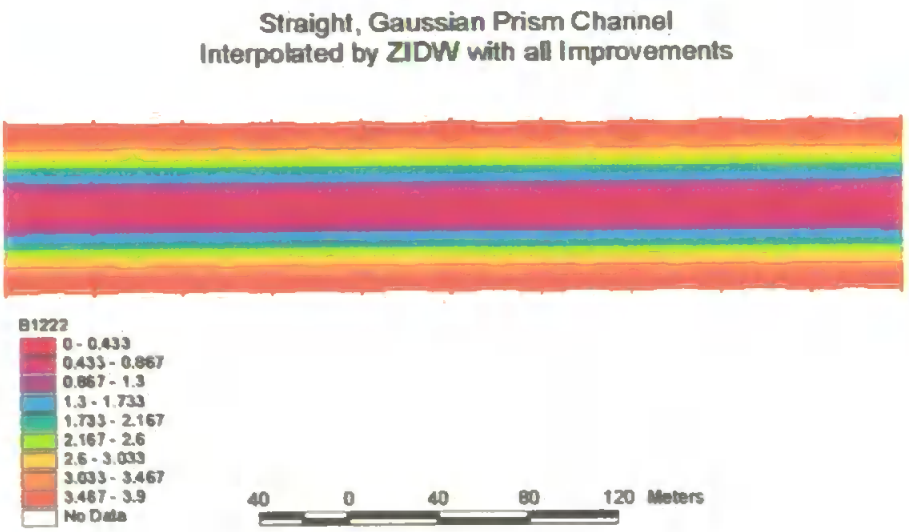

Figure 6.8 – Channel Interpolated by Improved ZIDW – Gaussian Prism.

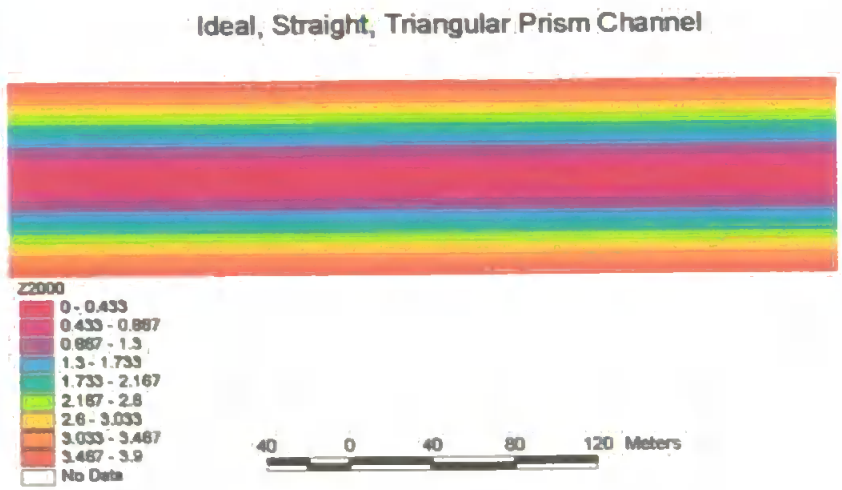

Figure 6.9 - Mathematically defined Channel – Triangular Prism.

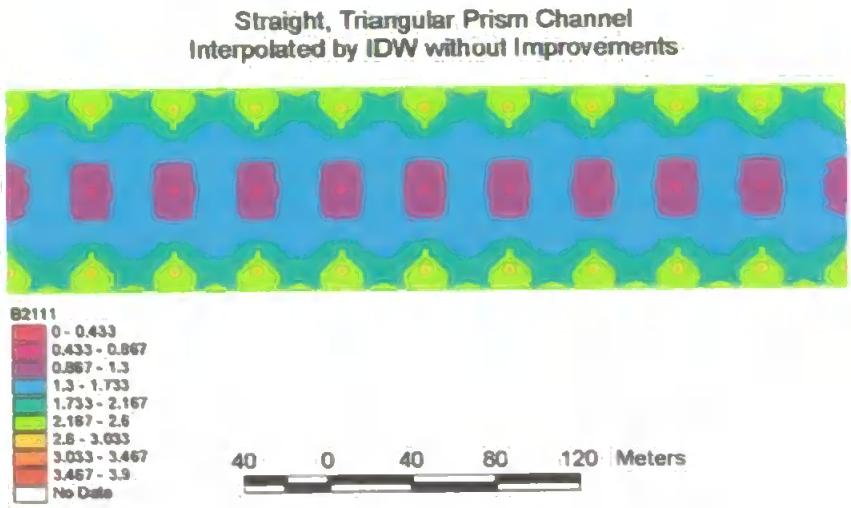

Figure 6.10 – Channel Interpolated by Standard IDW – Triangular Prism.

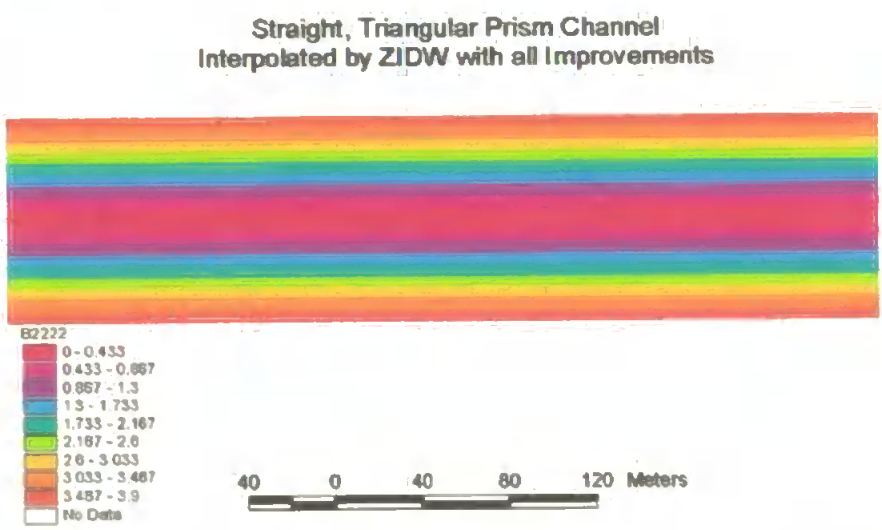

Figure 6.11 – Channel Interpolated by Improved ZIDW – Triangular Prism.

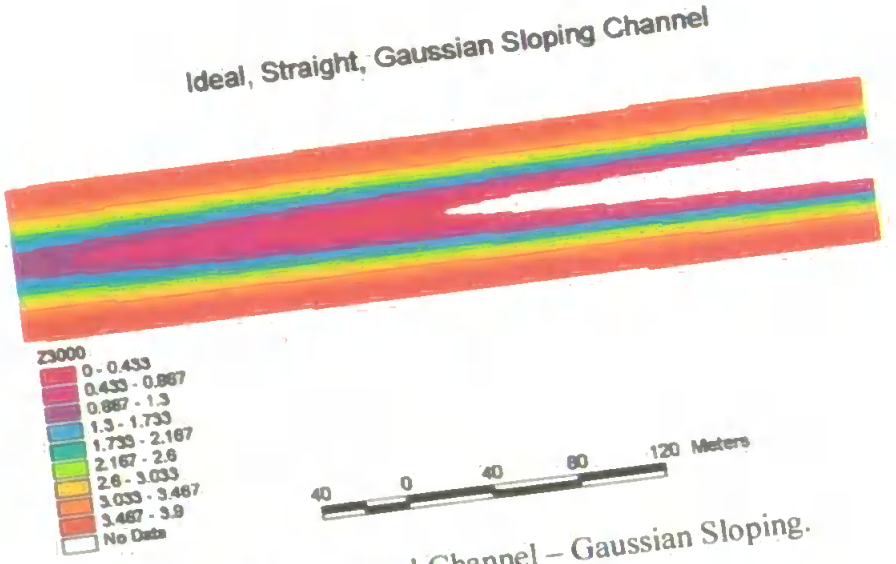

Figure 6.12 – Mathematically defined Channel – Gaussian Sloping.

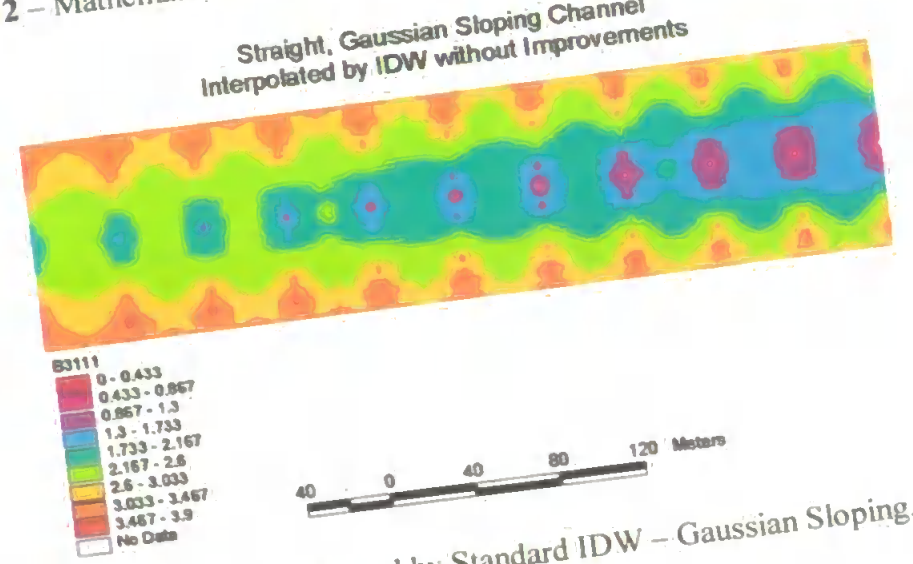

Figure 6.13 – Channel Interpolated by Standard IDW – Gaussian Sloping.

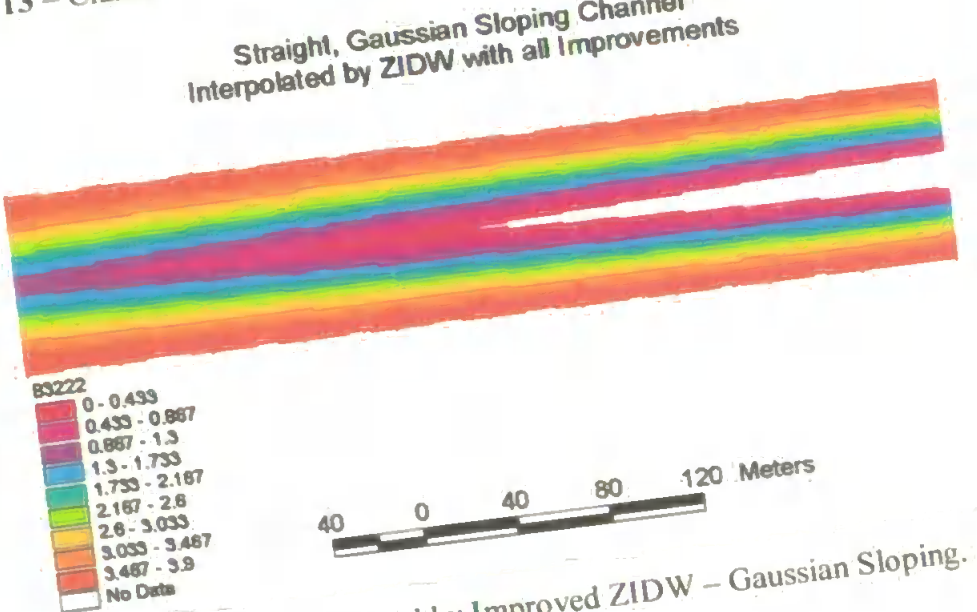

Figure 6.14 – Channel Interpolated by Improved ZIDW – Gaussian Sloping.

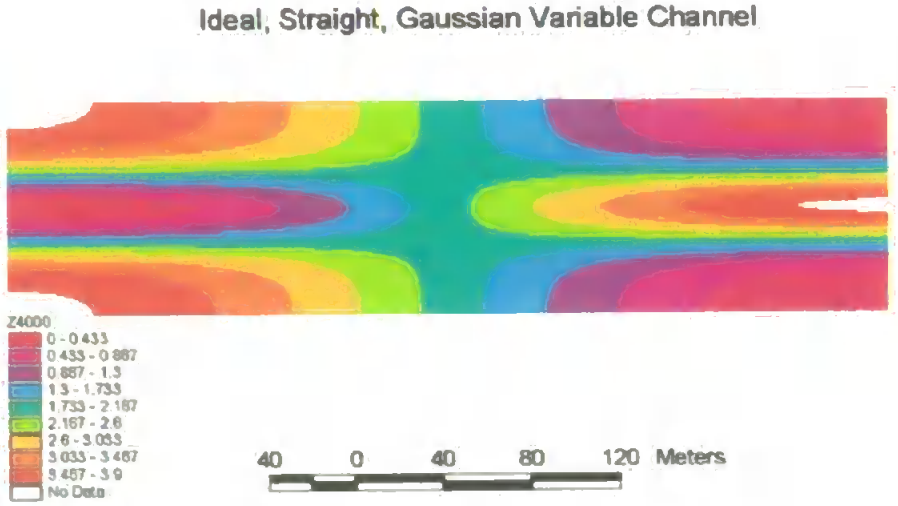

Figure 6.15 – Mathematically defined Channel – Gaussian Variable.

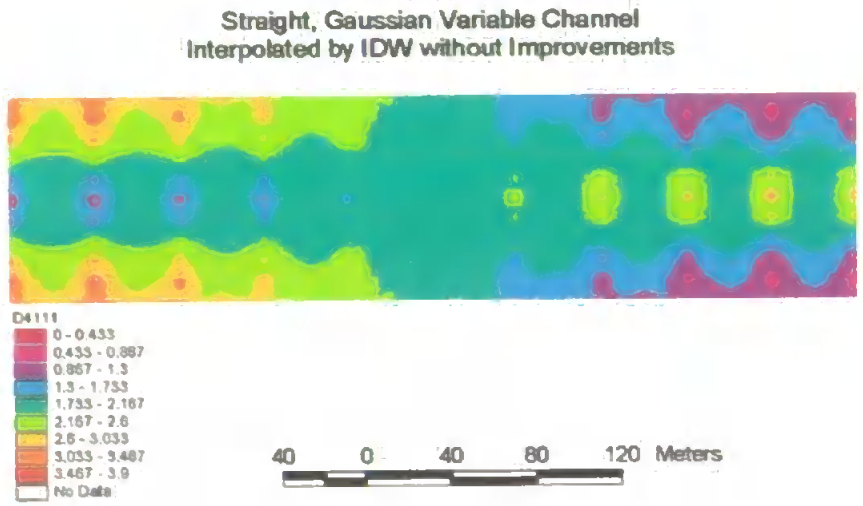

Figure 6.16 – Channel Interpolated by Standard IDW – Gaussian Variable.

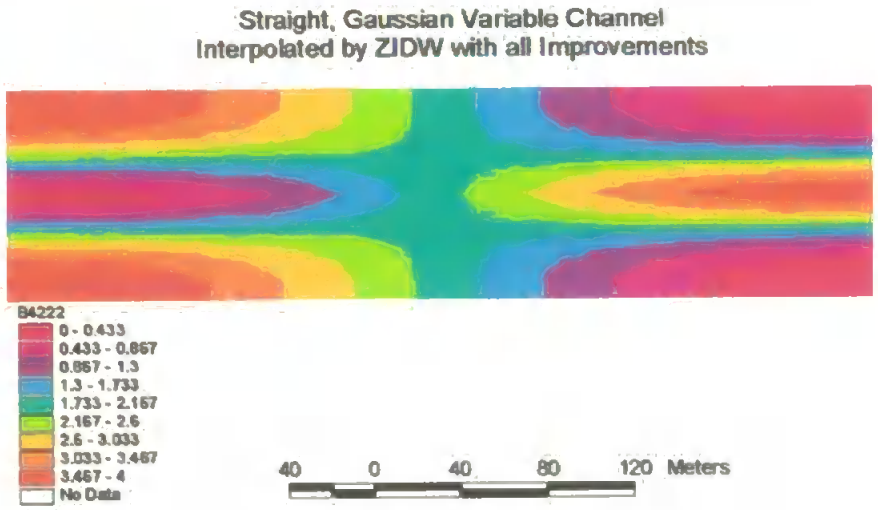

Figure 6.17 – Channel Interpolated by Improved ZIDW – Gaussian Variable.

6.3 Comparison with Conventional Methods of Interpolation

The idealised channel data was also interpolated by means of a TIN model and by Kriging, within the ArcInfo software. The best results using Kriging were produced using the locally variable, linear interpolation method referred to as 'Universal 1' within ArcInfo. The results reveal substantial artefacts resulting from the pattern of sounding lines (figure 6.18). The TIN model was vastly superior, to the Kriging, in avoiding interpolation artefacts. This method, produced very similar results to those derived by applying all three improvements to the IDW method, figures 6.19.

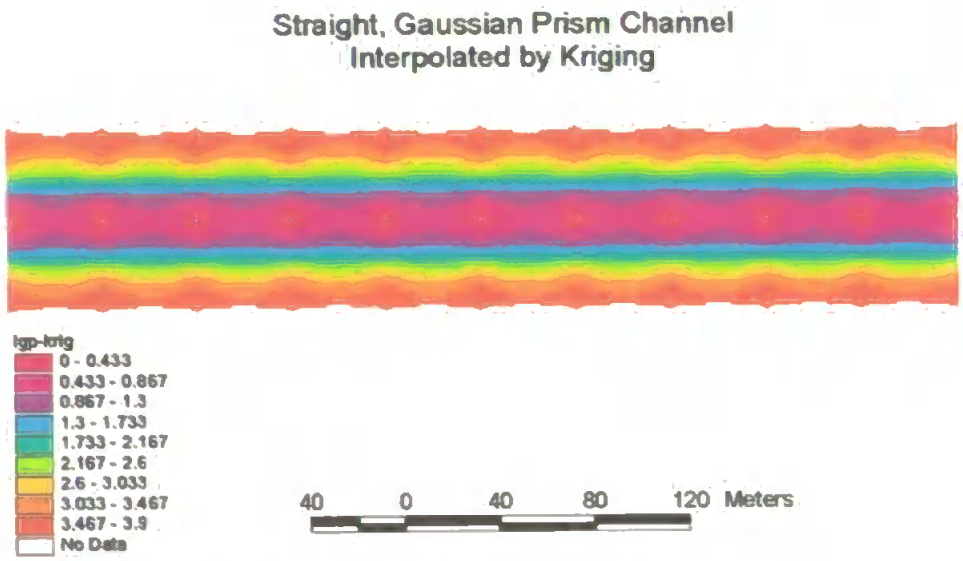

Figure 6.18 – Interpolation by Kriging – Gaussian Prism.

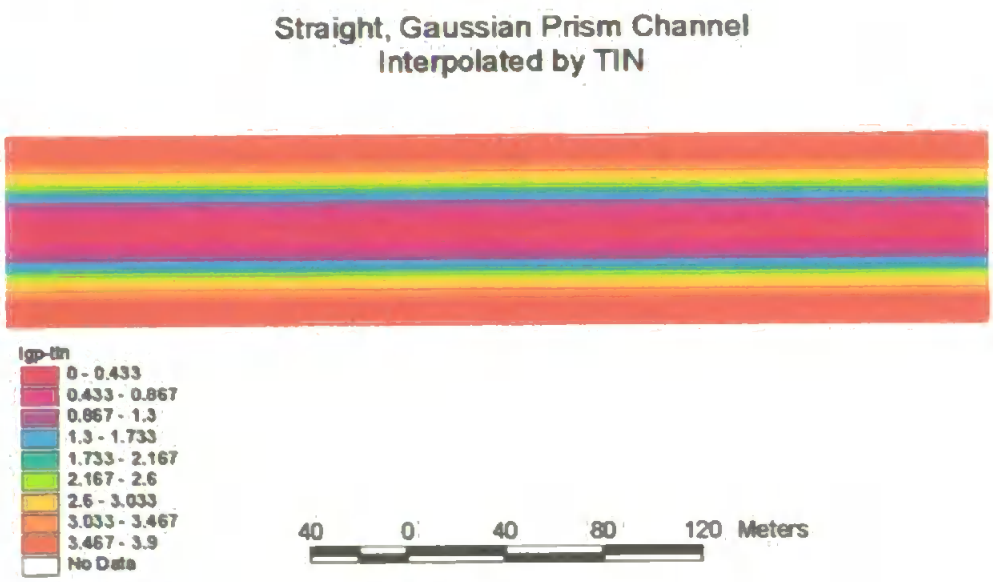

Figure 6.19 – Interpolation by TIN – Gaussian Prism.

The TIN model is, however, able to interpolate well only within the limits of the actual spatial extent of the data. For the 100 metre wide idealised channels only the central 80 metres were dealt with by the TIN method. Clearly this would present a disadvantage, compared to the improved inverse distance weighting technique, when applied to bathymetric data collected from bank to bank across an estuary.

In order to produce a fair comparison of standard errors between this method and the TIN model, it was necessary to exclude the 10 metre wide edge strip from both data sets and to apply the same degree of rounding (three decimal places) to all input values. The results of standard error calculations for the central 80 metres of each idealised channel are given in Table 6.2.

Channel	SE TIN Model	SE Improved IDW
Gaussian Prism	0.091	0.102
Triangular Prism	0.000	0.000
Gaussian Sloping	0.090	0.102
Gaussian Variable	0.073	0.079

Table 6.2 – Standard Error (SE) for Interpolation by improved IDW compared to use of a TIN Model applied to the four idealised channels.

The table clearly shows the TIN model to perform better than improved IDW for all the idealised Gaussian channels. This result appears to be in complete contradiction to the findings from interpolation of data in the Fal estuary (see Chapter 4). In the real case the TIN model produced significant interpolation artefacts across the channel; these were largely removed by using improved IDW interpolation. For the idealised channel, improvements to IDW reduced interpolation artefacts, but the TIN model performed slightly better, producing lower standard errors.

Investigation of profiles across the real channel in the Fal estuary reveal a cross-section closely approximating a Gaussian curve. Hence, the most likely explanation for the discrepancy in the performance between the two interpolation methods appears

to be caused by the spatial disposition of the input data. For the idealised channels sounding data were input along straight, equally spaced, parallel lines with soundings equally spaced along each line. Consequently the TIN interpolation would be performed on a regular network, producing high quality results. Interpolation artefacts were generated in the Fal estuary as a result of interaction between the channel shape and a very irregular network produced from the non-uniformly distributed sounding data.

6.4 Interpolation for Curved, Idealised Channels

This theory, proposed to explain the discrepancy between TIN interpolation applied to real and idealised channels, was tested by modifying the channel shapes and the regular distribution of soundings. The four profiles of idealised channel, as described in section 6.2, were maintained. A set of curved channels was generated from these, by bending each 100 metre wide idealised channel through 90° (figure 6.20). The sounding lines covering the channel formed radials about a central origin (figure 6.21), thus representing real sounding lines following the shape of an estuary.

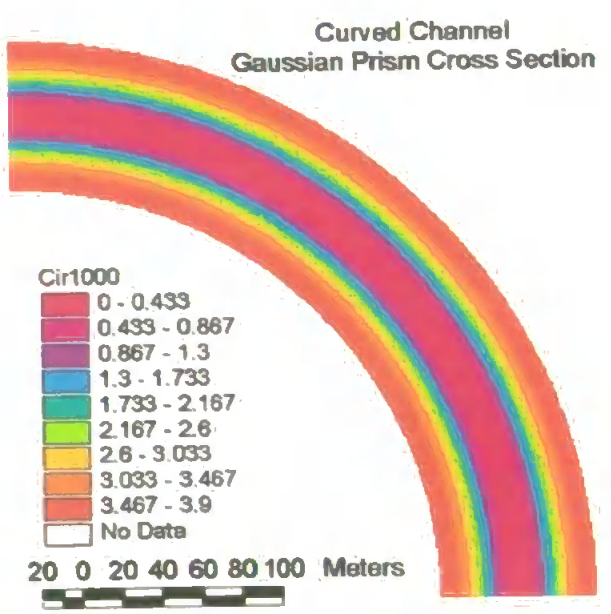

Figure 6.20 – Curved, Gaussian Prism Channel formed by Bending the Idealised Channels through 90°.

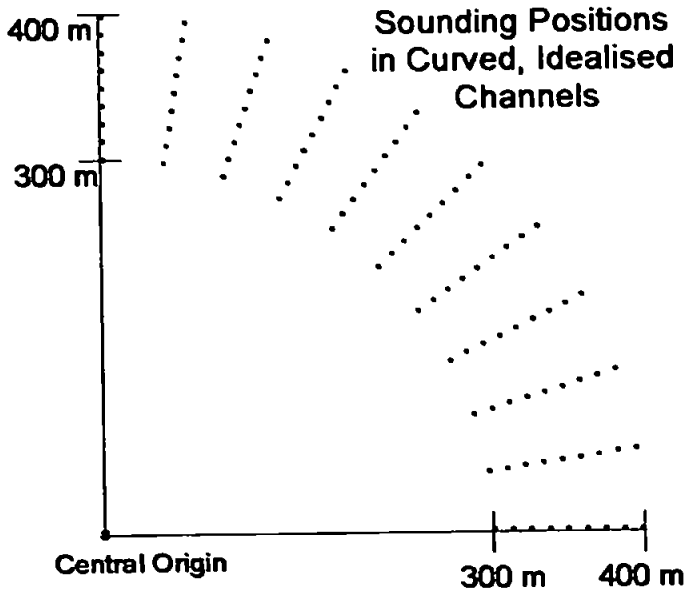

Figure 6.21 – Positions of the Soundings in the Curved, Idealised Channel.

These channels were interpolated using inverse distance weighting, combinations of the three improvements to inverse distance weighting (section 6.2) and TIN interpolation. An interpolation radius of 2.5 was used in the sounding line co-ordinate system, representing an ellipse of 25 by 100 metres in the real world, to ensure sufficient soundings for plane fitting at all points in the channel.

The standard errors for the interpolation of the curved channels using the improved IDW method and a TIN model are given in Table 6.3.

Channel	SE TIN Model	SE Improved IDW
Gaussian Prism	0.108	0.193
Triangular Prism	0.045	0.001
Gaussian Sloping	0.108	0.198
Gaussian Variable	0.086	0.158

Table 6.3 – Standard Error (SE) for Interpolation by improved IDW compared to use of a TIN Model applied to the four idealised, curved channels.

It can be seen from the table that for three of the four idealised, curved channels the TIN interpolation again produces a lower standard error than the improved IDW.

Clearly these results are not consistent with those for interpolation in the Fal estuary, as documented in Chapter 4. Having reinvestigated the case of the Fal, in some detail, it was established that this discrepancy between results for theoretical and real channels appeared to be due to the sounding lines in the real case being frequently non-perpendicular to the deep channel. Angles of as little as 10° between the perpendicular to the sounding lines and channel produce small artefacts using the TIN model, whilst angles of 40° or less result in extreme artefacts representing a complete failure of the TIN model to represent the channels in the real estuary. Clearly such cases will occur frequently in real estuaries as channels meander across the inter-tidal zone causing them to become non-parallel to the banks of the estuary. Even if a survey were to be planned with a pre-existing knowledge of channel patterns it would, in practice, be impossible to ensure that every survey line was perpendicular to each channel at all points along its length. This is especially the case in large estuaries, exhibiting complex patterns of channels and confluences, such as the Gironde, in western France, or the Humber, in north-east England. For the interpolation of historic data, clearly the only option is to work with the pattern of survey lines employed at that time.

An additional complication to the TIN model, for interpolating real data may result from irregularities in a sounding line caused by a combination of vessel handling, tide and wind conditions.

6.5 Development of a more Realistic Idealised Channel

In view of the results described above, a set of four more complex idealised channel was developed. These channels were designed to simulate reality better when testing the improved IDW interpolation method and comparing the results of this method with outputs produced using TIN interpolation.

These new channels again employed the four channel profiles, namely Gaussian Prism, Triangular Prism, Gaussian Sloping and Gaussian Variable, described in section 6.1. Each profile was shaped, in the horizontal, into a sinusoidal channel within a rectangular section of estuary, of width 100 metres and length 400 metres.

The bathymetry of each idealised channel was initially calculated mathematically, for every point in the channel. The results are displayed in figures 6.22 – 6.25.

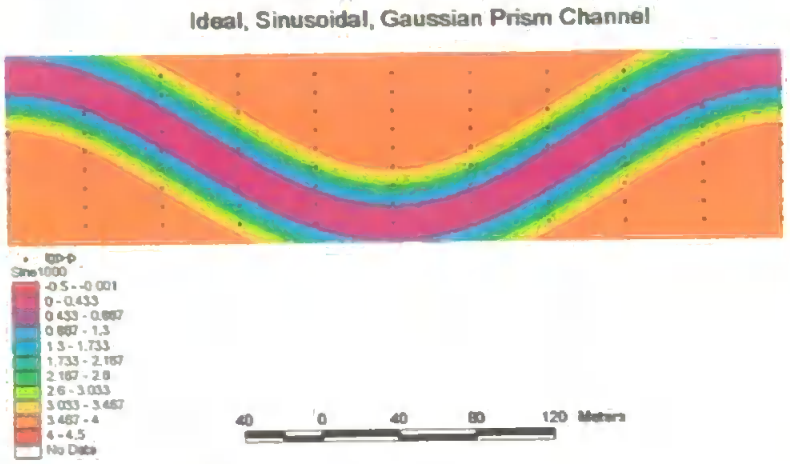

Figure 6.22 – Mathematically defined Sinusoidal Channel – Gaussian Prism.

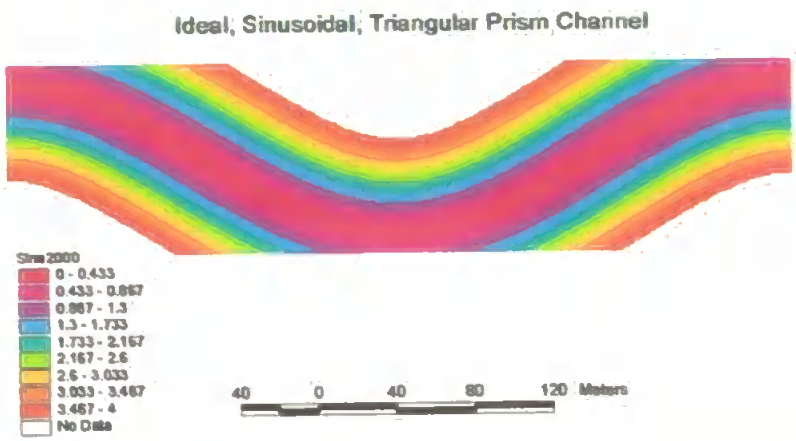

Figure 6.23 – Mathematically defined Sinusoidal Channel – Triangular Prism.

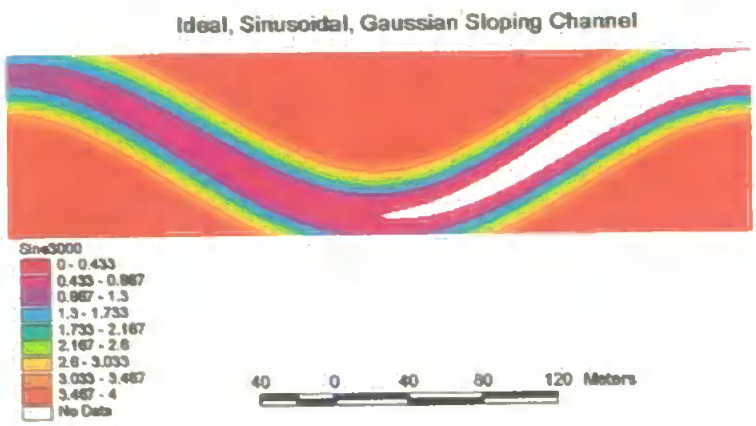

Figure 6.24 – Mathematically defined Sinusoidal Channel – Gaussian Sloping.

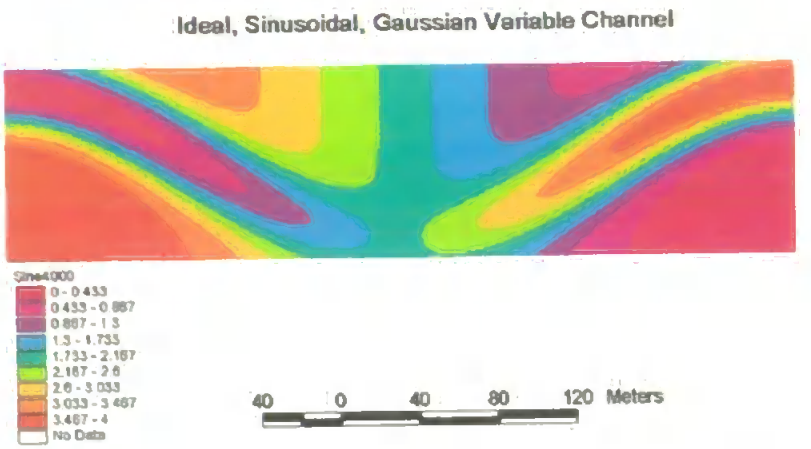

Figure 6.25 – Mathematically defined Sinusoidal Channel – Gaussian Variable.

Sounding lines across the four simulated estuaries were placed perpendicular to the banks of the estuary, at 40 metre intervals. These lines simulate a typical pattern of survey lines planned according to the shape of the estuary rather than the channels within it. Clearly, with no prior knowledge of the bathymetry within the estuary this would be the only possible way to plan a survey. For the sinusoidal channel this gives a minimum angle between sounding lines and channel of 60°.

The data from these sounding lines were interpolated using IDW with all improvements, i.e. sounding line co-ordinate system, zoning and plane fitting. The resulting standard errors are given in table 6.4. The results of this interpolation produced very poor results, with clearly visible artefacts of interpolation, figure 6.26. It can be seen from the figure that these artefacts form elliptical shapes directly influenced by transformation to the sounding line co-ordinate system. The improved co-ordinate system, based only on the positions of soundings, regardless of channel shape, is clearly inappropriate for interpolation of a channel non-perpendicular to the soundings.

Channel	SE Improved IDW	IDW with zoning and plane fitting only
Gaussian Prism	0.647	0.507
Triangular Prism	0.444	0.291
Gaussian Sloping	0.652	0.511
Gaussian Variable	0.474	0.365

Table 6.4 – Standard Error (SE) for Interpolation by improved IDW compared to IDW with zoning and plane fitting improvements only.

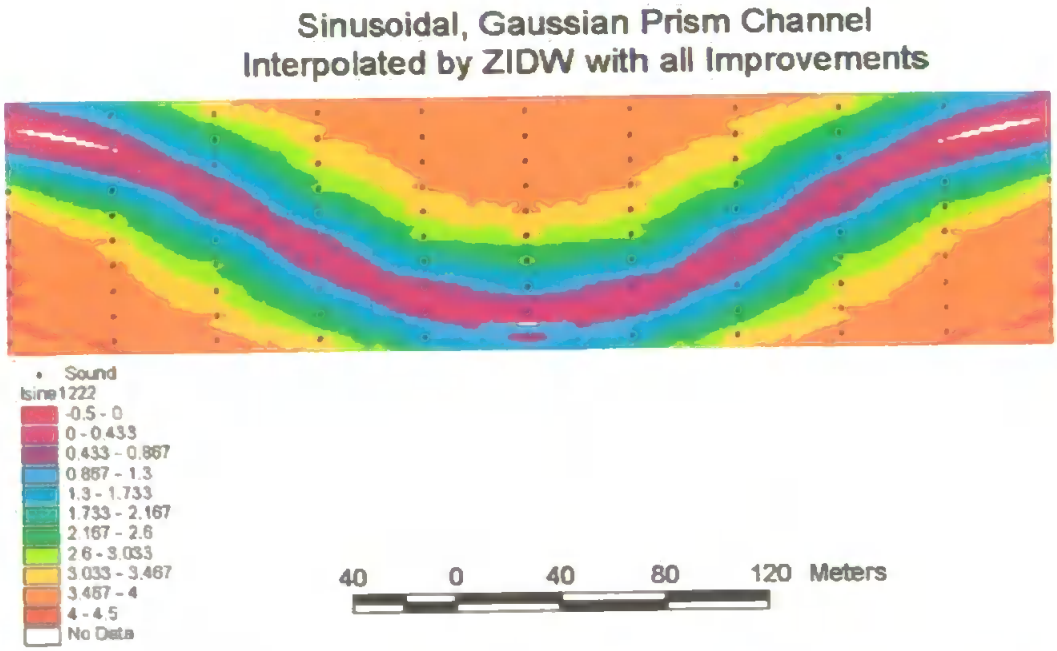

Figure 6.26 – Sinusoidal Channel Interpolated by Improved ZIDW – Gaussian Prism.

Hence, the IDW interpolation was repeated using only the zoning and plane fitting improvements. The result is an improved interpolation (see table 6.4), but artificial artefacts of the interpolation process are still produced (figure 6.27). These artefacts result from the use of a standard (x,y) co-ordinate system by default.

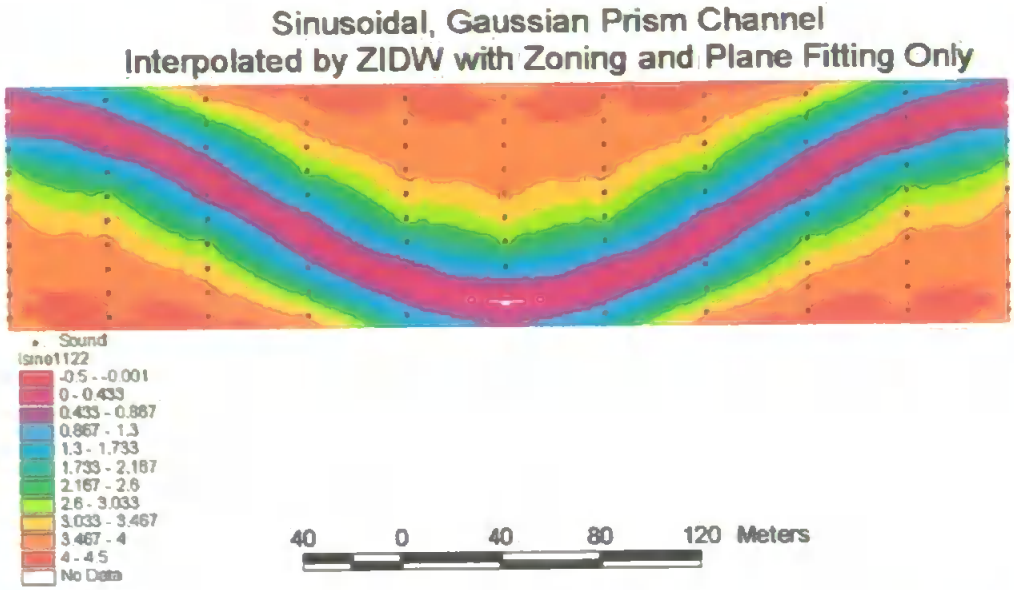

Figure 6.27 – Sinusoidal Channel Interpolated by ZIDW using zoning and plane fitting improvements only. A standard, circular interpolation radius of 50 metres has been used in this example – Gaussian Prism.

Interpolation of the four sinusoidal channels using a TIN model also produced significant artefacts of interpolation. An example of the Gaussian prism, sinusoidal channel interpolated using TIN forms Figure 6.28. This method is clearly failing, because the triangles produced are based entirely on the pattern of soundings, regardless of channel shape.

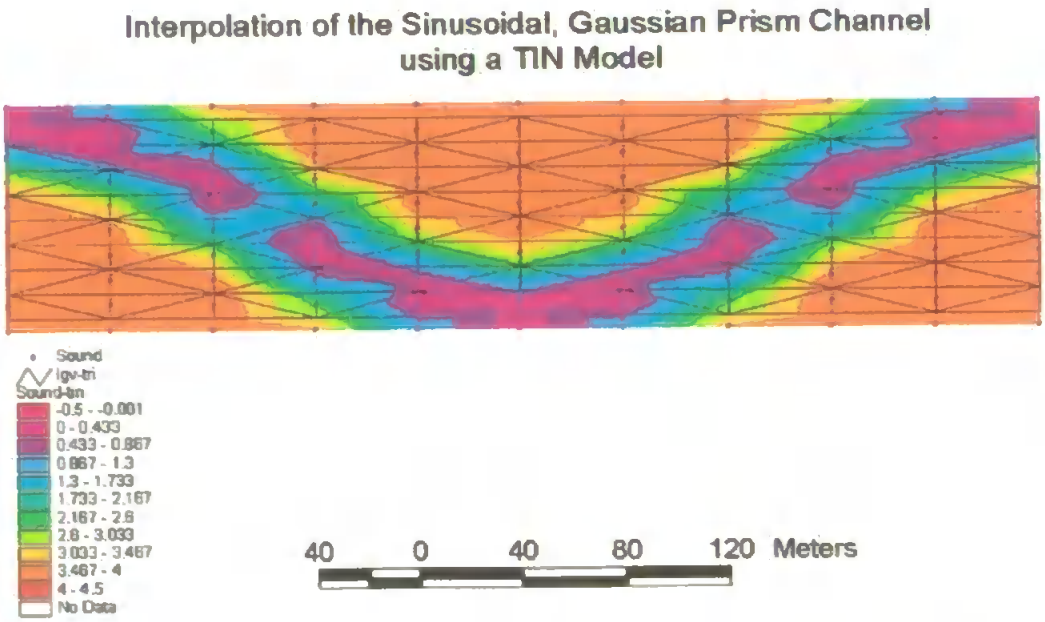

Figure 6.28 – Sinusoidal Channel Interpolated using a TIN model – Gaussian Prism.

6.6 Refining the Interpolation Process

A number of modifications were made to the ZIDW process, to improve its performance for the more realistic, sinusoidal channel cases described in section 6.5. These improvements were as follows:

1. Each sounding line was extended by addition of an extra sounding, whilst maintaining an along line sounding spacing of 10 metres, in order to provide sounding data to within 5 metres of the estuary bank. This was necessary to produce sensible results in the central area where the sinusoidal channel comes very close to the southern bank of the estuary.

2. A choice of methods for selecting soundings to be used in the interpolation was added to the program in place of the sounding line co-ordinate system. Three options were made available for selection of soundings. The first used a simple, circular interpolation radius of 50 metres, and thus performed identically to the earlier version of the program, when no change of co-ordinate system was applied. The second option was the use of an elliptical interpolation area with a semi-major axis parallel to the banks of the estuary, hence perpendicular to the sounding lines. The semi-major axis of this ellipse was chosen as 100 metres and the semi-minor axis as 25 metres. This option performs similarly to changing the co-ordinate system to a sounding line based system, as described in section 6.2. It can be seen from table 6.5 that such a system performs poorly when dealing with a channel which is not parallel to the banks of the estuary (see also section 6.5). The third option made available during revision of the program was that of a 'smart', elliptical search area. The smart ellipse uses a crude interpolation of the data to form an idea of the topography and then uses an iterative process to determine an elliptical search area with semi-major axis locally parallel to the channel at any point. Table 6.5 & figure 6.29 show that the smart ellipse produces the most realistic interpolation for the complex, sinusoidal channel.

	Circular Radius	Elliptical radius	Smart Ellipse
Gaussian Prism	0.345 0.380	0.428 0.447	0.336 0.359
Triangular Prism	0.099 0.099	0.270 0.260	0.227 0.240
Gaussian Sloping	0.350 0.384	0.435 0.452	0.339 0.360
Gaussian Variable	0.251 0.274	0.317 0.327	0.213 0.227

Table 6.5 – Standard Error (SE), in metres, for Interpolation by improved IDW using circular, elliptical and smart elliptical interpolation radii. The upper figure is the standard error for the whole, 100 metre wide channel. The lower value is the standard error calculated over the central 90 metres of the channel only. This is for comparison with results produced using a TIN model, which is capable of interpolation only for this restricted domain.

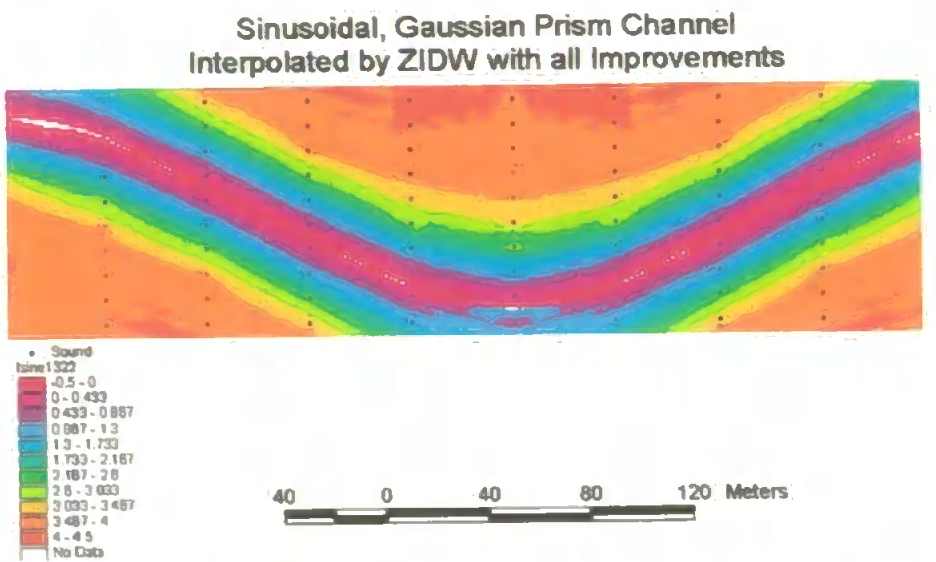

Figure 6.29 – Sinusoidal Channel Interpolated by ZIDW using Zoning, Plane Fitting and a 'Smart', Interpolation Ellipse - Gaussian Prism.

3. Equations of parametric form were employed, instead of polygonal zones (see Chapter 7), to avoid interpolation across the complex, sinusoidal channel. Here the equation, in x and y, describing each line segment is represented by two equations explicit in a parameter t, such that $x = x(t)$ and $y = y(t)$. This form can be used to determine where the two lines intersect (Angel, 1990) and hence

whether the line joining each sounding to an interpolated point crosses the channel.

The equations connecting (x_1, y_1) and (x_2, y_2) can be written, in parametric form, as:

$$x = (1-t)\, x_1 + t\, x_2$$

$$y = (1-t)\, y_1 + t\, y_2$$

$$0 \leq t \leq 1$$

As t goes from 0 to 1 all points in the segment joining (x_1, y_1) and (x_2, y_2) are generated. Equations of similar form are constructed for the second line segment, as follows:

$$x = (1-s)\, x_3 + s\, x_4$$

$$y = (1-s)\, y_3 + s\, y_4$$

$$0 \leq s \leq 1$$

At the intersection of the two line segments x and y are equal, hence:

$$(x_4 - x_3)s + (x_1 - x_2)t = x_3 - x_4$$

$$(y_4 - y_3)s + (y_1 - y_2)t = y_3 - y_4$$

Unless the two line segments are parallel, these equations may be solved for s and t. Values of both s and t between 0 and 1 indicate that the line segments intersect within the domain of interest. In the case of the interpolation program, the line joining a given sounding to the interpolated point locally intersects the channel. Further the position of this intersection point may be determined by substituting for t (or s) in the original parametric equations.

Comparison of the restricted zone standard errors, for the Gaussian Prism shaped, sinusoidal channel, interpolated using the improved ZIDW program compared to interpolation by a standard TIN model are given in table 6.6.

Interpolation Details	Standard Error for Restricted Channel
ZIDW with circular Interpolation Radius	0.380
ZIDW with Elliptical Interpolation Radius	0.447
ZIDW using the Smart Ellipse	0.336
TIN	0.496

Table 6.6 – Standard Error (SE) for Interpolation by improved IDW compared to use of a TIN Model for the Gaussian Prism shaped, sinusoidal channel.

Significantly Table 6.6 shows that for the more realistic, sinusoidal channel which is not perpendicular to the sounding lines at all points, all options of improved ZIDW perform better than the TIN model. Thus, the sinusoidal channel provides mathematical verification of the results produced practically for the Truro River. Secondly the smart elliptical search area can be seen, from the table, to produce the best interpolation of the channel data. These results will provide a theoretical basis for development of a universally applicable ZIDW program, to be tested on real sounding data from the Humber estuary, in North East England and the Gironde in Western France.

6.7 Conclusions

Improved IDW and TIN model both work well for interpolation of data in which the channel is perpendicular to the sounding lines (based on the banks of the estuary). Both methods, however, fail if the sounding lines are non-perpendicular to the channel. Partial failure occurs with angles, between sounding line and channel, of as great as 80°, with complete failure occurring for sounding line to channel angle of 60°. The development of improved IDW to incorporate a smart elliptical search radius for interpolation deals with this problem. An iterative process is used to define this smart search ellipse to be locally parallel to the channel at any point in the estuary. Such a system should be capable of successfully interpolating data from real estuaries containing meandering channels. Thus, this method will form the basis of

development of a universally applicable interpolation system to cope with multiple channels, flood and ebb channels and channel confluences, as described in Chapter 7.

Chapter 7 – Application of ZIDW to the Humber and Gironde

The continued development of ZIDW involved refining the method and suite of programs to achieve universal applicability to any estuary. Interpolation by ZIDW having been originally designed for a small estuary, the Fal (see Chapter 5), the Humber estuary, in north east England and the Gironde in western France, were chosen for this stage of the development as they represent examples of estuaries on a much larger scale. Both the Humber and Gironde, contain examples of complex hydrography, such as multiple channels and flood and ebb channels. For example, within Hull Roads, in the Humber, shipping using the docks in Hull use the deep channel along the north bank of the estuary, whilst vessels heading further upriver may follow the south channel. Such instances were highlighted previously (Chapters 5 and 6) as beyond the scope of early versions of the ZIDW software; this situation is addressed by the developments described in this chapter.

7.1 Considerations of Scale

In order to apply the ZIDW interpolation system to a range of it was first necessary to consider appropriate scaling of certain key parameters in the interpolation process. The basic parameter used to determine the interpolation radius is the average spacing between sounding lines (l). To include values from adjacent sounding lines, the radius of interpolation for each data set is taken to be equal to $1.2 \times l$. Additionally, the refinement of ZIDW by means of an elliptical search radius requires the spacing between soundings along a line (s) to be considered.

The data set obtained for the Humber estuary (from Associated British Ports, Port of Hull) contains straight, evenly spaced sounding lines. The line spacing is 100 metres throughout, whilst the soundings along each line are closely spaced at approximately 5 metres. For the Gironde estuary, however, the sounding lines appear in a considerable number of irregular blocks. Line spacing varies between blocks, exhibiting spacings of 100, 200, 400 and occasionally 800 metres. An average line spacing of 200 metres was identified as most appropriate where it was necessary to

define a single parameter, based on line spacing, in the Gironde. The average spacing of soundings along a line was taken as 20 metres.

Sounding line spacing (l), spacing between soundings along a line (s) and the corresponding interpolation radii are summarised, for each of the three test estuaries, in Table 7.1.

	Line Spacing (l)	Sounding Spacing (s)	Interpolation Radius
Fal Estuary	40 m	11 m	50 m
Humber	100 m	5 m	120 m
Gironde	200 m	20 m	240 m

Table 7.1 – Comparison of Sounding Line Spacing (l) and Sounding Spacing along a Line (s) for the test estuaries.

In addition to these fundamental parameters an appropriate method of identifying significant channels and ridges for estuaries of different scales was required. For the Fal estuary, inspection of each sounding and the sounding adjacent to it, on either side, was sufficient to determine the centre line of potential ridges and troughs. In the case of the Fal, a rise of 0.1 metres, or more, on either side of a sounding caused it to be labelled as a local channel. A fall of 0.1 metre to either side defined a ridge. During the extension of the ZIDW program suite to obtain universal applicability, however, this method of identifying channels and ridges was found to be unsuitable. For larger estuaries the method labelled an unrealistically large number of points as belonging to channels and ridges. On inspection many of these points were found to represent small undulations in the mud banks and even slight inaccuracies in the data. Clearly, a scale-dependent method of identifying channels and ridges was required.

Initially, the gradients of the channel and ridge sides were compared. The relatively narrow Fal estuary exhibited typical channel edge slopes of 60 mm/m, whilst the main channel in the Humber had edge gradients of 16 mm/m with shallower gradients, less than 10 mm/m, in the south channel. These gradients demonstrate the increased importance of using a zoned interpolation method in small estuaries, such as the Fal.

The half-width used to define channels was determined, experimentally, to be in a ratio of 1:4 with the interpolation radius. For example, a half width of 30 metres was used for defining channels and ridges in the Humber, where an interpolation radius of 120 metres was used (see above). The number of soundings within the half width, and therefore required to identify a channel or ridge, thus varies according to the spacing of soundings along the sounding line.

The half width was used to identify maxima and minima within the MAXMIN.EXE program (see section 7.2). In addition a height difference of 0.2 metres or more was specified to avoid false identification of data inaccuracies as channel or ridge points.

To prevent the data files becoming unmanageably large the cell size for interpolated data was determined by the area covered by each estuary. Whereas a 1 metre grid was appropriate in the Fal, coarser resolutions, of 2 metres for the Humber and 20 metres for the Gironde, were employed to prevent the number of cells from significantly exceeding 20×10^6.

7.2 Initial Development of Universally Applicable ZIDW

During the initial stages of automating the ZIDW process (Chapter 5, Section 5.1) a flow chart of the stages required for successful automation was developed (Figure 5.3). In the light of changes to the ZIDW process, devised as a result of testing on mathematically defined estuaries (Chapter 6), and the requirement for universal application of the program suite, an updated flow chart, (Figure 7.1) was produced.

For ZIDW programs to be made universally applicable it proved necessary to split the SLINES.EXE program, which previously identified sounding lines and located maxima and minima, into two separate programs. The new SLINES.EXE is applied to identify sounding lines only. It is used for data sets in their originally collected format, i.e. in sounding lines order; this applies to the Fal and Humber estuary data sets. If the data have been re-arranged, as in the Gironde estuary, a fundamentally different process of sounding line recognition is required (see Section 7.3). The second function of the original SLINES.EXE, namely locating channels and ridges, is

performed by a new program, MAXMIN.EXE. A user's guide to the suite of programs forms appendix 6, and the formats of files used by each program are given in appendix 7.

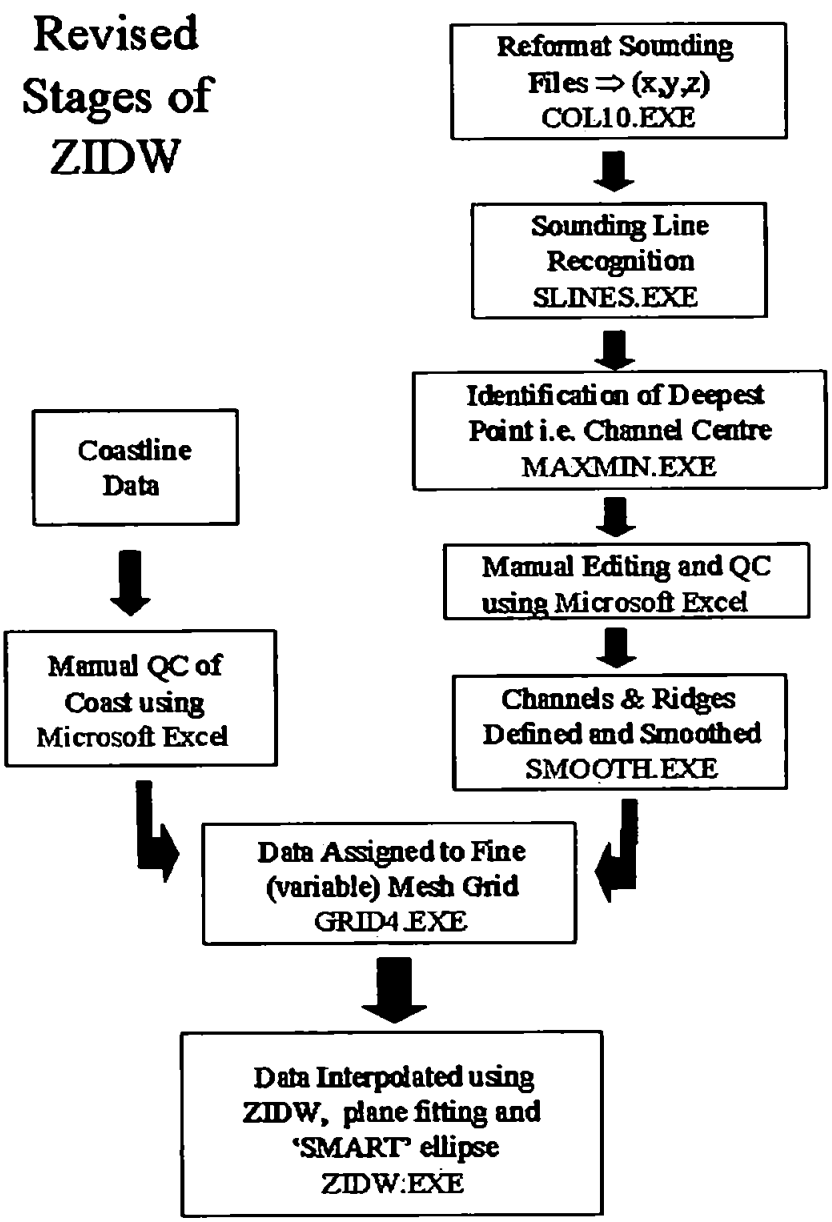

Figure 7.1 – Revised Stages of ZIDW. The program used to apply each process appears in blue.

MAXMIN.EXE initially identifies the deepest sounding in each sounding line and labels this as the main channel (C). Subsequently all other points in the line are examined to determine whether they represent local maxima (R) or minima (T). This part of the program uses a half width appropriate to the scale of estuary (see section 7.1). This half width is used to determine the average number of soundings, on either side of a given point, required to determine whether the point represents the centre point of a channel or ridge. In the case of the Humber, the half width (equal to interpolation radius divided by four) will be 30 metres. Given that the sounding spacing (s) in the Humber is 5 m, an average of 6 soundings will lie within the 30-metre radius. Hence, the MAXMIN.EXE program looks for a depth difference of 0.2 metres or more between the average and central depths over 6 soundings to either side of the central value, along a line. In the case of the Fal, with a half width of 50/4 = 12.5 metres and a sounding spacing of = 11 m., only 1 sounding to either side of the central point will be considered.

Having run the programs thus far, it is necessary manually to construct channels and ridges from the maxima and minima identified by MAXMIN.EXE. This process is carried out using a Microsoft Excel spreadsheet and scatter plots of the data points. To maintain consistency when joining maxima and minima into ridges and channels the scale of the estuary must, once again, be considered. Thus, the distance over which points may be considered as adjacent nodes is determined in terms of the number of spaces between lines. As a general rule, the number of line spaces across which a continuous channel or ridge may be joined should not exceed five. This represents a maximum distance of 200 metres in the Fal, 500 metres in the Humber and 1 kilometre (for lines spaced 200 metres apart) in the Gironde.

7.3 The Gironde Estuary

Owing to the unusual format in which the sounding data for the Gironde was supplied, some additional processes were required to produce data in a format compatible with the ZIDW program suite. Figure 7.2 shows an extension of the flow chart of stages of ZIDW (Figure 7.1) to include these special requirements.

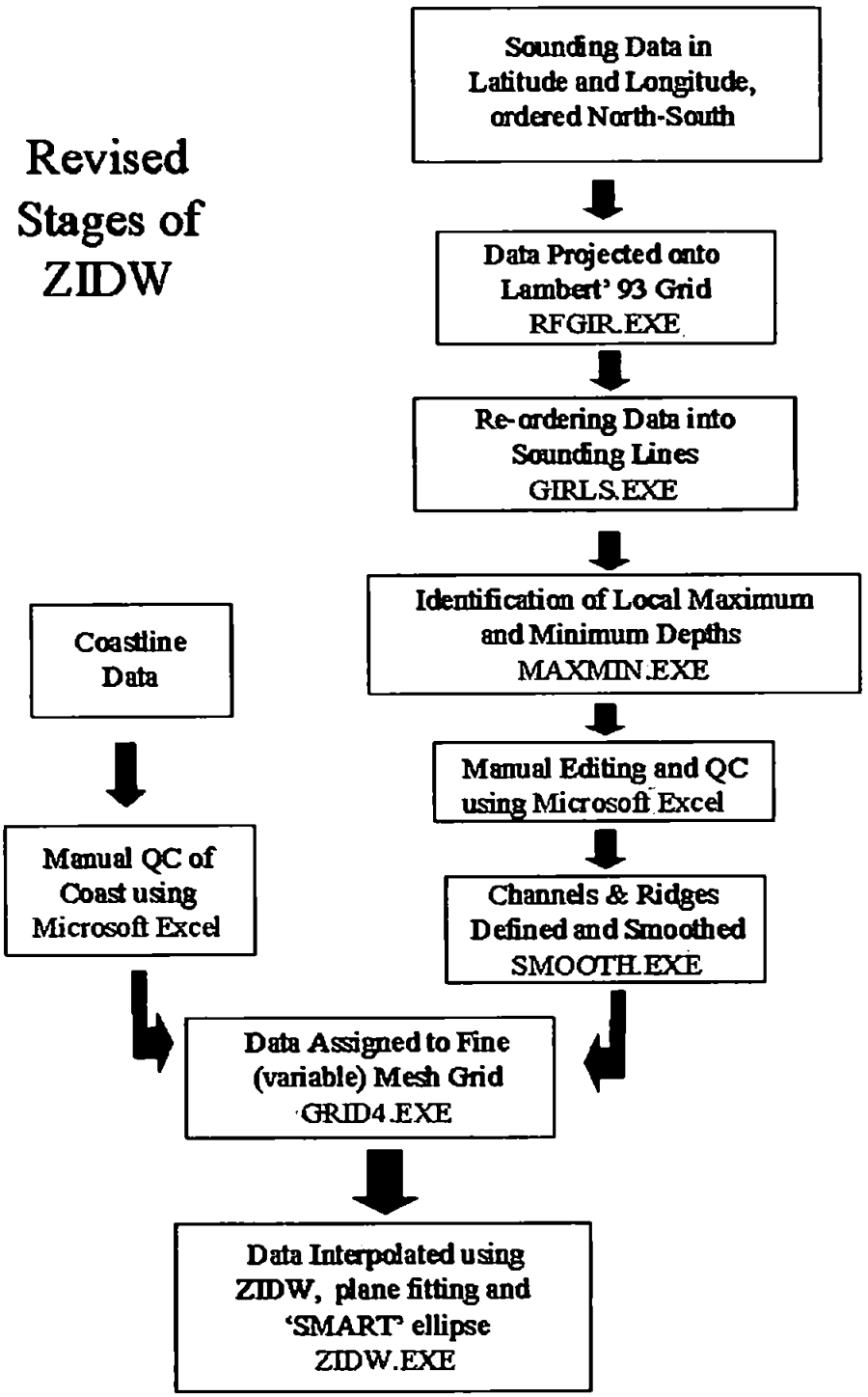

Figure 7.2 – Extension of the stages of ZIDW to allow for an unusual data format, such the data for the Gironde estuary. The program used to apply each process appears in blue.

Sounding data for the Gironde estuary were supplied as latitude and longitude with reference to the French geographic system. Hence, it was necessary to project the data, using a Lambert conical projection onto the new French grid system, Lambert '93. The technical details of this process appear in appendix 9. An additional program, RFGIR.EXE, was constructed to carry out this conversion, as the software available at the University of Plymouth did not include projections for France.

Unusually the data for the Gironde estuary were supplied in a format ordered from north to south, rather than the along sounding lines as it would have been when the data were collected. Hence, it was not possible to use the SLINES.EXE program, which considers the change in direction between adjacent soundings, in order to assign the soundings to lines. An alternative program, GIRLS.EXE, employing an entirely different principle, was devised to allocate the sounding data to lines. Here, the Gironde data were divided into a series of quadrilateral shaped areas. Each quadrilateral surrounded data, determined by visual inspection, to lie along lines of approximately equal spacing running in the same direction. The four vertices, of the quadrilateral, and the number of lines within it were then specified by means of an input file to the GIRLS.EXE program. From this information the program was able to determine the expected position of each sounding line and assign all soundings lying on or near these positions to the correct line (see figure 7.3). Initially a tolerance of ±20% was applied to the sounding allocation process. This resulted in about 1700 out of 2400 sounding-points been allocated to lines. Since all soundings were collected along sounding lines, the offline tolerance was increased to ±30% and later ±40%, increasing the number of points assigned to lines to about 2100 and 2300, respectively (see table 7.2).

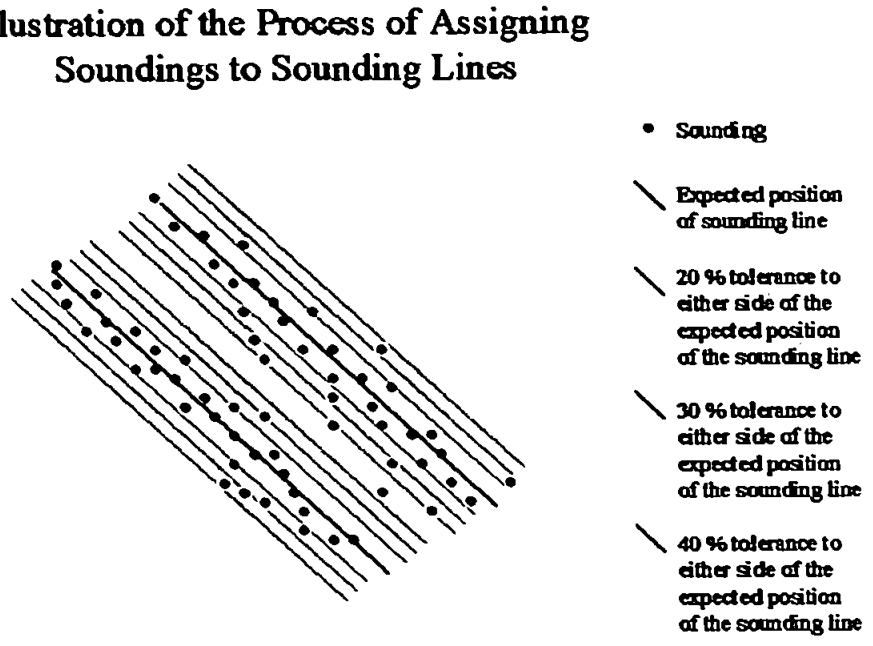

Figure 7.3 – Illustration of the allocation of soundings to expected positions of sounding lines, including the various offline tolerances.

Tolerance to either side of the identified position of the sounding line, as a percentage of the spacing between lines.	**Approximate number of soundings allocated to a line (total number of soundings = 2400).**
20%	1700
30%	2100
40%	2300

Table 7.2 – Summary of the number of soundings allocated to sounding lines, for various tolerances. Tolerances are given as a percentage of the spacing between sounding lines.

Having assigned the soundings to lines via the GIRLS.EXE program, the local maxima and minima on each line could be determined using the MAXMIN.EXE program, as for the other data sets (see section 7.2).

7.4 Refinements to the Interpolation Process

The final version of ZIDW employ a 'smart' interpolation ellipse, as described in section 7.6. The application of such an ellipse to real channels introduces a requirement that these channels are smooth. Previously channel points were joined using straight lines from one point to another, regardless of any scatter in the data (see section 6.3.1). This simple approach facilitated the unambiguous assignment of data to polygons. Since polygonal zones will no longer be defined (see section 7.6), combined with the necessity that the 'smart' ellipse follows the overall trends in channel direction, it was necessary to introduce a method of producing a best fit curve through the channel data. The 'smoothing' process was carried out by an additional program, within the ZIDW program suite, entitled SMOOTH.EXE. This program employs a subroutine from the Fortran mathematical programs library (Akima, 1978). The method of cubic splines in two directions (east and north) is used produce a best-fit curve through the data.

The method was first tested on a mathematically defined parabola. 201 equally spaced points were defined along the curve $y = x^2$, over the range $-2 < x < 2$. In order to randomise these points, 201 random numbers, between 0 and 1, were generated using a random number generator from the Fortran program library (RNUN). These random numbers were redistributed over the range -1 to 1, and multiplied by a factor of 0.2, to obtain a suitable range of scatter when added to the points on the parabola. The scattered points could then be smoothed, via the cubic splines method, employed by SMOOTH.EXE, and compared to the original parabola. The results of this test (shown in figure 7.4) clearly show the smoothed curve to be almost identical to the original parabola.

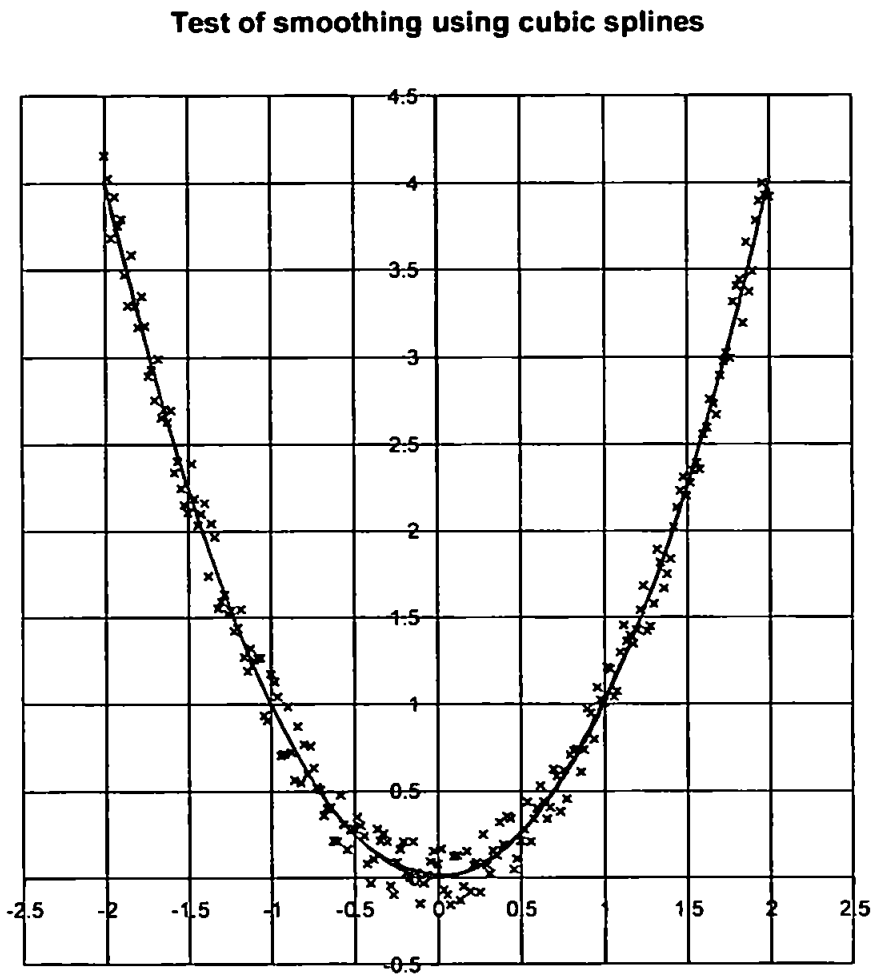

Figure 7.4 – Smoothing of data scattered randomly about a parabola. The dark blue curve shows the curve $y=x^2$, the dark blue crosses the randomly scattered data points and the red curve was generated through the points using SMOOTH.EXE.

Having ensured the subroutine was producing sensible results, the SMOOTH.EXE program was improved to determine of the actual point spacing by application of Pythagoras' Theorem between each adjacent pair of co-ordinates. To ensure successful operation of this part of the program, a facility to identify and eliminate duplicate sounding points was introduced into SMOOTH.EXE. The channel points, identified by MAXMIN.EXE, and the associated best-fit curves, generated by SMOOTH.EXE, for three reaches of the Gironde estuary are shown in figure 7.5.

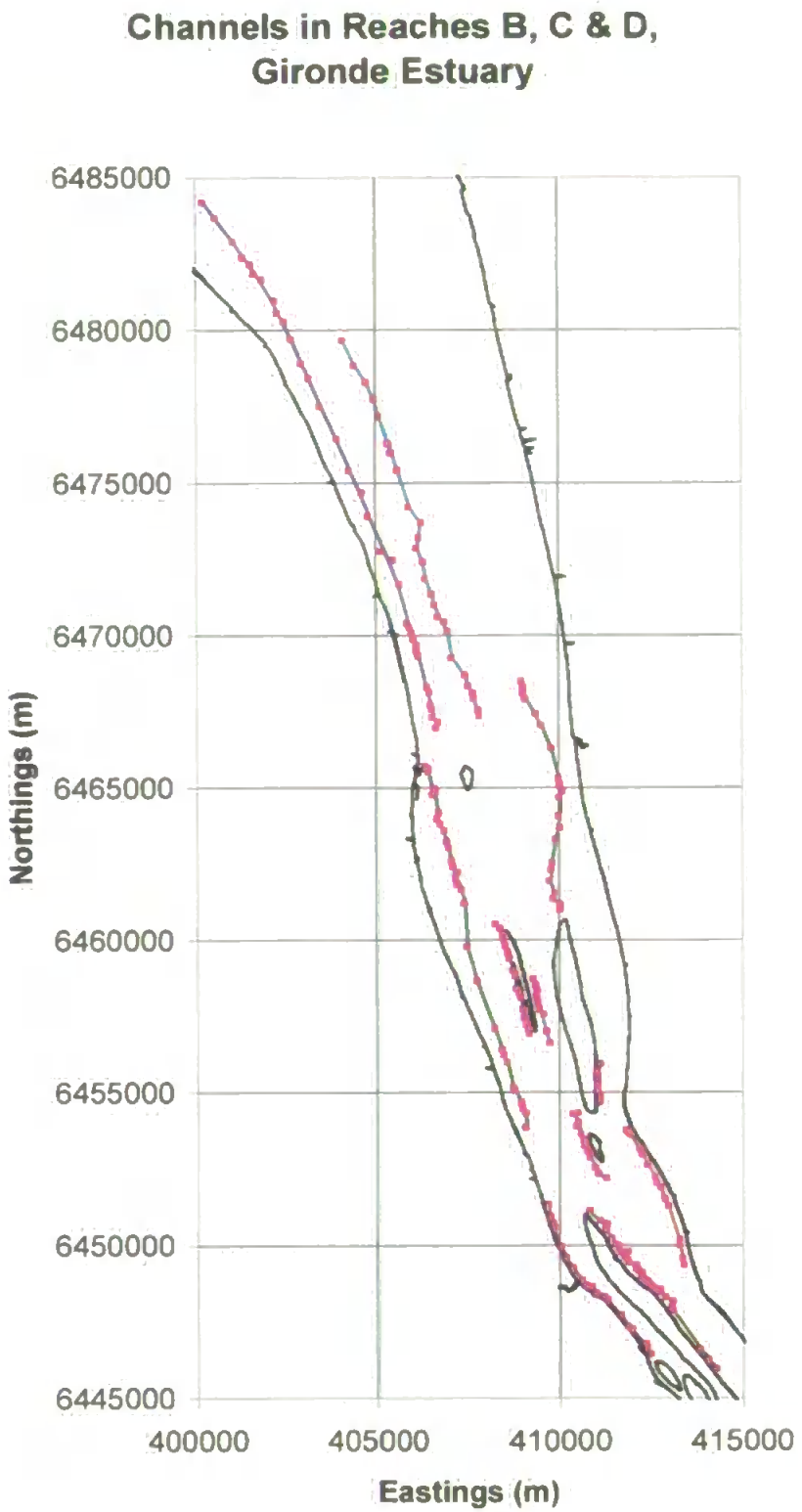

Figure 7.5 – Channels identified from scattered soundings (pink dots) with best-fit curves assigned by the SMOOTH.EXE program (dark coloured lines). Coastlines and islands are in black.

The application of SMOOTH.EXE is shown in greater detail, for a single channel (CO2) within the Gironde, in Figure 7.6.

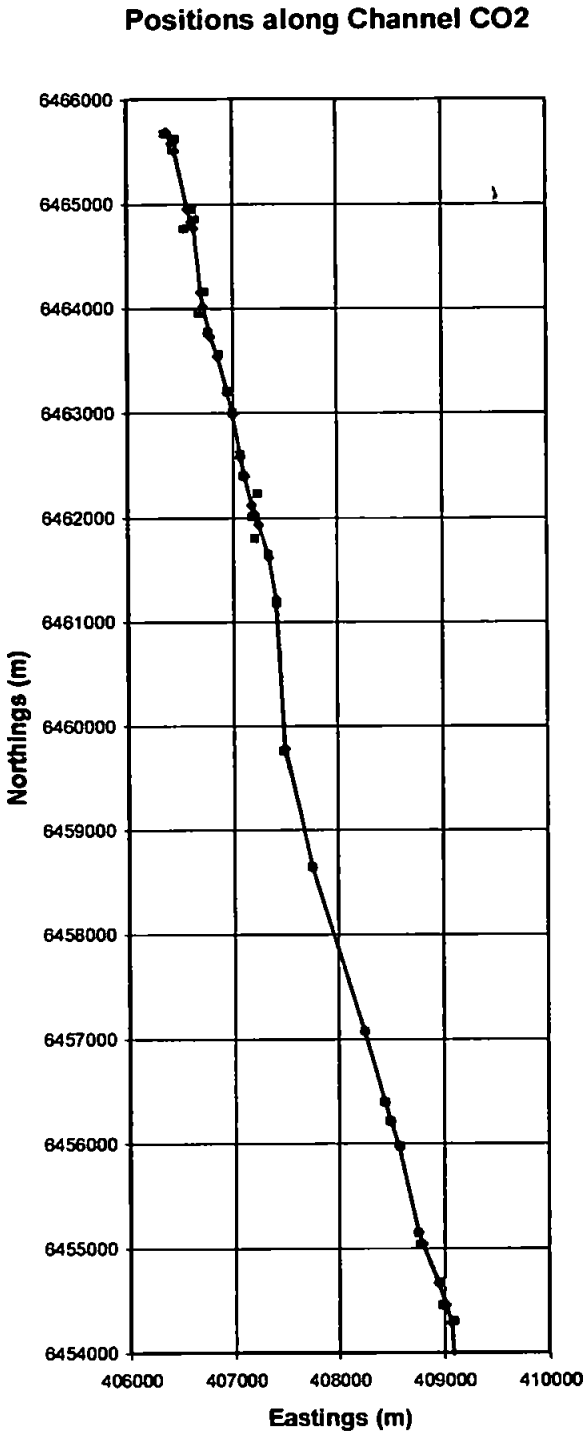

Figure 7.6 – Channel CO2, in the Gironde estuary, defined by scattered soundings (pink dots) and best-fit curve assigned by the SMOOTH.EXE program (dark blue line).

To apply ZIDW using the best-fit channel curve (defined as above), it was necessary to assign depth values to this curve. Clearly it would be inappropriate to assign the actual, known sounding values to the best-fit channel as these lie at scattered points, frequently several metres from the curve. The SMOOTH.EXE program was extended to calculate the required depths by use of the same curve fitting algorithm, based on cubic splines, as was employed in the x and y directions. The results were analysed using an Excel spreadsheet and found, by visual inspection, to be satisfactory. An example, showing the depths at scattered sounding positions and along the best-fit curve is given in Figure 7.7.

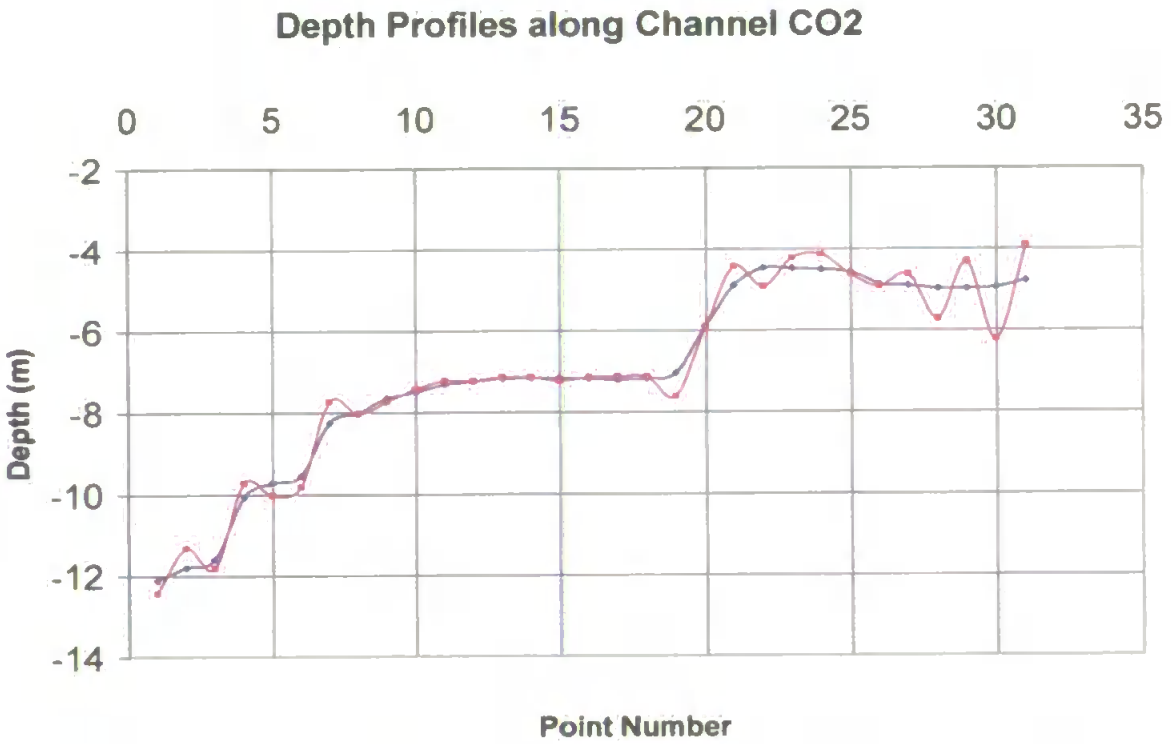

Figure 7.7 – Profile through the scattered, channel soundings (pink curve) in channel CO2 in the Gironde estuary and the profile along the corresponding best-fit channel curve (dark blue curve).

The smooth, best-fit channel, produced using SMOOTH.EXE, is then used to determine the direction of the 'smart' interpolation ellipse, as part of the interpolation program ZIDW.EXE. This was initially achieved by extending a perpendicular from each point within the interpolation grid to the smooth channel. The smoothing process should ensure that a unique segment of channel is intersected by this perpendicular. The direction of the semi-major axis of the 'smart' ellipse is given by the direction of this unique channel segment. As the co-ordinates of the ends of the

channel segment are known, segment direction is straightforwardly calculated, within the ZIDW.EXE program, using the rule governing the tangent of angles within a right angled triangle (see figure 7.8).

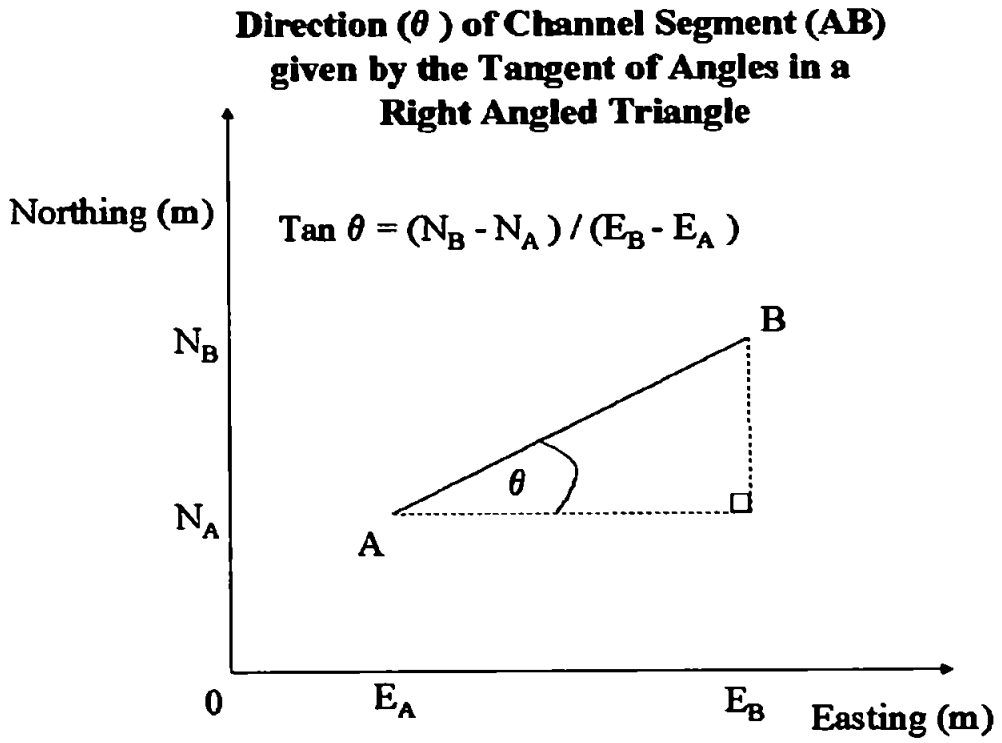

Figure 7.8 – Determination of the direction of a segment of channel using the rule governing the tangent of angles within a right angled triangle.

Where more than one channel exists locally to the interpolation point, an inverse distance weighted mean of the directions of each channel segment is used to give the direction of the 'smart' interpolation ellipse at the point. The distance from the point to each channel is determined using the theorem of rotation of axes. Here, one end of the channel segment is taken as the origin of the transformed co-ordinate system and the axes are rotated to be parallel and perpendicular to the channel segment. The perpendicular distance from the test point to the channel segment is then equal to the 'y' co-ordinate of the test point in the transformed co-ordinate system (see figure 7.9).

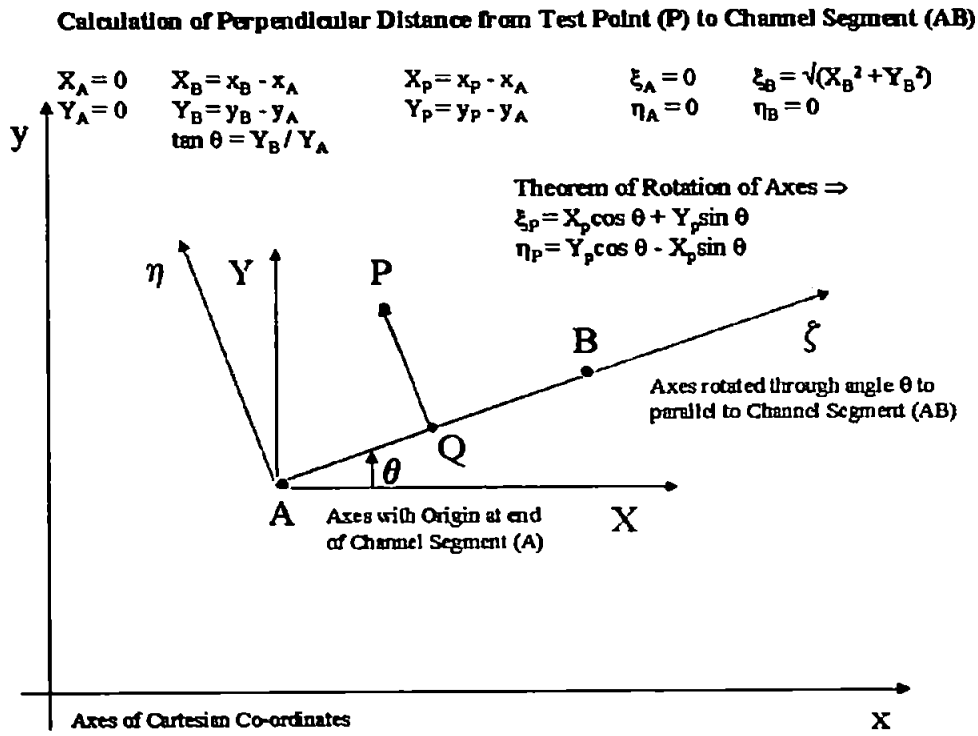

Figure 7.9 – Calculation of the distance between the test point and the segment of channel closest to it, using the Theorem of Rotation of Axes.

To allow for the problems associated with branching channels and flood and ebb channels, as described in sections 6.3 and 6.4, parametric equations (see section 7.6) rather than polygonal zones are used to prevent interpolation across the smoothed channels and ridges.

Having defined the 'smart' ellipse for each point, all soundings within a search area are tested, by the ZIDW.EXE program, to determine their effect on the depth of the point. A search area is used to prevent the need to consider every sounding within the entire data set, thus speeding up the operation of the program. The search area is defined as the large square, 100 grid cells by 100 grid cells, in which the test point lies and the 8 large squares surrounding it (see figure 7.10). This ensures that all soundings within the interpolation ellipse are included within the 'smart' ellipse even if the test point lies close to the edge of a large square. For the Fal estuary, the 1 metre cell size produces a large squares of 100 metres × 100 metres i.e. one hectare. Larger squares of 200 metres × 200 metres and 2 kilometres × 2 kilometres are generated by cell sizes of 2 and 20 metres in the Humber and Gironde, respectively.

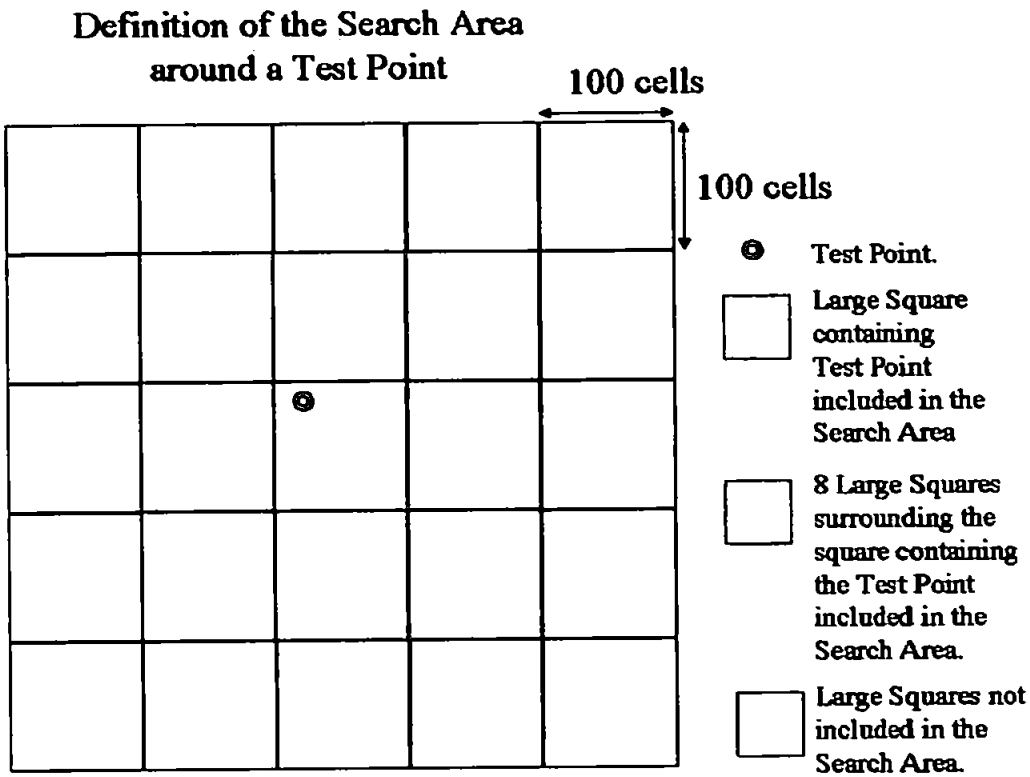

Figure 7.10 – Definition of Search Areas to improve the performance of the ZIDW.EXE program.

The procedure used to test each sounding point to determine whether it will affect a given test point is illustrated in figure 7.11.

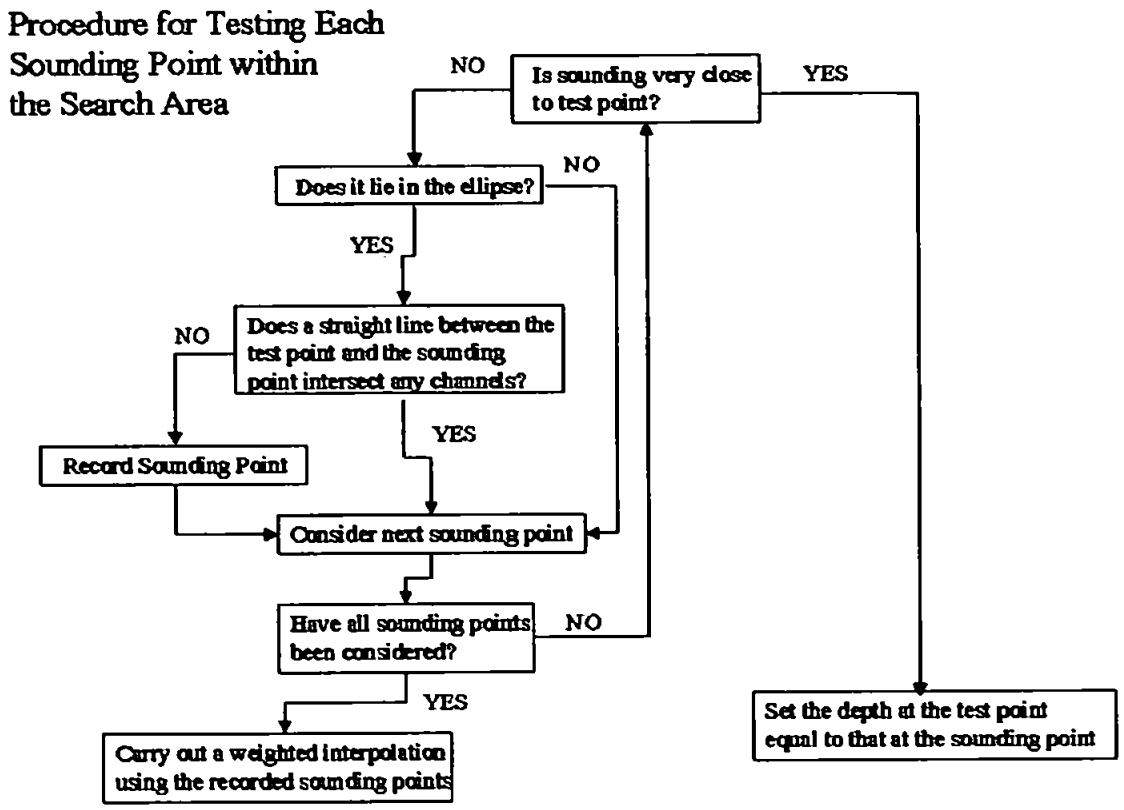

Figure 7.11 – Procedure for testing each sounding lying within the search area (as described above).

Finally, the data are interpolated, by the ZIDW.EXE program, using inverse distance weighting, with a 'smart' interpolation ellipse, interpolation prevented across all channels and plane fitting to improve the interpolation process.

This method of ZIDW, using channel boundaries rather than polygonal zones, results in interpolation of sounding data across the coastline. To avoid this 'leakage' of data onto the land, the concept of polygons was reintroduced. These new polygons prevent interpolation outside the banks of the estuary, whilst the system of parametric equations (section 7.6) continues to incorporate zoning as the method of avoiding interpolation across channels and ridges.

7.5 Improving the Universal ZIDW Program Suite

The initial version of the universally applicable ZIDW.EXE program defined a 'smart' ellipse for every point on the fine mesh grid, using the procedure described in section 7.4. This method proved to be extremely time-consuming, even when run on a fast, modern PC. In order to increase the speed of operation of the program, a method calculating the parameters of a 'smart' ellipse at the four-corners of each large square (100 cells × 100 cells) within the survey area was considered. In this case linear, two-dimensional interpolation could be employed to determine the parameters of the ellipse at all other points within the square. Whilst this revised method might present a suitable compromise for estuaries containing a single deep channel, such as the Fal, difficulties would arise when defining the direction of the 'smart' ellipse for large squares containing more than one channel. Hence, to maintain universal applicability of the ZIDW program, it was decided to concentrate on refining the method defining the angle of the 'smart' ellipse for every grid cell within the estuary.

The direction of the semi-major axis of the 'smart' ellipse was originally determined by extending a perpendicular from the point to be determined to the closest segment of channel to this point, as described in section 7.4. This approach, however, was found to produce a series of circular bands of data, clearly identifiable as artefacts of interpolation, near vertices in the channel. These artefacts are shown in figure 7.12.

These circular bands were generated as the method of defining the direction of the interpolation ellipse is unable to resolve situations where:

- test points are equidistant from two channel segments
- no perpendicular to a local channel segment exists.

The second of these unresolved cases is shown in figure 7.13.

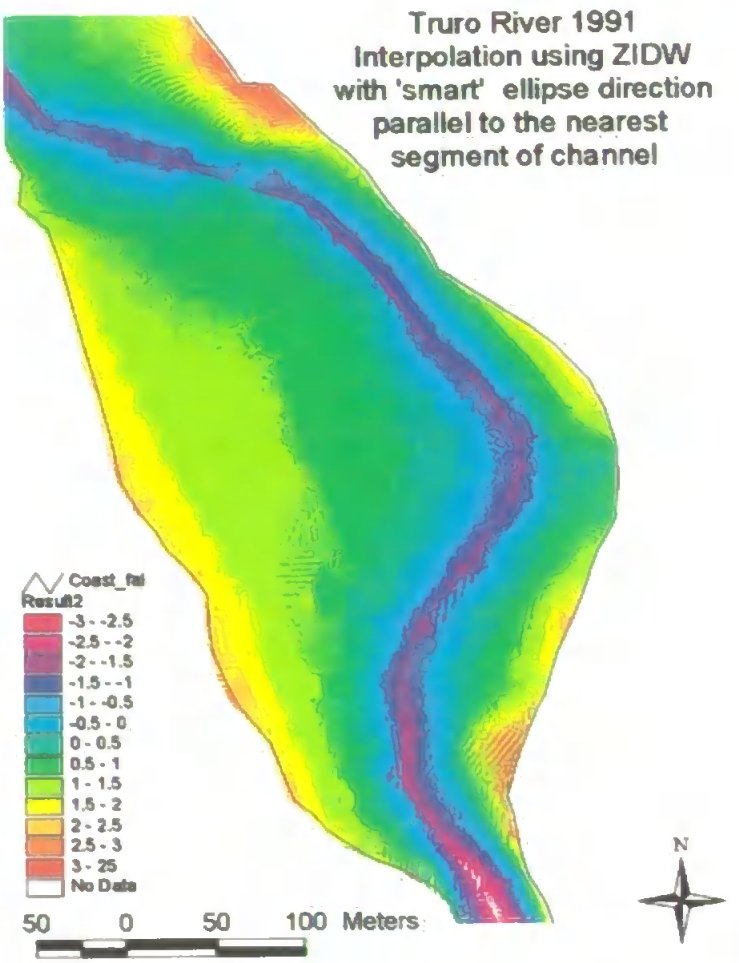

Figure 7.12 – Interpolation of bathymetric data from the Truro River by ZIDW using a 'smart' interpolation ellipse, with the direction of the semi-major axis of the ellipse parallel to the nearest segment of channel.

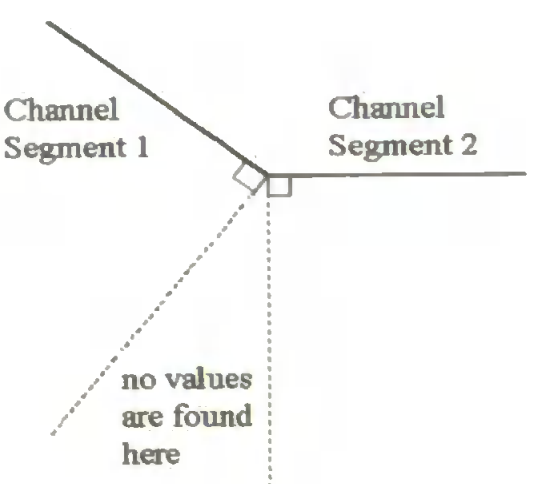

Figure 7.13 – Anomalous case where no perpendicular to a local channel segment exists.

In order to avoid the anomalies described above a weighted mean of the gradients of the two closest channel segments to each grid cell was applied to determine the direction of the 'smart' ellipse, as illustrated in figure 7.14.

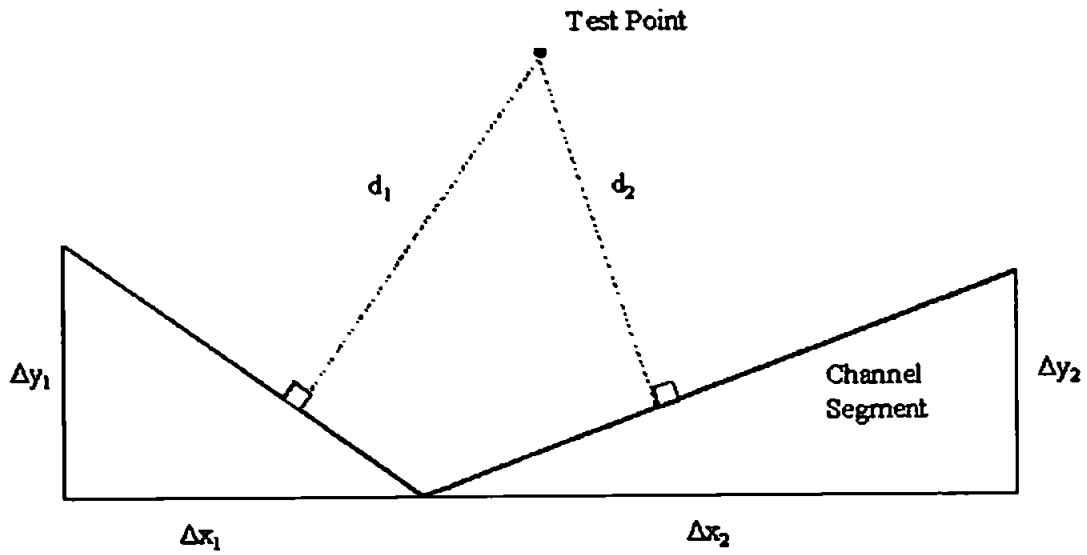

Figure 7.14 - Use of the weighted mean, of the direction of two channel segments, to determine the direction of the semi-major axis of the 'smart' ellipse.

The weighted mean of the direction of the two channel segments was applied using the following formula:

$$\tan \vartheta = \frac{\sum W_i \frac{\Delta y_i}{\Delta x_i}}{\sum W_i} \qquad \text{where: } \sum W_i = \sum \frac{1}{d_i}$$

This revised method, using weighted means, significantly reduced the interpolation artefacts around vertices of the channel. The results are shown in figure 7.15.

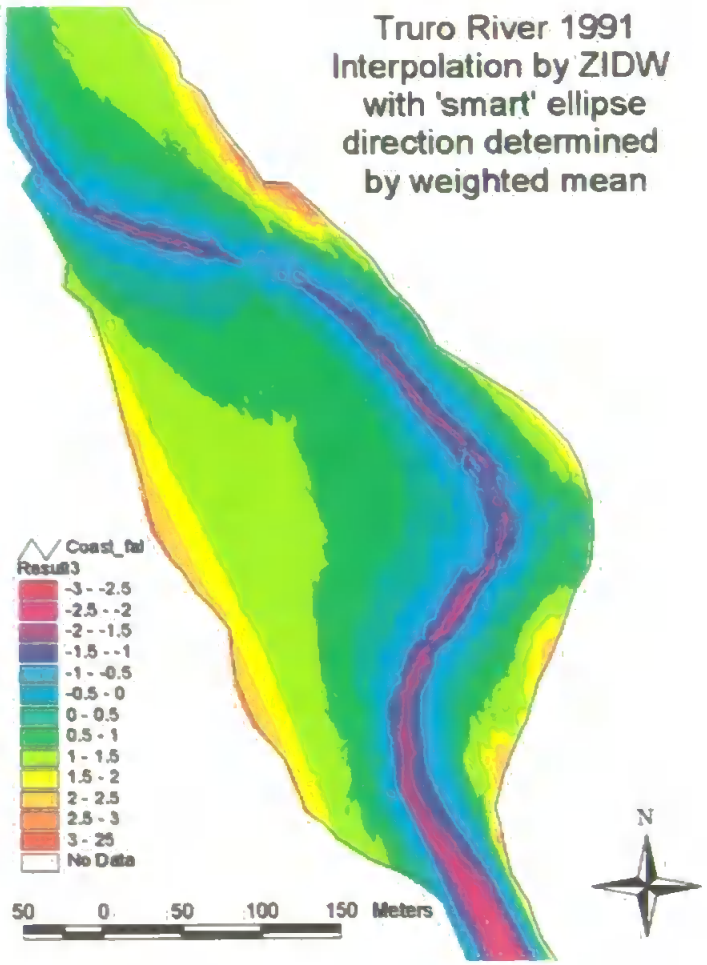

Figure 7.15 – Interpolation of bathymetric data from the Truro River by ZIDW, using a 'smart' interpolation ellipse, with the direction of the semi-major axis of the ellipse determined as a weighted mean of the direction of the nearest channel segments.

Relatively small anomalies, however, remain in the vicinity of channel vertices exhibiting significant changes in the direction of the channel. The formula used will also result in mathematical singularities at $\Delta x_i = 0$. In view of these remaining anomalies, an entirely new method of determination of the direction of semi-major axis of the 'smart' ellipse was formulated. Instead of concentrating on segments of the channel, as previously, this new approach defined ellipse direction relative to each vertex of the channel. Taking the direction of the semi-major axis of the 'smart' ellipse as that of the channel, at points on the channel to either side of a vertex, the direction at non-channel points will vary linearly between these two directions according to their angle around the vertex. This is illustrated in figure 7.16.

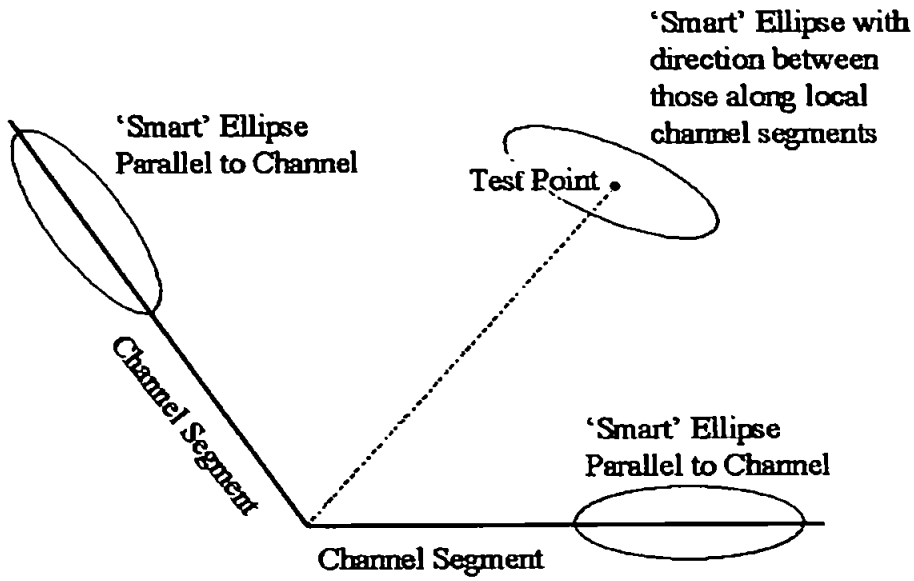

Figure 7.16 – Variation of the direction the 'smart' ellipse with angle about local channel vertices (not to scale).

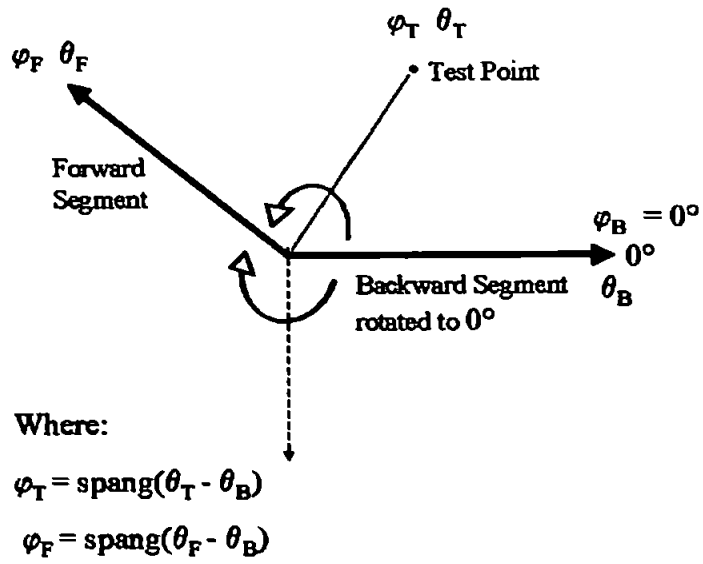

Figure 7.17 – Determination of the direction of the semi-major axis of the 'smart' ellipse, relative to the direction of local channel segments, derived about the local channel vertex.

The sense of variation of the ellipse direction is necessarily opposite for the obtuse angle, made by channel segments, compared to the corresponding reflex angle (see

figure 7.17). Hence, the direction of the semi-major axis of the 'smart' ellipse (D_T) is give by:

$$D_T = D_B + \frac{\varphi_T}{\varphi_F} \times (D_F - D_B) \qquad \text{for } \varphi_T < \varphi_F$$

$$D_T = D_B + \frac{spang(360° - \varphi_T)}{spang(360° - \varphi_F)} \times (D_F - D_B) \qquad \text{for } \varphi_T < \varphi_F$$

Where: *'spang'* is a subroutine developed to confine an angle to within the range 0° to 360°.

This method was shown to remove the interpolation artefacts seen previously in the vicinity of vertices of the channel, as shown in figure 7.18.

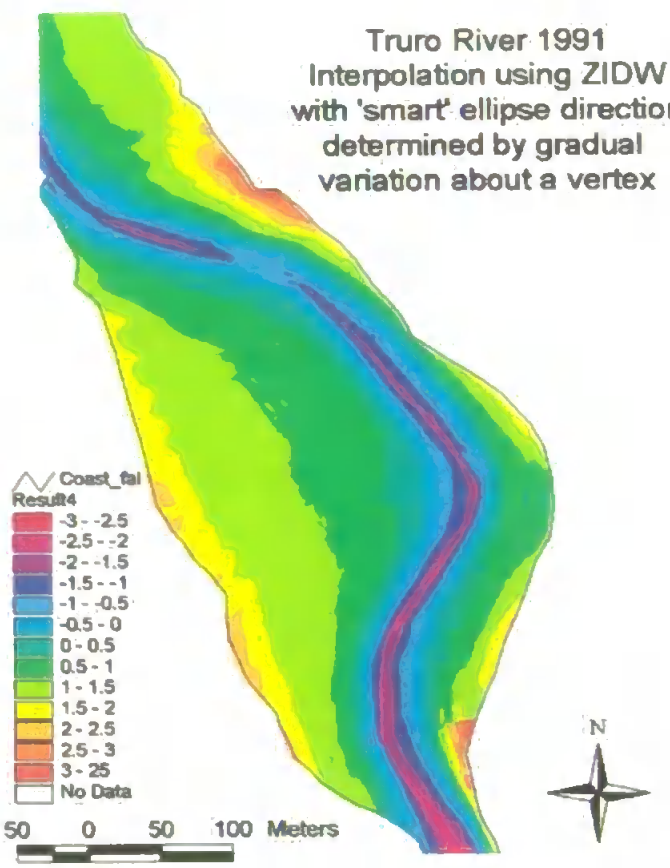

Figure 7.18 – Interpolation of bathymetric data from the Truro River using ZIDW and a 'smart' interpolation ellipse, with the direction of the semi-major axis determined by gradual variation about a vertex.

Finally, depths within the channel were overwritten by values interpolated from only other channel values, to produce a continuous channel avoiding visible artefacts of the interpolation process.

Having verified the final version of ZIDW in the Fal estuary (figure 7.18), the program suite was applied to bathymetric data from the Humber and Gironde estuaries (figure 7.19 and 7.20).

These figures clearly show the success of this version of ZIDW in dealing with multiple and non-continuous channels and ridges, highlighted, in chapter 5, as producing anomalous results when interpolated by earlier versions of the program suite.

The Humber data (figure 7.19) demonstrate the interpolation of major, non-continuous channels and ridges. In the eastern half of the figure, the non-continuous, deep channel on the north side of the estuary is used by vessels bound for Hull Docks, there is also a secondary, southern channel used at certain times by smaller vessels heading further upriver. From either channel it is necessary to cross a middle ground to reach the only channel, on the north side, in the western half of the displayed area.

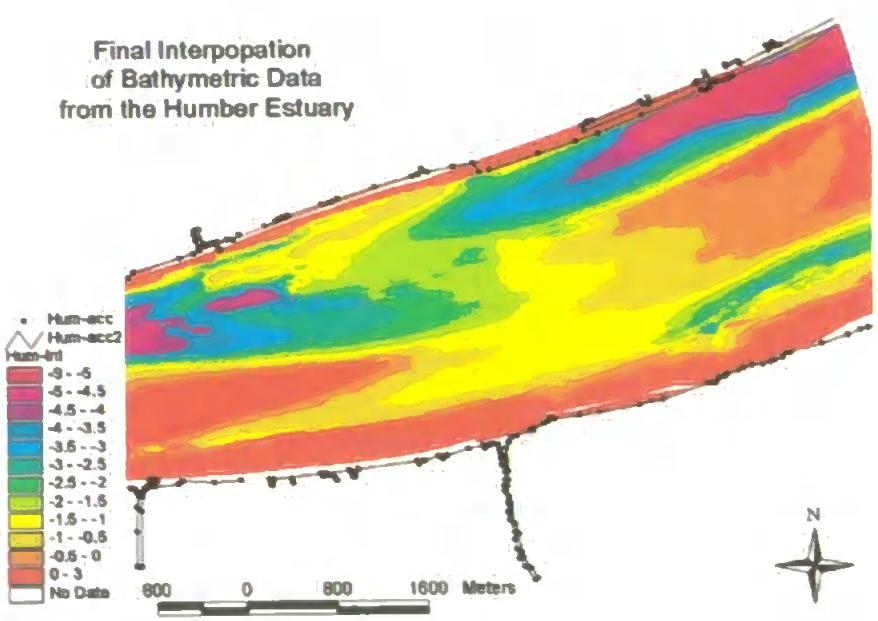

Figure 7.19 – Interpolation of bathymetric data from the Humber estuary using the ZIDW program suite

Figure 7.20 clearly shows the main, deep, navigation channel running along the west side of the Gironde estuary; a secondary channel close to the east bank and a number of non-continuous channels and ridges in the central part of the estuary. Interpolation around islands lying entirely above the high water mark is also performed successfully, by ZIDW, within the Gironde estuary (figure 7.20). Investigation of the occasional cells exhibiting erroneous or 'no-data' for the Gironde estuary (figure 7.20), revealed these apparent anomalies to result from the combination of data sets collected at different times, within the data supplied to this project, rather than from irregularities in the interpolation method.

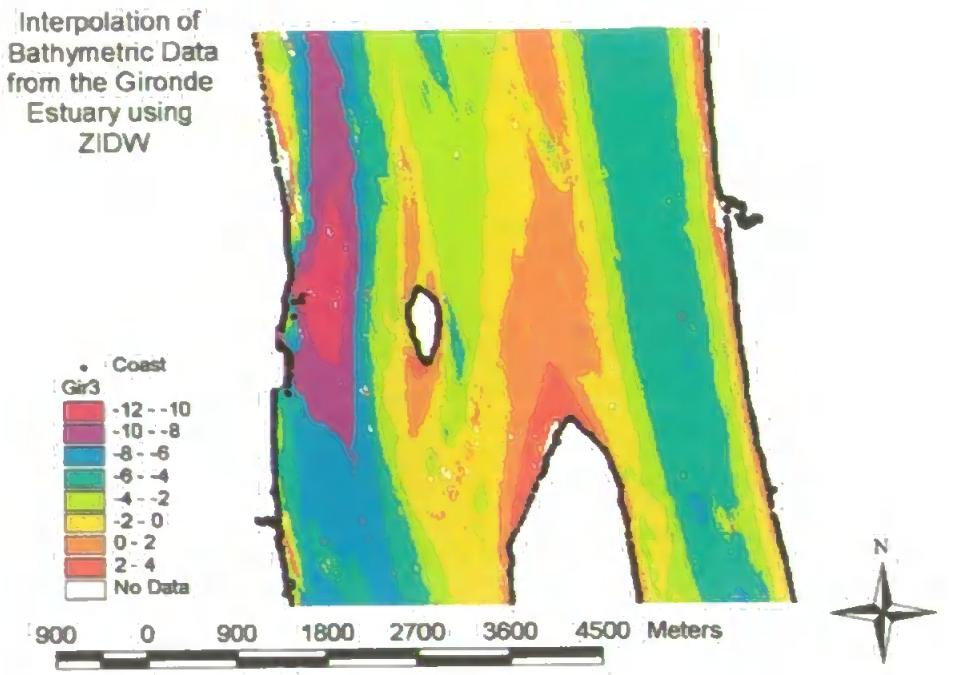

Figure 7.20 – Interpolation of bathymetric data from the Gironde estuary using the ZIDW program suite.

Chapter 8 – Discussion and Conclusions

8.1 Discussion

The formulation of the method, referred to as ZIDW, has provided a mechanism of interpolation for application to single beam, echo-sounding data. ZIDW successfully avoids the production of the visible artefacts of interpolation produced when interpolating inhomogenously distributed data using the methods available through conventional software. Rigorous, mathematical justification is provided for the method by means of application to theoretical channels of various shapes and a number of different cross-sections. Having undertaken extensive investigation of the literature it is believed that the ZIDW interpolation method represents an entirely new development within the field of hydrography. Clearly, this development is significant in terms of analysis of bathymetric trends within estuaries, in particular where older single beam data is to be compared with data collected by more recently developed swathe echo-sounders or scanning Lidar systems. In addition, interpolated bathymetry is required as a basis for various types of estuarine models, of which tidal modelling in estuaries provides an important example.

During the formulation and refinement of ZIDW a number of important new ideas have been adopted and refined. These include methods for identifying sounding lines and channels from reordered sounding data, as well as from data in its original form; the use of a channel following, 'smart' elliptical interpolation radius and construction of parameters designed to allow for variations imposed by estuaries of different scales. Through these ideas and the revision of ZIDW, to allow for non-continuous, flood and ebb type, channels, the latest interpolation system achieves universal applicability to estuaries of any scale and geographic location.

Although a TIN based interpolation model data was shown to be very effective in areas where the channel is exactly perpendicular to the sounding lines, slight deviations from the perpendicular produced significant interpolation artefacts. Such discrepancies will occur frequently in real estuaries as channels meander across the inter-tidal zone. Even if the survey is planned with a pre-existing knowledge of channel patterns it would, in practice, be impossible to ensure that every survey line

was perpendicular to each channel at all points along its length, especially in large complex estuaries such as the Humber or Gironde. The interpolation of historic data, vital for trend analysis, also relies on a method able to deal will the angle between channels and sounding lines being less than 90°, hence ZIDW represents an appropriate method of interpolation where methods available through existing software have been shown to be inappropriate.

Should additional funding become available, further testing, and possibly fine tuning, of ZIDW could be achieved by carrying out a single beam and a multi-beam survey of the same area of estuary at approximately the same time. Comparison of the results of the multi-beam survey with the single beam data, interpolated using ZIDW, would provide rigorous testing of the interpolation method for a real estuary. This type of testing would provide increased support for the commercial marketing of ZIDW.

The project has considered several methods of speeding up the operation of the ZIDW software. The use of the concept of 'large squares' to reduce the search area was adopted (section 7.4), whilst determination of the direction of the 'smart' ellipse at the corners of the large square only (section 7.5) was rejected for being unable to deal with multiple channels within a square. Possibly other methods of increasing the calculation efficiency of the software might be identified, in the future. However, speed of operation is not considered to represent a serious deficiency of the ZIDW software and as computer power continues to increase it is expected to become of less significance.

The development and application of the ZIDW program suite, described in this thesis, will allow single beam acoustic bathymetry to be compared with estuarine bathymetric data from different sources, collected by a variety of methods. Hence, a rigorously tested and verified basis now exists, from which a system to predict areas of bathymetric change within a small estuary, such as the Fal, may be formulated.

8.2 Conclusions

The initial aim of this project was to devise a system for prediction of areas of bathymetric change within small estuaries, exemplified by the Fal estuary, in south-west Cornwall. The following important conclusions were drawn from this phase of the study:

1. Red wavelength Lidar data provides sufficiently high resolution and accuracy, for use as part of a system to assess trends in mud bank heights within the inter-tidal zone, but not in channel depths.
2. Height information derived from stereo aerial photography is of insufficient accuracy for assessment of the inter-tidal zone. The data are therefore unsuitable for inclusion in a system to predict changes in estuarine bathymetry.
3. Single beam, acoustic bathymetry exhibits sufficient horizontal and depth accuracy for analysis of the inter-tidal zone. The data, however, require interpolation on to a regular grid for comparison with other data sets.
4. Interpolation for the single beam data, by IDW, TIN and Kriging, available within existing software packages, produces clearly identifiable interpolation artefacts along the centre line of channels and ridges.

This interpolation problem led to the second aim of the project, to formulate and evaluate a method for interpolating single beam acoustic bathymetry avoiding artefacts of interpolation. Formulation of this method produced an interpolation system using polygonal zones bounded by channels and coastlines in order to prevent interpolation across natural boundaries. This interpolation system successfully eliminates interpolation artefacts by preventing interpolation. Being based on Inverse Distance Weighting (IDW) the method was referred to as Zoned Inverse Distance Weighting (ZIDW).

In order to perform ZIDW on large and multiple data sets it was necessary to automate the interpolation method. The resulting suite of programs provides efficient automation of the processes of establishing sounding lines and channels, and of the allocation of soundings and output grid cells to polygons, required to perform ZIDW interpolation.

ZIDW was rigorously tested using a sequence of increasingly complex mathematically defined, ideal channels. ZIDW and TIN models were found to provide similar interpolation results for estuaries where all channels are perpendicular to the lines of soundings, represented by the theoretical straight and curved estuaries. The ZIDW method was also successful in eliminating artefacts of interpolation in cases where channels and ridges are not perpendicular to the sounding lines. This case, tested mathematically by a sinusoidal channel within a straight estuary and demonstrated visually by data from the Fal, is dealt with poorly by TIN interpolation.

Having verified ZIDW, both visually and mathematically, the method was developed to achieve universal applicability to interpolation of the single beam, echo sounding data from any estuary. This extension of the ZIDW software was investigated, developed and verified using single beam bathymetric from the Humber and Gironde estuaries.

In addition to incorporating natural boundaries to interpolation, the final, refined version of the ZIDW software provides:

- allowance for non-continuous, flood and ebb type, channels
- consideration of the effects of the scale of the estuary
- smoothing of the channels using cubic splines to support interpolation by a 'smart' ellipse.

The option to reconstruct sounding lines from data that has previously been re-ordered and a datum conversion program were also included in the final version of the ZIDW program suite.

Reference List

1. **ABP Ports Handbook** (1998). Associated British Ports.
2. Abrosimov, D. I. & Luchinin, A. G. (1999) Signal statistics of Lidar sounding of the upper ocean through its rough surface. **Izvestiya Akademi Nauk Fizika Atmofery I Okeana**, 35 (2) pp. 291-298.
3. **Admiralty Tide Tables** (1999). Volume 1, NP201-99, HMSO.
4. Ahrens, J. P. & Hands, E. B. (1998) Velocity parameters for predicting cross-shore sediment movement. **Journal of Waterway Port Coastal and Ocean Engineering-ASCI**, 124 (1) pp. 16-20.
5. Akima, H. (1978) A Method of Bivariate Interpolation and Smooth Surface Fitting for Irregularly Distributed data Points. **ACM Transactions on Mathematical Software** 4 (2) pp. 148-159.
6. Angel, E. (1990) **Computer Graphics**. Addison-Wesley Publishing Company, Inc.
7. Ashkenazi, V., Carne, A. S., Preiss, W. J. & Williams, J. W. (1980) **The 1980 readjustment of the triangulation of the United Kingdom and the Republic of Ireland OS(SN)80**. OS Professional Paper. New Series, No 31.
8. Ashkenazi, V., Cross, P. A., Davies, M. J. K. & Proctor, D. W. (1972) **The readjustment of the retriangulation of Great Britain and it's relationship to the European terrestrial and satellite networks**. OS Professional Paper. New Series, No 24.
9. Atkin, P., Tyler, A., Gilvear, D., Bryant, R., McDonald, P. & Teasdale, I. (1996) Remote sensing of radio-nuclide dispersion in the Ribble estuary, Lancashire, UK. Remote Sensing Science and Industry: **Proceedings of the 22nd Annual Conference of the Remote Sensing Society**.
10. Axelsson, R. & Alfreddsson, M. (1999) Optimisation of a Hydrographic Survey Organisation. **Proceedings of Hydro '99**, The Hydrographic Society, London.
11. Banic, J. (1995) Lidar Bathymetry – Looking into the sea. **Photonics Spectra**, 29 (6) pp. 98-100.
12. Bar, R., Watson, P. G., Ashcroft, C. R., Barnett, B. E. & Hilton, C. (1990) Humber Estuary – A case Study. **Hydrobiologia** 195 pp. 127-143.
13. Barbini, R., Colao, F., Fatoni, R., Palucci, A. & Ribezzo, S., (1999). Shipborne laser remote sensing of the Venice lagoon. **International Journal of Remote Sensing** 20 (12) pp. 2405-2421.
14. Black, K. S. (1998) Suspended sediment dynamics and bed erosion in the high shore mudflat region of the Humber estuary, UK. **Marine Pollution Bulletin** 37 (3-7) pp. 122-133.
15. Blomgran, S. (1999) A digital elevation model for estimating flooding scenarios at the Falsterbo Peninsula. **Environmental Modelling & Software** 14 (6) pp. 579-587.
16. Broadus, M., Whittaker, C., Young, R., Sharp, K. & Lingsch, S. (1997) New survey systems and technology for the littoral environment. **Marine Technology Society Journal** 37 (1) pp. 21-30.
17. Bukin, O. A., Major, A. Y., Pavlov, A. N., Shevtsov, B. M. & Kholodkevich, E. D. (1998) Measurement of the light scattering layers structure and detection of the dynamic processes in the upper layer by shipborne Lidar. **International Journal of Remote Sensing** 19 pp. 707-715.
18. Burnside, C. D. (1979) **Mapping from Aerial Photographs**. Granada Publishing.

19. Burnside, C. D. (1991) **Electronic Distance Measurement**: Third Edition. BSP Professional Books.
20. Burrough, P. A. (1986) **Principles in Geographic Information Systems for Land Resource Assessment**. Oxford Science Publications.
21. Burroughes, J. E., Abbott V. J. & Morris, K. P. (2000) Management of Hydrographic Survey Requirements. **Proceeding of Conference: Oceanology International 2000**, Brighton, UK.
22. Burroughes, J. E., George K. J. & Abbott V. J. (2001a) Interpolation of Hydrographic Survey Data. **The Hydrographic Journal** 99.
23. Burroughes J. E. & George K. J. (2001b) Automation of Interpolation by Zoned Inverse Distance Weighting for Linearly Distribution of Soundings. **GeoCoast**. In Press.
24. Campbell, J. B. (1996) **Introduction to Remote Sensing**: Second Edition. Taylor & Francis.
25. Chandler, J. (1999) Effective application of automated digital photogrammetry for geomorphological research. **Earth Surface Processes and Landforms** 24 (1) pp. 51-63.
26. Chandramohan, P., Kumar, V. S. & Kumar, S. J. (1996) Dredge spoil disposal off Kavaratti Island, Lakshadweep, India. **Indian Journal of Marine Sciences** 25 (1) pp. 67-70.
27. Chandrasekhar, M. G., Jayaraman, V. & Rao, M. (1996) Future perspectives of remote sensing. **Current Science** 70 (7) pp. 648-653.
28. Chester, T. J. & Ockenden, M. C. (1997) Numerical modelling of mud & sand mixtures. **Cohesive Sediments**. ed. Burt N, Parker R & Watts J. Wiley Publishers.
29. Churnside, J. H., Wilson, J. J. & Smolka, G. L. (1996) Airborne Lidar keeps tabs on underwater population. **Photonics Spectra** 30 (8) pp. 109-110.
30. Churnside, J. H., Wilson, .J J. & Tatarskii, V. V. (1997) Lidar profiles of fish schools. **Applied Optics** (36) pp. 6011-6020.
31. Conrad, P. E. (1988) Automatic depth estimation form Lidar wave forms. **Proceedings of Hydro '88** pp. 175.
32. Cooper, D. M. & Naden, P. S. (1998) Approaches to delivery modelling in LOIS. **Science of the Total Environment** 210 (1-6) pp. 483-498.
33. Cracknell, A. P. & Hayes, L. W. B. (1991) **Introduction to Remote Sensing**. Taylor & Francis pp. 70-80.
34. Cracknell, A. P. (1999) Remote sensing techniques in estuaries and coastal zones – an update. **International Journal of Remote Sensing** 20 (3) pp. 485-496.
35. Cross, P. A., Hollway, J. R. & Small, L. G. (1985) Working Paper No 2: **Geodetic Appreciation**. North East London Polytechnic, Department of Land Surveying.
36. Davidson, D. A. & Watson, A. I. (1995) Spatial variability in soil-moisture as predicted from airborne thematic mapper (ATM) data. **Earth Surface Processes and Lanforms** 20 (3) pp. 219-230.
37. Dobosiewicz, J (2001) Applications of Digital Elevation Models and Geographic Information Systmes to Coastal Flood Studies along the Shoreline of Raritan Bay, New Jersey. **Environmental Geosciences** 8 (1) pp. 11-20.
38. Duclos, B. J-C. C. (1998) **The use of Photogrammetry to monitor the effects of Sea Defences on Cliff Erosion and Beach Morphology on the Holderness Coast, North East England**. MSc Thesis, University of Plymouth.
39. Estep, L. (1993a) A review of airborne Lidar hydrographic (ALH) systems. **The Hydrographic Journal** 67 pp. 25.

40. Estep, L. (1993b) Passive optical bathymetry problem by a component analysis of the upwelling remote sensing signal: A suggested approach to the. **The Hydrographic Journal** 69 pp. 25.
41. Estep, L., Lillycrop, J. & Parson, L. (1994) Sensor fusion for hydrographic mapping applications. Proceedings, US Army Corps of Engineers 194 Training Symposium, **Surveying & Mapping, Remote Sensing/GIS**, New Orleans, LA . pp. SM: 2B 1-7.
42. Fent, L. (1999) Aerial films and solar angles: Influences on silver sagebrush inventory. **Journal of Range Management** 52 (1) pp. 32-38.
43. Ferrier, G. & Anderson, J. M. (1997) The application of remotely sensed data in the study of frontal systems in the Tay Estuary, Scotland, UK. **International Journal of Remote Sensing** 18 (9) pp. 1961-1975.
44. Field, C. T. & Millar, P. S. (1999) Laser remote-sensing system analysis for search and rescue. **Applied Optics** 38 (12) pp. 2586-2593.
45. Fox, A. J. (1995) Using multiple data sources to enhance photogrammetry for mapping Antarctic terrain. **Polar Research** 14 (3) pp. 317-327.
46. Gallacher, P. C. & Hogan, P. J. (1998) Hydrodynamical dispersion of dredged materials sequestered on the abyssal seafloor. **Journal of Marine Systems** 14 (3-4) pp. 305-318.
47. Galland, J. C., Laurence, D. & Teisson, C. (1997) Simulating turbulent vertical exchange of mud with a Reynolds stress model. **Cohesive Sediments**. ed. Burt N, Parker R & Watts J. Wiley Publishers.
48. Garciasoto, C., Sinha, B. & Pingree, R. D. (1996) Mapping a bloom of the Coccolithophorid Emiliania Huxleyi form airborne thematic mapper (ATM) data. **Journal of the Marine Biological Association of the UK** 76 (4) pp. 839-849.
49. George, D. G. & Happey-Wood, C. M. (1996) The remote sensing of a power station plume in Llyn Peris (Snowdonia). Remote Sensing Science and Industry: **Proceedings of the 22nd Annual Conference of the Remote Sensing Society**.
50. George, D. G. (1997a) Bathymetric mapping using compact airborne spectrographic imager (CASI). **International Journal of Remote Sensing** 18 (10) pp. 2067-2071.
51. George, D. G. (1997b) The airborne remote sensing of phytoplankton chlorophyll in the lakes and tarns of the English Lake District. **International Journal of Remote Sensing** 18 (9) pp. 1961-1975.
52. George, K. J. (1993) Hydrographic data bases for tidal numerical models. **International Hydrographic Review** 70 (2) pp. 135-149.
53. George, K. J. & Simon, B. (1984) The species concordance method of tide prediction in estuaries. **International Hydrographic Review** 61 pp 121-146.
54. Goff, J. R., Dunbar, G. B. & Barrett, P. J. (1998) **Journal of Coastal Research** 14 (2) pp. 461-471.
55. Gong, P. Pu, R. L. & Miller, J. R. (1995) Coniferous forest leaf-area index estimation along the Oregon transect using compact airborne spectrographic imager data. **Photogrammetric Engineering and Remote Sensing** 61 (9) pp. 1107-1117.
56. Gooch, M. J., Chandler, J. H. & Stojic, M. (1999) Accuracy assessment of digital elevation models generated using the Erdas Imagine Orthomax digital photogrammetric system. **Photogrammetric Record** 16 (93) pp.519-531.
57. Gorman, L., Morang, A. & Larson, R. (1998) Monitoring the coastal environment; Part IV: Mapping shoreline changes, and bathymetric analysis. **Journal of Coastal Research** 14 (1) pp. 61-92.

58. Graham, R. W. & Read, R. E. (1998) Practical experiences with films , cameras and navigation systems. **Photogrammetric Record** 16 (91) pp. 19-36.
59. Hamm, L., Chester, T., Fettiweis, M., Pathirana, K. P. P. & Peltier, E. (1997) An intercomparison exercise of cohesive sediment transport numerical models. **Cohesive Sediments**. ed. Burt N, Parker R & Watts J. Wiley Publishers.
60. Hartkamp, A. D., White, J. W. & Hoogenboom, G. (1999) Interfacing geographic information systems with agronomic modelling: A review. **Agronomy Journal** 91 (5) pp. 761-772.
61. Henderson, R. A. (1997) A guide to laser safety. Chapman & Hall Publishers.
62. Henning, I. (1998) A historic overview of radar imagery of sea bottom topography. **International Journal of Remote Sensing** 19 (7) pp. 1447-1454.
63. Hooijberg, M. (1997) **Practical Geodesy Using Computers**. Springer Publishers.
64. Hughes, S. H. (1999) The geochemical and mineralogical record of the impact of historical mining within estuarine sediments in the Fal Estuary, Cornwall, UK. **International Association of Sedimentologists**, Special Publication.
65. **Imagine Orthomax User's Guide** (1995) Erdas Imagine Version 8.1. Manchester Computing Centre, ISG 682.
66. Irish, J. L. & Lillycrop, W. J. (1997) Monitoring New Pass, Florida, with high density Lidar bathymetry. **Journal of Coastal Research** 13 pp. 1130-1140.
67. Irish, J. L. & Lillycrop, W. J. (1999) Scanning laser mapping of the coastal zone: the SHOALS system. **ISPRS Journal of Photogrammetry and Remote Sensing** 54 (2-3) pp. 123-129.
68. Jallow, B. P., Barrow, M. K. A. & Leatherman, S. P. (1996) Vulnerability of the coastal zone of The Gambia to sea level rise and development of response strategies and adaptation options. **Climatic Research** 6 (2) pp. 165-177.
69. Jerlov, N. G. (1976) Elsevier Oceanography Series 14: **Marine Optics**, Ch 5 & 6.
70. Jimenez, J. A., SanchezArcilla, A., Buo, J. & Ortiz, M. A. (1997) Analysing short-term shoreline changes along the Elbo delta (Spain) using aerial photographs.
71. Jouanneau, J. M. & Latouche, C. (1981) The Gironde Estuary. **Contributions to Sedimentology** 10. E Schweizerbart'sche Verlagsbuchhandlung (Nägele u. Obermiller) Stuttgart.
72. Kenward, T., Lettenmaier, D. P., Wood, E. F. & Fielding, E. (2000). Effects of Digital Elevation Model Accuracy on Hydrologic Predictions. **Remote Sensing of Environment** 74 (3) pp.432-444.
73. Kidner, D. B., Ware, J. M., Sparkles, A. J. & Jones, C. B. (2000) Multiscale Terrain and Topographic Modelling with the Implicit TIN. **Transactions in GIS** 4 (4) pp. 361-378.
74. Kilford, W. K. (1979) **Elementary Air Survey**, Fourth Edition. Pitman Publishers.
75. Koppari, K., Karlossen, U. & Steinvall, O. (1994) Airborne laser depth sounding in Sweden. **International Hydrographic Review** 71 (2) pp. 69-90.
76. Krekov, G. M., Krekova, M. M. & Shamanaev, V. S. (1998) Laser sensing of a subsurface oceanic layer I: Effect of the atmosphere and wind-driven sea waves. **Applied Optics** 37 pp. 1589,1595.
77. Kusuda, T., Watanabe, R. & Yamanishi, H. (1997) Mass fluxes in fluid-mud layers on an inclined bed. **Cohesive Sediments**. ed. Burt N, Parker R & Watts J. Wiley Publishers.
78. Lachapelle, G., Lethany, J. & Casey, M. (1984) Airborne single point and differential GPS navigation for hydrographic bathymetry. **The Hydrographic Journal** 34 p. 11.

79. Langran, G. (1992) **Time in Geographic Information Systems**. Taylor & Francis Publishers, London.
80. Lee, S. C. & Mehta, A. J. (1997a) Equillibrium hysometry of fine-grained shore profiles. **Cohesive Sediments**. ed. Burt N, Parker R & Watts J. Wiley Publishers.
81. Lee, S. C. & Mehta, A. J. (1997b) Problems in characterising dynamics of mud shore profiles. **Journal of Hydraulic Engineering**-ASCE 123 (4) pp. 351-361.
82. Leeks, G. J. L. & Walling, D. E. (1999) The river basin sediment dynamics and interactions within the UK Land –Ocean Interaction Study: the context. **Hydrological Processes** 13 (7) pp. 931-934.
83. LeHir, P. (1997) Fluid and sediment "integrated" modelling application to fluid mud flows in estuaries. **Cohesive Sediments**. ed. Burt N, Parker R & Watts J. Wiley Publishers.
84. Light, D. L. (1996) Film camera or digital sensors? The challenge ahead for aerial imaging. **Photogrammetric Engineering and Remote Sensing** 62 (3) pp. 285-291.
85. Light, D. L. (1999) C-factor for softcopy photogrammetry. **Photogrammetric Engineering and Remote Sensing** 65 (6) pp. 667- 669.
86. Lillycrop, W. J., Irish, J. L. & Parson, L. E. (1997) Shoals System. **Sea Technology** 38 (6) pp. 17-24.
87. Lin, C. S. (1996) Ocean surface profiling Lidar. **International Journal of Remote Sensing** 17 pp. 2667-2680.
88. Lindsay, P., Balls, P. W. & West, J. R. (1996) Influence of tidal range and river discharge on suspended particulate matter fluxes in the Forth estuary (Scotland). **Estuarine Coastal and Shelf Science** 42 (1) pp. 63-82.
89. Livingstone, D., Raper, J. & McCarthy, T. (1999) Integrating aerial videography and digital photography with terrain modelling: an application for coastal geomorphology. **Geomorphology** 29 (1-2) pp. 77-92.
90. **Lloyd's Ports of the World** 1999 (1998) LLP Ltd Publishers.
91. Longfield, S. A. & Macklin, M. G. (1999) The influence of recent environmental change on flooding and sediment fluxes in the Yorkshire Ouse basin. **Hydrological Processes** 13 (7) pp. 1051-1066.
92. Luman, D. E., Stohr, C. & Hunt, L. (1997) Digital reproduction of historical aerial photographic prints for preserving a deteriorating archive. **Photogrammetric Engineering and Remote Sensing** 63 (10) pp. 1171-1179.
93. Lyzenga, D. R. (1981) Remote sensing of bottom reflectance and water attenuation parameters in shallow water using aircraft and LANDSAT data. **International Journal of Remote Sensing** 2 pp. 71-82.
94. Macdonald, G. (1986) Airborne electromagnetic bathymetry system. **Proceedings of Hydro '86** pp. 17.
95. MacPhee, S. B., Dow, S. B., Anderson, A. J. & Reid, .D B. (1981) Aerial hydrography laser bathymetry and air photo techniques for obtaining inshore hydrography. **The Hydrographic Journal** 22 pp. 19.
96. Malthus, T. J., Place, C. J., Bennet, S. & North, S. (1996) An evaluation of the airborne thematic mapper sensor for monitoring inland waters. Remote Sensing Science and Industry: **Proceedings of the 22nd Annual Conference of the Remote Sensing Society**.
97. Mason, S., Ruther, H. & Smit, J. (1997) Investigation of the Kodak DCS460 digital camera for small-area mapping. **ISPRS Journal of Photogrammetry and Remote Sensing** 52 (5) pp. 202-214.

98. Matthews, J. P., Wisman, V. R,, Lwiza, K., Romeiser, R., Hennings, I. & Delor, G. P. (1997) The observation of the surface roughness characteristics of the Rhine plume frontal boundaries by simultaneous airborne thematic mapper and multi-frequency helicopter-borne radar scatterometer. **International Journal of Remote Sensing** 18 (9) pp. 2021-2033.
99. Matioli, G. S., Jansma, P. E., Jaramillo, L. & Smith, A. L. (1996) A desktop image processing and photogrammetric method for rapid volcanic hazard mapping: Application to air-photo interpretation of Mount Pelee, Martinique. **Bulletin of Volcanology** 58 (5) pp. 401-410.
100. McBride, R. A. & Byrnes, M. R. (1997) Regional variations in shore response along barrier island systems of the Mississippi River delta plain: Historical change and future prediction. **Journal of Coastal Research** 13 (3) pp. 628-655.
101. McCullagh, M. J. (1983) Transforamtion of contour strings to a rectangular grid based digital elevation model. **Euro-Carto II** pp. 18.
102. McLean, J. & Freeman, J. (1996) Effects of ocean waves on airborne Lidar imaging. **Applied Optics** 35 (4) pp. 24-25.
103. Menard, T., Nomine, M., Tatry, V. & Godet, Y. (1998) Technical evalution of optical remote detection instruments: DOAS and LIDAR. **Analusis** 26 (9) pp. M55-M59.
104. Mielke, B. (1991) **Integrated computer graphics**. West Publishing Co.
105. Miller, M. E. (1999) Use of historic aerial photography to study vegetation change in the Negrito Creek watershed, southwestern New Mexico. **Southwestern Naturalist** 44 (2) pp. 121-137.
106. Milton, E. J., Gilvear, D. J. & Hooper, I. D. (1995) Investigating change in fluvial systems using remotely sensed data. **Changing River Channels** pp. 227 - 301. ed. Gurnell, A. & Petts, G. John Wiley Publishers, London.
107. Mitra, K. & Churchside, J. H. (1999) Transient radiative transfer equation applied to oceanographic Lidar. **Applied Optics** 38 (6) pp. 889-895.
108. Mittenzwey, K. H., Sinn, G., Roof, N. & Harsdorf, S. (1997) An improved Lidar method for monitoring surface waters: Experiments in the laboratory. **International Journal of Remote Sensing** 18 pp. 2271-2276.
109. Moore, R. V. (1997) The logical and physical design of The Land Ocean Interaction Study database. **Science of the Total Environment** 194 pp. 137-146.
110. Moore, T., Morris, K., Blackwell, G. & Gibson, S. (1997) Extraction of Beach Landforms from DEMs using a Coastal Management Expert System. **Proceedings of Geocomputation '97 & SIRC '97.**
111. Moore, T., Morris, K., Blackwell, G., Gibson, S. & Stebbing, A. (1998) An expert system for integrated coastal management: A geomorphological case study. **Marine Pollution Bulletin** 37 (3-7) pp. 361-370.
112. Mortensen, P. (1996a) Airborne fluorosensor may find underwater treasure. **Laser Focus World** 32 (9) pp. 46-48.
113. Mortensen, P. (1996b) Laser system charts Australia's coastline. **Laser Focus World** 32 (7) pp. 22-23.
114. Naden, P. S. & Cooper, D. M. (1999) Development of a sediment delivery model for application in large river basins. **Hydrological Processes** 13 (7) pp. 1011-1034.
115. Nairn, R. (1994) Royal Australian Navy laser airborne depth sounder, the first year of operation. **International Hydrographic Review** 71 (1) pp. 109-119.
116. Naisset, E. (1997) Estimating timber volume of forest stands using airborne laser scanner data. **Remote Sensing Environment** 61 pp. 246-253.

117. Narayanan, R. M. & Kalshoven, J. R. (1997) Advances in Laser Remote Sensing for Terrestrial and Oceanographic Aplications, **Proceedings SPIE 3059**.
118. Neilson, B. & Costello, M. J. (1999) The relative lengths of seashore substrate around the coastline of Ireland as determined by digital methods in a geographical information system. **Estuarine Coastal and Shelf Science** 49 (4) pp. 501-508.
119. Netzband, A., Christiansen, H., Maass, B. & Werner, G. (1998) Relocation of dredged material form Hambourg harbour in the River Elbe. **Water Science and Technology** 37 (6-7) pp. 241-248.
120. Nieke, B., Vincent, W. F., Therriault, J-C., Legrendre, L. Berthon J-F. and Condal, A. (1997) Use of ship-borne laser fluoresensor for remote sensing of chlorophyll in a coastal environment. **Remote Sensing Environment** 60 pp. 140-152.
121. O'Connor, B. A. & Nicholson, J. (1993) An estuarine and coastal sand transport model. **Dynamics & Exchanges in Estuaries & the Coastal Zone**. ed. Prandle D. American Geophysical Union Publishers.
122. O'Connor, T. P. (1998) Comparative criteria: Land application of sewage sludge and ocean disposal of dredged material. **Marine Pollution Journal** 36 (3) pp. 181-184.
123. Oberthur, T., Goovaerts, P. & Dobermann, A. (1999) Mapping soil texture classes using field texturing, particle size distribution and local knowledge by both conventional and geostatistical methods. **European Journal of Soil Science** 50 (3) pp. 457-479.
124. Oliver, M. A. (1990) Kriging: A method of interpolation for Geographic Information Systems. **International Journal of Geographic Information Systems** 4 (4) pp. 313-332.
125. Orum, T. V., Bigelow, D. M., Cotty, P. J. & Nelson, M. R. (1999) Using predictions based on geostatistics to monitor trends in Aspergillus flavus strain composition. **Phytopathology** 89 (9) pp. 761-769.
126. Parson, L. E., Lillycrop, W. J., Klein, C. J., Ives, R. C. P. & Orlando, S. P. (1997) Use of Lidar technology for collecting shallow water bathymetry of Florida Bay. **Journal of Coastal Research** 13 pp. 1173-1180.
127. Penny, M. F., Abbott, R. H., Phillips, D. M., Billard, B., Rees, D., Faulkner, D. W., Cartwright, D. G., Woodcock, B., Perry, G. J., Wilsen, P. J., Adams, T. R. & Richards, J. (1986) Airborne Laser Hydrography in Australia. **Applied Optics** 25 (13).
128. Petrie, G. (1997) Developments in Digital Photogrammetric Systems for Topographic Mapping Applications. **ITC Journal** 2 pp. 121-135.
129. Petrie, G. & Kennie, T. J. M. (1990) **Terrain Modelling in Surveying and Civil Engineering**. Whittles Publishing.
130. Phillips, J. M., Webb, B. W., Walling, D. E. & Leeks, G. J. L. Estimating the suspended sediment loads of rivers in the LOIS study area using infrequent samples. **Hydrological Processes** 13 (7) pp.1035-1050.
131. Pickard, G. L. & Emery, W. J. (1990) **Descriptive Physical Oceanography: An Introduction**: Fifth (SI) Enlarged Edition. Pergamon Press.
132. Pirrie, D. & Camm, G. S. (1999) The impact of mining on sedimentation in the coastal zone of Cornwall, UK. **Quaternary Research** |Association Field Guide (in press).
133. Pirrie, D., Camm, G. S., Sear, L. G. & Hughes, S. H. (1997) Mineralogical and Geochemical signature of mine waste contamination, Tresillian River, Fal Estuary, Cornwall, UK. **Environmental Geology** 29 pp. 58-65.

134. Pirrie, D., Hughes, S. H. & Camm, G. S. (1999) Late Holocene sedimentation due to mine waste discharge; Fal Estuary, Cornwall, UK. **Quaternary Research** Association Field Guide (in press).
135. Pirrie, D., Hughes, S. H. & Pullin, H. (1996) The effect of mining on sedimentation over the last 500 years in the Fal Estuary, Cornwall, UK. Late Quaternary coastal change in West Cornwall, UK, Field Guide. **Environmental Research Centre, University of Durham, Research Publication** 3, pp. 75-82 ed. Healy M G.
136. Pozdnyakov, D. V. & Kondratyev, K. (1996) Lidar fluorescence technique application for studying hydrodynamic processes. **Marine Technology Society Journal** 30 pp. 46-53.
137. Rainey, M., Tyler, A., Bryant, R., Gilvear, D., McDonald, P. & Teasdale, I. (1996) Spectral characteristics of radio-nuclide bearing intertidal sediments in the Ribble estuary, Lancashire, England. Remote Sensing Science and Industry: **Proceedings of the 22nd Annual Conference of the Remote Sensing Society.**
138. Ratcliff, J. (1997) **Fal estuary historic audit.** Cornwall Archaeological Unit, Cornwall County Council.
139. Rees, W. G. (2000) The Accuracy of Digital Elevation Models Interpolated to Higher Resolutions. **International Journal of Remote Sensing** 21 (1) pp. 7-20.
140. Richards, J. A. (1997) **Study of Ords and Cliff Erosion on the Holderness Coast using Digital Elevation Models derived from Stereo Aerial Photographs.** MSc Thesis, University of Plymouth.
141. Rocadenbosch, F. & Comeron, A. (1999) Error analysis for the Lidar backward inversion algorithm. **Applied Optics** 38 (21) pp. 4461-4474.
142. Roy, D. P., Devereux, B., Grainger, B. & White, S. J. (1997) Parametric geometric correction of airborne thematic mapper imagery. **International Journal of Remote Sensing** 18 (9) pp. 1865-1887.
143. Sagar, B. S. D., Venu, M. & Srinivas, D. (2000) Morphological operaotrs to extract channel networks from Digital Elevation Models. **International Journal of Remote Sensing** 21 (1) pp.21-29.
144. Saito, Y. M., Kanoh, M., Hatake, K., Kawahara, T. D. & Nomura, A. (1998) Investigation of laser-induced flourescence of several natural leaves for application to Lidar vegetation monitoring. **Applied Optics** 37 pp. 431-437.
145. Sanderson, P. G., Eliot, I. & Fuller, M. (1998) Historical development of a foredune plain at Desperate Bay, Western Australia. **Journal of Coastal Research** 14 (4) pp. 1187-1201.
146. Scheffner, N. W. (1996) Systematic analysis of long-term fate of disposed dredged material. **Journal of Waterway Port Coastal and Ocean Engineering-ASCI** 122 (3) pp. 127-133.
147. Shinn, E. A., Reich, C. D., Locker, S. D. & Hine, A. C. (1996) A giant sediment trap in the Florida Keys. **Journal of Coastal Research** 12 (4) pp. 953-959.
148. Shoshany, M., Golik, A., Degani, A., Lavee, H. & Gvirtzman, G. (1996) New evidence for sand transport direction along the coastline of Israel. **Journal of Coastal Research** 12 (1) pp 311-325.
149. Shuey, R. W. (1996) Using aerial photography. Pollution Engineering 28 (9) pp. 58-59.
150. Simpson, H. (2000) Investigation of dune morphology using GIS and remote sensing techniques. **MSc Thesis**, University of Plymouth, Unpublished.

151. Sinclair, M. (1997) LADS MK II aircraft launched. **Proceedings of Hydro' International.**
152. Sinclair, M. (1999) Airborne Laser Bathymetry – Acceptance Grows in 1998/1999. **Proceedings of Hydro '99.**
153. Spinnard, R. W., Carder, K. L. & Perry, M. J. (1994) **Ocean Optics: Oxford Monographs on Geology and Geophysics** No. 25. Oxford University Press.
154. Stebbing, A. R. D., Huntley, D. & Leeks, G. J. L. (1998) Integrated riverine, estuarine and coastal research in the UK Land –Ocean Interaction Study (LOIS). **Marine Pollution Bulletin** 37 (3-7) pp. 115-121.
155. Steele, B. M., Winne, J. C. & Redmonnd, R. L. (1998) Estimation and mapping of misclassification probabilities for thematic land cover maps. **Remote sensing of Environment** 66 (2) pp. 192-202.
156. Steinvall, O. & Koppari, K. (1996) Depth sounding Lidar – an overview of Swedish activities and with future prospects. **Proceedings SPIE** 2964 pp. 2-25.
157. Stevens, D. L. & Olsen, A. R. (1999) Spatially restricted surveys over time for aquatic resources. **Journal of Agricultural Biological and Environmental Statistics** 4 (4) pp. 415-428.
158. Stapleton, C. & Pethick, J. (1995) **The Fal Estuary: coastal processes and conservation**. Report to English Nature. Institute of Estuarine and Coastal Studies, Hull pp. 63.
159. Sunberg, P. (1992) The use of airborne laser in hydrographic surveys. **Proceedings of Hydro '92**, The Hydrographic Society, London.
160. Teisson, C. (1997) A review of cohesive sediment transport models. **Cohesive Sediments**. ed. Burt N, Parker R & Watts J. Wiley Publishers.
161. Thomson, A. G., Eastwood, J. A., Fuller, R. M., Yates, M. G. & Sparks, T. H., (1996) Remote sensing of the intertidal zone in the LOIS project. Remote Sensing Science and Industry: **Proceedings of the 22nd Annual Conference of the Remote Sensing Society**.
162. Thorne, M. G. (1983) Studies of Fal estuary sediment I: early diagenetic sulphide mineralisation. **Proceedings of Ussher Society** 5 pp. 437-444.
163. Tindall, C. I. & Moore, R. V. (1997) The Rivers Database and the overall data management for the Land Ocean Interaction Study programme. **Science of the Total Environment** 194 pp. 129-135.
164. Townsend, P. A. & Walsh, S. J. (1998) Modelling floodplain inundation using an integrated GIS with radar and optical remote sensing. **Geomorphology** 21 (3-4) pp. 295-312.
165. **Truro Harbour Authority records** (1999).
166. VanHorssen, P. W., Schott, P. P. & Barendregt, A. (1999) A GIS-based plant prediction model for wetland ecosystems. **Landscape Ecology** 14 (3) pp. 253-265.
167. Vitsinkii, S. A., Divin, V. D., Keller, A. V., Lovchii, I. L. & Svetlykh, A. A. (1996) Cooper-vapour lasers for hydrooptics applications. **Journal of Optical Technology** 63 (5) pp. 401-405.
168. Walling, D. E., Owens, P. N. & Leeks, G. J. L. (1999) Rates of contemporary overbank sedimentation and sediment storage on the floodplain of the main channel systems of the Yorkshire Ouse and River Tweed, UK. **Hydrological Processes** 13 (7) pp. 993-1009.
169. Wass, P. D. & Leeks, G. J. L. (1999) Suspended sediment fluxes in the Humber catchment, UK. **Hydrological Processes** 13 (7) pp. 935-953.

170. Watson, A. & Gilvear, D. J. (1993) Examination of the use of imagery for mapping river channels and floodplain sediments. **Proceedings of the NERC Symposium on Airborne Remote Sensing** pp. 117-136.
171. Wells, N. (1986) **The Atmosphere and Ocean: A Physical Introduction**. Taylor & Francis.
172. Wensink, H. & Sidhu, H. (1997) Bathymetric assessment system – BAS. **Proceedings of Hydro' International**.
173. Whiteman, D. N. (1999) Application of statistical methods to the determination of slope in Lidar data. **Applied Optics** 38 (15) pp. 3360-3369.
174. Wilkinson, W. B., Leeks, G. J. L., Morris, A. & Walling, D. E. (1997) Rivers and coastal research in the Land Ocean Interaction Study. **Science of the Total Environment** 194 pp. 5-14.
175. Williams, J. & Higginson, J. J. **Sea & Air: The Marine Environment**: Second Edition. Naval Institute Press.
176. Willis, D. H. & Crookshank, N. L.(1997) Modelling multiphase sediment transport in estuaries. **Cohesive Sediments**. ed. Burt, N., Parker, R. & Watts, J. Wiley Publishers.
177. Winterbottom, S. J. & Gilvear, D. J. (1997) Quantification of channel bed morphology in gravel-bed rivers using airborne mutispectral imagery and aerial photography. **Regulated Rivers-Research Management** 13 (6) pp. 489-499.
178. Winterbottom, S. (1996) The use of airborne remotely sensed data for mapping habitats within gravel- bed rivers. Remote Sensing Science and Industry: **Proceedings of the 22nd Annual Conference of the Remote Sensing Society**.
179. Wolf, P. R. (1974) **Elements of Photogrammetry**. McGraw-Hill, USA.
180. Zurabyan, A. Z., Yakonlev, V. A., Zhurenkov, A. G. & Kachurin, V. K. (1997) Effect of wind waves on the spatial resolution of airborne Lidar in the bathymetry of a marine medium. **Journal of Optical Technology** 64 pp. 781-782.

Appendix 1 -

Example of Satellite Elevation Plots

used for GPS Survey Planning

Total Satellites In View

To change any parameter, including the plot type, see below. **Please note:** In order to view the graph, you need Internet Explorer or Netscape browsers greater than version 3.XX

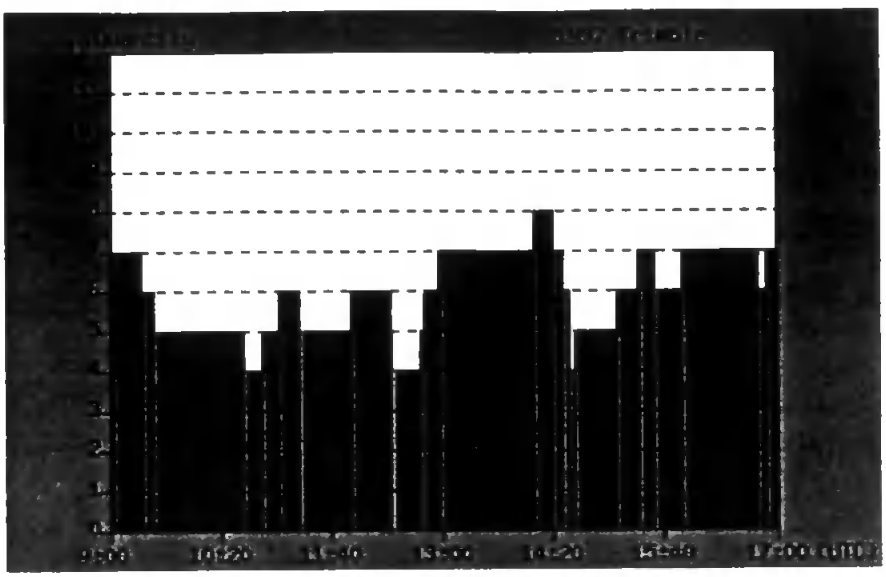

Lat: 50.20 **Long:** -5.00 **Mask:** 13.0
Date: 04-05-2000 **Starting Hour:** 9:00 (GMT) **Duration:** 8 hours

Total-In-View:

The total-in-view plot displays the total number of satellites with elevation angles that exceed the mask angle you specify. This plot is useful for a quick look at the time periods when there are enough satellites available for your receiver to calculate a GPS position.

Latitude: 50.20 **Date:** 04-05-2000
Longitude: -5.00 **Starting hour:** 9 (GMT)
Mask: 13.0 degrees **Duration:** 8 hours
Plot type: Total in View

send reset

help

Elevation

To change any parameter, including the plot type, see below. **Please note:** In order to view the graph, you need Internet Explorer or Netscape browsers greater than version 3.XX

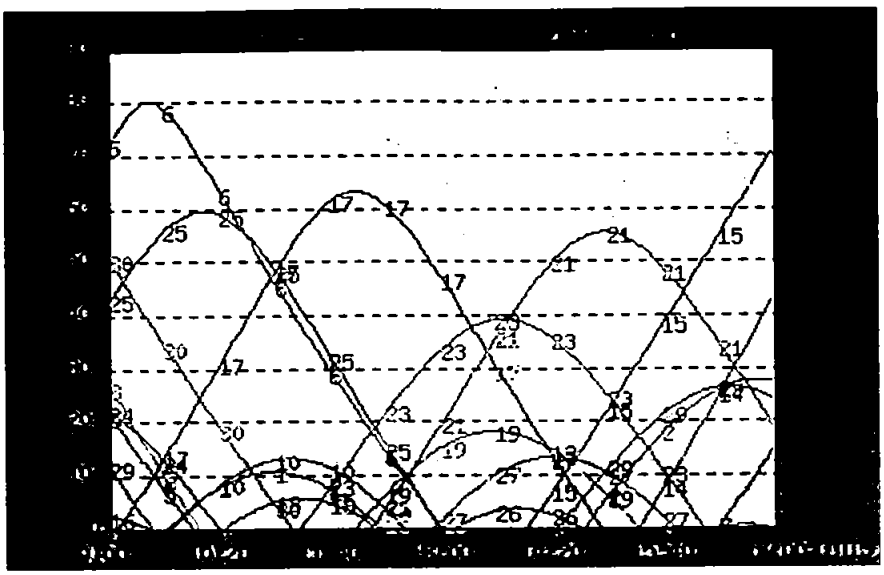

Lat: 50.20 **Long:** -5.00 **Mask:** 13.0
Date: 04-05-2000 **Starting Hour:** 9:00 (GMT) **Duration:** 8 hour:

Elevation:

The elevation plot shows the elevation angle above the horizon for all satellites in view during the time period you specify. An elevation of 90 degrees is directly overhead.

Latitude: 50.20 **Date:** 04-05-2000
Longitude: -5.00 **Starting hour:** 9 (GMT)
Mask: 13.0 degrees **Duration:** 8 hours
Plot type: Elevation

send reset

help

Appendix 2 -

Example of Station Description Form

used during GPS Ground Control Survey

and Co-ordinates of Ground Control Points

Description of Trigonometrical Station

tion:- 1. Area:- Newham Industrial estate

tangular .....E.	Projection .....
ordinates .....N.	Grid .....

ght of Mark above i) Land Survey Datum .....m. ii) M.H.W.S. ..... m.

cription of Station:-

Corner of small garage.

Rivetty nail.

Location Map:-

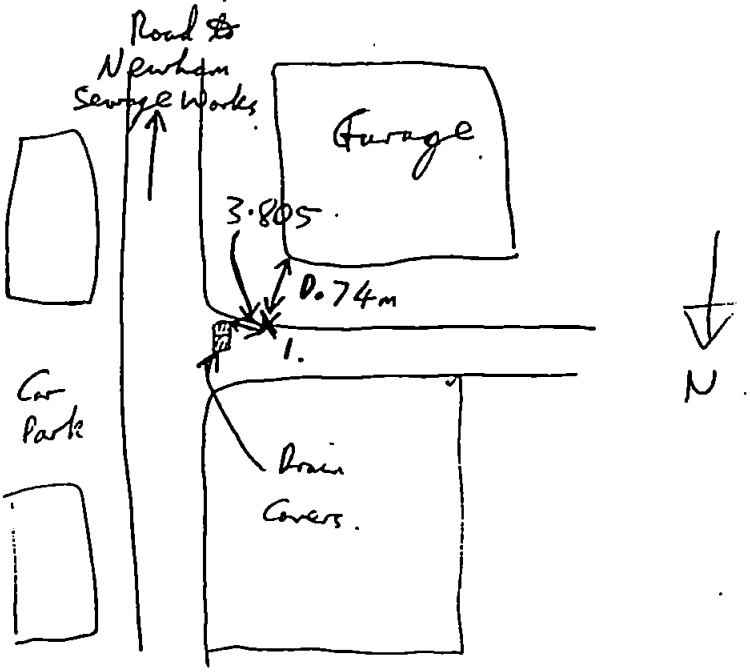

pable life of Mark ..... Years

rvisability:-

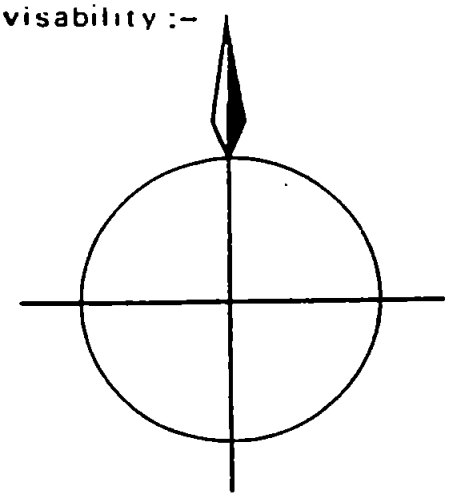

Site Sketch:-

SVs = 6.

Obs time = 8 minutes.

Start time = 16:00. (BST)

Antennae Ht = 1.276m

(Photo No. = 21)

o Cover Held:-

Handheld: 50° 15' 22.1" N.
05° 02' 45.9" W.

tact for Permission:-

:-

Described by:- JEB

Date:- 5-4-00.

Ground Control Points - OSBG36

WGS84

Point No	E (m)	N (m)	H (m)	Point No	Lat.	Long.	Ht.
BASE2	181612.75	41159.36	99.6	BASE2	50ø13'47.99700"N	5ø03'48.41290"W	152.504
BASE1	181612.75	41159.36	99.6	BASE1	50ø13'47.99700"N	5ø03'48.41290"W	152.504
1	182978.744	44027.728	4.138	1	50ø15'22.54466"N	5ø02'45.47834"W	57.047
2	182912.287	44394.758	3.849	2	50ø15'34.32313"N	5ø02'49.58717"W	56.758
3	182893.563	44721.462	4.96	3	50ø15'44.86094"N	5ø02'51.20588"W	57.87
4	183528.373	44907.214	50.178	4	50ø15'51.70537"N	5ø02'19.57127"W	103.091
5	184043.453	44592	52.796	5	50ø15'42.19299"N	5ø01'52.94431"W	105.711
6	184244.079	43796.57	70.032	6	50ø15'16.73960"N	5ø01'41.19412"W	122.947
7	183684.996	44096.311	45.524	7	50ø15'25.69457"N	5ø02'10.00369"W	98.437
8	184195.897	43330.45	75.885	8	50ø15'01.60593"N	5ø01'42.66780"W	128.799
9	184136.943	42564.186	8.412	9	50ø14'36.75402"N	5ø01'44.06895"W	61.325
10	183323.813	42507.278	13.654	10	50ø14'33.84295"N	5ø02'24.94638"W	66.564
11	183373.511	43248.472	5.87	11	50ø14'57.87212"N	5ø02'23.96628"W	58.781
12	183419.68	43897.068	17.602	12	50ø15'18.90285"N	5ø02'22.97337"W	70.513
13	182641.504	42185.892	60.142	13	50ø14'22.55035"N	5ø02'58.68118"W	113.05
14	182235.944	42387.016	85.94	14	50ø14'28.51542"N	5ø03'19.54177"W	138.846
15	182099.367	43070.784	7.458	15	50ø14'50.44081"N	5ø03'27.84226"W	60.363
16	182713.818	43746.53	55.789	16	50ø15'13.10275"N	5ø02'58.25742"W	108.697
17	183329.202	41478.756	65.018	17	50ø14'00.59676"N	5ø02'22.55859"W	117.928
18	184241.762	40883.703	49.988	18	50ø13'42.55921"N	5ø01'35.34186"W	102.902
19	182967.502	40681.708	10.121	19	50ø13'34.34974"N	5ø02'39.14828"W	63.03
20	183792.063	40803.373	3.146	20	50ø13'39.37070"N	5ø01'57.84199"W	56.058
21	184010.569	41746.778	22.86	21	50ø14'10.15986"N	5ø01'48.76361"W	75.772
22	184568.526	42103.546	52.487	22	50ø14'22.42770"N	5ø01'21.36757"W	105.402
23	184336.125	40706.688	48.424	23	50ø13'36.95994"N	5ø01'30.22367"W	101.339
24	No Access	Replaced by 38					
25	No Access	Replaced by 37					
26	185720.057	42354.39	85.471	26	50ø14'32.04491"N	5ø00'23.82602"W	138.393
27	185702.055	41532.466	73.971	27	50ø14'05.44688"N	5ø00'23.06101"W	126.893
28	185053.793	41049.704	3.184	28	50ø13'48.99099"N	5ø00'54.75348"W	56.103
29	185541.604	42730.678	65.625	29	50ø14'43.97806"N	5ø00'33.58945"W	118.545
30	184352.345	41276.658	31.2	30	50ø13'55.40930"N	5ø01'30.57276"W	84.115
31	183212.658	43598.804	3.449	31	50ø15'08.98634"N	5ø02'32.79851"W	56.359
32	184665.646	43021.356	8.807	32	50ø14'52.22941"N	5ø01'18.34885"W	61.723
33	183945.378	41721.601	23.603	33	50ø14'09.26009"N	5ø01'51.99815"W	76.515
34	184256.254	41301.51	30.417	34	50ø13'56.08661"N	5ø01'35.46703"W	83.331
35	185103.696	39426.85	80.769	35	50ø12'56.58617"N	5ø00'48.92950"W	133.691
36	185142.845	39617.849	84.65	36	50ø13'02.81276"N	5ø00'47.34608"W	137.572
37	184418.205	41597.041	4.57	37	50ø14'05.85429"N	5ø01'27.90879"W	57.485
38	184095.394	41265.491	32.671	38	50ø13'54.71067"N	5ø01'43.50124"W	85.584

Appendix 3 -

Results of the Triangulation of Aerial Photography,

with GPS Ground Control,

for 1988 and 1996

1988:

```
Discrepancy List for Solution:
------------------------------
   Point 4 was ignored - no image points
   Point 19 was ignored - no image points
   Point 20 was ignored - no image points
   Point 30 was ignored - no image points
```

Frame Description	Control Points	Tie Points
88_089	6	0
88_090	13	0
88_091	12	0
88_092	7	0
88_187	7	0
88_188	12	0
88_189	8	0
88_194	7	0
88_195	7	0

```
                    ----- Results for Iteration  1 -----

                          Statistics Summary
                          ------------------
                     Number of Equations:  308
                     Number of Unknowns:   150
                     Degrees of Freedom:   158

               Standard Deviation of Unit Weight: 24.176958


                    ----- Results for Iteration  2 -----

                          Statistics Summary
                          ------------------
                     Number of Equations:  308
                     Number of Unknowns:   150
                     Degrees of Freedom:   158

               Standard Deviation of Unit Weight: 1.556546


                    ----- Results for Iteration  3 -----

                          Statistics Summary
                          ------------------
```

```
                    Number of Equations:  308
                    Number of Unknowns:   150
                    Degrees of Freedom:   158

          Standard Deviation of Unit Weight: 0.671321


               ----- Results for Iteration  4 -----

                         Statistics Summary
                         ------------------
                    Number of Equations:  308
                    Number of Unknowns:   150
                    Degrees of Freedom:   158

          Standard Deviation of Unit Weight: 0.671192


               ----- Results for Iteration  5 -----

                         Statistics Summary
                         ------------------
                    Number of Equations:  308
                    Number of Unknowns:   150
                    Degrees of Freedom:   158

          Standard Deviation of Unit Weight: 0.671191
```

1996:

```
Discrepancy List for Solution:
------------------------------
   Point 32 was ignored - no image points
   Point 35 was ignored - no image points
   Point 36 was ignored - no image points

Frame Description         Control Points  Tie Points
------------------------  --------------  ----------
96_047                             5          10
96_048                            15          16
96_049                            14          17
96_050                            10          10
96_233                             9          10
96_234                            10          10
96_288                            10          10
96_289                            14          14
96_290                             8          10

----- Results for Iteration  1 -----

                                   Statistics Summary
                                   ------------------
                              Number of Equations:  698
                              Number of Unknowns:   294
                              Degrees of Freedom:   404

                    Standard Deviation of Unit Weight: 66.952757
```

----- Results for Iteration 2 -----

Statistics Summary

Number of Equations: 698
Number of Unknowns: 294
Degrees of Freedom: 404

Standard Deviation of Unit Weight: 6.552553

----- Results for Iteration 3 -----

Statistics Summary

Number of Equations: 698
Number of Unknowns: 294
Degrees of Freedom: 404

Standard Deviation of Unit Weight: 1.921917

----- Results for Iteration 4 -----

Statistics Summary

Number of Equations: 698
Number of Unknowns: 294
Degrees of Freedom: 404

Standard Deviation of Unit Weight: 1.897176

Appendix 4 -

Conversion of Heights from

OD Liverpool to OD Newlyn

for the Fal Estuary

Conversion of Heights to OD Newlyn

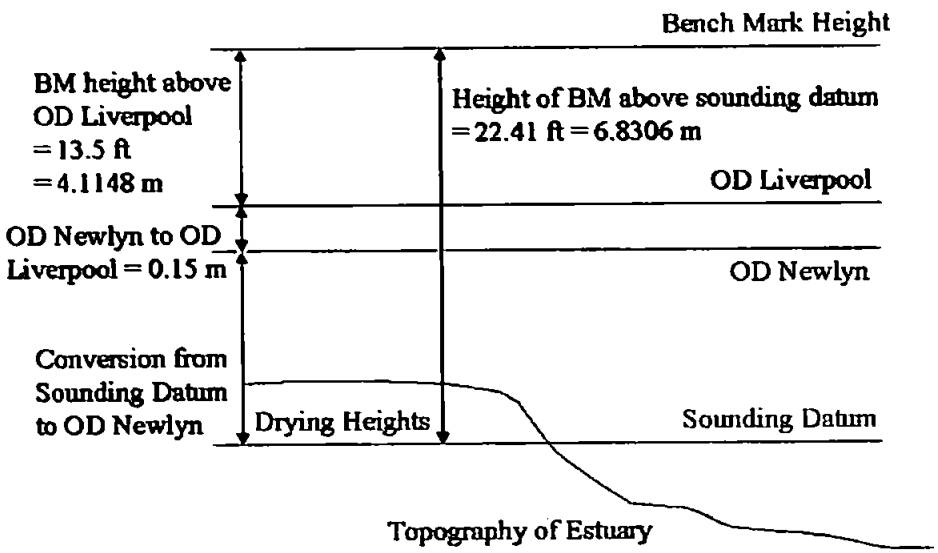

⇒ Conversion from Sounding Datum to OD Newlyn = 6.8306 - 4.1148 - 0.15 = 2.57 m

Appendix 5 -

Publications Resulting from this Project

1. Burroughes, J. E., Abbott V. J. & Morris, K. P. (2000) Management of Hydrographic Survey Requirements. **Proceeding of Conference: Oceanology International 2000**, Brighton, UK.

2. Burroughes, J. E., George K. J. & Abbott V. J. (2001a) Interpolation of Hydrographic Survey Data. **The Hydrographic Journal** 99.

3. Burroughes J. E. & George K. J. (2001b) Automation of Interpolation by Zoned Inverse Distance Weighting for Linearly Distribution of Soundings. **GeoCoast**. In Press.

Management of Hydrographic Survey Requirements

Authors

Miss J E Burroughes
Researcher, University of Plymouth, UK

Mr V J Abbott
Senior Lecturer, University of Plymouth, UK

Dr K P Morris
GIS Researcher, Centre for Coastal Marine Sciences, UK

Paper presented at Oceanology International (OI) 2000 Conference.

Abstract

As a result of frequent hydrographic surveys within large estuaries, such as the Thames or Humber, data is available to allow the recognition of sedimentary patterns, even if they are not always fully understood. In the case of smaller estuaries with fragmented commercial interests, such as the Fal estuary in Cornwall, sufficient resources are rarely available to carry out frequent and comprehensive hydrographic surveys.

Despite this limitation a variety of data providing mudbank heights and/or channel depths is available, though widely scattered amongst various authorities. This data includes occasional hydrographic surveys, aerial photography at low water and Lidar flights. Research, that is ongoing at the University of Plymouth, uses the Fal estuary as a typical example of a small port and aims to rationalise this information into a standard format and refer it to a single datum, within a Geographic Information System (GIS). The result of this process will provide a basis for a statistical, prediction model of depths within the estuary. The development of such a model, in conjunction with airborne data to be acquired in the future, will aid the port authorities in evaluating sediment movement within their area of jurisdiction and manage further hydrographic survey requirements economically.

The paper expands on the aim of the project outlined above and considers the approach to be used in tackling this problem. Available data sets are identified and displayed graphically along with data format and datum problems experienced. Possible solutions to these problems are investigated and the results of these initial stages of the project are shown by graphical displays from the GIS.

Introduction

Despite forming the largest estuarine system in Cornwall the Fal estuary (figure 1) exhibits problems of fragmented commercial interests and limited resources for carrying out hydrographic surveys identified. This is typical of a small estuary. The lower section of the estuary forms a deep tidal basin, know as Carrick Roads, which does not, in general, present navigational restrictions. The situation experienced within the six major tributaries flowing into this basin is, however, less favourable towards shipping. Large areas of these tributaries consist of inter-tidal mud flats, which cover some 26% of the total area covered by the Fal estuary (Hughes, 1999) and navigation channels are often narrow, shallow and convoluted. Strong tidal currents and rapid water level changes are produced by the fairly large spring tidal range of 4.6 m (Admiralty Tide Tables, 1999) experienced within the estuary. Additionally the River Fal, Tresillain River, Truro River and Restronguet Creek, which flow into the head of the estuary, have historically experienced rapid siltation as a result of mine waste deposits (Pirrie et al, 1996, 1997).

Figure1 - Location of the Fal Estuary, Cornwall, UK

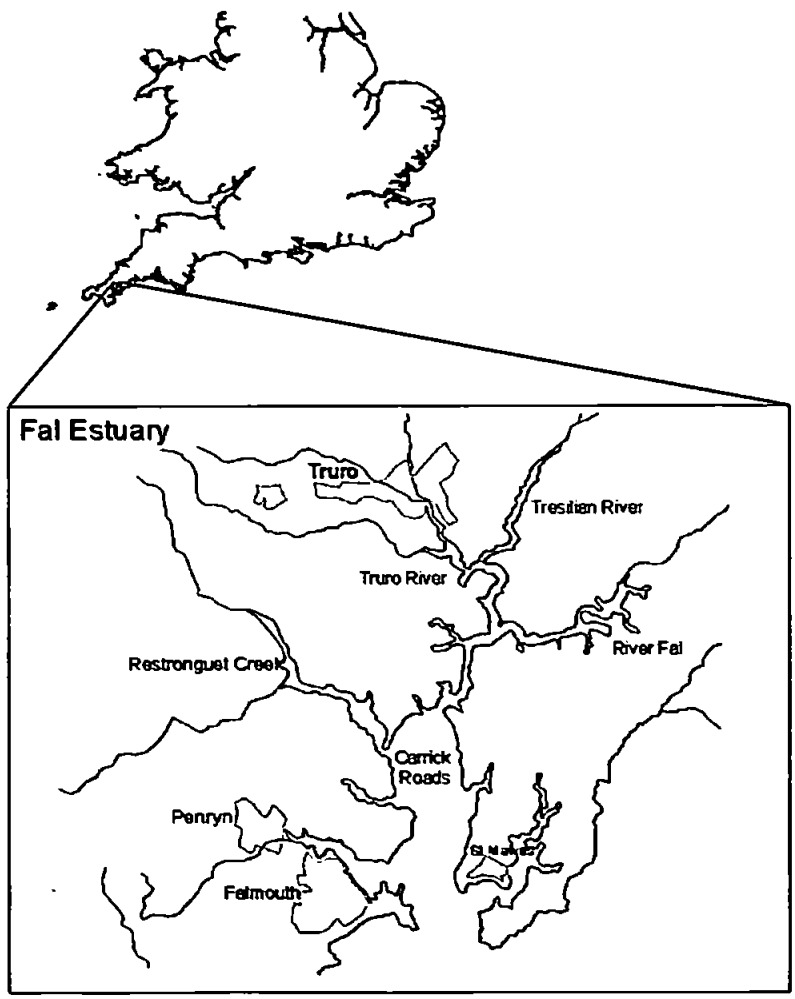

The main commercial ports within the Fal estuary are those of Truro, Penryn and Falmouth, with major waterfront activities consisting of:

- Cargo handling and the landing of calcified seaweed at Newham and Lighterage Quays in the Truro River.
- Fishing activities at Penryn Quay, Bowyers Cellars and Little Falmouth.
- Boatyards, lay ups and maintenance on the south bank of the Penryn River.

The main commercial area is at Falmouth Docks, supporting cargo handling, ship repair and maintenance, dry docking facilities and the building and fitting of large yachts. Bunkering services for ships using the English Channel and sheltered anchoring for large vessels in Carrick Roads and Falmouth Bay are also commercially important to the Falmouth area (Ratcliffe, 1997).

The small Truro Harbour Authority handles approximately 50,000 tonnes per annum, with cargoes including primary and secondary aggregates, scrap metal, barley, timber, animal feed, fertiliser and china clay (Truro Harbour Records, 1999). The port is only accessible to small vessels, the largest of 1748 dwt (Lloyd's Ports of the World, 1999).

In view of the physical conditions and commercial requirements outlined above, it was decided that this study would concentrate on the Truro River section of the Fal estuary. This waterway is important in linking the deep basin of the lower estuary to the Truro Harbour Authority and small commercial quays along the riverbank.

This paper will initially describe the major types of topographic and bathymetric data available for the Truro River. Sources of ancillary information, such as volumes of material dredged from this area and climatic data prior to the various surveys, will also be identified. Methods adopted in the rationalisation of these data sets to a common format, referred to a single datum will be addressed, and problems experienced during this process identified, with discussion of their possible solutions. Finally the results of this phase of the project will be displayed using output from a GIS.

Data Inputs

Acoustic bathymetry collected by the Harbour Masters Department has, to-date, provided the only basis for monitoring siltation and assessing survey requirements within the Truro River. Such data is limited, by financial constraints and equipment availability, to relatively infrequent surveys gathered using a single beam echo sounder. This project aims to accumulate such data, in conjunction with data from other types of survey and supporting historic information to provide a fuller picture of changes within this part of the Fal estuary. Data has been accumulated for the Truro River from 1960 to the present.

The major bathymetric and topographic data sets for inclusion within the GIS are as follows:

- Depths and drying heights are provided by a number of boat-based acoustic surveys. The United Kingdom Hydrographic Office and Truro

Harbour Authority have supplied this data, collected using a single beam echo sounder. Coverage of the entire Truro river is provided for 1974 and the 1990s (Comprising three surveys: 1991, 1995 and 1996) with partial coverage from 1961. Data along a survey line is gathered every 0.1 second. Data interval supplied on a chart is scale dependent, with a typical sounding spacing of 12 metres at the scale of 1:2,500. Survey line spacing is variable due to the curved course followed by the river; the average spacing is approximately 40 metres.

- Lidar data collected in 1998 has been obtained from the Environment Agency (figure 2). The red wavelength Lidar used provides very little penetration into the water column, thus mud bank heights but not water depths are obtainable from this data set. Since the Lidar data was flown at low water, coverage of all drying areas in the Truro River was achieved at very high resolution, using a pixel size of 2 metres.

Figure 2 - Environment Agency Lidar data
Truro River

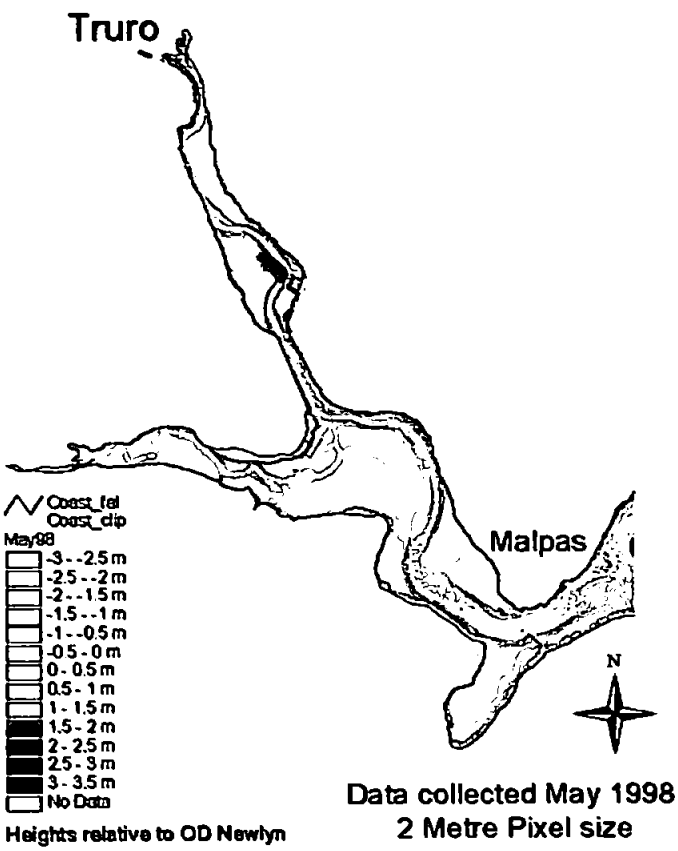

- Sets of aerial photographs, forming vertical, stereo pairs were obtained from the National Remote Sensing Centre Ltd (NRSC) and BKS Surveys Ltd, Londonderry, Northern Ireland with the permission of Cornwall

County Council. Two sets of nine photographs flown at low water will provide mud bank height information for 1988 and 1996. Camera calibration certificates, necessary for stereo interpretation from the photography, have also been obtained from NRSC and BKS Surveys Ltd. Ground control for the aerial photography will be surveyed in using a real time kinematic (RTK) global positioning system (GPS). The carrier phase system, manufactured by Trimble and loaned to the project by the University of Plymouth, will provide centimetric accuracy in both horizontal position and height.

Identification of trends within these topographic and bathymetric data sets will be carried out in the context of supporting information, as follows:

- Datum information provided by Truro Harbour Authority and the United Kingdom Hydrographic Office.
- Tidal information obtained from Truro Harbour Authority and the Admiralty Tide Tables.
- Daily rainfall totals for at least one month prior to surveys, supplied by the United Kingdom Meteorological Office.
- Dredging quantity data provided by Truro Harbour Authority.

Data Format and Datums

To provide a basis for comparison, the diverse data sets described above required rationalisation to a common unit system, reference datum and data format. This process was carried out within an Arc/Info based GIS. The completed system will provide a tool for data integration and modelling within later stages of the project.

The first stage of the rationalisation process was to convert depth and height data from early surveys from feet into metres. All positions were resolved to the Ordnance Survey (OS) grid, OSGB36. OSGB36 was selected because it is widely used and well understood within the British scientific community. In addition, the choice of grid co-ordinates, rather than latitude and longitude, will simplify geometric issues associated with interpolation of spatial data. Limitations imposed on OSGB36 by internal inconsistencies within the system (Ashkenazie et al 1972 & 1980) were not considered to represent a major problem over the size of the survey area covered by the Truro River. The variety of data to be included within the project made issues of datum conversion inevitable. The choice of OSGB36 results in a requirement for conversion from the GPS reference ellipsoid, WGS84, to OSGB36 for Lidar data and aerial photographic ground control.

It was decided to relate all depth and height information to Ordnance Datum (OD) Newlyn. This datum provides a vertical reference level coincident with a horizontal plane throughout the area of interest, unlike the more obvious choice of local chart datum. This forms a series of six steps along the Truro River, between the north end of Carrick Roads and Truro.

To allow intercomparison of the data spatial and depth resolution required rationalisation between the various data sets. A 10 metre cell size was chosen as the most suitable resolution in both horizontal directions. This choice of optimum resolution represents a compromise between requirements for a sufficiently high resolution to allow comparison of fine detail within channel bed structure and limitations imposed by the single beam sounding data with average resolutions of 12 metres along line and 40 metres between lines. Averaging of the high resolution, Lidar data (figure 2) to this cell size unfortunately resulted in the loss of interesting detail, but presented no technical difficulties within the GIS. Interpolation of the lower resolution single beam echo sounder data to the 10 metre cell size was, however, far less straightforward.

Interpolation Results

Initially a triangular irregular network (TIN) model was used to interpolate point depths onto the 10 metre grid. This method creates a network of triangles joining each point to all its near neighbours; point values are maintained and intermediate values are interpolated within the triangles. Interpolation of the linearly inhomogeneous, single beam echo sounder data by the TIN technique produced features identified as 'artificial interpolation artefacts'. These features formed shoal 'ridges' across the centre line of the deep water channel between lines of depth data (figure 3). Interpolation between shoal depths on either side of the channel was identified as the cause of such artefacts.

Figure 3 - Example of TIN Model Interpolation

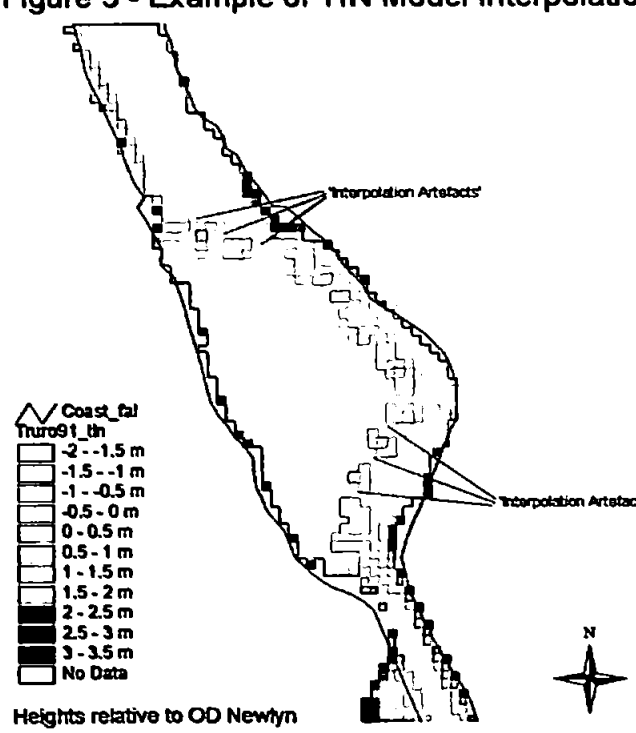

Data collected 6 - 17 March 1991
Interpolation by TIN Model to 10 metre cell size
Interpolation ' Artifacts' along channel centre

A number of techniques were identified as possible methods of eliminating this interpolation problem. Manual interpolation and addition of data points along the centre line of the channel before re-running the TIN model was attempted. This method proved moderately successful in reducing interpolation artefacts, but some artefacts of smaller horizontal extent and lesser depth differential were still generated by the TIN model.

The use of Inverse Distance Weighting (IDW) as an interpolation technique was also investigated. The method weights surrounding depth values according to their distance from each point where an interpolated depth value is required. A number of interpolation radii were tested during the investigation of the IDW technique. The method was, however, rejected due to a tendency to produce channel bed contours consisting of small spikes and hollows not realistic in sediment consisting of mud particles. An example of sounding data interpolated using the IDW method is given in figure 4.

Figure 4 - Example of IDW Interpolation

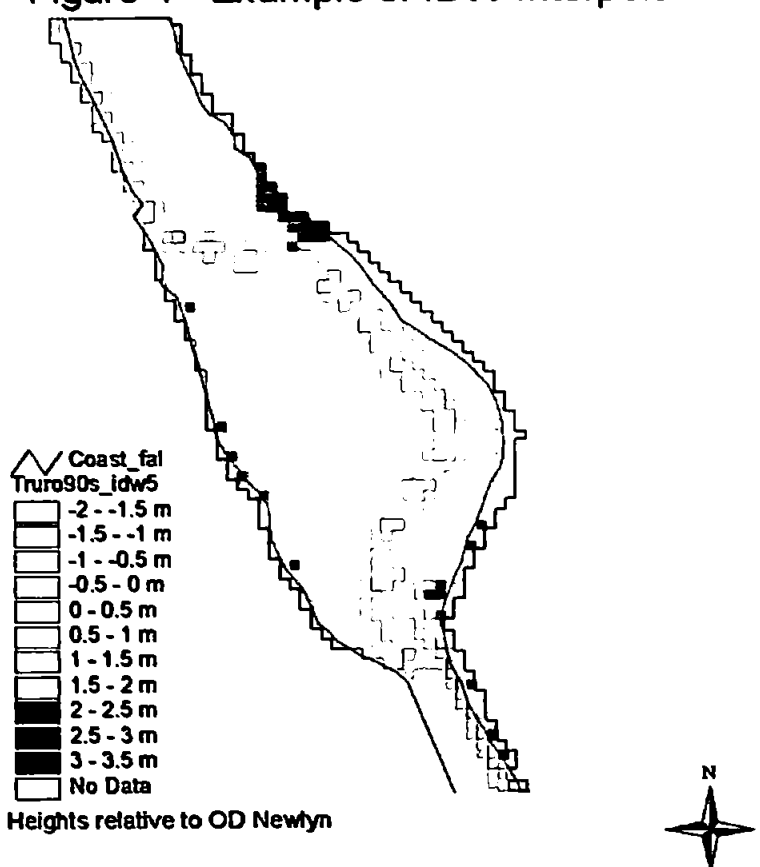

Data collected 6 - 17 March 1991
Interpolated cell size 10 metres
Interpolation radius 50 metres

Finally the statistical interpolation technique of Kriging was applied to the bathymetric data. Investigation of the most suitable type of interpolation model and interpolation radius required was carried out through the study of semi-variograms

and contoured variance models produced within the GIS. A Gaussian interpolation model with a radius slightly larger than the maximum line spacing of the point data (a 50 metre radius for 40 metre line spacing) produced results apparently free from identifiable, interpolation artefacts. An example of sounding data interpolated using the Kriging by the Gaussian model is given in figure 5. It is worth noting that interpolation by Kriging is relatively slow and computer intensive compared to the other interpolation methods mentioned above.

The aerial photographic data, supplied as photo prints, were scanned onto a Personal Computer (PC) at high resolution. Stereo interpolation using Erdas Imagine software will be carried out once the RTK system becomes available to carry out the ground control survey.

Depth data has been displayed at decimetre resolution using Arc/View legend files constructed to highlight depth bands of particular interest whilst masking out land heights within the Lidar and aerial photographic data.

Figure 5 - Example of Kriging Interpolation

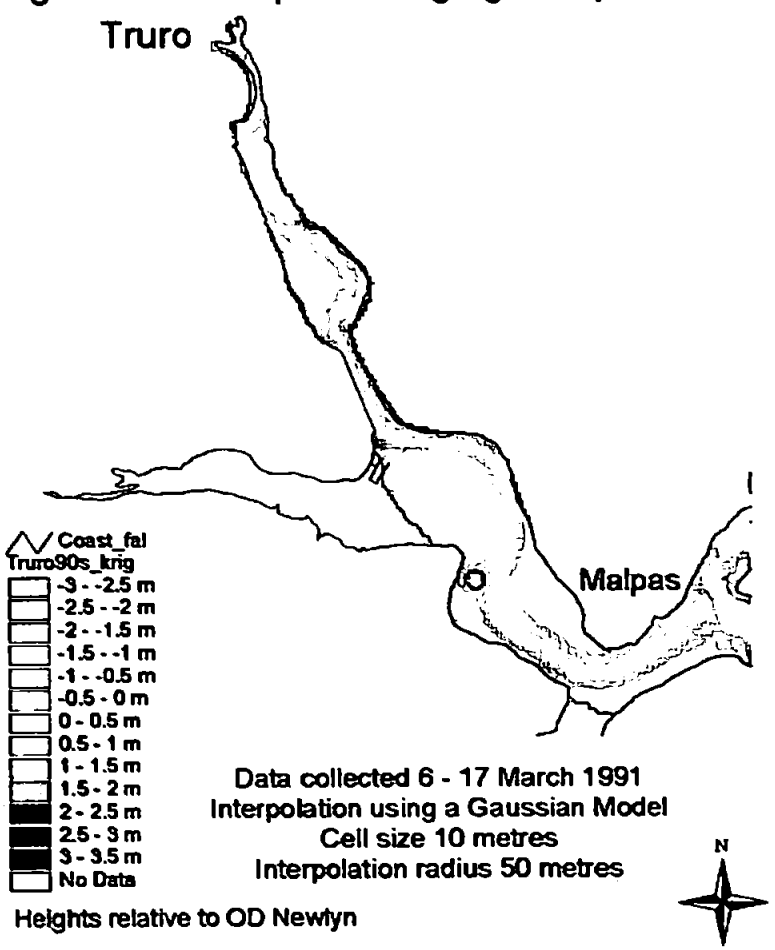

Discussion & Conclusions

The paper describes the types of topographic and bathymetric data available for a small estuary with fragmented commercial interests, such as the Fal estuary in SW Cornwall. In order to provide a basis for investigation and modelling of long term changes within such an estuarine system it was necessary to use data collected by the vastly differing methods of single beam acoustic bathymetry, Lidar and aerial photography. The rationalisation of these hydrographic data sets to a common reference framework and format within the Arc/Info GIS, as a basis for meaningful data comparison, has been discussed in some detail. The choice of the OSGB36 grid system to provide the horizontal reference framework and the vertical datum, consistent with a horizontal plane, OD Newlyn for water depths are explained with justification of this choice. Problems experienced within the process of data format rationalisation are highlighted, with discussion of possible solutions. The particularly problematic area of interpolating data from a single beam echo sounder into a regular grid format, is especially focussed upon.

It is proposed that the result of the data collection and rationalisation process described will provide a basis for a statistical, prediction model of depths within the Truro River. This model, in conjunction with airborne data to be acquired in the future, will aim to aid Truro Harbour Authority in evaluating sediment movement within its area of jurisdiction. This evaluation should allow limited resources available for hydrographic surveying to be managed more efficiently, by targeting resources to particular areas at varying time intervals.

Acknowledgements

We acknowledge Dr K M Miller, University of Plymouth, for his numerous inputs to this paper and the project as a whole. Capt. A Brigden, Head of Maritime Services and Harbour Master (Truro & Penryn), is also acknowledged for providing bathymetric data and ancillary information to the project.

References

Admiralty Tide Tables, 1999. Volume 1, NP201-99, Taunton.

Ashkenazi V, Carne A S, Preiss W J & Williams J W, 1980. The 1980 readjustment of the triangulation of the United Kingdom and the Republic of Ireland OS (SN) 80. OS Professional Paper. New Series No. 31.

Ashkenazi V, Cross P A, Davies M J K & Proctor D W, 1972. The readjustment of the retriangulation of Great Britain and its relationship to the European terrestrial and satellite networks. OS Professional Paper. New Series No. 24.

Hughes S H, 1999. The geochemical and mineralogical record of the impact of historical mining within estuarine sediments in the Fal Estuary, Cornwall, UK. International Association of Sedimentologists, Special Publication.

Lloyd's Ports of the World 1999. Published by: LLP Ltd., 1998.

Pirrie D, Camm G S, Sear L G & Hughes S H, 1997. Mineralogical and Geochemical signature of mine waste contamination, Tresillian River, Fal Estuary, Cornwall, UK. Environmental Geology, Vol 29, pp 58-65.

Pirrie D, Hughes S H & Pullin H, 1996. The effect of mining on sedimentation over the last 500 years in the Fal Estuary, Cornwall, UK. Late Quaternary coastal change in West Cornwall, UK, Field Guide. Environmental Research Centre, University of Durham, Research Publication 3, pp 75-82. Ed: Healy M G.

Ratcliff J, 1997. Fal estuary historic audit. Cornwall Archaeological Unit, Cornwall County Council, Truro.

Truro Harbour Authority, 1999, general records, Truro.

A Paper Reprinted from

THE HYDROGRAPHIC JOURNAL

serving the interests of the

world hydrographic surveying community

No 99

JANUARY 2001

Interpolation of Hydrographic Survey Data

ABSTRACT

This paper considers the interpolation of historic data, collected using a single beam echo sounder, onto a regular grid. The use of conventional software provides a number of interpolation methods, including the application of Triangular Irregular Networks (TINs), Inverse Distance Weighting (IDW) and Kriging. These methods are, however, found to produce artificial, interpolation artefacts when applied to sounding data, concentrated along lines which cross narrow, deep channels. The paper develops an interpolation method to overcome this problem, based on the inverse distance weighting (IDW) technique. The results obtained during testing of the method on historic, single beam, echo sounder data collected in the Truro River, south west Cornwall, UK are presented. These results demonstrate significant success in reducing artificial artefacts of interpolation.

Janet Burroughes, Dr Ken George and Dr Vic Abbott

Institute of Marine Studies, University of Plymouth, UK.

INTRODUCTION

This paper considers the interpolation of single beam, echo sounder data collected in the Truro River, south west Cornwall. It forms part of a study into long term changes in the river and is based on surveys carried out over the past forty years, using a number of different surveying techniques.

Bathymetric data are usually available in one of two forms:

1. Published navigational charts, providing both spot soundings and depth contours, known as isobaths. The isobaths may be reduced to a series of depth values by specifying the position and depth at frequent intervals along their length.
2. Unpublished soundings charts or working drawings, comprising a larger number of spot soundings. Frequently these soundings are concentrated along survey lines running approximately perpendicular to the direction of the depth contours, with relatively large areas devoid of depth information existing between each line.

For several applications, depth information needs to be specified on a grid (often a rectangular grid). These include:

1. The comparison of bathymetric data sets from diverse sources.
2. Analysis of temporal trends.
3. Numerical modelling using finite differences.

This process involves the application of a method of spatial interpolation between the soundings. In order to achieve this interpolation at a specified point, one of a variety of methods must be applied. The details of this process vary from method to method; three commonly used methods are as follows:

1. *Inverse Distance Weighting (IDW)*, in which a radius of interpolation is defined around each specified point. All data values, linearly weighted, within this radius are then used to contribute to the value assigned at the point. The weighting applied to each value is inversely proportional to the distance of the sounding from the point. Since the output values form a weighted average they cannot be greater than the highest or less than the lowest input value. Hence, IDW cannot create ridges or valleys (Watson & Philip, 1985). Furthermore, as the influence of each input point on the interpolated values is distance related, IDW will not preserve ridges or valleys, (Philip & Watson, 1982).
2. *Triangular Irregular Network (TIN)*, where the domain is divided into triangles, with the criterion that each triangle should be as close to equilateral as possible. This method maintains existing sounding values, with interpolation between these data points being performed along the edges of the defined triangles.
3. *Kriging* is a statistical interpolation method, based on regionalised variable theory. This method assumes that the spatial variation in depth values exhibits the same pattern of variation over all parts of the surface. The mathematical function to be applied during kriging is chosen by consideration of the spatial variation of depth values within a particular data set. This is achieved by comparing graphs of semi-variance of the actual data with those of data values predicted by each mathematical function, plotted against the distance between pairs of data points. These graphs are known as semi-variograms. For more details of the kriging interpolation method see Oliver (1990).

APPLICATION TO THE TRURO RIVER

The Truro River forms one of the major tributaries flowing into the Fal estuary, in southwest Cornwall, UK. The area of the Truro River of particular interest to commercial navigation stretches northwards from its confluence with the Fal estuary in the south, to the tidal limit of the river, situated in the centre of Truro. The relative locations of the Fal Estuary and its tributaries are shown in Figure 1.

The upper section of this stretch of river varies in width from less than 40m to more than 200m. It practically dries out at low water, revealing extensive mud flats on either side of a steep-sided channel some 30m wide. This channel contains a stream of river water, which continues to flow even at extreme low tide. The bathymetric data collected in the Truro River, and supplied by Truro Harbour Master, takes the form of a large number survey lines forming cross sections across the river channel. The data was

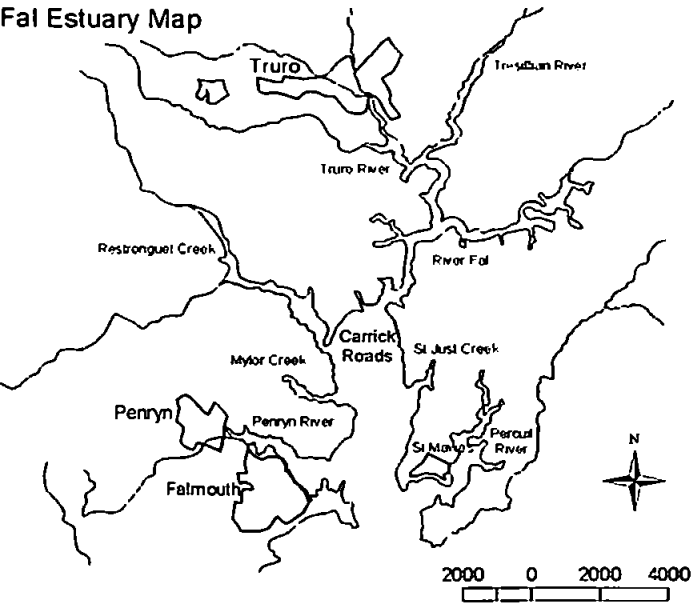

Fig. 1: Relative locations of the Fal estuary and Truro River

pplied at a scale of 1:2500, giving an average along line sounding acing of 11m and between line intervals of about 40m. Additional undings have been input, manually along the centre line of the main annel.

It is evident that in order to obtain reasonable results from lines soundings spaced 40m apart, a radius of 50m is appropriate for use a method of spatial interpolation. Since the channel is only proximately 30m wide, the use of a circular zone of interpolation ound each specified point means that averaging will take place ross the channel. The extreme case is a point in the bed of the channel, whose depth will be determined by averaging depths on the slopes on either side, as well as soundings adjacent to it within the channel. Consequently, the averaged depth assigned to points in the vicinity of the channel will be unrealistically shoal. The overall effect of this limitation with each interpolation method is to produce a series of artificial ridges across the channel, the centre of which correspond with the centre of the 40 metre 'gap' between lines of soundings (Figure 2).

OVERCOMING THE INTERPOLATION PROBLEM

Initial attempts to eliminate this interpolation problem involved locating the line of maximum depths along the channel. Additional data points were added to the sounding data along this line, by means of manual interpolation between adjacent deepest depths. The IDW interpolation model was then reapplied to this manually improved point data file. This method exhibited a moderate degree of success in reducing interpolation artefacts, but some artificial ridges of smaller horizontal extent and lesser depth differential remained after the interpolation process. The results are displayed in Figure 3.

At University of Plymouth, a program is being developed to completely overcome this interpolation problem. Within this program each sounding in the data set is assigned to one of three categories. Bearing in mind the general trend of the river channel is north south, the categories are assigned as follows:

1. W = west of the channel bed
2. C = in the channel bed
3. E = east of the channel bed

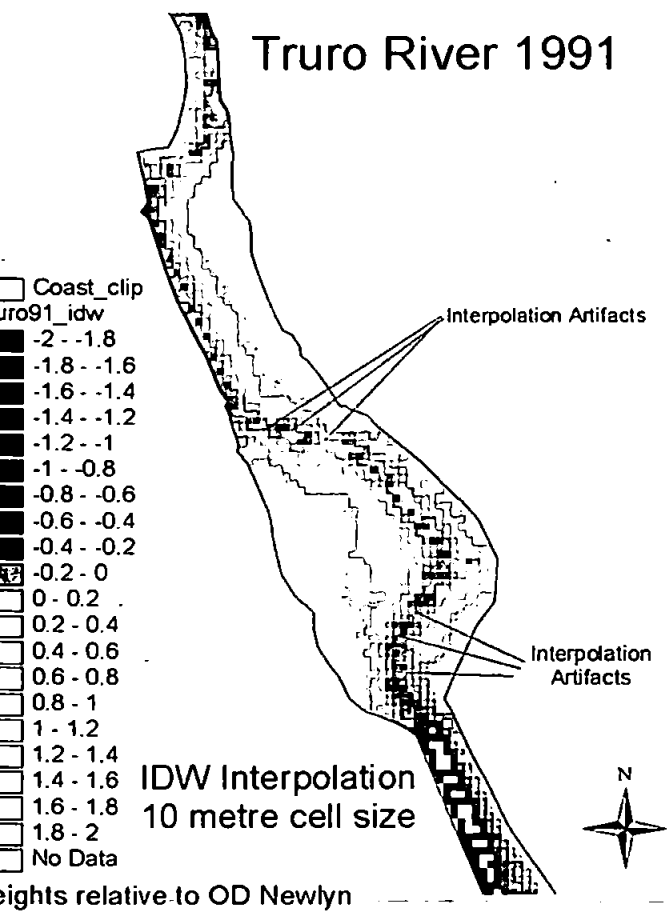

Fig. 2: Interpolation of bathymetric data without special consideration of the channel

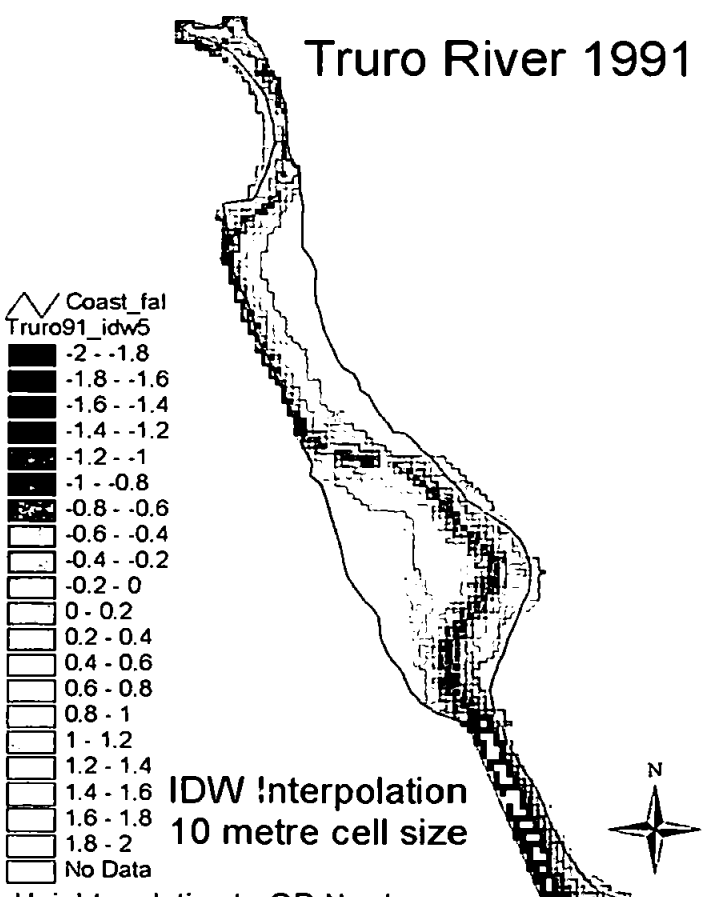

Fig. 3: Interpolation of bathymetric data with manual interpolation of soundings along the centre line of the channel

Each point in the rectangular grid on to which points are to be interpolated is similarly assigned to one of the three zones W, C or E. The allocation of zones to the sounding data is illustrated in Figure 4.

To date, these zones have been assigned by manually editing soundings and grid cells within the data files. Clearly for large and/or multiple data sets it would be desirable to devise a method of automating this process.

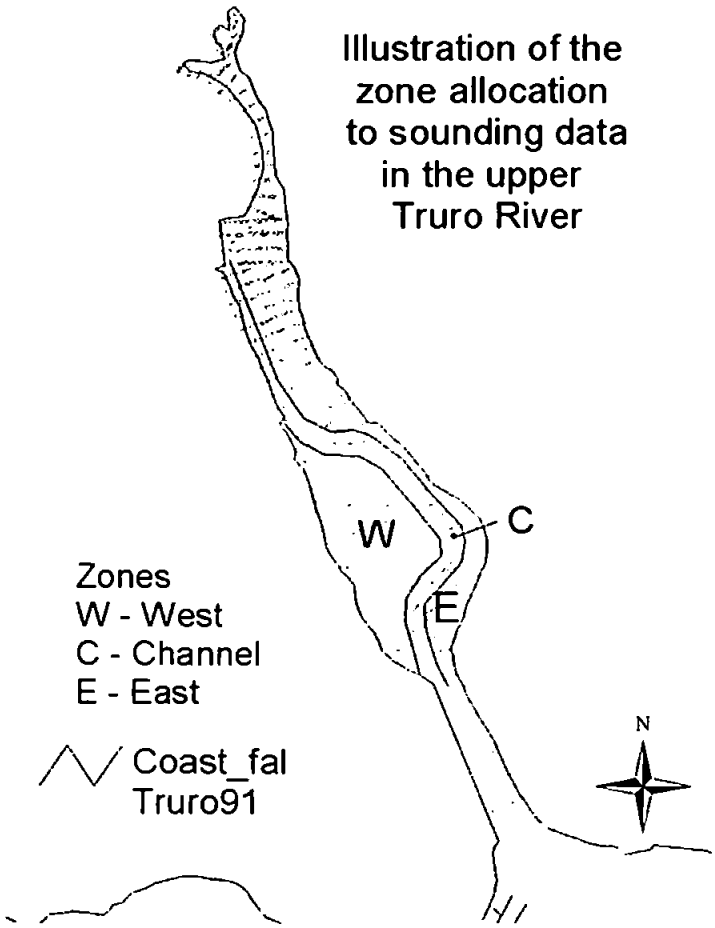

Fig. 4: Allocation of the three zones to bathymetric data in part of the upper Truro River

Interpolation was performed by the method of inverse distance weighting, with an interpolation radius of 50m, but taking the zones into account, thus:

Zone of Specified Point	Zone of Sounding
West	West or Channel
Channel	Channel
East	Channel or East

The success of zoning the channel and mud bank areas in the interpolation process is clearly shown in Figure 5. It can be seen that allowing for the channel by zone allocation removes artificially interpolated ridges across the channel otherwise produced by interpolation (previously illustrated in Figure 2).

DISCUSSION AND CONCLUSIONS

The results of interpolation of lines of soundings onto a regular, rectangular grid were found to be far more realistic, particularly when the existence of the narrow, relatively deep channel was

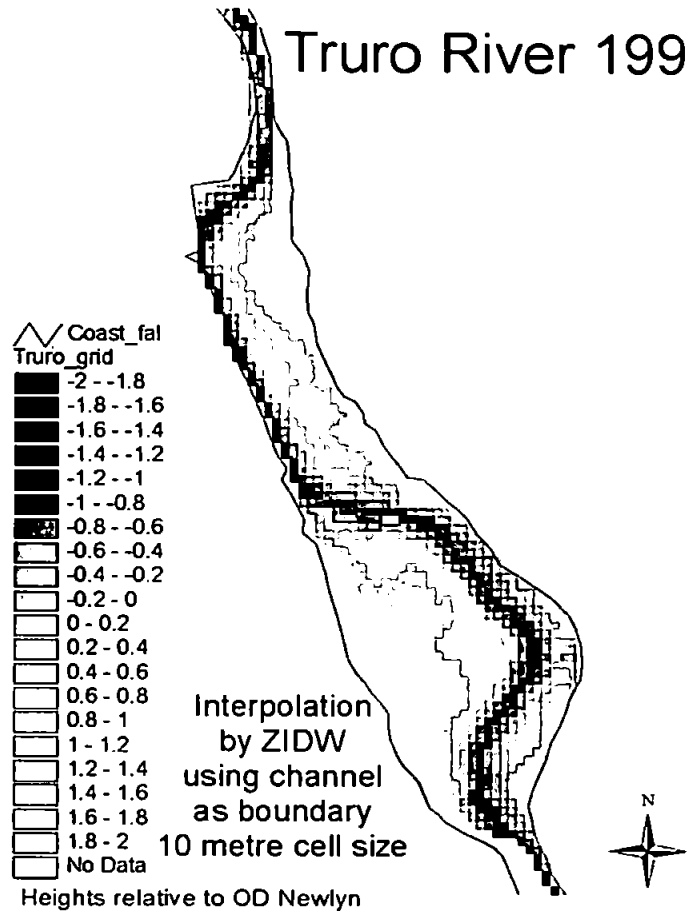

Fig. 5: Interpolation of bathymetric data using Zoned Inverse Distance Weighting to allow for the channel

specifically taken into account during the interpolation process. The characteristics of fine, tide washed sediments, such as those found in the Truro River, would be inconsistent with the formation of the series of holes and ridges placed in the channel by interpolation without specific treatment of the existence of this channel. The zoning method proposed is intended to eliminate this problem successfully.

Currently the program developed at the University of Plymouth requires manual assignment of the zones (west, channel or east), in order to perform this refined method of data interpolation. To allow the program to be easily applied to large and/or multiple data sets further development would be desirable to automate the zone assignment process. Trend analysis using a number of historic data sets, from the Truro River, illustrates an application which would benefit from the automation of zone assignment within the program.

REFERENCES

Oliver, M.A. 'Kriging: A Method of Interpolation for Geographical Information Systems'. *International Journal of Geographic Information Systems* 4: no. 4, pp 313-332, 1990.

Philip, G.M. and Watson, D.F., (1982). 'A Precise Method for determining Contoured Surfaces', *Australian Petroleum Exploration Association Journal* 22: pp 205-212.

Watson, D.F. and Philip, G.M., (1985). 'A Refinement of Inverse Distance Weighted Interpolation', *Geo-Processing*, 2: pp 315-327.

THE HYDROGRAPHIC SOCIETY

2002 DIARY

Interested in sponsoring The Hydrographic Society's 2002 Diary ?

... READ ON & ACT NOW

If you look inside the covers of The Hydrographic Society's Diary you can read the profiles of the sponsors of this year's diary and see their advertisements

This time next year you could be looking at *your* company's profile and full-page advertisement

Remember every Member of the Society will receive a copy of the 2002 Diary

Corporate and Associate Corporate Members interested in taking advantage of sponsorship opportunities in the 2002 Diary are invited to provide the following by the 31st May 2001 deadline:

Sponsorship of £450 plus VAT

Full-page black & white camera-ready advertising material

250-word company profile

See order form enclosed

* * * * *

Additional Diaries & Presentation Diaries

The Hydrographic Society is proud of its Diary: it looks stylish and is a convenient size. It is also an excellent way to promote your company's name and profile; your aims, purpose and operation will be broadcast to the Society's membership and beyond for a whole year.

Corporate Members and Associate Corporate Members are invited to order special presentation copies of the Diary with their own name and logo on the front cover. These presentation copies can be distributed to your existing and potential new clients or used for other promotional purposes.

Sponsorship is good value for money

* * * * *

To discuss special discount packages combining Diary sponsorship with advertising in The Hydrographic Journal or on the Society's website, please contact the Media Manager

For further details and order forms for Presentation Diaries or extra Diaries, please contact:

Helen Atkinson, Media Manager, The Hydrographic Society, PO Box 103, Plymouth, PL4 7YP, UK

Tel. & Fax. +44 (0)1752 223512 *e-mail: helen@hydrographicsociety.org*

If you would like to see your company's profile in next year's diary, pass this information on to your advertising manager

DON'T MISS THE DEADLINE – 31st MAY 2001

Automation of Interpolation by Zoned Inverse Distance Weighting for Linearly Distribution of Soundings

By Janet Burroughes and Dr Ken George, Institute of Marine Studies, University of Plymouth.

Published in the on-line journal GEOCOAST in September 2001.

Abstract

This paper documents the development of a suite of programs to automate the Zoned Inverse Distance Weighting (ZIDW) method of interpolation. ZIDW was devised, (Burroughes et al, 2001), after extensive testing revealed that standard interpolation methods were unable to deal, in a sensible manner, with estuarine bathymetry, containing relatively deep, narrow channels. The initial stages of the ZIDW method consist of the definition of sounding lines, identification of channels and allocation of soundings to zones. At first these processes were performed manually (Burroughes et al, 2001). The manual method was acceptable, although time consuming, for small data sets. Over larger survey areas, however, even within a fairly small estuary, manual allocation of soundings was not feasible. Hence, it became necessary to develop a suite of programs to automate the ZIDW process.

The paper describes, in detail, the development, and testing, of this suite of programs, using data sets from the Fal estuary, in Southwest Cornwall. Careful consideration, during the design process, will allow the programs to be generally applicable to estuaries containing mud-banks crossed by relatively narrow deep channels. The method is currently being applied on a much larger scale, in the Gironde estuary, in western France, as part of ongoing research work at the University of Plymouth.

Introduction

The vast majority of existing bathymetric data, particularly historic data, have been collected using a single beam echo sounder. Working charts produced from this type of data contain a high density of soundings, limited only by the space required to print each value, along the sounding line with comparatively large gaps between the lines. For example, the sounding data, displayed on charts at a scale of 1:2500, being used in this study demonstrates an average sounding spacing of 11 metres along sounding lines, but a line spacing of around 40 metres.

In order to use this type of depth data for numerical modelling and trend analysis it becomes necessary to interpolate the data on to a regular grid. Such interpolation can be performed by numerous proprietary software packages using one of several interpolation methods, for example Inverse Distance Weighting (IDW), Triangular Irregular Networks (TIN) and Kriging. These methods will produce apparently realistic results for interpolation over areas exhibiting smooth, uniformly trending water depths. However, when applied to estuarine bathymetry, consisting of mudflats crossed by a narrow, relatively deep channel, prominent 'interpolation artefacts' are produced.

Examples of these artefacts, appearing as ridges across the deep channel, were generated when single beam echo sounder data for the Truro River, in Southwest Cornwall, UK, were interpolated. Figure 1 shows these data interpolated using IDW within Arc/Info software. A 50 metre interpolation radius has been used to include adjacent lines given an approximate line spacing of 40 metres.

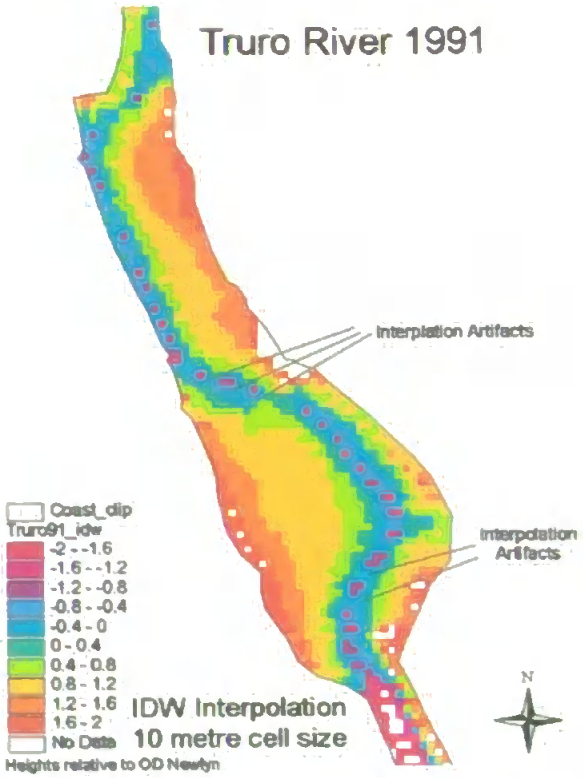

Figure 1 – Interpolation of inhomogeneous sounding data on to a regular grid, by means of IDW, without special consideration of the deep channel.

These artefacts are clearly shown by two cross-sections through the Truro River (see Figure 2a). Despite being only 20 metres apart the two cross sections reveal substantial differences depending whether the profile is along a sounding line or between lines. The profile along the channel (Figure 2b) shows non-existent ridges across the channel occurring at approximately 40 metres intervals. These ridges correspond to the gap between each sounding line.

The interpolation artefacts, described above, result from interpolation of depths within the channel, using shoaler points on either side in addition to adjacent channel data. Similar artefacts were generated when bathymetric data were interpolated by means of Triangular Irregular Networks or Kriging (Burroughes et al. 2000).

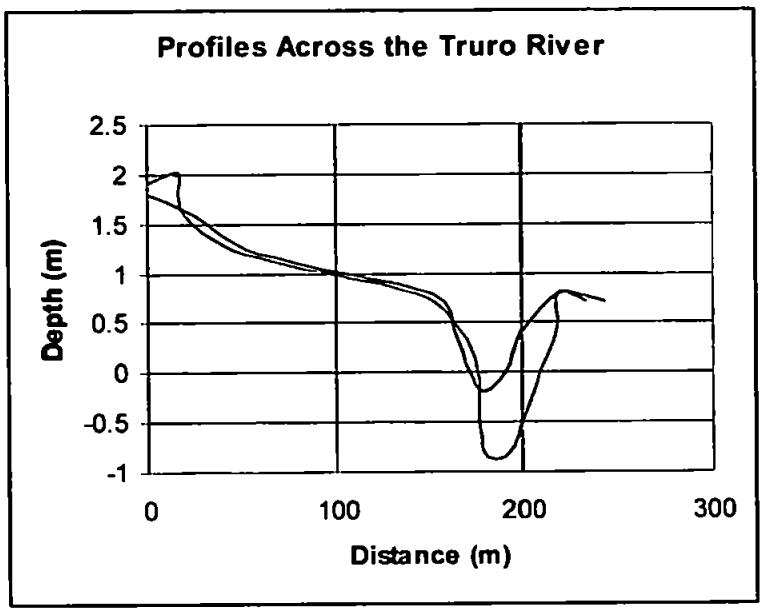

Figure 2a – Two profiles across the Truro River 20 metres apart, along a sounding line (red line) and between sounding lines (blue line).

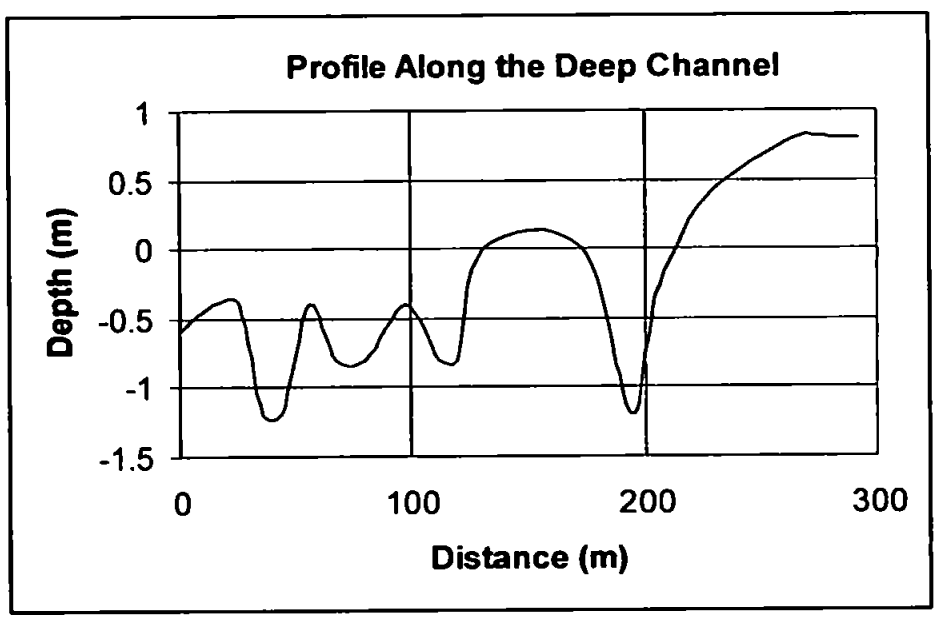

Figure 2b – Profile along deep channel of the Truro River, as shown in Figure 1.

A method has been developed to overcome this limitation in standard interpolation procedures. This method, referred to as Zoned Inverse Distance Weighting (ZIDW), recognises and accounts for the deep channel during interpolation. A program to perform ZIDW has been developed at the University of Plymouth, the initial stages of which are described in Burroughes et al. (2001). In essence, this program requires

each input sounding and cell in the output grid to be assigned to one of three categories, as follows:

1. W = west of the channel bed
2. C = in the channel bed
3. E = east of the channel bed

The zone assignment process is illustrated in Figure 3.

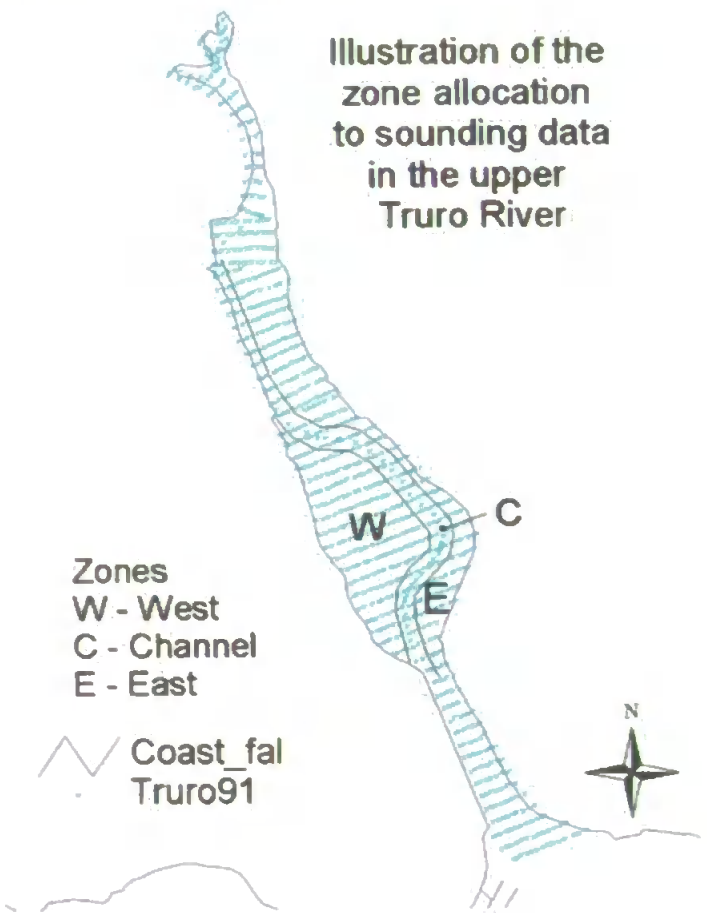

Figure 3 – Allocation of the three zones to bathymetric data in part of the Upper Truro River

Interpolation is then performed by inverse distance weighting, but taking the zones into account, thus:

Zone of Specified Point	Zone of Sounding
West	West or Channel
Channel	Channel
East	Channel or East

The results of this ZIDW interpolation, using a 50 metre radius of interpolation, for historic data from the Truro River, are shown in Figure 4.

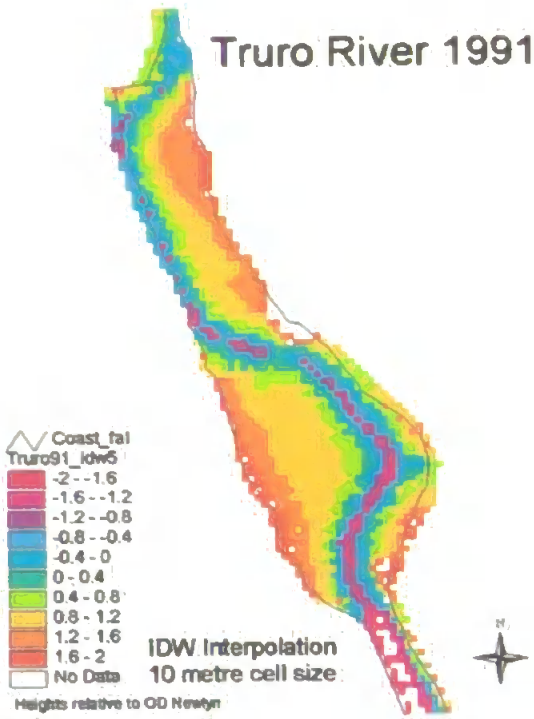

Figure 4 – Interpolation of bathymetric data using Zoned Inverse Distance Weighting to allow for the channel

A comparison of Figure 4 with Figure 1, produced by standard IDW interpolation performed on the same data set, clearly shows the effectiveness of the ZIDW method in eliminating artefacts of the interpolation process from the output grid data.

Previously (Burroughes et al., 2001) the assignment of zones to soundings and output cells was performed manually. Clearly this limited the use of ZIDW to the interpolation of single, small data sets. This paper describes the stages involved in

automating the process of allocating zones to produce a suite of programs allowing ZIDW to be applied to large and multiple bathymetric data sets.

Automation of the Zoning Process

The stages of producing ZIDW with automated zone allocation are shown in Figure 5.

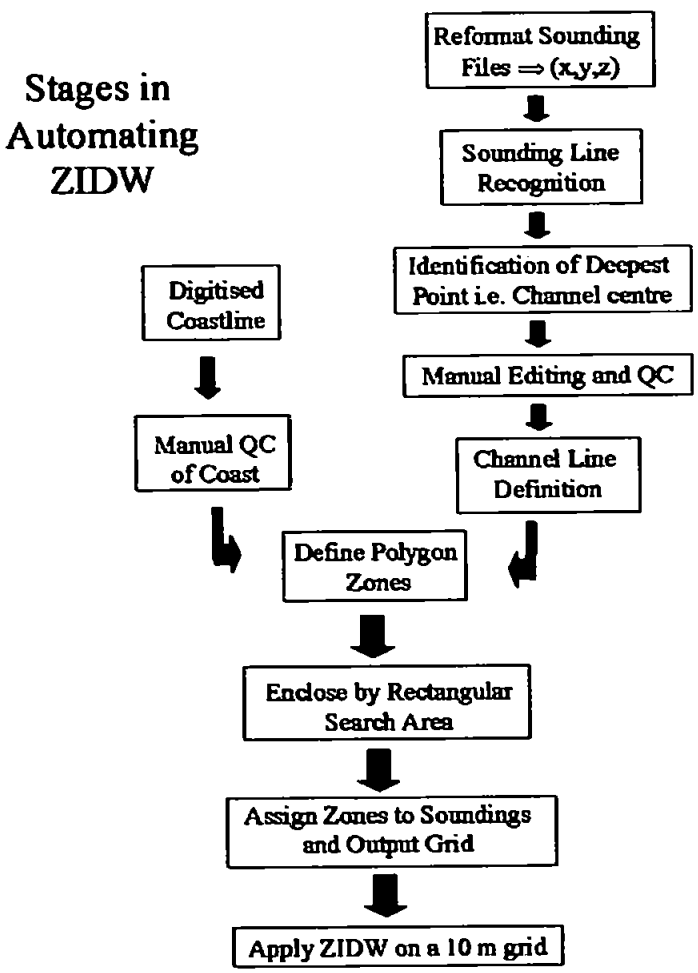

Figure 5 – Flow Diagram illustrating the processes involved in producing automated ZIDW software.

The first stage of the automation process was to define the centre line of the deep channel (right branch of the flow diagram, Figure 5). Initially the separate position (x, y) and depth (z) files produced by digitising depth data within Arc/Info were

combined into a single file of co-ordinates and depth (x, y, z) which could be input into the ZIDW software suite.

As the depth within the deep channel is unlikely to be uniform (in the case of the Truro River the channel shoals moving landward) an overall depth threshold can not be used to identify the line of deep soundings delineating this channel. Instead advantage was taken of the requirement for survey lines of single beam echo sounding data to be run at a high angle (near perpendicular) to depth contours, and hence to the channel. Consequently the deepest sounding on each line will represent the point of intersection of the deep channel with that line. Identification of this intersection point on all sounding lines will thus produce a series of points through which the channel line may be drawn.

To apply this process it was first necessary for the program to recognise sounding lines within the (x, y, z) data file. Here it was possible to have recourse to the order by which linearly distributed data are most straightforwardly digitised, i.e. across the river along the first line then returning in the opposite direction via the next. The program considered the direction between consecutive pairs of soundings to determine whether they lie on the same line. An inter-sounding direction of less then 60° implies that the pair of soundings lie on the same line, whilst a directional change of greater than 60° identifies a change from one line to the next. Hence, a column containing line numbers can be added to the (x, y, z) data file.

This method would also operate successfully for sounding data digitised line by line in the same direction. Digitally logged data will normally contain line numbers, and thus allow this stage of the automated ZIDW process to be by-passed, or at least simplified. However, the line identification method within ZIDW would deal with data logged consecutively along vessel survey lines if required.

Having identified the survey lines the program then determined, and allocated a code number, to the deepest sounding within each line. The record (co-ordinates, depth, line number, and code) for each of these deepest points was automatically copied to the end of the data file, to allow straightforward investigation and display of the results. Local minima were also ascertained, with a different code number, to facilitate interpolation in the area of any subsidiary channels.

Examination of the program outputs from this stage of the ZIDW software revealed a number of anomalies. These anomalies resulted from peculiarities in the survey method and complex channel features, supporting the decision to incorporate a manual quality control (QC) stage within the program at this point, see Figure 5.

Details of Anomalies

Anomalous channel points selected by the program were identified as resulting either from unusual survey practice or from genuine anomalies in the estuarine channel system. Within these two broad categories a number of specific problem factors were detected:

1) Factors of unusual survey practice

   a) Partial survey lines - where occasional large gaps between survey lines have been in-filled by a line stretching only part way across the estuary. Anomalies occur where these part lines do not cross the deep channel, as the deepest sounding covered is selected rather than the deep channel (Figure 6a).

   b) Lines run parallel to the deep channel – an unusual practice undertaken in a small part of the Truro River where channel straightening has produced a very narrow channel. The program is not designed to select the channel in these areas (Figure 6b).

   c) Very wobbly lines – where direction changes of greater than 60° occur within a survey line. These direction changes will be wrongly identified as a line change (Figure 6c).

   d) Gaps in the line corresponding to the deep channel – induced by the deliberate practice of selection of shoal soundings for navigational safety. May result in secondary minima being labelled as the main channel (Figure 6d).

2) Complex features of the channel system

a) Discontinuities in the channel – In tidal estuaries separate flood and ebb channels may occur. These channels do not join producing a discontinuity in the channel line identified (Figure 7a).

b) Branching channels and middle grounds – areas where the channel branches or divides around an island or central mudbank (Figure 7b).

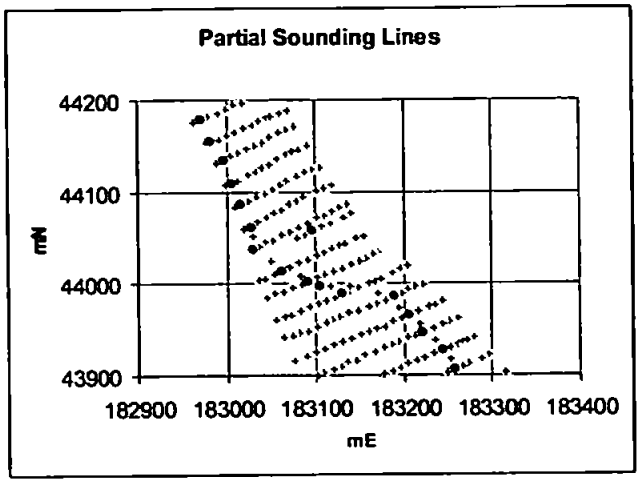

Figure 6a – Partial Survey Lines

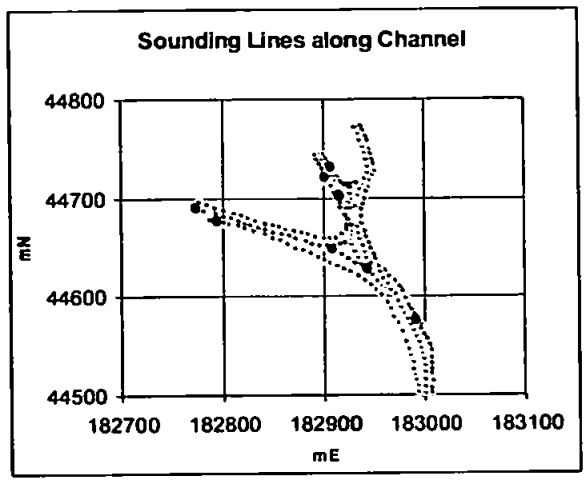

Figure 6b – Lines Near Parallel to Channel

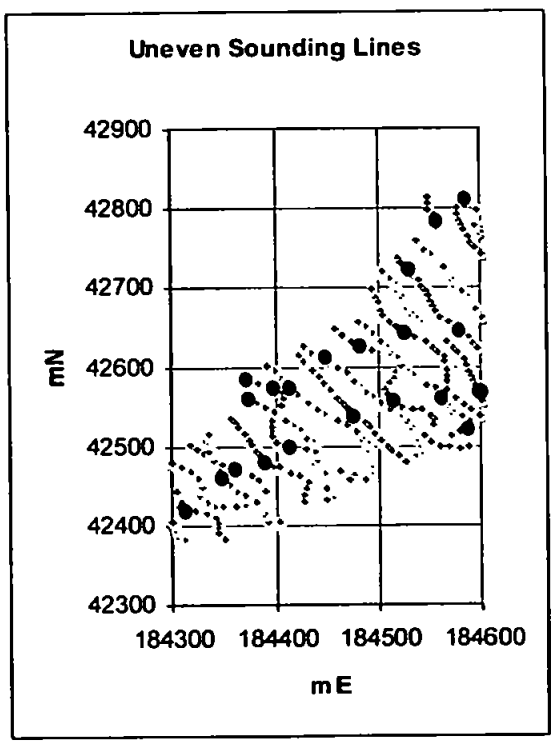

Figure 6c – Bends in Survey Lines > 60°

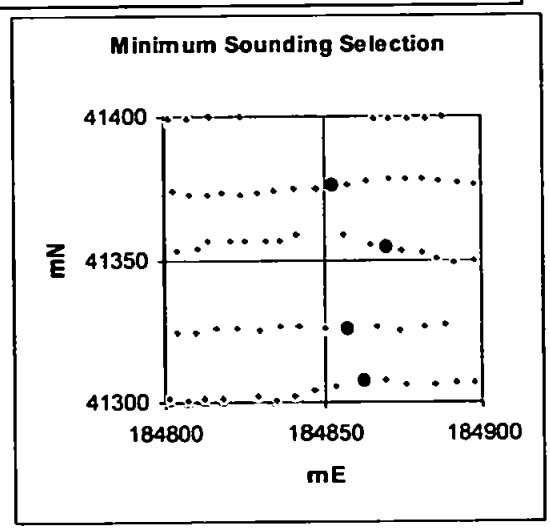

Figure 6d – Sounding Gap Corresponding to Deep Channel

Figure 6 – Anomalous Channel Selection due to Unusual Survey Practice. Large, black dots represent selected channel points, small crosses give the positions of all non-channel soundings.

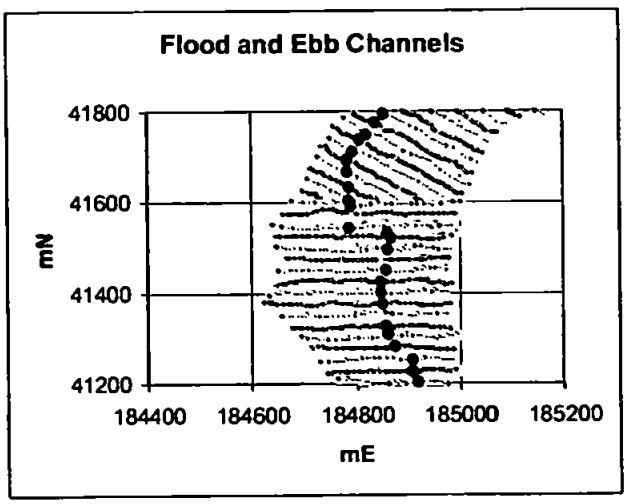

Figure 7a – Flood and Ebb Channels

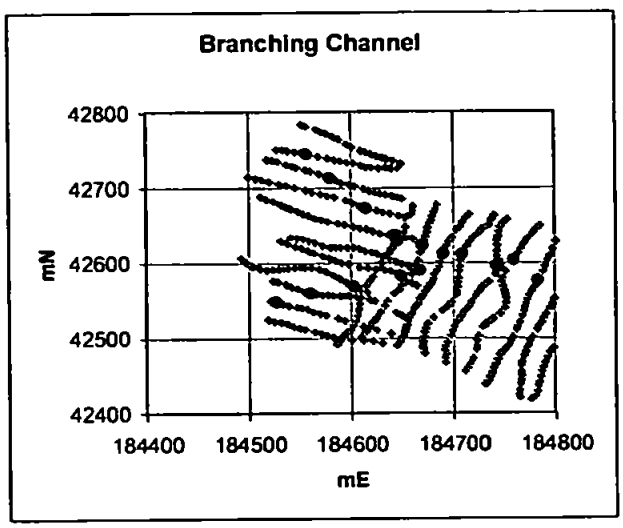

Figure 7b – Channel Branching

Figure 7 – Anomalies in Channel Selection due to Complex Natural Systems. Large, black dots represent selected channel points, small crosses give the positions of all non-channel soundings.

Despite the presence of these unusual features, the automated channel selection process was found to select the deep channel correctly on more than 91% of survey lines when tested on four historic data sets surveyed in the Truro River between 1961 and 1996. Inclusion of the fifth available data set surveyed in the same area, in 1995, produced a lower rate of correct channel selection, just over 82%, due to a large number of survey lines containing bends of > 60° (one can only speculate on the reason for this poor survey practice).

Manual Quality Control

Manual quality control was used to identify erroneous channel points resulting from the anomalies identified above. The number and complexity of their causal factors made automation of the quality control process unrealistic (and, the authors would suggest, undesirable) to ensure adequate treatment of unusual channel features.

During quality control rogue channel points were given an error code in place of the channel code assigned by the program, to avoid incorrect channel definition in the next stage of the ZIDW automation process. Out of sequence points resulting from bends and branches in the main channel and the presence of secondary channels were reordered in preparation for the fitting of channel lines to the data. A separate number code was allocated to each subsidiary channel to facilitate correct joining of channel systems.

Defining the Channel and Coastline

The channel line was defined by linking all deepest points determined above by means of straight lines. On investigation of small samples of data the use of actual data points joined by straight lines, eliminating the assumptions involved in curve fitting, was determined to be the most sensible method of producing an interpolation boundary.

The line definition program, originally designed to join points along a coastline, was edited to recognise a change in point code. Thus, by allocating different codes to the main channel and each subsidiary channel, joining points lying in different channels was avoided. The input channel data files, generated above, were edited to include a duplicate, joining point at confluences of channels. This prevented gaps occurring at junctions of channels and thus 'leakage' in the polygons outlined by the channels and coastline. The channel was specified in an upriver direction.

For consistency the coastline was to be specified in a clockwise direction. The start of this file was taken as the southernmost data point; necessarily the point on the opposite bank must become the last data point. Free boundary lines across the estuary

were necessarily added, during the polygon construction phase, to join the coastline and channels thus creating closed polygons.

Construction of Interpolation Polygons

Two vector topology files were constructed for the purpose of defining the required polygons. The first file contained node names and their co-ordinates (nodes being points at the junctions of every line (arc) forming the edge of one or more polygon). The second file defined each polygon according to the nodes surrounding it in clockwise order; the type of line joining consecutive pairs of nodes, e.g. main channel (MC), coast (AC) or free boundary (F), and the direction to be followed along each line (positive '+' or negative '-'). Samples from these node and polygon topology files are given in Figure 8.

Node Identifier	Easting (m)	Northing (m)
96 A1	184812	40563
96 A2	184519	42445
96 M1	184910	40422

Start Node	Type and Direction of Joining Arc
A1	AC+
A2	F
M3	MC-

Figure 8 – Top Diagram: An example node definition file, '96' gives the year of survey, 'A' represents a node on the coastline and 'M' a node on the main channel

and nodes are numbered consecutively along the relevant arc. **Lower Diagram:** Node numbers identify arcs enclosing each polygon, with associated arc type and direction. **Note:** Free boundaries join nodes with a straight line having no direction.

An algorithm was then be developed to produce interpolation polygons from a file containing coded coastline and channel vertices according to the relevant vector topology files.

For the successful operation of this program it was necessary to avoid anomalous topologies of two types:

1. Polygons must not be specified starting with a free section (Code F). This is easily avoided by careful choice of start node.

2. Two free sections must not occur consecutively within the polygon topology. Two very closely spaced nodes on the same arc, joined by a short section of this arc, must be input between free sections to allow the program to correctly define the polygons.

The codes of defined nodes were maintained in the output file to allow them to be distinguished from vertices for checking purposes. The vertices were allocated a code 'v' within the polygon definition program.

Allocation of Soundings and Output Grid Cells to Polygons

To facilitate the sounding and output cell allocation process a rectangular domain covering the entire survey area was defined. This rectangle had dimensions 4 km by 5 km for the Truro River study, thus enclosing all areas covered by various surveys carried out over the 40 year study period. The domain contained within this rectangle was then covered by a fine mesh of 1 metre cells. This cell size was chosen on the basis of a compromise between a sufficiently high resolution to maintain data accuracy for any sounding and output resolutions to be dealt with in the Truro River study, whilst maintaining manageable file sizes.

The program was then able to represent all coastline and channel data on the 1 metre grid by allocating their data codes to the appropriate grid cells. At this stage any grid cells containing neither coastline nor channels, i.e. cells covered by land or non-channel parts of the estuary were allocated a blank code.

To avoid difficulties resulting from boundaries shared by more than one polygon the program would fill each polygon individually, using a different code letter for each. For example, all cells on the 1 metre grid within the western polygon, i.e. between the western shore of the estuary and the channel would be assigned a code 'W'. A single character code was chosen to maintain manageable file sizes, whilst using a grid of 1 metre cell size over and area of several square kilometres.

Polygon filling was undertaken using the method of scan-line filling (as explained in Mielke, 1991). Within the polygon-filling program, it was necessary to design an algorithm to resolve the anomalous situation of polygon boundaries and turning points of these boundaries appearing identical when detected by the line by line scanning approach. For example, scanning across the grid in Figure 9:

1. The first scan line encounters no polygon boundaries
2. The second scan detects only one turning point and thus would require no filling
3. The third line finds two turning points, also requiring no filling
4. The fourth line contains four polygon boundary crossings, conforming to the odd-even rule (Mielke, 1991) and would therefore be filled correctly
5. The fifth scan line would detect two polygon boundaries, require fill between, but also a minimum turning point which does not represent a boundary where filling is stopped.

.	.	.	.	.	.	.	.	.	.	.
.	.	.	.	B	.	.	.	.	.	.
.	.	.	B	B	B	.	.	B	.	.
.	.	B	B	.	B	.	B	.	B	.
.	B	B	.	.	.	B	.	.	B	.
.	B	.	.	.	.	.	.	.	B	.
.	B	.	.	.	.	.	.	.	B	.

Figure 9 – Part of a polygon, defined on the grid, illustrating typical problems associated with the polygon filling process.

Performing ZIDW

Having successfully assigned all cells, within the 1 metre grid, to a polygon, the ZIDW interpolation process could be performed. Provision was made in the interpolation for averaging the data onto a 10 metre grid, required for comparison with other data sets, during this interpolation. Clearly, it was necessary to take the polygonal zones into account during any averaging processes. If the zones were not taken into consideration the benefits of zoned interpolation would be partially negated by the effects of averaging across channels. It was decided to maintain the high resolution, 1 metre grid during interpolation, despite the subsequent requirement for zoned averaging. This would provide data at 1 metre grid scale, for comparison and calculations, in addition to the 10 metre scale required later.

According to the zoning theory the choice of soundings to be included in the determination of each point on the grid must obey the following rules:

1. Each trial point in the channel, i.e. coded C or c, only soundings within the channel are allowed in the ZIDW process.

2. For non-channel trial points, i.e. points in any polygon, only soundings in the same polygon or in the channel are permitted in ZIDW

The method employs the fitting of a plane through selected sounding points fitting and inverse distance weighting. All soundings lying within a circle, of radius 50 metres, centred on the test point (except those outside the polygon containing the test point and not in the channel) were considered. A plane equation of the form $z = a + bx + cy$ was fitted to the selected soundings, using an origin coincident with the test point, such that the equations of condition are:

$$a + bx_1 + cy_1 = z_1$$

$$a + bx_2 + cy_2 = z_2$$

$$a + bx_3 + cy_3 = z_3$$

Hence the solution, for 'a' gives the value of depth (z) at the test point, where:

$$a = \begin{vmatrix} z_1 & x_1 & y_1 \\ z_2 & x_2 & y_2 \\ z_3 & x_3 & y_3 \end{vmatrix} \div \begin{vmatrix} 1 & x_1 & y_1 \\ 1 & x_2 & y_2 \\ 1 & x_3 & y_3 \end{vmatrix}$$

The method of sounding selection results in up to 40 soundings being used to interpolate the depth at certain test points. Hence a least squares solution was required to fit the plane through the soundings. The normal equations were as follows:

$$(\Sigma W_i)a + (\Sigma W_i\, x_i)b + (\Sigma W_i\, y_i)c = (\Sigma W_i\, z_i)$$

$$(\Sigma W_i\, x_i)a + (\Sigma W_i\, x_i^2)b + (\Sigma W_i\, x_i\, y_i)c = (\Sigma W_i\, x_i\, z_i)$$

$$(\Sigma W_i\, y_i)a + (\Sigma W_i\, x_i\, y_i)b + (\Sigma W_i\, y_i^2)c = (\Sigma W_i\, y_i\, z_i)$$

The results of this interpolation method produce a smoothly contoured surface; apparently consistent with the smooth shape expected for mud bank features (see Figure 10).

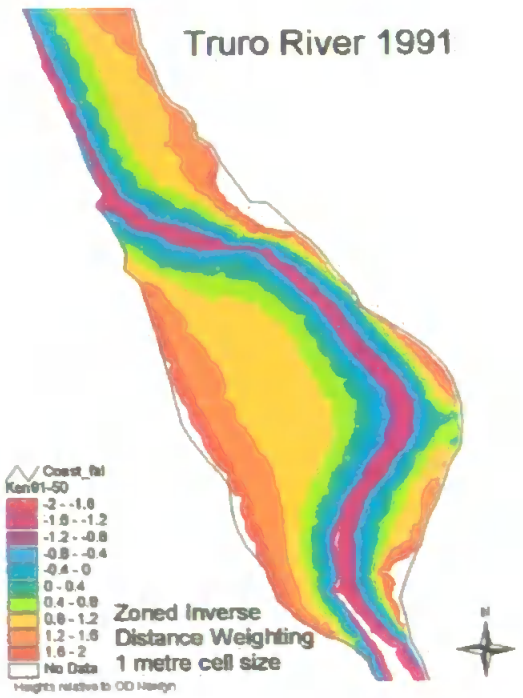

Figure 10 – Interpolation of the 1991 data set using Zoned Inverse Distance Weighting, with a 30 metre radius of interpolation.

For certain data sets the isobaths exhibit slight arcuate cusps in some areas. These features appear to coincide with the intersection of the isobaths and sounding lines. To minimise these effects the program was improved to remove rounding errors imposed on the locations of sounding points. Also, various interpolation radii were tested to determine which was best suited to the average line spacing exhibited by each data set. For the 1991 and 1996 data the arcuate cusps were removed from the interpolated isobaths by reduction of the 50 metre interpolation radius to 30 metres. The 1961 data, however, exhibits a greater spacing between certain pairs of sounding lines than the more recent data sets, probably as a result of running lines along transects. This early data set contains line spacings of up to 50 metres compared to 40 metres for subsequent surveys. Consequently, the use of a 30 metre interpolation radius for 1961 produced narrow bands of 'no data' between some survey lines. After experimenting with various interpolation radii, a 50 metre radius was determined to produce the most realistic isobath model from this data set.

Modifications and Improvements

After testing on a number of data sets, it was necessary to make some modifications to the programs.

The program to allocate soundings to polygons was originally limited to a maximum of 5 intersections of each scan line with the coastline and channel. For the 1974 and 1995 data sets, more than 5 intersections were encountered causing a 'Fatal Error' in the program. After examination of the data, these errors were found to result from repeated intersections along short sections of very uneven channel.

The uneven nature of the channel was investigated by means plotting profiles across the channel, along each sounding line within the problem area. A number of consecutive profiles were plotted coincidentally on the same axes for comparison purposes. The results this investigation ascertained that the data set contains insufficient information to determine whether the uneven channel is a genuine phenomenon, resulting from complex hydrography at the confluence of the Truro and Tresillian Rivers, or due to factors of the survey. These factors could result from the selection method used to determine which sounding values are displayed on the chart combined with the closeness and irregularity of sounding lines in this area.

In the light of this investigation it was considered inappropriate to apply any form of spatial smoothing to the uneven channel. If it were possible to ascribe channel irregularities to aspects of the survey process it would be relatively straightforward to assign a best-fit curve through the channel points. To avoid the danger of losing genuine channel information via a smoothing process, however, it was necessary to edit the program to cope with more than 5 intersections of the coastline and channel.

The counting of intersections is a fundamental part of polygon definition within the suite of programs; hence this alteration is not straightforward. Initially part of the program was modified to count the maximum number of intersections that could be encountered within a data set representing the worst case scenario. A maximum of eight intersections was detected in the 1995 data set from the Fal estuary. Clearly more might be present in data for other areas.

In order, to maintain the universal applicability of the ZIDW program suite. It was decided to reconstruct the point allocation program, employing a different approach for assigning grid cells to the appropriate polygonal zone. The revised program initially ensures that no vertices of polygons fall exactly on a scan line. This is achieved, within the program, by displacing all vertices with co-ordinates of a whole number of metres by a negligibly small amount. Consequently a scan line will never exactly intersect with a maximum or minimum turning point of a polygon boundary. This ensures that every scan line will encounter an even number intersections with polygon boundaries. Each consecutive pair of intersections will, therefore, represent entering and then leaving the polygon. By this method the program is able to deal with any number of boundary intersections, and it is no longer necessary to specify each unique combination of intersections individually.

This modification resulted in listings of intersections being generated in a non-sequential order. This difficulty was overcome by the addition of a simple sorting sub-routine to place the previously identified intersection points into numerically ascending order according to their east-west co-ordinates, that is parallel to the direction of scanning.

The ZIDW program suite has been developed, and successfully tested, on the basis of polygonal zones bounded by coastline, channels and edge boundaries. All the sounding points were required to construct the ZIDW surface. Hence, it was not possible, in this investigation, to use independent sounding points to verify accuracy. Instead, rigorous, theoretical testing of the method has been carried out for a number of mathematically defined channels of increasing complexity. The visual and statistical results of these tests provide numerical validation of the theory behind ZIDW, and will form the basis of a further paper.

Clearly, an anomalous case to the ZIDW method arises where channels are not contiguous to the limit of the polygon. This occurs in the case of flood and ebb channels following different routes. The use of a free boundary, to join such channels into a continuous feature, necessarily results in an interpolation boundary, where no physical discontinuity exists. As a result artificial artefacts of interpolation are generated in the vicinity of this boundary. Realistic interpolation in the vicinity of such features, in-conjunction with extending the ZIDW program suite for application

to larger scale estuaries, is the subject of ongoing research at the University of Plymouth.

Conclusions

The Zoned Inverse Weighting (ZIDW) method, described by Burroughes et al (2001), has been successfully automated and tested, using data sets from the Fal estuary, in Southwest Cornwall. The method involves automating the processes of sounding line definition; identification of the main and subsidiary channels and allocation of input sounding data and output grid cells to polygonal zones. The interpolation polygons are defined in vector form by means of a file containing co-ordinates of nodes and a polygon topology file. ZIDW is then performed using inverse distance weighted interpolation, taking into account the polygonal zones outlined by the coastline and channels. The user has the option to select an appropriate radius of interpolation according to the spacing of soundings within the original data set.

Careful consideration, during the design process, will allow the programs to be generally applicable to estuaries containing mud-banks crossed by relatively narrow deep channels. The method is currently being tested on a much larger scale, in the Gironde estuary, in western France, as part of ongoing research work at the University of Plymouth.

References

Burroughes J E, Abbott V J and Morris K P, 2000. Management of Hydrographic Survey Requirements. Proceedings of Oceanology 2000 Conference, Brighton.

Burroughes J E, George K J and Abbott V J, 2001. Interpolation of Hydrographic Survey Data. The Hydrographic Journal – In press.

Mielke B, 1991. Integrated Computer Graphics. Published by: West Bay Publishing Company.

Appendix 6
Users Guide to the ZIDW Program Suite for Interpolation of Bathymetric Data

Notes:
1. *** is a 3-character tag used to identify the data set used
2. The file formats given in this document are intended to provide a guide to the information required in each file. For more details of file formats see appendix 7.

Phase 1: To Identify the Channels

COL10.EXE

To combine input from Arc-Info into a single file.

Input files:	***-XY.TXT	Cartesian co-ordinates of sounding-points.
	***-Z.TXT	Heights of sounding-points above datum.
Output file:	***-XYZ.TXT	Cartesian co-ordinates and heights of sounding-points.

RFGIR.EXE

To reformat bathymetric and coastline data from the lower Gironde estuary, from latitude and longitude on the Clarke 1880 spheroid, to the Lambert 93 grid, based on the GRS 1980 spheroid.

Input files:	***-BLZ.TXT	Latitude, longitude and height of sounding-points.
	***-COST.TXT	Latitude and longitude of coastline.
Output files:	***-XYZ.TXT	Cartesian co-ordinates and heights of sounding-points.
	***-ACC.TXT	Cartesian co-ordinates of coastline.

Either:

SLINES.EXE

To identify sounding lines for data arranged in original, line order. For example, data from the Fal and Humber.

Input file:	***-XYZ.TXT	Cartesian co-ordinates and heights of sounding-points.
Output file:	***-SPTS.TXT	Sounding points ordered along sounding lines.

Or:

GIRLS.EXE

To identify sounding lines for data no longer arranged in line order. For example, data from the Gironde estuary.

Input files:	***-XYZ.TXT	Cartesian co-ordinates and heights of sounding-points.
	***-SLD.TXT	Positions of vertices of quadrilaterals and number of sounding lines within the quadrilateral.
Output file:	***-SPTS.TXT	Sounding points ordered along sounding lines.

MAXMIN.EXE

To locate the deepest sounding and any local minima on each line.

Input file:	***-SPTS.TXT	Sounding points ordered along sounding lines.
Output file:	***-TPTS.TXT	Turning points.

SMOOTH.EXE

To smooth the channel data using cubic splines.

Input file:	***-TPTS.TXT	Turning points.
Output file:	***-SMOC.TXT	Smoothed channel data.

Phase 2: To Interpolate the Data using ZIDW

GRID5.EXE

To define the boundaries of the interpolation area.

Input files:	***-ACC.TXT	Positions of vertices on the coastline, listed anticlockwise around the country.
	***-GRID.TXT	Parameters of the fine mesh grid covering the survey area.
Output files:	***-PIXL.DAT	1 character labels of all the pixels within the fine mesh grid, covering the survey area.
	***-BMAP.TXT	Labelled fine mesh grid suitable for display in bitmap form, for checking purposes.

ZIDW.EXE

To determine the height above datum of all possible points on the 1 m grid, using zonated least-squares weighted by inverse distance from the sounding-points.

Input files:	***-XYZ.TXT	Cartesian co-ordinates of sounding-points.
	***-GRID.TXT	Parameters of the fine mesh grid covering the survey area.
	***-SMOC.TXT	Smoothed channel data.
	***-PIXL.DAT	1 character labels of all the pixels within the fine mesh grid, covering the survey area.
Output files:	***-POSN.TXT	Positions, in Cartesian co-ordinates, of pixels for which a height has been determined, for use in Arc-Info.
	***-HODN.TXT	Heights, relatice to datum, of pixels for which a height has been determined, for use in Arc-Info.

Input of ***-POSN.TXT & ***-HODN.TXT into Arc-Info:

1) Create a Point Coverage
   a) Use GENERATE to produce a new coverage from ***-POSN.TXT
   b) Use DEFINE (in TABLES) to add depths to the point coverage from ***-HODN.TXT
   c) Use BUILD to build the topology of the point coverage
   d) Use JOINITEM to link the coverage and attribute table together

2) Create a Grid from the Point Coverage
   a) Use POINTGRID <point coverage> <grid coverage> <item = depth>
   b) Select SPATIAL ANALYST in Arc-View to view the grid coverage

Appendix 7

File Formats for the ZIDW Program Suite

*****-XYZ.TXT** ⇒ Cartesian co-ordinates of all sounding points.

Format:

Point Number	Easting (m)	Northing (m)	Height (m) relative to Datum
	To the nearest decimetre (1 d. p.)	To the nearest decimetre (1 d. p.)	To the nearest centimetre (2 d. p.)

Example: From the Truro River 1991 (T91-XYZ.TXT)

```
 1   183567.7    43277.3      1.60
 2   183556.8    43272.1      1.20
 3   183545.8    43267.2       .50
 4   183531.4    43261.3     -3.10
 5   183521.7    43257.1     -3.10
 6   183512.8    43253.5     -2.80
 7   183502.5    43250.8     -2.90
 8   183493.6    43246.5     -2.40
 9   183484.4    43242.1     -2.40
10   183473.9    43237.9     -2.00
```

*****-SPTS.TXT** ⇒ Sounding Points in ordered along sounding lines.

Format:

Point Number	Sounding Line Number	Point Number within the Sounding Line	Easting (metres)	Northing (metres)	Height (metres) relative to Datum
			To the nearest decimetre (1 d. p.)	To the nearest decimetre (1 d. p.)	To the nearest centimetre (2 d. p.)

Example: From the Humber (HUM-SPTS.TXT)

```
 1    1    1  508828.8  427493.9     3.60
 2    1    2  508828.8  427493.9     3.70
 3    1    3  508825.5  427491.3     3.40
 4    1    4  508823.0  427488.1     2.70
 5    1    5  508821.3  427484.4     2.00
 6    1    6  508820.3  427480.2     1.60
 7    1    7  508820.3  427476.3     1.20
 8    1    8  508821.0  427472.1      .70
 9    1    9  508823.6  427466.2      .60
10    1   10  508824.8  427464.3      .40
```

***-SLD.TXT ⇒ Positions of vertices of quadrilaterals and number of sounding lines within the quadrilateral.

Format:

Reach Code and Quadrilateral No.	Geodetic Reference	Co-ordinates of each vertex of the quadrilateral	No. of sounding lines within the quadrilateral
e.g. C01 = Reach C, quadrilateral 1	e.g. L = Lambert '93	To nearest metre	

Example: From the Gironde (GIR-SLD.TXT)

C01 L	406983	6465893	406300	6465839	405517 6470339	406533 6470694	24
C02 L	408467	6467455	406717	6467145	406233 6470829	407817 6470282	18
C03 L	409167	6467655	407867	6467473	407833 6470710	408767 6470875	17
C04 L	410500	6465944	409433	6465750	408533 6470927	409983 6471145	14
C05 L	406737	6464642	406100	6464857	406233 6465911	406966 6465929	6
C06 L	407767	6465759	406900	6465607	406717 6467107	407517 6467214	15
C07 L	409450	6465250	407885	6465161	407650 6467236	409183 6467304	11
C08 L	407459	6463018	406133	6462911	406033 6465571	407230 6465625	14
C09 L	409733	6464536	407180	6464125	407133 6464946	409617 6465399	5
C10 L	410933	6463179	409836	6463036	409433 6465607	410500 6465750	14

***-TPTS.TXT ⇒ Maximum and minimum turning point.

Format:

Point Number	Sounding Line Number	Point Number within the Sounding Line	Easting (metres)	Northing (metres)	Height (metres) relative to Datum	Channel Code
e.g. 1	e.g. 1	e.g. 1	To the nearest decimetre (1 d. p.)	To the nearest decimetre (1 d. p.)	To the nearest centimetre (2 d. p.)	e.g. C

Example: From the Humber (HUM-TPTS.TXT)

47	1	47	508854.1	427316.2	-8.20	C
1191	2	574	508772.4	427257.0	-8.40	C
1283	3	47	508686.3	427233.0	-8.60	C
2420	4	567	508574.9	427182.1	-8.90	C
3611	6	559	508336.9	427010.9	-7.60	C
4272	7	611	509131.0	427522.4	-7.60	C
4331	8	38	509064.2	427421.2	-7.60	C
5491	9	579	508961.5	427367.7	-7.80	C
5580	10	49	508441.7	427070.8	-7.50	C

-TPTS.PRN ⇒ Channels and ridges manually identified from turning points file (-TPTS.TXT).

Format:

5 columns each 8 characters wide ≡ *.prn format out from Microsoft Excel, without changing column widths:

Unique Channel Code	Point Number within the Channel	Easting (m)	Northing (m)	Height (m) relative to Datum
e.g. C01	e.g. 1	To the nearest metre	To the nearest metre	To the nearest centimetre (2 d. p.)

Example: From the Humber (HUM-TPTS.PRN)

```
M1          1   508229   426968    -7.40
M1          2   507933   426927    -8.80
M1          3   507842   426884    -8.20
M1          4   507745   426860    -7.30
M1          5   507656   426848    -7.10
M2          1   507288   426650    -5.40
M2          2   505836   425524    -3.00
M2          3   505758   425443    -2.90
M2          4   505548   425355    -2.60
```

***-SMOC.TXT ⇒ Smoothed channel data.

Format:

Unique Channel Code	Number of Points within that channel				
Easting (m) of point on smoothed channel	Northing (m) of point on smoothed channel	Height (m) relative to Datum of point on smoothed channel	Easting (m) of original sounding point	Northing (m) of original sounding point	Height (m) relative to Datum of original sounding point
To the nearest metre	To the nearest metre	To the nearest centimetre (2 d. p.)	To the nearest metre	To the nearest metre	To the nearest centimetre (2 d. p.)

Example: From the Humber (HUM-SMOC.TXT)

```
M1                 5
    508228.    426974.      -7.40    508229.    426968.      -7.40
    507938.    426910.      -8.80    507933.    426927.      -8.80
    507840.    426888.      -8.20    507842.    426884.      -8.20
    507743.    426867.      -7.30    507745.    426860.      -7.30
    507656.    426848.      -7.10    507656.    426848.      -7.10
M2                30
    507288.    426650.      -5.40    507288.    426650.      -5.40
    505836.    425516.      -3.00    505836.    425524.      -3.00
    505758.    425454.      -2.86    505758.    425443.      -2.90
    505548.    425351.      -2.67    505548.    425355.      -2.60
    505283.    425234.      -3.05    505283.    425234.      -3.10
    505190.    425198.      -3.30    505190.    425199.      -3.20
```

***-GRID.TXT ⇒ Parameters of the fine mesh grid covering the survey area.

Example: From the Humber (HUM-GRID.TXT)

2.	Size of hyperfine mesh, in metres
504000.	Easting of SW point
423000.	Northing of SW point
6000.	E-W distance
5000.	N-S distance
100.	Smallest spacing between lines, in metres

***-POSN.TXT ⇒ Positions of pixels for which height has been determined, for input into Arc-Info.

Format:

Point Number	Easting (m)	Northing (m)
e.g. 1	To the nearest metre	To the nearest metre

Example: From the Truro River 1991 (T91-POSN.TXT)

```
    1   182700.    44500.
    2   182700.    44506.
    3   182700.    44510.
    4   182700.    44512.
    5   182700.    44516.
    6   182700.    44517.
    7   182700.    44520.
    8   182700.    44523.
    9   182700.    44525.
   10   182700.    44528.
```

***-HODN.TXT ⇒ Height at each position given in ***-POSN.TXT, for input into Arc-Info.

Format:

Point Number	Height (m) relative to Datum
e.g. 1	To the nearest centimetre (2 d. p.)

Example: From the Truro River 1991 (T91-HODN.TXT)

```
 1     -3.56
 2     -3.73
 3     -8.53
 4       .12
 5    -16.71
 6     -3.36
 7     -4.69
 8    -16.35
 9      5.29
10     -3.57
```

***-ACC.TXT ⇒ Coastline File

Format:

Segment Number	Easting (m)	Northing (m)
e.g. 1	To the nearest centimetre (2.d.p.)	To the nearest centimetre (2.d.p.)

Example: From the Fal Estuary (FAL-ACC.TXT)

```
1      184068.80  39601.65
1      184080.60  39600.11
1      184089.80  39612.90
1      184061.00  39615.34
1      184071.40  39627.24
1      184092.70  39628.50
1      184097.30  39650.82
1      184095.60  39679.77
1      184099.00  39709.79
1      184105.10  39746.06
```

Note: The formats of other files mentioned in the text, for example ***-POLY.TXT, are not detailed here, as these files are no longer used.

Appendix 8 - Glossary of Technical Terms

Large Square – Square area 100 grid cells by 100 grid cells. For the examples used in this study:

Estuary	Cell Size	Area of Large Square
Fal	1 m	100 m by 100 m
Humber	2 m	200 m by 200 m
Gironde	20 m	2 km by 2km

Search Area – the large square containing the test point, in question, and the 8 large squares surrounding it:

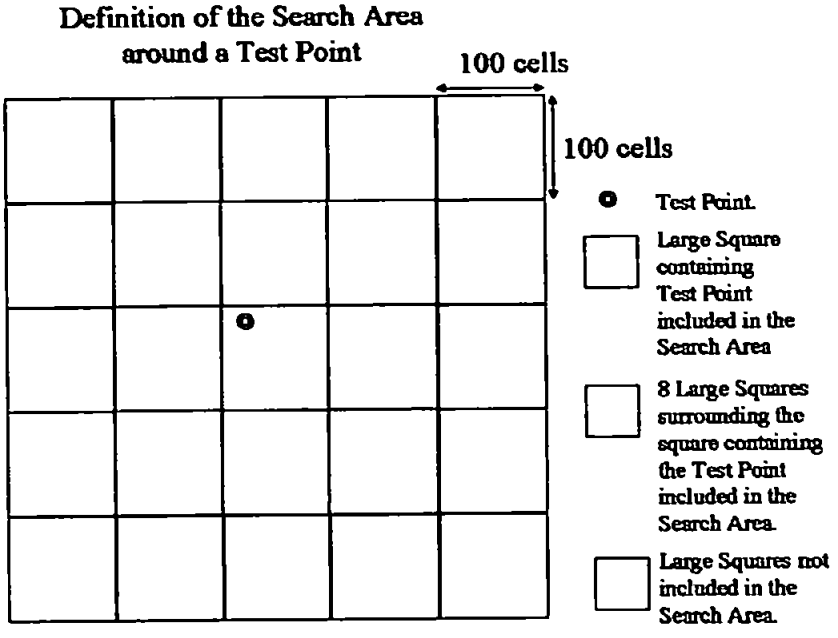

SMART ellipse – elliptical area, centred on the test point and with semi-major axis given by 1.2 × sounding line spacing and semi-minor axis equal to 0.25 × semi-major axis. The orientation of the smart ellipse is such that the semi-major axis is parallel to the channel segment closest to it. All soundings lying within the smart ellipse contribute to the determination of depth at the test point unless separate from it by the centre line of a channel or crest of a ridge.

Half width – the distance to either side of a test point, along the sounding line, within which all soundings are considered, in order to determine whether the test point represents part of the centre line of a channel or the crest of a ridge.

Appendix 9 -

Transformation of Gironde Data

From Latitude and Longitude on Clarke 1880 Spheroid

To Lambert 1993 Grid Co-ordinates

Process:

Transformation of the Gironde Data

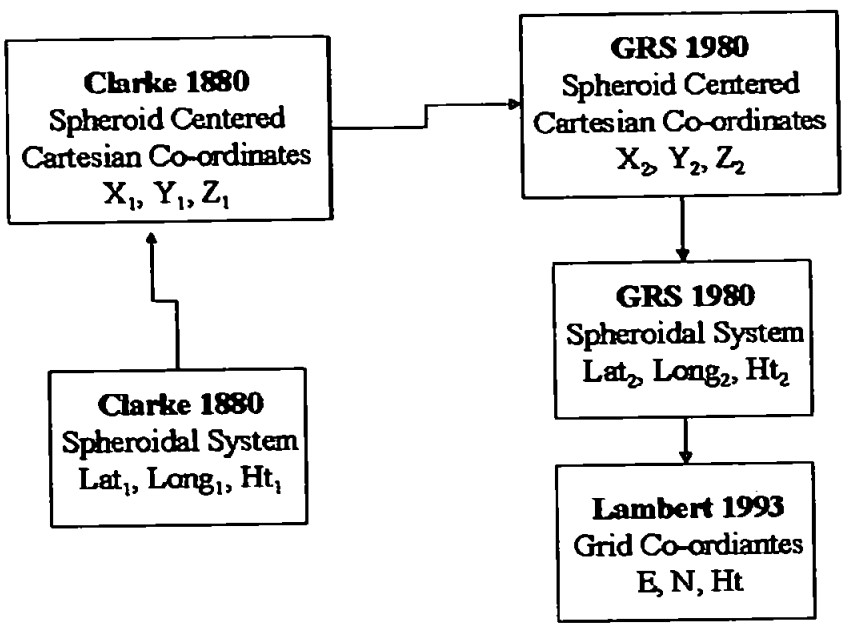

1. Computation of Cartesian Co-ordinates from Latitude (φ) and Longitude (λ):
(Equations from Hooijberg, 1997)

$$h_0 = H + Ns_0$$

$$RN = \frac{a}{\left(1 - e_0^2 \sin^2 \varphi\right)^{\frac{1}{2}}}$$

$$X_0 = \left(RN_0 + h_0\right)\cos\varphi_0 \cos\lambda_0$$

$$Y_0 = \left(RN_0 + h_0\right)\cos\varphi_0 \sin\lambda_0$$

$$Z_0 = \left(RN_0\left(1 - e_0^2\right) + h_0\right)\sin\varphi_0$$

Where:
o = old co-ordinate
n = new co-ordinte
a = semi-major axis of the ellipsoid

e^2 = first eccentricity of ellipsoid squared
H = geoidal orthometric height
h = elevation of the datum
Ns = geoidal separation of the datum (N)
RN = radius of curvature in the meridian
φ = geodetic latitude
λ = geodetic longitude

2. 7-Parameter Transformation Algorithm used to transform, used from Clarke 1880 to GRS 1980:
(Equations from Hooijberg, 1997)

$$X_n = \Delta X + (X_0 + \omega Y_0 - \psi Z_o) \times (1 + \Delta k)$$
$$Y_n = \Delta Y + (Y_0 - \omega X_0 + \varepsilon Z_o) \times (1 + \Delta k)$$
$$Z_n = \Delta Z + (Z_0 + \psi X_0 - \varepsilon Y_o) \times (1 + \Delta k)$$

Where:
o = old co-ordinate
n = new co-ordinte
ΔX = component of origin translation X
ΔY = component of origin translation Y
ΔZ = component of origin translation Z
ω = rotation of XYZ system about Z-axis
ε = rotation of XYZ system about X-axis
ψ = rotation of XYZ system about Y-axis
Δk = change in scale of datum

3. Computation of Latitude (φ) and Longitude (λ) from Cartesian Co-ordinates:
(Equations from Hooijberg, 1997)

Latitude:

$$p = \left(X_n^2 + Y_n^2\right)^{\frac{1}{2}}$$
$$\vartheta = \tan^{-1}\left[\frac{(a_n Z_n)}{(b_n p)}\right]$$
$$\varphi_n = \tan^{-1}\left[\frac{\left(Z_n + e'^2_n\, b_n \sin^3 \vartheta\right)}{p - e_n^2 a_n \cos^3 \vartheta}\right]$$

Longitude by iteration using a corrected value of θ:

$$\varphi'_n = \varphi_n$$

$$\vartheta = \tan^{-1}\left[\frac{b_n}{a_n \tan\varphi'_n}\right]$$

$$\varphi_n = \tan^{-1}\left[\frac{\left(Z_n + e'^2_n\, b_n \sin^3\vartheta\right)}{\left(p - e^2_n a_n \cos^3\vartheta\right)}\right]$$

$$\lambda_n = \tan^{-1}\left(\frac{Y_n}{X_n}\right)$$

$$Rn_n = \frac{a_n}{\left(1 - e^2_n \sin^2\varphi_n\right)^{\frac{1}{2}}}$$

$$h_n = \frac{p}{\left(\cos\varphi_n - RN_n\right)}$$

$$Ns_n = h_n - H$$

Where:
o = old co-ordinate
n = new co-ordinate
a = semi-major axis of the ellipsoid
b = semi-minor axis of the ellipsoid
e^2 = first eccentricity of ellipsoid squared
e'^2 = second eccentricity of ellipsoid squared
H = geoidal orthometric height
h = elevation of the datum
Ns = geoidal separation of the datum (N)
RN = radius of curvature in the meridian
φ = geodetic latitude
λ = geodetic longitude

4. Projection from GRS 1980 to Lambert 1993:
(Equations from Hooijberg, 1997)

$$Q = \frac{1}{2}\left[\ln\left((1+\sin\varphi)/(1-\sin\varphi)\right) - e\ln\left((1+e\sin\varphi)/(1-e\sin\varphi)\right)\right]$$

$$R = \frac{K}{\exp\left(Q\sin\varphi_0\right)}$$

$$E = E_0 + R\sin\gamma$$

$$N = R_b + N_b - R\cos\gamma$$

$$\gamma = \left(\lambda_0 - \lambda\right)\sin\varphi_0$$

$$k = \left(1 - e^2\sin^2\varphi\right)^{\frac{1}{2}}\left(R\sin\varphi_0\right)/\left(a\cos\varphi\right)$$

Where:

a = semi-major axis of the ellipsoid
e^2 = first eccentricity squared
φ_0 = Central Parallel (CP), latitude of projection origin
φ_b = Latitude of (false) grid origin, in case of 2 parallels
λ_0 = Central, Reference Meridian (RM, λ_0), longitude of true and grid origin
E_0 = false easting constant at grid and projection origin, (RM, λ_0)
N_b = false northing constant for φ_b, at the RM, λ_0
R = mapping radius at latitude, φ
R_b = mapping radius at latitude, φ_b
K = mapping radius at the equator
Q = isometric latitude

φ = parallel of geodetic, positive north
λ = meridian of geodetic longitude, positive east
E = easting co-ordinate
N = northing co-ordinate
γ = convergence angle
k = grid scale factor at a general point